PREPARATION OF POROUS CARBON FROM PALM SHELL USING PHOSPHORIC ACID ACTIVATION: PROCESS OPTIMISATION, ADSORPTION, REAGENT RECOVERY AND REUSEABILITY

Lim Wah Ching

B. Eng (Chemical and Process Engineering) (Hon)

M. Sc (Integrated Process Plant Management System)

A thesis submitted in fulfilment of the requirement for the degree of Doctor of Philosophy

Faculty of Engineering

Monash University

December 2011

ABSTRACT

The objective of present work is to develop chemically activated carbons from palm shell using H_3PO_4 via optimisation on the process parameters such as impregnation ratio, activation temperature and activation time, with the aim of achieving high yield and well developed pore structure. The process optimisations have been conducted utilising the optimisation tool Response Surface Methodology (RSM). Various issues associated with chemical activation process such as the activation in inert media/self-generated atmosphere (SGA) and activation with reclaimed reagent were also been addressed. The kinetics of the H_3PO_4 activation and significance of SGA have been assessed using thermogravimetric analysis (TGA). The activated carbon have been characterised for (i) pore size distribution, average pore size and the surface area using the BET surface area analyser, (ii) the surface textures and structure of the pores using SEM, FT-IR and XRD. Based on the pore structure and the surface area, suitability of the PSAC for adsorption on specific macromolecules, Methylene Blue (MB) and dairy COD have been developed. Effectiveness of an adsorbent is assessed by the equilibrium adsorption capacity and the rate of adsorption of the adsorbent. Experiments on adsorption isotherm and kinetics of the mentioned adsorbates have been established. The recovery and reusability of H_3PO_4 for subsequent activation of palm shell under identical experimental conditions were also being thoroughly investigated. PSAC with BET surface area exceed $2000 m^2/g$ has been developed, coupled with high carbon yield of approximately 50%. The good adsorption value on MB and dairy COD correspond with high mesopore content in PSAC, a unique character of the carbon. The significance of SGA has been demonstrated from TGA analysis. The reclaimed H_3PO_4 is found to have almost similar activation capability as that of fresh acid in terms of yield and textural characteristics.

STATEMENT OF AUTHORSHIP

The thesis contains no material which has been accepted for the award of any other degree or diploma in any university or other institution. I affirm that, to the best of my knowledge, the thesis contains no material previously published or written by another person, except where due reference is made in the text of the thesis.

Signed: .....

Lim Wah Ching

December 2011

ACKNOWLEDGEMENTS

I wish to express my deep appreciation to my supervisor Dr. Veena Doshi for her guidance, encouragement and perseverance throughout the course of my research. I would also like to thank my co-supervisor Associate Professor Chandrasekar Srinivasakannan for his advice and valuable feedbacks. Fourth-year students and laboratory staffs of School of Engineering, Monash University, Prasana Seheran, Lim Pek See, Jason Soh, Amahl and Farisha for their support throughout the my research. Fellow researchers Jason, Darwin, Mark, Alpha, Oon-Ee and Yoges for providing a cohesive environment. Century Chemicals Sdn Bhd & Kekwa Indah Sdn Bhd for contributing industrial feedback that shaped my research objectives. Finally and most of all to Joey, Sasha, Venezia, my mum and family members for their support and patient.

Lim Wah Ching

December 2011

TABLE OF CONTENTS

PAGE

LIST OF TABLES

LIST OF FIGURES

CHAPTER I

INTRODUCTION

1.1 Background

This work explores the non-conventional chemical activation method using palm shell as precursor with phosphoric acid (H_3PO_4) as reagent. The utilization of self-generate atmosphere in place of a continuous flow of inert gas for activation, holds the potential for process scale-up due to its simplicity and low energy loss. Evident by the ability of H_3PO_4 to generate carbon with favorable textural characteristics, this work attempts to add new knowledge through comprehensive study to establish the optimum condition for palm shell activated carbon (PSAC) development.

Although chemical activation by H_3PO_4 has been reported for many biomass, its application to the palm shell is very limited. With the awareness of heteroporous nature of AC through H_3PO_4 activation, this work focuses on development of significantly higher mesoporous AC specifically targeted for adsorption of macromolecule such as dye and dairy waste with intention to simultaneously generate high surface area and carbon yield. The recovery and reusability of the reagent have also been thoroughly investigated.

1.2 Research objective

Objective I: Process development

The desired characteristics of PSAC such as the well developed pore size and surface area depends on factors namely precursor material, activating agent, impregnation ratio and activation method. The range of these independent variables was estimated from the literature survey and a Design of Experiment (DOE) using Response Surface Method (RSM) was carried out to find the minimum number of experiments and to optimize the process conditions. Regression analysis and analysis of Variance (ANOVA) was utilized for fitting the model and for examining the statistical significance of the model terms. The result of second-order response surface model was evaluated. Subsequently, mathematical regression models for responses of PSAC on BET surface area, pore size and yield was established.

Objective II : Characterization of palm shell activated carbon

The developed PSAC were characterized for its textural and surface characteristics. The surface area, average pore size and pore distribution were evaluated using surface area analyser. Thermogravimetric analysis (TGA) was conducted on palm shell, its char and PSAC to assess the implication of H_3PO_4 activation under self-generate atmosphere. The structure of the pores was examined using Scanning Electron Microscope (SEM) while its surface functional groups were assessed by Fourier transform infrared (FT-IR) and X-ray diffraction (XRD) analysis.

Objective III: Adsorption isotherm and kinetics

The equilibrium adsorption capacity of the PSAC with respect to methylene blue and dairy COD was carried out to assess the effectiveness of PSAC in adsorb macromolecules. This objective involves identifying appropriate models that explain the mechanism of adsorption. Adsorption isotherms were experimentally established before being tested with the well

known models such as Langmuir, Freundlich and Temkin. The kinetics of adsorption was also modeled to establish a complete adsorption mechanism based on industrial environment.

Objective IV: Recovery and reusability of H_3PO_4 in palm shell activated carbon generation

This part of the work evaluates the recovery and reusability of H_3PO_4 in PSAC generation. Upon activation, the H_3PO_4 was reclaimed and reused for subsequent activation under identical process conditions. The effectiveness of the reclaimed reagent was assessed for three cycles covering an activation temperature between 325 to 525 °C.

1.3 Thesis plan and publications

A review of the literature was carried out in Chapter 2 to assess available AC development methods particularly using palm shell as precursor. This review, together with the result in PSAC development (Chapter 4) has been published as *Activation of palm shells by phosphoric acid impregnation for high yielding activated carbon, W.C. Lim, C. Srinivasakannan, N. Balasubramanian, Journal of Analytical and Applied Pyrolysis 88 (2010) 181-186 (attached in appendix)*. This paper highlights the non-conventional H_3PO_4 activation method yielding carbon with well developed textural characteristics from less complex processes. These findings were also presented at the *Annual World Conference on Carbon 2010* at Clemson University, U.S.A. The outcome of methylene blue adsorption investigation as discussed in Chapter 5, has also been published in Journal of Separation Science and Technology [*Preparation of high surface area mesoporous activated carbon: Kinetics and equilibrium isotherm, W. C. Lim, C. Srinivasakannan, V. Doshi, 2012, Separation Science and Technology, 47: 886-895, as attached in appendix*]. The findings of reagent recovery and reusability as discussed in chapter 6, has been presented in the *Annual*

World Conference on Carbon 2011, Shanghai, China. The manuscript is in final process of submission to Chemical Engineering and Processing: Process Intensification [*Significance of activation temperature on recovery and reusability of phosphoric acid in preparation of activated carbon from palm shells, Wah Ching Lim, C. Srinivasakannan, Veena Doshi, 2011*]. Finally the conclusions derived from the current research were discussed in Chapter 7 along with the suggestions for further works in the same chapter.

CHAPTER II

LITERATURE REVIEW

2.1. Introduction

This chapter provides a review of AC activation and the precursors especially palm shell, its methods of generation as well as the recovery and reusability of reagents. In addition, it describes the textural characteristics of AC in terms of surface area, pore characteristics and surface chemistry. The last section of this chapter discusses about the adsorption characteristics of AC specifically towards macromolecules pollutant such as methylene blue and dairy COD.

2.2 Activated carbon

AC is generally recognised as carbonaceous solid substance with large surface area and well developed interconnected network of porous structure [1-4]. Its high degree of porosity and extended inter-particulate surface area allows AC to exhibit superior and indiscriminative adsorption capacity. AC is widely considered as the most versatile adsorption technology for effluent treatment, potable water treatment, solvent recovery, air treatment, decolorizing, metal ore processing and many general domestic applications [5,6,7,8,9,10,11,12,13,14]. Besides, AC are also used as capacitor [15], sieve separator [16] and electrode [17].

The world demand for AC is expected to expand 5.2% per year through 2012 to 1.2 million tons [18]. The adsorption capability of AC is usually substantiated with reasonable mechanical strength (to minimise structural collapse that leads to lost function), unique pore structure and high degree of surface reactivity [19]. Carbon is the major chemical composition found in AC, with approximately 50% of mass weight, while the residue comprises of H, N, S, O and a trace amount of inorganics. Structurally, AC could be considered as disorganised amorphous material with a network of hexagonal carbon layer which are cross-linked by aliphatic bridging. AC is also associated with a low degree of graphitization [20]. The characteristic of heteroatom bound to the carbon surfaces provide the unique functional groups characteristics to AC. These imbalance charges influence the surface chemistry of AC, and thus the adsorption properties of carbon [19].

2.2.1 Structure of carbonaceous materials

AC and other carbonaceous materials mainly contain carbon with the atomic structure of ls^2, $2s^2$, $2p^2$. Different orientations of carbon structure and the C-C bonding interaction gives rise to 3 major forms of carbons [20]:

i) sp^3 based (or rigid and isotropic structure): Each C atom is bonded with 4 neighbouring C atoms, as demonstrated in diamond.

ii) sp^2 based (or graphite layered structure): Each C atom is bonded with 3 neighbouring C atoms into single hexagonal carbon (graphite) layer.

iii) 3-dimensional carbon (or fullerenes structure): A configuration likely due to the re-hybridisation resulting from intermediate between sp^2 and sp^3. Such carbon complex is usually found in carbon nanotubes [20].

Fig. 2.1 shows the major forms of carbon and its derivative. Most of the carbonaceous materials available exhibit graphite orientations (sp^2 based) whilst the planar layers tend to exhibit parallel alignment and the configuration. These carbon layers are maintained by its dispersive and Van der Waals forces [20]. These graphite materials could be further classified by its crystallographic order, into graphitic carbons and non-graphitic carbons. Most AC (powdered or granular) exhibits two-dimensional order but not three-dimensional graphitic ordering, as illustrated in Fig. 2.2 [21]. This is due to the intense pyrolytic decomposition and reorganisation experienced during carbonization and activation which results in a random orientation crystallographic framework on the material. As such, AC is considered as non-graphitic with highly disordered microstructure.

2.2.2 Classification of activated carbon

AC could be generally classified into granular activated carbon, powdered activated carbon and its derivatives such as shaped or impregnated activated carbon [22].

2.2.2.1 Granular activated carbon (GAC)

GAC is a category of AC with average particle size between 1 and 5 mm. It is the most widely used AC particularly as column filler for gas or liquid treatments. Its larger particle size (as compares to PAC) enables lower pressure drop in it application, a key criterion of low energy and economical adsorption. GAC could also be regenerated, which is an important economic benefits for large scale applications [23].

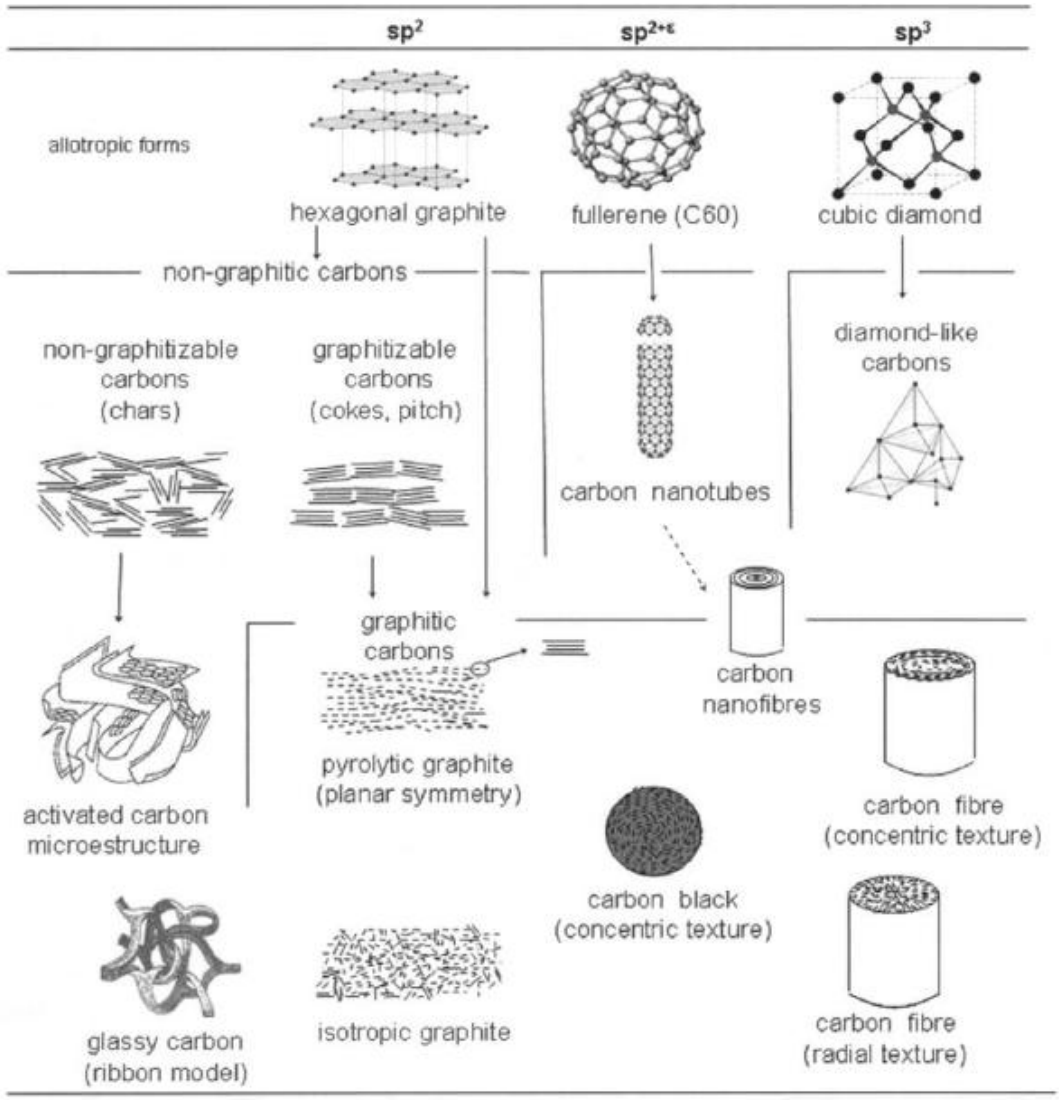

Fig. 2.1. Major allotropic forms of carbon and a schematic representation of some of the carbon structures derived from these forms. *Extracted from J.A. Menendez-Diaz, I. Martin-Gullon, Types of carbon adsorbents and their production, Interface Science and Technology Volume 7 (2006) 1-47*

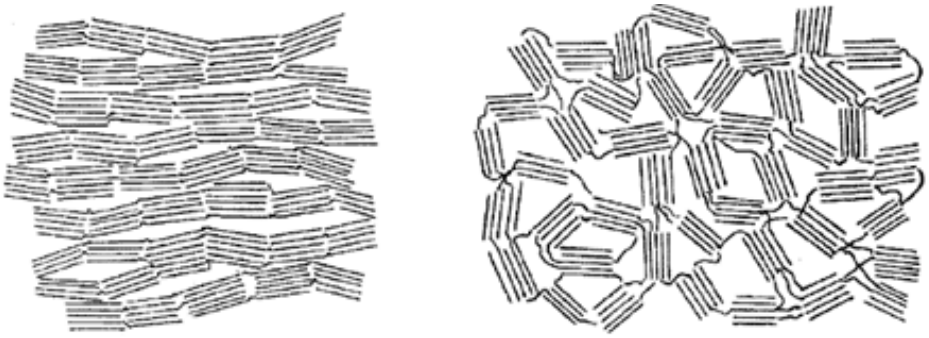

Fig. 2.2. Graphitizable and non-graphitizable carbons. *Extracted from Carbon Adsorption, R.C. Bansal, M. Goyal, CRC Press 2005, ISBN: 978-0-8247-5344-3*

2.2.2.2 Powdered activated carbon (PAC)

Powdered activated carbon (PAC) is considered as AC with the average particle size between 15 and 25 um [20]. High diffusivity of the adsorbate is the key factor to effective adsorption by PAC. With lower density than GAC, this adsorbent demonstrates better suspension and is distributed more evenly amongst the adsorbate molecules, creating a vast adsorption area and reducing the diffusion distance for adsorbate transportation to the pores [24]. As such, the time required for adsorption equilibrium in PAC application is shorter. In practice, PAC is usually utilized in blending or fluidised mode while GAC which is regularly found in fixed adsorber beds. Unlike GAC, PAC is normally disposed of upon treatment [25]. Although PAC adsorption is very effective due to its even suspension, the time for reaching its settling tends to be more challenging [24]. PAC requires longer residence time and could affect its application in large scale.

Studies have established numerous advantages of adding PAC in activated sludge systems. The presence of PAC in conventional systems improves sludge settling, increases organics removal, reduces the impact of organic shock loadings, increases organic carbon loading, suppresses aerator foaming and reduces sludge bulking [25,26]. A search in literature found limited works in PAC particularly with those with high mesopores content. It is a known fact that a key application of PAC are in large adsorbates (such as dye, protein and pharmaceuticals) removal. This gap of knowledge would be the fundamental of this research; i.e. development of mesoporous PAC for macromolecules adsorption.

2.2.2.3 Shaped activated carbon

Shaped activated carbon is a carbon derivative usually associated with special application. Using mainly PAC, shaped AC is produced by mechanically entrust or palletised into specific

shape such as cylinder, monolith or even paper [20], usually with the assistance of a binding agent. These shaped carbons have a higher internal porosity, density and hardness but a lower abrasion index than broken GAC, making it favourable for certain application.

2.2.2.4 Impregnated activated carbon

Some AC is impregnated with inorganics such as Ag, S, Cu and Hg for specific adsorption application. AC loaded with Ag is used as an adsorbent for purifications of domestic water, whilst AC impregnated with S [22] have been found to enhance the elemental mercury sorption very well [27,28]. On the other hand, impregnated AC is found to enhance removal of tail gas, arsenic and cation in water [29,30,31]. Cu-impregnated coconut husk AC can be used as an adsorbent for the effective removal of As(III) from aqueous solutions [32].

2.3 Precursors for activated carbon

It is a challenge to prepare AC with desired textural characteristics and at the same time commercially attractive; i.e. using low-cost raw materials and low energy processes (or low process temperature) [24,33]. Utilization of such materials for the production of AC has been adequately reviewed [24,32,34,35]. Generally, any carbonaceous solids could to be converted into AC as evident in the vast works reported on AC using a wide range of materials and activation methods [5,13,14,36,37,38]. In practice, some associated conditions such as molten formation during thermal treatment. Materials with tendency to turn into a fluid or pseudo-fluid state, such as thermoplastics or coking coal, which is often observed as a form of molten during heat treatment, would not be a suitable precursor for AC [20]. As such, a large number of studies focus on the use of waste materials of considerable rigidity (often measured as hardness), such as the shells or stones of fruit nuts [24].

In recent years, these carbonaceous materials have lost its traditional role as a major source of energy due to environment concerns on carbon footprint. These materials however hold the potentials as renewable sources for AC (traditionally using coal). Precursors from fresh biomass origin offer the most economical option as they is copious renewable supplies, with low mineral and sulphur content than coal based materials with appreciable hardness [6,39]. In the last few decades, many AC investigations were made concerning the recycling of these agricultural wastes. Some works suggest they are compatible, if not better, than the commercial AC as demonstrated in removal toward specific adsorbates [40,41].

Generally, a precursor is expected to meet the following technical and economical criteria:

- Available at low cost: Literature survey indicates that there have been many attempts to obtain low-cost AC or adsorbent from lignocellulosic materials such as *Arundo donax* cane [42], bamboo [43], cotton stalks [38], coconut shell [44], corn cob [45,46,47], coffee bean endocarp [48], date pits [6], durian shell [49], evergreen oak [50], *Eucalyptus camaldulensis Dehn* bark [51], jackfruit peel [14], olive-waste cakes [52], oil palm fibre [53], oil palm empty fruit bunch [54], olive husk [41], olive kernel [55], peach stones [56], palm shell [57,58,59], peanut hull [39], rattan sawdust [60], pistachio-nut shell [61,62], rubber wood [63], rosewood [12] and vetivers root [64]. Readily available feedstock is the key to precursor selection. While almost all of the raw materials for AC production are dependent on geographical condition and production cycle (harvest season) [7,12,37,38], local availability would be a huge advantage and viewed as an important assurance towards long terms supply. Palm shell for instance, are vastly available in production country and available throughout the year while seasonal based agricultural waste such as apricot [65], cherry stone [66], plum stone [67] and rice hull [36] may not meet the objective of constant supply.

- High carbon content: The produced AC consists between 75 and 90% carbon [64] and all carbons originate from its precursor. A typical chemical composition of lignocellulosic materials make up of 48% C, 6% H and 45% O and trace of inorganics, corresponding atomic ratios are: O/C = 0.73, H/C = 1.5 and H/O = 2.07 [68]. Most of the reported element analysis on shells and stones based wastes such as coconut [69], almond [70], apricot [70], hazelnut [70], palm shell [71], walnut [70] are in agreement with the mentioned report with approximately 50% of C contents. Marsh & Rodriguez-Reinoso reported that these materials composed of cellulose (42-50%), hemicelluloses (19-25%) and lignin (16-25%) [68], However, Daud & Ali [69] reported different observation with lignin content above 30% and 50% in coconut and palm shell respectively.

- Low inorganic content: The presence of inorganics tend to reduce the adsorption capacity in resulted carbon. AC from almond shell, nut shell, apricot and cherry stones are with low ash content in contrast with those from grape seed and rice hull [32,72,73]. For instance, rice husk with high ash content (cellulose: 32.24%; hemicellulose: 21.34%; lignin: 21.44% and ash: 15.05%) [74] has been associated with adverse activation conditions such as high activation temperature and pore widening [72].

- Sufficient volatility: Volatilisation during heat treatment is the main mechanism to release non-carbon substances, a prerequisite to effective pore development [8]. Raw materials with poor volatility may require a relatively higher activation temperature for effective textural development. On the other hand, material with high volatility would result a low carbon yield. For instance, pyrolysis of wheat, straw, olive husks,

grape residue, rice husks, etc, produce char twice the yield of char issued from wood [32]. Hence, only raw materials with the right volatility character could provide well developed AC as well as meeting the economy criteria.

- Ability to yield the required textural characteristics: Good adsorption capacity, sufficient hardness and potential for effective regeneration are some desired textural characteristics [75]. Coconut shell, for instance, are high in density, an advantageous evident in the resulted AC which is high in density and purity [44]. Similar characteristics is also seen in palm shell.

2.3.1 Palm shell

Oil palm plantation is one of the successful stories of Malaysian agricultural development. In line with the rapid growth of palm oil to become world's largest source of edible oil [38.5 million tonnes or 25% of the world total edible oil and fat production], Malaysia is now the second largest producer of palm oil with 15.88 million tonnes or 43% of the total world supply [76]. However, this industry generates a large amount of biowaste in form of shell, kernel and fibre. At present, there is little utilization reported to this waste materials. Palm shell generated by the palm oil mills are traditionally used as solid fuel for steam boilers for electricity production. The problems associated with the burning of these solid fuels are the emissions of dark smoke and the carryover of partially carbonized fibrous particulates due to incomplete combustion of the fuels [77].

The composition of a raw material dominates their reactivity in the pyrolysis and activation reactions [32]. Palm shell is reported to have the characteristic of a good precursor: high in density but low in ash [71,75]. The proximate and ultimate analyses show that palm shells

typically consist of 50% carbon element with 17-21% of fixed carbon and 76-80% of volatile matters, 3.3% ash and elemental analysis shows 50-54% C, 6-7% H, 0.2-2% N and 41-44% O [69,78]. Besides, principal components of oil-palm shell are lignin (over 50%) [79], an element which in comparison with cellulose and hemicellulose is more readily to be depolymerised during activation, a condition for quality AC [79,80].

Daud & Ali compared the influence of shell materials as precursor and found that the rate for micropores and mesopores creation at any burn-off in palm shell is higher than that in the coconut shell [69]. All these have positive criteria has made palm shell a potential precursor for large scale commercial AC production [75].

2.4 Physical activation

Physical activation utilizes oxidating agents such as air, steam or CO_2 (or the mixture) to partially oxidise the precursor (carbonization) and followed by gasification on the char (activation) at an elevated temperature [32,61,81].

2.4.1 Carbonization

Carbonization is a volatilization process of which non-carbon elements such as O, H, N and S are eliminated and released as volatile matters (H_2O, hydrogen, light hydrocarbons and tar) [82]. This thermal treatment process initiates structural alteration as residual C atoms tend to group themselves into stack of aromatic sheets via cross-linking reactions, creating a non-graphitizing carbon structure [83].

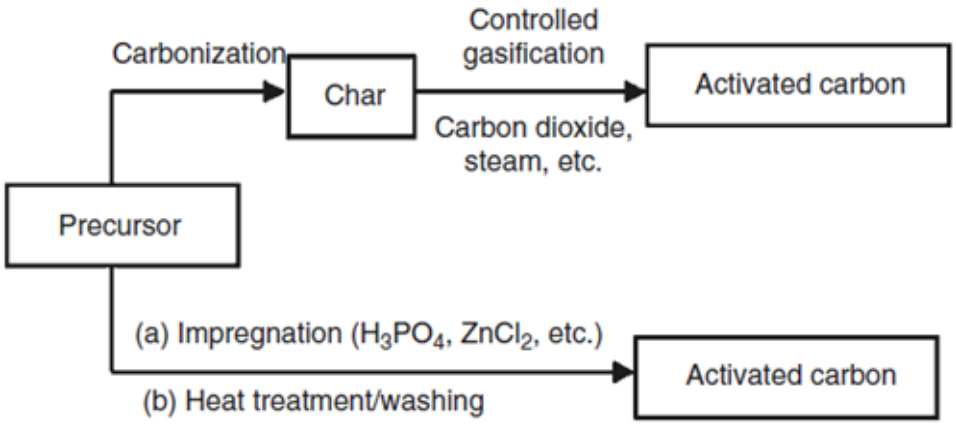

Fig. 2.3. General flow sheet for manufacture of activated carbon. *Extracted from Activated Carbon, H. Marsh, F. Rodriguez-Reinoso, First ed., Elsevier Ltd., Oxford, 2006*

2.4.2 Activation

Carbonization solely is not sufficient to develop desired porosity. The char requires further thermal treatment, known as activation and at much higher temperature, to make incipient pores accessible [82] and at the same time create the new ones. Coupled with intensive structural re-organisation, activation could give rise to extremely high surface area and unique pore characteristics in the produced AC.

While most of the physical activations are conducted in conventional 2-stage, a number of researchers investigated a single-stage activation where carbonization and activation take place simultaneously. The one-step activation process is desirable due to lower energy consumption, capital expenditure and shorter, processing time that can significantly improve the process economics [81,84]. Experimental results testify that high surface area AC can be prepared using one-step CO_2 activation. Yang et al. reported a better textural characteristics in coconut AC (BET surface area: 1667 m^2/g) than conventional two-step method [81]. High BET surface area was also reported for apricot stone (1190 m^2/g) while moderate values for

almond shell and cherry stone (998 m^2/g and 875 m^2/g) but low on grape seed at 497 m^2/g [85].

2.4.3 Physical activation with O_2

Activation with O_2 yields CO and CO_2 simultaneously as the primary product Eq. (2.1) & (2.2) with the ratio of CO to CO_2 increases with temperature [20]:

$$C + O_2 \rightarrow CO_2 \qquad \Delta H = -387 \text{ kJ mol}^{-1} \qquad (2.1)$$

$$2C + O_2 \rightarrow 2CO \qquad \Delta H = -226 \text{ kJ mol}^{-1} \qquad (2.2)$$

As indicated in the enthalpies, both reactions are highly exothermic and often result in runaway reactions that lead to undesired pore widening [86]. As such O_2 activation is rarely applied as a sole activation agent in physical activation [87], correspond to almost no works in open literature on O_2-activated AC.

2.4.4 Physical activation with steam (H_2O)

The gasification reaction in steam activation on carbon materials is as shown below.

$$C + H_2O \rightarrow H_2 + CO \qquad \Delta H = 132 \text{ kJ mol}^{-1} \qquad (2.3)$$

CO, by products from reaction (2.3) may further react among themselves, yielding H_2, CO_2 and CH_4 as shown in Eq. (2.4) and (2.5).

$$CO + H_2O \rightarrow H_2 + CO_2 \qquad \Delta H = -41.5 \text{ kJ mol}^{-1} \qquad (2.4)$$

$$C + 2H_2 \rightarrow CH_4 \qquad \Delta H = -87.5 \text{ kJ mol}^{-1} \qquad (2.5)$$

Steam activation is an endothermic process and does not result in any runaway reactions. It is easy to control even at high temperature. Under atmospheric condition, steam activation

works only on the particle surface while leaving internal structure are unaltered. As such, it is usually conducted at high temperature (up to 1000 °C) to extend the chemical reactions inside to the char particles to achieve full porosity potential.

Steam activation is by far the most widely used for commercial AC. It is usually conducted in kiln and often associated with injection of a certain amount of air. The exothermic reaction between O_2 in the air with carbon material provides the heat required in maintaining the temperature for the steam-precursor reaction [20]. Generally steam activated AC are predominantly microporous [88]. Azargohar & Dalai [89] and Arriagada et al. [90]observed AC produced from steam spruce whitewood and activated peach stone are predominantly microporous.

2.4.5 Physical activation with CO_2

The reaction between carbon and CO_2 yields CO as by-product as shown in Eq. (2.6) & (2.7) [48]. Several studies have associated CO_2 activation with development of narrow micropore, a unique pore size for gas adsorption.

$$C + CO_2 \rightarrow 2CO \qquad \Delta H = +159\ kJmol^{-1} \qquad (2.6)$$

$$C + H_2O \rightarrow 2CO + H_2 \qquad \Delta H = +117\ kJmol^{-1} \qquad (2.7)$$

CO_2 activation is regularly associated with diffusion issues. Ahmedna et al. [91] observed of a lower reaction rate as compared to steam in pecan shell AC studies. This is further supported by Gergova et al. [92] who did similar investigation and it was found the reaction rate of CO_2 at 800 °C is 3 times lower than steam. The larger molecular size (compares to H_2O) has resulted in slower diffusion of CO_2 into the porous structure of the char correspondent to low activation rate [91].

Higher production cost (than steam) holds another obstacle for CO_2 to be actively applied for commercial AC. Although these mentioned disadvantages exist, a majority of physical activation mechanism use CO_2 as the activating agent. CO_2 activation is clean, easy to produce and control than steam in laboratory. Furthermore, the flowrate of CO_2 is reported to have little effect of the textural characteristics [54].

2.5 Chemical activation

Chemical activation is regularly applied on lignin-based precursors such as wood sawdust, fruit shells and stones [14]. This method utilizes inorganic additives to dehydrate the lignocellulosic materials and simultaneously prevent shrinkage during carbonization [58,19]. H_3PO_4, $ZnCl_2$ and KOH are amongst the most popular activating agents in comparison to H_2SO_4, K_2CO_3 and $FeCl_2$. The produced AC is usually in powder form or soft solid that can be easily milled into powder.

Chemical activation starts with impregnation; i.e. aqueous reagent is blended with the precursor particles, usually at a fixed ratio. Sufficient soaking time is required to initiate chemical changes. During activation, these reagents catalyse the reactions that lead to tunneling, channeling and pitting and result in generation of fine pores on char surface. Simultaneously, non-carbon content in the structure is being released in form of volatile matters (water, furan derivatives and levoglucosan) [19]. Hence, chemical activation is a less thermal dependent carbon enrichment process (compared to physical activation) with the entire development completed in single step.

2.5.1 H_3PO_4 activation

H_3PO_4 is the most preferred chemical reagent as evident in works over a wide range of botanical materials namely palm shell [19,57], bamboo [8], cotton stalks [5], coconut shell [44], *Arundo donax* cane [42] rubber wood [63], peach stones [93], woods [94], *Eucalyptus camaldulensis Dehn* bark [51], vetivers root [64], olive seed [95], date pits [6], evergreen oak [50], peanut hull [39] and jackfruit peel [14].

The interaction between H_3PO_4 and precursor begins as early as upon mixing [96]. Under heat treatment, H_3PO_4 catalyse reactions that lead to bond cleavages and hydrolysis of lignocellulosic materials, resulting in release of volatile matters. Such early reactivity brings the advantage of a lower activation temperature for H_3PO_4 [97]. The cross-linking reactions among the cellulose fibres would also lead to dilation of the structure and formation of a larger rigid cross-linked solid [6,98]. Observations such as swelling or elastic paste composition have been regularly reported. Jagtoyen et al. hypothesised the swelling is due to insertion of H_3PO_4 between the cellulose chains that disrupts the existing hydrogen bonds, and simultaneously separates the chains and dilate the structure [96].

H_3PO_4 is known to attack lignin (and hemicellulose) at low temperature, hydrolysing the glycosidic linkage and cleaving the aril ether bonds [99]. Menendez-Diaz & Gullon [20] reported that microporosity development begins at temperature as low as 200 °C and attaining a maximum at 300 °C. Jagtoyen et al. observed the formation of ester linkages with -OH groups by phosphorus compound at below 200 °C [96]. Compared to $ZnCl_2$, H_3PO_4 is a Bronsted acid; i.e. a stronger impregnant as well as dehydrating agent and thus more effective to induce bond cleavage. Furthermore, it forms phosphate esters or polyphosphates with the chains of degraded biopolymers [100]. The potential of H_3PO_4 in developing high surface area AC without excessive heating has been observed in a large number of works (Precursor/

activation temperature/ BET surface area): coffee bean husk/ 450 °C/1402 m^2/g [101]; wood/ 500 °C/ 1730 m^2/g [94]; bamboo/ 600 °C/ 1869 m^2/g [102]; vine shoot/ 400 °C/ 1666 m^2/g [103] and evergreen oak/ 450 °C/ 1723 m^2/g [50].

Activation at higher temperature sees the increase in mesoporous fraction in H_3PO_4-ACs as the wall of micropores begins to collapse, turning some into mesopores [7]. As activation temperature further increases (>500 °C), excessive heat breaks the phosphate cross-linkages between the cellulose fibres and result in carbon structural contractual, regularly seen in decrease of micro- and mesopores surface area and reduction of pore volume. Corcho-Corral et al. [103] and Gomez-Tamayo et al. [50] reported a 30% decrease in BET surface area for vine shoot and evergreen oak AC respectively when activation temperature increase from 450 °C to 550 °C. This is in agreement with Diao et al. who reported 500 °C [104] as optimum temperature for grain sorghum AC while Jagtoyen & Derbyshire [96] observed maximum mesoporous in yellow poplar and while oak AC at 500-550 °C. On the other hand, Marsh & Rodriguez-Reinoso [68] reported that the amount of phosphorus introduced into the precursor is the main factor in porosity development and that the degree of mesoporosity achieved is large only when the concentration of H_3PO_4 is high. In the works on coffee bean husk, Baquero et al. [101] reported no mesopores in H_3PO_4 activated AC when impregnation ratio (IR) is low but the mesopores start to develop and become essential when IR increase from intermediate to high. This is further evident in works by Munoz-Gonzalez et al. [56] and Yavuz et al. [105] on AC for pine sawdust and olive stone respectively.

The H_3PO_4 solution also comprises of a variety of polyphosphoric acids (general formula of $H_{n+2}P_nO_{3n+1}$) and as a result, the textural outcome of H_3PO_4 activation is complex and less predictable. At equilibrium the exact constituent composition of the polyphosphoric acids

depends on the content of P_2O_5 in the solution [68]. These acidic reagents are able to interact with oxygen functional groups and thus catalyse the dehydration and dehydrogenation reactions, resulting in charring and aromatization of the carbon skeleton and creation of the pore structure [98].

2.5.2 $ZnCl_2$ activation

$ZnCl_2$ is known to be a dehydrator which subtracts H and O from raw material to develop carbonaceous microporous structure [106]. It is amongst the most popular activating agents and investigations on $ZnCl_2$ activation has been reported on hazel nut [13], rice husk [36], sugarcane bagasse [36,107,108], palm shell [109,110], peanut hull [39], Tamarind wood [111], coffee residue [112,113], walnut shells [106,114] and pistachio-nut shell [115].

$ZnCl_2$-AC are dominantly microporous as evident in type I N_2 adsorption isotherm [39,112,116]. Exceptional observation was reported by Khalili et al. [117] on paper mill sludge AC as samples with highly mesopores were observed, probably due to high IR. Well developed $ZnCl_2$-activated ACs were reported on peach stones [118] and sugar beet bagasse (BET surface area of 3000 and 1826 m^2/g respectively) [107] while fair result in tamarind wood (1322 m^2/g) [111], dates stone (1270 m^2/g) [119], hazelnut husk (1092 m^2/g) [13]. $ZnCl_2$-AC from rice husk and sugarcane bagasse were reported of low surface area (811 and 864 m^2/g) [36]. Lua and Yang [115] reported of well developed pistachio nut AC for $ZnCl_2$ activation under N_2 atmosphere and vacuum conditions (BET surface area of 1635 and 1647 m^2/g respectively). There is however a drop in interest using $ZnCl_2$ as reagent in recent years due to issue such as pollution, corrosion and non-compliance to pharmaceutical and food requirements [14,63].

2.5.3 KOH activation

Activation with KOH were used for AC from corn cob [45,46,120], durian shell [49], peanut hull [39], Oil palm fibre [53], oil palm empty fruit bunch [121], palm shell [122], Olive husk [41] and coffee bean endocarp [48].

El-Hendawy hypothesised KOH activation as a series of chemical reactions [120]:

$$\text{Ligno.} + KOH \rightarrow \text{Ligno.}K_2O + H_2O \quad (2.8)$$

$$\text{Ligno.} + H_2O \rightarrow \text{Char,C} + H_2O + \text{Tar} \quad (2.9)$$

$$C + H_2O \rightarrow H_2 + CO_2 \quad (2.10)$$

$$K_2O + H_2 + CO_2 + \text{Char, C} \rightarrow \text{Char} + K_2CO_3 + K \quad (2.11)$$

The primary reaction in KOH activation is indicated in Eq. (2.8), involving dehydration, cracking, partial polymerisation and distortion to the lignocellulosic material. Subsequent transformation of the lignocellulosic material to char is as seen in Eq. (2.9). The process release tars and metallic potassium which may react with the produced char yielding an abundant fine pores under the high diffusion and pyrolysis action. KOH-AC are reported predominantly with micropores with narrow pore sizes [46,61]. Lua et al. [61] observed AC from pistachio nut are dominated by micropores and development of larger pore (meso- and macropores) occurred only after 800 °C. CO_2, by-product in KOH activation may further react with K to produce K_2CO_3 before it decomposes to K_2O and CO_2, at high temperature [as shown in Eq. (2.10) & (2.11)]. As observed by Hsu et al., the potassium compounds (K_2O and K_2CO_3) become significant at above 700 °C [98]. It was also observed that the atomic K enhances pore formation upon intercalating and expanding the interlayers of adjacent network carbon planes and result in AC with very high SBET surface area [123]. As such, well developed KOH ACs are associated with extreme process conditions. Cao et al. [46]

reported of extremely high surface area in corn cob AC (BET value of 2700 m^2/g) but at a temperature comparable to physical activation of 850 °C. Similarly, Michailof et al. [41] reported high surface area (1800 m^2/g) KOH based olive husk AC occurred upon excessive treatment: heating at 900 °C for 3 hr under excessively high IR of 4. High activation temperature for quality AC has also been recorded for maize stalks (1811 m^2/g at 700 °C) [120] and pistachio nuts (1926 m^2/g at 800 °C) [124].

2.6 Palm shell activated carbon

The first recorded published work on PSAC is by Hussein et al. in the year 1996 using $ZnCl_2$ as reagent [109]. Well developed PSAC was reported (BET about 1500 m^2/g) with the textural character transformed from essentially microporous at low IR (15%) to a fair fraction of mesopores at 25% IR. Since then, there has been a considerable amount of studies on PSAC and the use in removal various adsorbates.

Physical activation investigations on PSAC were generally using CO_2 as reagent even though this is contradictory to industrial practice (use steam). CO_2 is clean, easy to handle and it facilitates control of the activation process due to the slow reaction rate at temperatures around 800 °C [32]. On the other hand, chemical activation on PSAC has also been frequently investigated due to the advantages of the carbonization-activation process that could be carried out simultaneously. H_3PO_4 [57], K_2CO_3 [125], NaOH [126], KOH [127] has been utilized as the activation reagents.

Among the basic reagents, KOH and NaOH have been applied in PSAC development [116,122,126,127] with the BET value of 2247 m^2/g being reported for NaOH activation. The

process is however, highly complex and requires CO_2 as part of physiochemical treatment. Strong dependencies of IR in KOH activation have been reported by Guo & Lua. The BET surface area was found to increase with IR to maximum of 1214 m^2/g at 30% impregnation before a sharp reduction to 870 m^2/g at 40% impregnation [19]. H_2SO_4 and K_2CO_3 are the other types of reagents activated palm shell by Guo & Lua [128] and Adinata et al. [59] The PSAC with respective BET surface areas of 1250 and 1170 m^2/g, however, were not high quality as PSAC with physio-chemical activation.

The potential of combined physical-chemical activation on PSAC has been widely explored. Generally, the produced char from chemical activation using reagents H_3PO_4, $ZnCl_2$ KOH and H_2SO_4 are further treated again using CO_2. PSAC are found to be better in quality with BET surface area between 1200 and 2247 m^2/g. However, the mechanisms are complex (3 stage activation and longer treatment duration), required high energy input and as such, more challenging for up-scale. Research on PSAC using non-conventional activation methods have been reported. Lua & Jia pyrolysed palm shell under vacuum before steam activation. They hypothesised the quick removal of volatile matters under vacuum condition which minimised pore blockage. PSAC with reasonable developed surface area (1183m^2/g) and high in mesopores (45%) were reported [129]. On the other hand, the feasibility of using microwave-induced CO_2 reaction to prepare PSAC was explored [130]. The produced PSAC were found to be high in density and predominantly micropores but the surface was not well developed (BET surface area < 500 m^2/g). Well developed PSAC (BET surface area >1400 m^2/g) were successfully prepared using one-step CO_2 activation in a single heating from room to activation temperature of 850 °C. The carbon yield was however low at only 15% [131].

Thus far, only Guo & Lua [19,58,132] and Lim et al. [57] investigated the prospect of H_3PO_4 as reagent for PSAC. The earlier author reported achievement of high surface area (BET: 1563 m^2/g) with well-developed microporosity [132]. Their work highlighted the characteristic of H_3PO_4 as a quality reagent: effective in promoting necessary chemical changes (for surface area development), the ability to form internal linkage and as a great inhibitor to excessive burn-off (for high AC yield). On the other hand, Lim et al. have successfully developed PSAC using a non-conventional and yet simple activation method: low temperature and short duration at 425 °C at 30 min, under self-generate atmosphere. PSAC with reasonable well developed surface area (1109 m^2/g) and high carbon yield (> 50%) was obtained. The potential of this work can be seen in a few aspects: inert gas flow during activation is no longer a requirement (cost saving and simplify process control); low activation temperature (energy saving, low heat stress on design and equipments), high yield (in-line with economical criteria) and highly mesoporous (ability to uptake macromolecule adsorbates). While conventional AC development sees the inverse relationship between textural characteristic (such as surface area) and carbon yield, this work paves the way for process optimization based on desired process criteria: high surface area and high carbon yield.

Activation temperature has been reported to have the most significant effect on PSAC textural characteristics, followed by reagent type and activation time. Generally, increase temperature (up to an optimum value) leads to a better developed PSAC as seen in higher BET surface area and pore volume [75,133,134]. Daud et al. investigated the influence of carbonization temperature on pore development in PSAC and concluded there is no clear pattern of the effects of carbonization temperature on development of meso- and macropores [82]. The same author has also investigated the influence of activation time on PSAC

development to be between 30 to 120 min using steam and concluded that prolonging the activation time resulted in widening of micropores as it destroys the walls between adjacent pores. Contradicting observations were reported on the effect of CO_2 flowrate. Sumathi et al. observed that the flow of CO_2 (between 100 and 500 cm^3/min) has minor effect on surface area development on PSAC, especially when low activation temperature was utilized [78]. This is different from the observation by Lua et al. [131], who found the BET surface area of PSAC to increase almost 200% to 1440 m^2/g for CO_2 flow from 25 to 100 cm^3/min, before reduced drastically to 750 m^2/g at excessive flow rate. The author highlighted the need of a minimum CO_2 flow to effectively carry out its duties for pore generation and volatile matter removal. The adverse effect of excessive CO_2 flow which results in severe burn off was also mentioned.

Almost all works done on PSAC utilized N_2 gas flow to create an inert atmosphere during the charring process, with few exceptions using vacuum or vacuum & steam [135,136]. Guo & Lua [130] and Sumathi et al. [78] investigated the influence of N_2 flow on PSAC development of flow rate between 5 and 500 cm^3/min and 100 and 500 cm^3/min respectively. However, both studies reported BET surface area of less than 400 m^2/g due to unfavourable process conditions. Hence, no solid conclusion on the influence of this inert gas was made. On the other hand, Jia et al. [135] reported activation under vacuum environment in PSAC generation could speed up volatile matters removal from pore to reduce pore blockage for steam during the subsequent activation process. The highest BET surface area in CO_2 activation was reported by Lua & Guo at 1410 m^2/g [131]. Daud et al. [137] produced PSAC with steam with the highest BET value of 1319 m^2/g.

Response surface methodology (RSM), a statistical optimization tool, has been widely used to investigate the effect of process variables on AC development from raw materials namely bamboo waste [138], mangosteen peel [139], rambutan peel [140], rattan sawdust [141], olive-waste cakes [142], coconut shell [44], oil palm fiber [53], coffee bean endocarp [48], coconut husk [143,144], oil palm empty fruit bunch [54,121], oil palm frond [145], palm shell [78]. All the works found the correlations developed were able to predict the values of the responses quite well as evidenced by the generally acceptable values of the percentage errors. The only available RSM work on PSAC was based on physical activation [78]. It was found the statistical analysis is reliable to optimize the production of PSAC with activation temperature found to have the largest effect while interaction between the activation temperature and activation time has considerable effect on producing PSAC. The PSAC developed was however with average BET surface area of 1053 m^2/g.

Majority of the PSAC investigations reported of AC predominantly with micropores [78,128,132,133,146] disregard the process condition (unless excessively treated). Guo and Lua compared influence of different reagents under inert atmosphere. It was observed that PSAC from $ZnCl_2$, KOH and H_3PO_4 are rich in micropores [132]. The authors also reported similar observation on PSAC prepared using physiochemical activation (KOH & CO_2) [146] as well as microwave induced CO_2 activation [130]. This is further established for work done on PSAC using CO_2 [133,134], H_2SO_4 [128] and $ZnCl_2$ [109]. First attempt to develop PSAC with improved mesoporosity was reported by Hu & Srinivasan [110]. They hypothesised that the surface area and mesopore content in PSAC could be tuned by controlling the experiment parameters such as IR ($ZnCl_2$ is the reagent), duration of exposure to CO_2 atmosphere and activation temperature. The process developed is complex involving both physical and chemical activation at high activation temperature of 800 °C. PSAC developed are 94%

mesopores (based on pore volume) but BET surface area is less than 1300 m^2/g. Such high fraction of mesopores are likely due to the wall of pores collapse caused by high activation temperature and long treatment time (more than 3 hours). This is further evident in the low carbon yield of 26%. However, there is no direct evident of how the mesopore development relates to a process conditions such as influence of reagent used, activation atmosphere or pretreatment process.

A summary of relevant data on PSAC process condition is shown in Table 2.1(a) to (c). It was observed that a majority of the PSAC study reports only the pore structure and pore characteristics of the AC, without the due mention to the carbon yield. The characteristics namely surface area and carbon yield strongly depend on both the precursor and the activation procedure. Generally, AC with high BET surface area is the result of activation at high temperature, which in turn, results in low carbon yield. Consequently, it is not possible to preview which is the activation procedure that develop a PSAC with the highest surface area as well as carbon yield. As such, no conclusion could be drawn from available works in the prospect for higher porosity-high yield PSAC. Among the reported literature the yield of AC using physical activation methods is found to be less than 17%, with the activation temperatures around 900 °C. While the physiochemical activation methods reported yield less than 30% with the activation temperatures of around 800 °C (with an exception of $ZnCl_2/CO_2$ activation resulting in a yield of 37%). Among the chemical activation methods the K_2CO_3 activation produced a very low yield of 19%, while the H_3PO_4 activation at 500 °C resulted in a yield of 40%, which is significantly higher than the other activation methods and activating agents. It can be observed that the yield of AC varied widely depending upon the processing methods

Table 2.1 (a) Process condition of PSAC: Physical activation

Activating agent	Carbonization (°C/h)	activation (°C/h)	Inert/ activating gas	BET surface area (m^2/g)	Total pore volume (cm^3/g)	Yields (% wt/wt)	Additional information	Reference
CO_2		850/2	N_2 &CO_2	1410	0.71		One stage activation	[130]
CO_2		800/2	CO_2	1062		17	One stage activation	[58]
CO_2	600/3	900/0.5	CO_2	1366	0.69	10.2	two stages activation	[133]
CO_2	600/3	900/0.5	N_2 &CO_2	1366	0.48	10.3	Two stages activation	[134]
CO_2		1100/1.5	N_2 &CO_2	1052	0.76		Two stages activation	[78]
CO_2	300-700/2	900/2	N_2 &CO_2	1062			Two stages activation	[75]
CO_2	600/2	900/0.5	CO_2	1366			Two stages activation	[127]
CO_2	850	850/1	N_2 &CO_2				Two stages activation	[69]
CO_2	600/2	900/0.5	N_2 & CO_2	1366	0.6	10	Two stages activation	[217]
CO_2		900/2	CO_2	1062			One stage activation	[122]
Steam	400	900/1	vacuum & N_2	1183	0.69		Carbonization under vacuum	[136]
Steam	675/2	900/1	vacuum & N_2	998			Carbonization under vacuum	[135]
Steam	500-900	500-900/1	N_2				Two stages activation	[82]
Steam	900/1	900/7	N_2	1319	0.73		Two stages activation	[218]

Table 2.1 (b) Process condition of PSAC: Chemical activation

Activating agent	Optimum activation (°C/h)	Inert gas	BET surface area (m^2/g)	Total pore volume (cm^3/g)	Yields (% wt/wt)	Additional information	Reference
H_3PO_4	500/2	N_2	1135		40	IR used is 8.0	[58]
H_2SO_4	700/2	N_2	1014			IR used is 8.0	[122]
KOH	700/2	N_2	1148			IR used is 6.0	[122]
H_2SO_4	700/2	N_2	1250			IR used is 6.0	[75]
K_2CO_3	800/ 1	N_2	1200	0.5		One stage activation	[151]
K_2CO_3	800/2	N_2	1170		18.9	IR 1.0	[59]

Table 2.1 (c) Process condition of PSAC: Physical-chemical activation

Activating agent	Carbonization (°C/h)	Optimum activation (°C/h)	Inert/ activating gas	BET surface area (m^2/g)	Total pore volume (cm^3/g)	Yields (% wt/wt)	Additional information	Reference
$ZnCl_2$ & CO_2	500/3	500/1	N_2 & CO_2	1500			IR 0.1-0.4	[109]
$ZnCl_2$ & CO_2	600/2	800/1	N_2 & CO_2	1837	1.27	30	Sample washed before carbonization; IR 0.2	[132]
$ZnCl_2$ & CO_2	800	800/2-3	N_2 & CO_2	1291	1.26	25.5	No cooling on the char; IR 0.25-3.0	[110]
H_3PO_4 & CO_2	600/2	800/1	N_2 & CO_2	1563	1.03	28	Sample washed before carbonization; IR 0.4	[132]
H_3PO_4 & CO_2	600/2	800/1	CO_2	1563			Sample were pretreated with H_3PO_4; IR 0.4	[127]
NaOH & CO_2	800/2	800/1.5	N_2 & CO_2	2247	0.80	30	Sample washed before carbonization; IR 2.0	[126]
KOH & CO_2	600/2	800/1	N_2 & CO_2	1408	0.77	25	Sample washed before carbonization; IR 0.4	[132]
KOH & CO_2	600/2	800/1	CO_2	1408	0.72		Sample were pretreated with KOH	[127]
KOH & CO_2	700/2	850/2	N_2 & CO_2	596	0.34		Impregnation on char; IR 1.0	[219]
KOH & CO_2	600/2	800/1	N_2 & CO_2	1562	0.75		Sample washed before carbonization; IR 0.1	[127]
H_2SO_4 & CO_2	600/2	800/1	N_2 & CO_2	1408	0.72		Sample washed before carbonization; IR 0.3	[127]

2.7 Influencing factors on activated carbon development

The textural outcome of AC is very much dependant on the combined effect of the precursor, reagent and activation conditions. Natures of precursor and activation temperatures have the most significant effect followed by impregnation ratio (activation gas flow rate for physical activation) and activation time.

The textural AC is highly dependent on the nature of precursor [106]. Lignin content for instance, results in high surface area development with strong presence of mesopores [147,148] and its inorganic tends to produce AC with undesirably high ash content (seen in rice hall AC, discussed in section 2.5).

The activation temperature directly influences the volatilization which in turn, greatly affects the textural outcome and yields of the AC [146,149]. Generally, BET surface area and pore volume increases with the activation temperature to an optimum value after which they begin to decrease [75,150]. Hayashi et al. [151] produced AC from almond shell (AM), coconut shell (CN), oil palm shell (OP), pistachio shell, (PT) and walnut shell (WN) using K_2CO_3 and found the BET surface area to increase with activation temperature from 500 to 800 °C. On the other hand, Kalderis et al. found similar trend on $ZnCl_2$ activation of bagasse and rice husk with optimum temperature of 700 °C [152]. Such observations were also reported on other precursors involving chemical or physical activation methods [133,153].

Excessively high activation temperatures bring destruction to the surface area and shifts pore size distribution. Jagtoyen et al. observed the increase of mesopore volume (begins at 250 °C and at the highest at 550 °C) corresponds with the decrease of microporosity; signifying the transformation of micropore to wider pore due to increase in temperature [96].

The yield of the AC is widely reported to be influenced by the activation temperature, activation time and the impregnation ratio. Generally, increased temperature leads to a decreased yield of carbon [51,58,59]. This could either be due to greater primary decomposition of biomass at higher temperatures or through secondary decomposition of char residue. Chandra et al. [49] reported a significant drop in durian shell AC, from 37% to 21% when activation temperature increased from 400 to 650 °C. In contrast, Prahas et al. [14] found yield in jackfruit peel AC remain almost constant for activation temperature from 350 °C to 550 °C. Hence, the influence of temperature is complex and varies, corresponding to the combined effect of the nature of precursor, reagent and degree of burn-off.

The selection of activating agent influences the textural characteristic of the AC generated. Steam activation tends to result in AC with wider pores as compared to that produced using CO_2 (as discussed in section 2.6.4). Such influence is more obvious in chemical activation. H_3PO_4 is regularly associated to heteroporosity; accredited to a mesoporous rich outcome while KOH activated AC are high in narrow-micropore [68]. Girgis et al. [39] investigated influence of different reagents on peanut hull and reported a mesoporous rich AC with high surface area using H_3PO_4 as compared to $ZnCl_2$ and KOH. In contrary, Kalderis et al.[152] found $ZnCl_2$ more effective as reagent than H_3PO_4 and NaOH on activation on rice husk and sugarcane bagasse.

Intensity of reagent (such as steam, CO_2 flowrate) has considerable effect on textural of AC. BET value increased progressively with steam or CO_2 flowrate to reach an optimum value [78]. Similarly for chemical activation, adequate amount of reagent is essential to minimise the formation of tarry matters which could otherwise clog up the pores [128,38]. Surface area and pore volume generally increases with impregnation to an optimum ratio [8,75,149,154].

High IR intensifies pyrolysis of starting materials and thus enhances the pore development as evident in BET surface areas [149]. Reffas et al. observed the pore size distribution of Coffee bean AC (H_3PO_4 as reagent) transforms from no mesopore to exclusively mesoporous by increase the IR from 0.6 to 1.8 [155]. Similar observation were reported on other H_3PO_4 [50,8] activation as well as other reagents such as H_2SO_4 [75] and $ZnCl_2$ [117].

Excessive impregnation however leads to pore widening and result in larger pores (meso and macropores) due to more activation agent being incorporated into precursor matrix [7,44,75,104,149]. On the other note, Girgis et al. observed a high amount of H_3PO_4 could result in formation of an unwanted phosphorus layer covering the particles and reduce the contact with the surrounding atmosphere. This obstruction limits the activation potential considerably thus resulting in the reduction of porosity [38]. IR influences the AC yields at different degrees: Sudaryanto et al. [33] found the KOH activated cassava peel AC decrease from 29% to 22% when IR increases from 0.5 to 2.5, while Prahas et al. [14] found little changes in H_3PO_4 activated jackfruit peel AC yield when IR increases from 1 to 4. Liou et al. [156] investigated rice husk AC and found the yield reduce more significantly due to IR when H_3PO_4 was used as the chemical reagent as compared to $ZnCl_2$.

For both physical and chemical activation the increase in activation time encourages burn off and results in changes of textural characteristics and decreases the overall yield of AC. Surface area and total pore volumes generally increase with time to an optimum value as sufficient time is required to eliminate all the moisture and volatile matters in the precursor before giving path to pore development [32]. However, the values thereafter are observed to decrease gradually at longer soaking time, attributed to the gasification which resulted in the collapse of the wall of the pore [32].

2.8 Chemical reagent recovery

The feasibility of chemical activation processes is strongly dependent upon efficiently recovering the reagent for recycling. This involves subsequent leaching stage, followed by an additional operation consisting of drying the washed AC. Of all the research related to AC, there are only a few investigations reported on the quantitative aspect of the reagent recovery and even lesser reports on the quality of the AC using reclaimed reagents. Reagent recovery investigations focus on the percentage recovery of the impregnation reagent [65] while reusability investigations report on ability of the reclaimed reagent on the textural characteristics of the AC.

Table 2.2 summarises all the reported works in the area of reagent recovery as well as its subsequent reusability in open literature. Most of the earlier work reports on percentage reagent recovery, while the potential of the recovered reagent on quantity and quality of the AC prepared on subsequent usage has not been reported. Adinata et al. [59] reported that K_2CO_3 reagent recovery increases with IR (from 0.5 to 2.0) in PSAC while Boudrahem et al. [112] reported same observation on preparation of $ZnCl_2$-AC from coffee residue. Similarly a number of observations have been reported on the reduction in the reagent recovery with activation temperature [59,157]. It should be noted that Tay et al. [158] have reported the highest recovery of above 97% with K_2CO_3 and KOH as activating agents for soybean oil cake precursor at 600 °C and at IR of 1.

The loss of H_3PO_4 upon activation has been well established and widely reported by earlier investigators. The H_3PO_4 was reported to be physically entrapped inside the carbon as insoluble metal phosphates. Jagtoyen et al. [80] highlighted the loss of recoverable H_3PO_4 in coal activation, credited to the consumption of reactions with mineral matters resulting in

formation of insoluble metal phosphates. Solum et al. [159] reported that 0.9 wt% phosphorus is retained in AC produced after extensive leaching. Toles et al. [160] reported a presence of 3 wt% phosphorous in the carbon by XRF analysis even after intensive washing. Guo & Rockstraw [7] found an increase in the phosphorus contents of final AC products with IR or final activation temperature. Girgis et al. [6], accredited to unleached residual phosphates in AC based on low adsorption of N_2 molecules at low pressure during characterisation. The increase in ash content of the AC has been reported to be due to the presence of H_3PO_4 due to the formation of phosphates within the carbon [80]

Different authors have followed different patterns of final washing step to remove the activating agent and reported incomplete H_3PO_4 recovery even upon intensive repeated washing. Reffes et al. [155] reported a two-week duration for complete recovery of H_3PO_4 from coffee AC using distilled water in a Soxhlet extractor method. Vernersson et al. [42] and Liou et al. [156] highlighted the presence of poorly soluble water phosphorus compounds in the carbon structure after washing.

In general the recovery of H_3PO_4 is found to be relatively lower as compared to other reagents. Soleimani et al. [65] and Suarez-Garcia et al. [161] reported a recovery of only 85-90% for H_3PO_4 based activation process while a recover of above 97% has been reported for K_2CO_3 and KOH based activations [158]. Guo and Lua [58] investigated the effectiveness of activation process comparing the fresh H_3PO_4 and the reclaimed acid, for activation on palm shell. PSAC produced using reclaimed H_3PO_4 were found to have a much lower BET surface areas in comparison with the fresh acid. The surface areas were reported to decline sharply from 1135 m^2/g (fresh H_3PO_4 activation) to 1007, 849 and 376 m^2/g for three consecutive reclaimed runs. Similar claims were asserted by Toles et al. [162] for H_3PO_4 activation of

almond shell. However the reagent recovery of H_3PO_4 were not reported or measured in both works. The subsequent impregnation-activation with the reclaimed acid was based on the assumption of no loss or decomposition of H_3PO_4 during process of activation and washing.

Chemical activation is a complex process and the usefulness of recovered reagent could only be confirmed by experiments. Regent such as H_3PO_4 are costly and an effective recovery mechanism is critical for commercial realisation as well as minimizing environment pollution. To the knowledge of the authors, there is no in-depth investigation on H_3PO_4 recoverability and its subsequent reusability.

2.9 Characterization of activated carbon

2.9.1 Surface area and pore characteristics

The pore size classification method adopted by the International Union of Pure and Applied Chemistry (IUPAC) is based on their width. The pores could be divided into three groups: the micro-, meso- and macropores.

Generally, the pore structure could be visualised as having many small pores (micropores) branching off from larger ones (mesopores), which are open through the entire particle (macropores), as shown in Fig. 2.3. The larger pores act as the transport pores while the smaller ones, which may be dead-end which play the role of adsorption pores.

Micropores are pores with effective dimension of less than 2 nm while mesopores are with average pore diameter between 2 and 50 nm. Pore with larger width are classified as macropores. Micropores could be further categorised based on the adsorbent-adsorbate interactions. Primary micropores (less than 0.8 nm) seen as the pore filling physisorption at

very low P/P_0 is enhanced by adsorbent-adsorbate interaction while in secondary micropores (average pore diameter: 0.8-2 nm), the filling occur by a cooperative adsorption mechanism at higher relative pressures.

Conventional AC development focuses on micropore porous development but the interest in mesopore rich AC has increased in recent years. The importance and significance of mesoporous carbon is seen in the number of works done in this area [110,117,154,163,164]. Mesopores in AC provide the rapid mass transport into adsorption pore and reduce the barrier correspond and result in shorter adsorption equilibrium time. The potential of these carbon materials is seen in macromolecule adsorption, catalytic support, battery electrode material, capacitor and biomedical engineering applications. High surface in mesoporosity is required to meet these criteria to allow macromolecules and ions to penetrate easily to the surface of carbon [116]. There has been a great deal of interest in the synthesis of mesoporous carbon [163]. The process is complex and high cost, prompting a continuing search for low-cost potential adsorbents, especially from botanical mass [165].

Table 2.2 Reagent recovery and reusability in chemical activation

Precursor	Activation			Chemical reagent		Observation	Reference
	I.R.	Temperature	Time				
	$wt_{reagent}$ / $wt_{precursor}$	°C	min	Type	Recovery, %($wt_{recovered}$/ $wt_{impregnated}$)		
Soybean oil cake[1]	1	600	60	K_2CO_3	98	Reagent recovery were investigated at 600 & 800 °C with recovery above 98%	[158]
Soybean oil cake[1]	1	600	60	KOH	96	Reagent recovery were investigated at 600 & 800 °C with recovery above 96%	[158]
Polyaramid fibres[1]	0.75	400- 950	30	H_3PO_4	82-25	Increase in carbonization temperature resulted a decrease in reagent recovery	[161]
Palm shell[1]	0.50-2.00	600-1000	120	K_2CO_3	0.5-2.0	Reagent recovery increase with IR but reduced with activation temperature	[59]
Apricot stone[1]	1	400	Not stated	H_3PO_4	90	Single sample investigation. Reagent recovery is about 90%	[65]
Coffee residue[1]	0.25-1.00	600	60	$ZnCl_2$	92-68	Reagent recovery decrease with IR	[112]
Sunflower oil cake[1]	0.85 & 1.90	600	Not stated	H_2SO_4	78 & 81	Reagent recovery is slightly increase at higher IR	[147]
Almond shell[2]	1	450	60-120	H_3PO_4	Not measured	Activation by reclaimed acid produced AC with much lower BET surface areas than the fresh acid	[168]
Palm shell[2]	2	500	120	H_3PO_4	Not measured	Activation by reclaimed acid produced AC with much lower BET surface areas	[58]

Remarks:
1. No investigation on activation by reclaimed reagents
2. All reclaimed activations are at same precursor weight

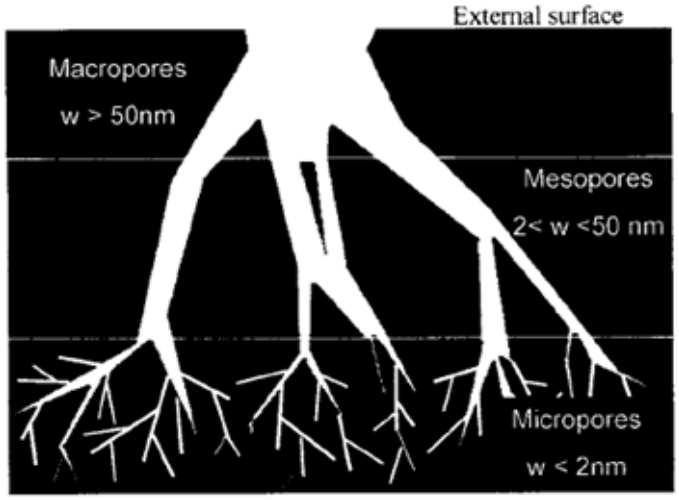

Fig. 2.4. Schematic representation of the pore network of activated carbon

Six general types of isotherms have been observed and the characteristic isotherms are as described below:

Type I isotherms are typical of microporous solids where only monolayer adsorption occurs. In these, micropore filling occurs significantly at relatively low partial pressure <0.1 $P=P_o$, the adsorption process being complete at approximately 0.5 $P=P_o$. The potential field of force between neighbouring wall in the very fine micropores causing an increase in the interaction energy between the solid surface and the gas molecules corresponds with the increase in adsorption, especially at low relative pressures. These isotherms are thus characterized by a plateau that is almost horizontal and parallel to the pressure axis. Type II isotherms correspond to multilayer physical adsorption and could be recognised from a long linear portion and do not attain a limiting value as seen in the plateau. The monolayer coverage is succeeded by multilayer adsorption at higher $P=P_o$ values.

Type III isotherms, characterized by being convex to the pressure axis, are generally obtained in the case of nonporous adsorbents or carbons with mixed micro-and mesoporosity, as the

results of adsorbate-adsorbate interactions will tend to promote the adsorption of more molecules.

Type IV isotherm, a multilayer adsorption where complete filling of the smallest capillaries occurred, are obtained for solids containing pores in the mesopore range. The unique adsorption-desorption hysteresis is due to greater amount adsorbed along the desorption branch than along the adsorption branch at any given relative pressure.

Type V isotherm is similar with Type III but with a plateau at fairly high relative pressures and often seen in polar and non-polar adsorbates with weak adsorbent-adsorbate interactions. The type VI isotherm are recognised in the sharp steps, an outcome of stepwise multilayers adsorptions on a uniform nonporous surface.

2.9.2 Surface morphology

The presence of O, N and P provides unique characteristics to the surface chemistry of AC [166]. These surface functional groups influence the adsorption capacity [19], catalytic properties, acid-base character and moisture content [167]. FT-IR, X-ray photoelectron spectroscopy (XPS), thermal analysis (TA), thermal programmed desorption (TPD), Boehm and potentiometric titrations are methods commonly applied in surface chemistry studies [167].

Abundant in quantity, oxygen surface groups are the main contributors to the surface chemistry. Among them, carboxylic, lactone and hydroxyl groups would give rise to acidic characteristic [168] while pyrone, chromene and quinone are basic in nature [168,169] (Fig. 2.5 & 2.6). On the other hand, phosphorus (in the form of phosphate derivatives) leads to

acidic surface characters [5,170]. Numerous works on palm shell [127,132], cotton stalk [5], bamboo [8] and rice hull [72] verified the development of acidic functional group due to H_3PO_4 activation, with groups of carboxylic, phenolic, and lactones have been reported [5,19].

The amount of oxygen, nitrogen and phosphorus on AC varies considerably with activation temperatures. The oxygen content in AC decreases significantly (from 25 % to 1%) with activation temperature; due to decomposition of oxygen-based acidic groups at temperatures above 250 °C. As such, ACs from low activation temperatures (< 500 °C) are dominated with acidic surface (mainly phenolic hydroxyl groups) while basic surface oxide groups are reported for activation above 800 °C. Guo & Rockstraw reported high acidic group in low temperature H_3PO_4 activated AC from rice hull [72] while Ip et al. [8] observed the decreased in acidic site in bamboo AC preparing H_3PO_4 activated at 900 °C.

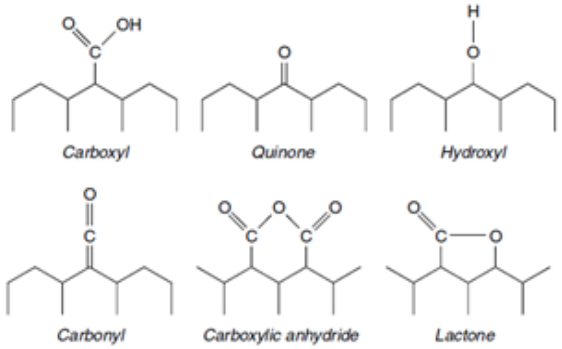

Fig. 2.5. Simplified schematic of some acidic surface groups of activated carbon

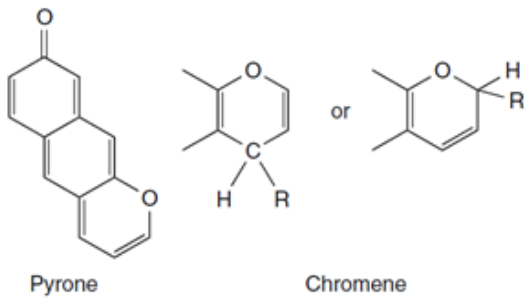

Fig. 2.6. Schematic of basic groups on activated carbon

2.10 Activated carbon adsorption

The AC adsorptivity, be it physical or chemical adsorption depends on the nature of the adsorbent, its effective surface area and adsorption conditions [83]. In the case of physical adsorption or physiosorption, the adsorbate is bound to the surface by relatively weak van der Waals forces. Chemisorption, on the other hand, involves exchange or sharing of electrons between the adsorbate molecules and the surface of the adsorbent resulting in a chemical reaction. The bond formed between the adsorbate and the adsorbent is essentially a chemical bond and is thus much stronger than in the physisorption.

Physical adsorption is non-specific and occurs between any adsorbate-adsorbent systems while chemisorption tends to be specific. These differences mainly arises from the enthalpy of adsorption. In physical adsorption, the enthalpy of adsorption is usually between 10 and 20 $kJmol^{-1}$ whereas it is generally of the order of 40 to 400 $kJmol^{-1}$ for chemisorption. The thickness of adsorbate between both adsorption are different, with multilayer being observed in physical adsorption while monolayer for chemisorption. Physical adsorption process is reversible under the same temperature of adsorption whereas chemisorptions are generally irreversible. This is due to chemisorption involves significant electron transfer between the adsorbate and the adsorbent [19].

AC is the most widely practiced adsorption treatment used to remove pollutant [171,172,173]. The main advantage of carbon adsorption over other processes is that it can remove both organic and inorganic compounds either at generally low cost [174]. AC removes pollutant even at concentrations as low as 100 mg/l in batch and continuous processes. The system for AC adsorption is less expensive than advanced system such as

membrane filtration and ion exchanger [175]. Furthermore, it is safe and easy to operate while the spent AC such as GAC could be regenerated under simple treatment before reused.

Despite its prolific use in water and waste water industries, commercial AC remains as an expensive material, leading to a search for low cost material as alternative adsorbent materials, such as AC prepared from rattan sawdust [60], palm ash [176], coconut shell [44], hazelnut shell [177] and palm kernel fibre [178], Sunflower oil cake [147], acorn [95] and olive seed [95].

The selection of AC depends on the nature of precursor. Removal of heavy metal ions from water phase required acidic AC which demonstrates cation-binding capacities in treatment conditions [149]. The surface charges on AC also influences sorption properties of AC. With surface containing both hydrophobic and hydrophilic sites, the sorption characterise of AC is different between adsorbates. Adsorption of non-polar adsorbate would not be affected by the differences between both sides while a polar adsorbate is preferentially adsorbed on polar sites [179].

Modified or impregnated AC is used for its specific sorption properties. Langley et al. reported HNO_3 treatment of ACs increases the material's ability to remove both Cr and Cu ions from aqueous solution [180]. Kuang et al. credited the existence of oxygen surface functional groups Ag loaded AC in promoting mercury adsorption [181].

2.10.1 Adsorption of methylene blue (MB)

Effluent discharged from the dye industries impede light penetration, retards photosynthetic activity and resulted in aqua-toxic components fish and other organisms [12]. Most of the

used dyes are stable to photo-degradation, bio-degradation and oxidizing agents [182]. It is estimated that more than 100,000 commercially available dyes with over 50,000 tonnes of dyes are discharged via effluent into environment annually [183].

The adsorbate MB, with molecular structure as shown in Fig. 2.8, is the most common among all other dyes in dyeing cotton and silk [184]. In practice, the most commonly used adsorbent for the removal of MB by adsorption is coal based commercial AC [147]. While most of these adsorbent are with well-developed surface area, they are at the same time predominately microporous. Guo et al. [34] demonstrated that the MB adsorption does not only influence by surface area available but also by other factors such as chemical nature of the surface while Girgis et al. [6] has observed the advantage of mesoporous AC in MB removal. In addition, various works has substantiated the favour of mesoporous AC in removal of these large size molecules of contaminants such as MB dye [154,155,185].

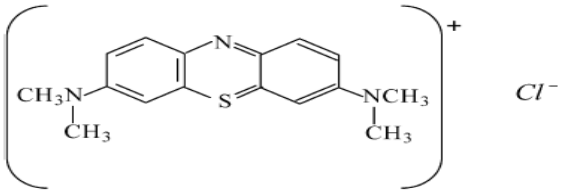

Fig. 2.7. Chemical structure of methylene blue

The mechanism for the removal of MB dye by adsorption may be assumed to involve the following steps [186]:

- Migration of dye from bulk of the solution to the surface of the AC
- Diffusion of dye through the boundary layer to the surface of the adsorbent
- Adsorption of dye at an active site on the surface of AC, and
- Intra-particle diffusion of dye into the interior pores of the AC particle

MB adsorption from aqueous solution onto the AC has been reported as a function of initial dye concentration, temperature, pH, and stirring speed [187]. High initial concentration of MB enhances the sorption process by providing a driving force to overcome all mass transfer resistances of all molecules between the aqueous and solid phases [177]. Increase in temperature is generally resulted in increase in the amount of MB adsorped. Implying a kinetically controlling process, increased temperature leads to highly mobility of the molecules, thereby facilitating the formation of surface monolayer and result in an increase in the rate of adsorption. In addition, adsorption of MB onto the adsorbent surface is an endothermic reaction. Increase in temperature shifts the equilibrium according the Le Chatelier Principle, resulting in higher MB molecules being adsorped. The adsorption of MB increased as the pH increases with varying degree. Increase in pH changed the AC surface chemistry by increasing the number of negative charged sites, providing a favourable adsorption opportunity on MB cation due to electrostatic attraction [188]. On the other hand, the surface charge density decrease with an increase in the solution pH and the electrostatic repulsion between the positively charged MB and the surface of the adsorbent is lowered thus increasing the rate of adsorption.

MB uptakes by different adsorbent such as agricultural waste, its carbon or ash have been reviewed by Rafatullah et al. [34], Bhatnagar & Sillanpaa [35], Demirbas [37], Dias et al. [24], Ioannidou & Zabaniotou [32] and Yin et al. [189]. It is quite obvious that MB adsorptivity of natural materials could be boosted significantly upon activation. Using lignin material as base, Zou & Han observed the AC has an adsorption capacity of 604 mg/g or approximately 20 times higher than in untreated form [190.]. Similar observation also reported on rice husk (41 mg/g and 343 mg/g). This should however, not be used as a platform to undermine MB uptake ability among natural materials. Review by Rafatullah et

al. [34] has shown that teak wood bark, papaya seeds and grass waste has exceptionally high MB adsorptivity (914 mg/g, 555 mg/g and 457mg/g), more effective than the highest recorded by ACs from agricultural waste (Straw AC: 472 mg/g). Similarly, not all ACs demonstrated reasonable MB uptakes. ACs from hazelnut shell, apricot stones, walnut shell and almond shell has shown poor adsorptivity with less than 10 mg/g uptake reported.

MB adsorption by AC is influenced by many factors such as pore size, surface area and surface chemistry as shown in a vast number of works. AC with high surface area usually provides a favorable condition for large adsorption capacity. Besides of the highest uptake recorded on mentioned straw AC , high adsorptivity (over 400 mg/g) by agricultural based AC has been reported on bamboo [43], vetiver roots [64], peach stone [93] and oil palm fiber [53].

Equilibrium sorption isotherms and kinetics of MB by AC were extensively investigated, much due to the fact to use MB uptake to characterise AC's adsorptivity [183,191,192]. A search in available literature reveals that only Tan et al. investigated MB adsorption using PSAC. The MB adsorptivity was good at 244 mg/g with equilibrium data best described by the Langmuir isotherm model [193]. The PSAC development process is complex: physio-chemical activation (KOH & CO_2) with high activation temperature and long duration (850 °C and 4 h) while the PSAC quality is poor with BET surface area was found to be 596 m^2/g.

2.10.2 Adsorption of dairy COD

Dairy industry produces different products such as milk, butter, cheese, yogurt, milk powder, ice-cream, various types of desserts [194]. The hygienic requirement results in a large effluent discharge from washing and cleaning operation [195]. Ramasamy et al. reported 2 to

5 litre of wastewater produced for each litre of milk processed [196]. These plants differ widely both in quantity and quality depending on a given dairy factory production characteristics [197], resulting in effluents vary greatly in characteristics [198, 194]. The dairy industry is usually characterized by high biological oxygen demand (BOD), chemical oxygen demand (COD) concentrations [195,199,200,201,202]. Constituted mainly of lactose, the COD content of these effluents could be as high as 6000 to 8000 mg/l [203,204]

Aerobic, anaerobic, membrane technology (ultrafiltration, nanofiltration, reverse osmosis)[205], coagulation, flocculation and precipitation are available treatment technology for dairy waste. Aerobic treatment processes are commonly used together with anaerobic processes for dairy wastewater treatment [206]. These aerobic processes include activated sludge processes or trickling filters or aerated lagoons, or a combination of these [207]. The high energy requirement of aerobic treatment is well documented [201]. On the other hand, anaerobic treatment doesn't require aeration equipment, use less energy, while require lesser land and produce less sludge [194]. It also holds the potential of producing methane [196,208]. As such due to the tremendous area requirement for aerobic treatment lagoons, most lagoons are thus usually anaerobic lagoons.

The conventional wastewater treatment technologies as adopted in industrialized nations are expensive to build, operate and maintain [209], especially for decentralized communities. Research efforts are going on [210] for the development of treatment technologies suited to these applications. Low cost adsorbent such as PAC can be used as a promising adsorbent for removal of various types of pollutants from dairy wastewater. There has been significant amount of works on COD adsorption in dairy waste; however, only limited investigation using AC. Kushawa et al. [201] reported a COD adsorption value of 134 mg/g from synthetic

dairy COD using commercial AC. Devi et al. [210] conducted similar investigation using mixture adsorbent carbon and commercial AC and reported the maximum adsorption capacity reported is less than 30 mg/g. Kennedy et al. [205] achieved 87% and 96% removal of BOD and COD respectively from tannery wastewater using rice husk-AC. Hami et al. [211] elucidated significant increases in BOD and COD removal efficiencies using AC in a dissolved air flotation unit treating refinery wastewater. It has been reported that COD adsorption process of dairy waste decrease with increase of pH especially in basic environment [201]. It was also reported that the intra-particle diffusion of dairy COD components into meso-pores is the rate-controlling step in the adsorption process. Sarkar et al. utilized coagulation as a pretreatment step prior to adsorption with PAC before treating the dairy wastewater by membrane separation method [195,212]

2.11 Adsorption isotherm and kinetics

Adsorption is a complex process and depends on electrostatic and non-electrostatic (hydrophobic) interactions. Much works are still necessary to identify the sorption mechanisms clearly [34] and it is the crucial component to design and run an industrial adsorption plant [173]. Adsorption isotherm is a graphical representation showing the relationship between the amount adsorbed by a unit weight of adsorbent (such as AC) and the amount of adsorbate remaining in the test medium at equilibrium. On the other hand, adsorption kinetics provides information about the mechanism of adsorption [177].

2.11.1 Adsorption isotherm

2.11.1.1 Langmuir Isotherm

Adsorption isotherms can be generated based on numerous theoretical explanations. The simplest theoretical model that can be used to describe monolayer adsorption is the Langmuir

equation [213]. Langmuir isotherm assumes monolayer adsorption onto a surface containing a finite number of adsorption sites of uniform strategies of adsorption with no transmigration of adsorbate in the plane of surface [214]. The Langmuir equation, which is applicable to homogeneous sorption, can be described by the linearised form:

$$\frac{C_e}{q_e} = \frac{1}{bQ_0} + \frac{C_e}{Q_0}$$

The Langmuir constants Q_0 (mg/g) and b (L/mg) are determined from the slope and intercept of the plot of specific adsorption, C_e/Q_e against the equilibrium concentration, C_e. The close proximity of the experimental data with the model equation evidenced from the R^2 value which demonstrates suitability of the Langmuir isotherm model.

The essential characteristics of the Langmuir isotherm can be expressed in terms of a dimensionless equilibrium parameter R_L which is defined by:

$$R_L = \frac{1}{1 + bC_0}$$

where b is the Langmuir constant and C_0 is the highest adsorbate concentration (mg/l). The value of R_L indicates the type of the isotherm to be either favourable ($0< R_L< 1$), unfavourable ($R_L>1$), linear ($R_L=1$) or irreversible ($R_L=0$).

2.11.1.2 Freundlich Isotherm

The Freundlich model is an empirical equation based on the distribution of solute between the solid phase and aqueous phase at equilibrium [213]. Freundlich isotherm assumes heterogeneous surface energies in which the energy term in Langmuir equation varies as a function of the surface coverage thus allowing multi-layer adsorption [214]. The logarithmic form of Freundlich isotherm is given by the following equation:

$$\mathrm{Log}(\mathrm{Q_e}) = \mathrm{Log}(\mathrm{K_F}) + \frac{1}{\mathrm{n}}\mathrm{Log}(\mathrm{C_e})$$

where Q_e is the amount adsorbed (mg/g), C_e is the equilibrium concentration of the adsorbate, K_F (mg/g)(L/mg)$^{1/n}$ and n are the Freundlich adsorption constant. 1/n is the heterogeneity factor that measure of the adsorption intensity as well as its favourability of the adsorption process. For this isotherm model, the slope 1/n ranging between 0 and 1 is a measure of adsorption intensity or surface heterogeneity, becoming more heterogeneous as its value gets closer to zero. A value of 1/n below 1 indicates a normal Langmuir isotherm while 1/n above 1 is indicative of cooperative adsorption [214]. From the linearised Freundlich plot of log(Q_e) versus log(C_e), Freundlich constants K_F and 1/n could be obtained. The R^2 value corresponds to the magnitude of variation between the experimental data and the model equation.

2.11.1.3 Temkin Isotherm

Temkin isotherm considers the effect of indirect adsorbate-adsorbate interactions on adsorption isotherms. The heat of adsorption of all the molecules in the layer would decrease linearly with coverage due to adsorbate-adsorbate interactions [214]. The linearised form of Temkin isotherm has the following form:

$$Q_e = \frac{RT}{b}\ln(A) + \frac{RT}{b}\ln(C_e)$$

where Q_e is the amount adsorbed (mg/g), C_e is the equilibrium concentration of the adsorbate, while A (L/g) is the equilibrium binding constant corresponding to the maximum binding energy and B (= RT/b), is the Temkin constant related to heat of sorption. R (8.314 J/mol K) is the universal gas constant and T (K) is the absolute solution temperature. From the plot of the above equation, the Temkin isotherm constants A and B could be obtained. The R^2 value corresponds to the magnitude of variation between the experimental data and the model equation.

2.11.2 Adsorption kinetics

2.11.2.1 Pseudo-First-Order Kinetic Model

The pseudo-first-order kinetic Lagergren equation [215] is derived as:

$$\log(Q_e - Q_t) = \log Q_e - \frac{k_1}{2.303}t$$

Where Q_e and Q_t are the amounts of MB adsorbed (mg/g) at equilibrium and at time t (min), respectively, and k_1 (min^{-1}) is the adsorption rate constant of pseudo-first-order adsorption. The validity of the model can be checked by linearised plot of $\log(Q_e - Q_t)$ versus t. Constants k_1 and Q_e could be obtained from the plot along with the R^2 values which evidence the acceptability of the model in representing the experimental data.

2.11.2.1 Pseudo-Second-Order Kinetic Model

The second-order kinetic model is conveniently expressed in the linearised form as:

$$\frac{t}{Q_t} = \frac{1}{k_2 Q_e^2} + \frac{t}{Q_e}$$

Where Q_e and Q_t are the amounts of MB adsorbed (mg/g) at equilibrium and at time t (min), respectively, and k_2 is the rate constant (min^{-1}). From the linear plots of t/ Q_t against t the degree of agreement between the experimental and the calculated adsorption $Q_{e,exp}$ and $Q_{e,cal}$ could be obtained. In addition, the correlation coefficient values, R^2 from the plot could also provide indication on the suitability of pseudo-second-order kinetic model to describe the adsorption dynamics.

2.11.2.3 Intraparticle Kinetic Model

The intraparticle diffusion equation [216] can be described as:

$$Q_t = K_p t^{1/2} + C$$

Where C is the intercept and k_p is the intraparticle diffusion rate constant ($mg.g^{-1}min^{-1/2}$), which can be evaluated from the slope of linear plot of Q_t versus $t^{1/2}$. The R^2 values for the Intraparticle diffusion would determine the suitability of this model describing the adsorption scenario. Though adsorption isotherm an kinetics have been extensively investigated on a vast amount of materials, there has been no conclusion on adsorption trends. Experimental investigation is still required to get identify the adsorption mechanism.

2.12 Conclusions

AC are powerful adsorbents that can efficiently remove several pollutants; however, their large-scale application is limited by high production costs. In this review, an attempt has been made to focus on the recent developments of AC related to the low cost agricultural wastes. The differences in the textural characteristics of these AC indicate the dominant influences of the precursors' strucrure and process conditions on their reactivity in the pyrolysis/activation reactions. With both conventional physical and chemical activation, AC with high surface areas might be obtained and adsorption behaviour might be controlled by carefully manipulating preparation parameters. Some produced AC, such as from palm shell, hold the potential to be economically viable and compete with the commercial ones. Although the amount of available literature data on AC adsorption is increasing at a tremendous pace, there are still several gaps which need to be filled. The conditions for the production of AC after surface modification for higher uptake of pollutants need to be optimized. Environmentally safe disposal of pollutants-laden reagent is another important topic of concern which should not be overlooked. As such, reagent recovery studies need to be performed in detail to enhance the economic feasibility of the activation process. It is also suggested that the research should be expanded to pilot-plant studies to check their feasibility on commercial scale.

2.13 References

1 R.R. Bansode, J.N. Losso, W.E. Marshall, R.M. Rao, R.J. Portier, Adsorption of volatile organic compounds by pecan shell and almond shell-based granular activated carbons, Bioresource Technology 90 (2003) 175-184

2 C.P. Dwivedi, J.N. Sahu, C.R. Mohanty, B.R. Mohan, B.C. Meikap, Column performance of granular activated carbon packed bed for Pb(II) removal, Journal of Hazardous Materials 156 (2008) 596-603

3 Z. Aksu, E. Kabasakal, Adsorption Characteristics of 2,4-Dichlorophenoxyacetic Acid (2,4-D) from Aqueous Solution on Powdered Activated Carbon, Journal of Environment Science and Health, Part B. 40 (2005) 545-70

4 M.A. Diaz-Diez, V. Gomez-Serrano, C. Fernandez Gonzalez, E.M. Cuerda-Correa, A. Macias-Garcia, Porous texture of activated carbons prepared by phosphoric acid activation of woods, Applied Surface Science 238 (2004) 309-313

5 B.S. Girgis, E. Smith, M.M. Louis, A.A. El-Hendawy, Pilot production of activated carbon from cotton stalks using H_3PO_4, Journal of Analytical and Applied Pyrolysis 86 (2009) 180-184

6 B.S. Girgis, A.N.A. El-Hendawy, Porosity development in activated carbons obtained from date pits under chemical activation with phosphoric acid, Microporous and Mesoporous Materials 52 (2002) 105-117

7 Y. Guo, D.A. Rockstraw, Physical and chemical properties of carbons synthesized from xylan, cellulose, and Kraft lignin by H_3PO_4 activation, Carbon 44 (2006) 1464-1475

8 A.W.M. Ip, J.P. Barford, G. McKay, Production and comparison of high surface area bamboo derived active carbons, Bioresource Technology. 99 (2008) 8909-8916

9 S. Ichcho, E. Khouya, S. Fakhi, M. Ezzine, H. Hannache, R. Pallier, R. Naslain, Influence of the experimental conditions on porosity and structure of adsorbents elaborated from Moroccan oil shale of Timahdit by chemical activation, Journal of Hazardous Materials A118 (2005) 45-51

10 R-S. Juang , S-H. Lin, C-H. Cheng, Liquid-phase adsorption and desorption of phenol onto activated carbons with ultrasound, Ultrasonics Sonochemistry 13 (2006) 251-260

11 S. Gaspard, S. Altenor, N. Passe-Coutrin, A. Ouensanga, F. Brouers, Parameters from a new kinetic equation to evaluate activated carbons efficiency for water treatment, Water Research 40 (2006) 3467-3477

12 V.K. Garg, M. Amita, R. Kumar, R. Gupta, Basic dye (methylene blue) removal from simulated wastewater by adsorption using Indian Rosewood sawdust: a timber industry waste, Dyes and Pigments 63 (2004) 243-250

13 M. Imamoglu, O. Tekir, Removal of copper (II) and lead (II) ions from aqueous solutions by adsorption on activated carbon from a new precursor hazelnut husks, Desalination 228 (2008) 108-113

14 D. Prahas, Y. Kartika, N. Indraswati, S. Ismadji, Activated carbon from jackfruit peel waste by H_3PO_4 chemical activation: Pore structure and surface chemistry characterization, Chemical Engineering Journal 140 (2008) 32-42

15 G. Issabayeva, M.K. Aroua, N.M. Sulaiman, Electrodeposition of copper and lead on palm shell activated carbon in a flow-through electrolytic cell, Desalination 194 (2006) 192-201

16 J.S. Tan, F.N. Ani, Carbon molecular sieves produced from oil palm shell for air separation, Separation and Purification Technology 35 (2004) 47-54

17 M.K. Aroua, S.P.P. Leong, L.Y. Teo, C.Y. Yin, W.M.A.W. Daud, Real-time determination of kinetics of adsorption of lead(II) onto palm shell-based activated carbon using ion selective electrode, Bioresource Technology 99 (2008) 5786-5792

18 P. Girods, A. Dufour, V. Fierro, Y. Rogaume, C. Rogaume, A. Zoulalian, A. Celzard, Activated carbons prepared from wood particleboard wastes: Characterisation and phenol adsorption capacities, Journal of Hazardous Materials 166 (2009) 491-501

19 J. Guo & A.C. Lua, Surface Functional groups on oil-palm-shell adsorbents prepared by H_3PO_4 and KOH activation and their effects on the adsorptive capacity, Institution of Chemical Engineers, Trans IChemE, Part A, 81 (2003) 585-590

20 J.A. Menendez-Diaz, I. Martin-Gullon, Types of carbon adsorbents and their production, Interface Science and Technology Volume 7 (2006) 1-47

21 E. Bottani, J. Tascon, Adsorption by Carbons, Elsevier 1st Ed. 2008, ISBN 978-0-08-044464-2

22 S.M. Manocha, Porous carbons, Sadhana Vol. 28, Parts 1 & 2 (2003) 335-348

23 F.Y. Yuen, B.H. Hameed, Recent developments in the preparation and regeneration of activated carbons by microwaves, Advances in Colloid and Interface Science 149 (2009) 19-27

24 J.M. Dias, M.C.M. Alvim-Ferraz, M.F. Almeida, J. Rivera-Utrilla, M. Sanchez-Polo, Waste materials for activated carbon preparation and its use in aqueous-phase treatment: A review, Journal of Environmental Management 85 (2007) 833-846

25 O. Aktas, F. Cecen, Bioregeneration of activated carbon: A review, International Biodeterioration & Biodegradation 59 (2007) 257-272

26 F.B. DeWalle, E.S.K. Chian, Biological regeneration of powdered activated carbon added to activated sludge units, Water Research 11 (1977) 439-446

27 I.V. Bylina, S. Tong, C.Q. Jia, Thermal analysis of sulphur impregnated activated carbons with mercury adsorbed from the vapour phase, Journal of Thermal Analysis and Calorimetry 96 (2009) 91-98

28 D. Karatza, A. Lancia, D. Musmarra, C. Zucchini, Study of mercury absorption and desorption on sulfur impregnated carbon, Experimental Thermal and Fluid Science 21 (2000) 150-155

29 L. Ma, P. Ning, Y. Zhang, X. Wang, Experimental and modeling of fixed-bed reactor for yellow phosphorous tail gas purification over impregnated activated carbon, Chemical Engineering Journal 137 (2008) 471-479

30 K.T. Klasson, L.H. Wartelle, J.E. Rodgers III, I.M. Lima, Copper(II) adsorption by activated carbons from pecan shells: Effect of oxygen level during activation, Industrial Crops and Products 30 (2009) 72-77

31 P. Mondal, C.B. Majumder, B. Mohanty, Effects of adsorbent dose, its particle size and initial arsenic concentration on the removal of arsenic, iron and manganese from simulated ground water by Fe^{3+} impregnated activated carbon, Journal of Hazardous Materials 150 (2008) 695-702

32 O. Ioannidou, A. Zabaniotou, Agricultural residues as precursors for activated carbon production- A review, Renewable and Sustainable Energy Reviews 11 (2007) 1966-2005

33 Y. Sudaryanto, S.B. Hartono, W. Irawaty, H. Hindarso, S. Ismadji, High surface area activated carbon prepared from cassava peel by chemical activation, Bioresource Technology 97 (2006) 734-739

34 M. Rafatullah, O. Sulaiman, R. Hashim, A. Ahmad, Adsorption of methylene blue on low-cost adsorbents: A review, Journal of Hazardous Materials 177 (2010) 70-80

35 A. Bhatnagar, M. Sillanpaa, Utilization of agro-industrial and municipal waste materials as potential adsorbents for water treatment-A review, Chemical Engineering Journal 157 (2010) 277-296

36 D. Kalderis, D. Koutoulakis, P. Paraskeva, E. Diamadopoulos, E. Otal, J.O. del Valle, C. Fernandez-Pereira, Adsorption of polluting substances on activated carbons prepared from rice husk and sugarcane bagasse, Chemical Engineering Journal 144 (2008) 42-50

37 A. Demirbas, Agricultural based activated carbons for the removal of dyes from aqueous solutions: A review, Journal of Hazardous Materials 167 (2009) 1-9

38 B.S. Girgis, M.F. Ishak, Activated carbon from cotton stalks by impregnation with phosphoric acid. Materials Letters 39 (1999) 107-114

39 B.S. Girgis, S.S. Yunis, A.M. Soliman, Characteristics of activated carbon from peanut hulls in relation to conditions of preparation, Materials Letters 57 (2002) 164-172

40 H.L. Mudoga, H. Yucel, N.S. Kincal, Decolorization of sugar syrups using commercial and sugar beet pulp based activated carbons, Bioresource Technology 99 (2008) 3528-3533

41 C. Michailof, G.G. Stavropoulos, C. Panayiotou, Enhanced adsorption of phenolic compounds, commonly encountered in olive mill wastewaters, on olive husk derived activated carbons, Bioresource Technology 99 (2008) 6400-6408

42 T. Vernersson, P.R. Bonelli, E.G. Carrella, A.L. Cukierman, Arundo donax cane as a precursor for activated carbon preparation by phosphoric acid activation. Bioresource Technology 83 (2002) 95-104

43 B.H. Hameed, A.T.M. Din, A.L. Ahmad, Adsorption of methylene blue onto bamboo-based activated carbon: Kinetics and equilibrium studies. Journal of Hazardous Materials 141 (2007) 819-825

44 M.K.B. Gratuito, T. Panyathanmaporn, R.A. Chumnanklang, N. Sirinuntawittaya, A. Dutta, Production of activated carbon from coconut shell: Optimization using response surface methodology. Bioresource Technology 99 (2008) 4887-4895

45 N. Bagheri, J. Abedi, Preparation of high surface area activated carbon from corn by chemical activation using potassium hydroxide, Chemical Engineering Research and Design 87 (2009) 1059-1064

46 Q. Cao, K-C. Xie, Y-K. Lv, W-R. Bao, Process effects on activated carbon with large specific surface area from corn cob, Bioresource Technology 97 (2006) 110-115

47 R-L. Tseng, S-K. Tseng, F-C. Wu, C-C. Hu, C-C Wang, Effects of micropore development on the physicochemical properties of KOH-activated carbons, Journal of the Chinese Institute of Chemical Engineers 39 (2008) 37-47

48 J.V. Nabais, P. Carrott, M.M.L.R. Carrott, V. Luz, A.L. Ortiz, Influence of preparation conditions in the textural and chemical properties of activated carbons from a novel biomass precursor: The coffee endocarp, Bioresource Technology 99 (2008) 7224-7231

49 T.C. Chandra, M.M. Mirna, J. Sunarso, Y. Sudaryanto, S. Ismadji, Activated carbon from durian shell: Preparation and characterization, Journal of the Taiwan Institute of Chemical Engineers 40 (2009) 457-462

50 M.D.M. Gomez-Tamayo, A. Macias-Garcia, M.A.D. Diez, E.M. Cuerda-Correa, Adsorption of Zn(II) in aqueous solution by activated carbons prepared from evergreen oak (*Quercus rotundifolia L.),* Journal of Hazardous Materials 153 (2008) 28-36

51 P. Patnukao, P. Pavasant, Activated carbon from *Eucalyptus camaldulensis Dehn* bark using phosphoric acid activation. Bioresource Technology, 99 (2008) 8540-8543

52 R. Baccar, J. Bouzid, M. Feki, A. Montiel, Preparation of activated carbon from Tunisian olive-waste cakes and its application for adsorption of heavy metal ions, Journal of Hazardous Materials 162 (2009) 1522-1529

53 B.H. Hameed, I.A.W. Tan, A.L. Ahmad, Optimization of basic dye removal by oil palm fibre-based activated carbon using response surface methodology, Journal of Hazardous Materials 158 (2008) 324-332

54 M.Z. Alam, E.S. Ameem, S.A. Muyibi, N.A. Kabbashi, The factors affecting the performance of activated carbon prepared from oil palm empty fruit bunches for adsorption of phenol, Chemical Engineering Journal 155 (2009) 191-198

55 A. Zabaniotou, O. Ioannidou, E. Antonakou, A. Lappas, Experimental study of pyrolysis for potential energy, hydrogen and carbon material production from lignocellulosic biomass, International Journal of Hydrogen Energy 33 (2008) 2433-2444

56 Y. Munoz-Gonzalez, R. Arriagada-Acuna, G. Soto-Garrido, R. Garcia-Lovera, Activated carbons from peach stones and pine sawdust by phosphoric acid activation used in clarification and decolorization processes. Journal of Chemical Technology Biotechnology 84 (2009) 39-47

57 W.C. Lim, C. Srinivasakannan, N. Balasubramanian, Activation of palm shells by phosphoric acid impregnation for high yielding activated carbon. Journal of Analytical and Applied Pyrolysis 88 (2010) 181-186

58 J. Guo, A.C. Lua, Textural and chemical properties of adsorbent prepared from palm shell by phosphoric acid activation. Materials Chemistry and Physics 80 (2003) 114-119

59 D. Adinata, W.M.A.W. Daud, M.K. Aroua, Preparation and characterization of activated carbon from palm shell by chemical activation with K_2CO_3, Bioresource Technology 98 (2007) 145-149

60 B.H. Hameed, L.H. Chin, S. Rengaraj, Adsorption of 4-chlorophenol onto activated carbon prepared from rattan sawdust, Desalination 225 (2008) 185-198

61 A.C. Lua, T. Yang, Effects of vacuum pyrolysis conditions on the characteristics of activated carbons derived from pistachio-nut shells, Journal of Colloid and Interface Science 276 (2004) 364-372

62 T. Yang, A.C. Lua, Characteristics of activated carbons prepared from pistachio-nut shells by potassium hydroxide activation, Microporous and Mesoporous Materials 63 (2003) 113-124

63 C. Srinivasakannan, M.Z. Abu Bakar, Production of activated carbon from rubber wood sawdust, Biomass & Bioenergy 27 (2004) 89-96

64 S. Altenor, B. Carene, E. Emmanuel, J. Lambert, J-J. Ehrhardt, S. Gaspard, Adsorption studies of methylene blue and phenol onto vetiver roots activated carbon prepared by chemical activation, Journal of Hazardous Materials 165 (2009) 1029-1039

65 M. Soleimani, T. Kaghazchi, Adsorption of gold ions from industrial wastewater using activated carbon derived from hard shell of apricot stones - An agricultural waste, Bioresource Technology 99 (2008) 5374-5383

66 M. Olivares-Marin, C. Fernandez-Gonzalez, A. Macias-Garcia, V. Gomez-Serrano, Thermal behaviour of lignocellulosic material in the presence of phosphoric acid. Influence of the acid content in the initial solution, Carbon 44 (2006) 2347-2350

67 P. Nowicki, H. Wachowska, R. Pietrzak, Active carbons prepared by chemical activation of plum stones and their application in removal of NO_2, Journal of Hazardous Materials 181 (2010) 1088-1094

68 H. Marsh, F. Rodriguez-Reinoso, Activated carbon, First ed., Elsevier Ltd., Oxford, 2006

69 W.M.A.W. Daud, W.S.W. Ali, Comparison on pore development of activated carbon produced from palm shell and coconut shell, Bioresource Technology 93 (2004) 63-69

70 A. Aygun, S. Yenisoy-Karakas, I. Duman, Production of granular activated carbon from fruit stones and nutshells and evaluation of their physical, chemical and adsorption properties, Microporous and Mesoporous Materials 66 (2003) 189-195

71 T.L. Kelly-Yong, K.T. Lee, A.R. Mohamed, S. Bhatia, Potential of hydrogen from oil palm biomass as a source of renewable energy worldwide, Energy Policy 35 (2007) 5692-5701

72 Y. Guo, D.A. Rockstraw, Activated carbons prepared from rice hull by one-step phosphoric acid activation, Microporous and Mesoporous Materials 100 (2007) 12-19

73 A.F. Martins, A.D.L. Cardoso, J.A. Stahl, J. Diniz, Low temperature conversion of rice husks, eucalyptus sawdust and peach stones for the production of carbon-like adsorbent, Bioresource Technology 98 (2007) 1095-1100

74 W.S.W. Ngah, M.A.K.M. Hanafiah, Removal of heavy metal ions from wastewater by chemically modified plant wastes as adsorbents: A review, Bioresource Technology 99 (2008) 3935-3948

75 J. Guo, W.S. Xu, Y.L. Chen, A.C. Lua, Adsorption of NH_3 onto activated carbon prepared from palm shells impregnated with H_2SO_4, Journal of Colloid and Interface Science 281 (2005) 285-290

76 S.H. Shuit, K.T. Tan, K.T. Lee, A.H. Kamaruddin, Oil palm biomass as a sustainable energy source: A Malaysian case study, Energy Volume 34 (2009) 1225-1235

77 S. Yusoff, Renewable energy from palm oil- innovation on effective utilization of waste, Journal of Cleaner Production 14 (2006) 87-93

78 S. Sumathi, S. Bhatia, K.T. Lee, A.R. Mohamed, Optimization of microporous palm shell activated carbon production for flue gas desulphurization: Experimental and statistical studies, Bioresource Technology 100 (2009) 1614-1621

79 Suhas, P.J.M. Carrott , M.M.L. R. Carrott, Lignin - from natural adsorbent to activated carbon: A review. Bioresource Technology 98 (2007) 2301-2312

80 M. Jagtoyen, F. Derbyshire, Activated carbons from yellow poplar and white oak by H_3PO_4 activation, Carbon 36 (1998) 1085-1097

81 K. Yang, J. Peng, H. Xia, L. Zhang, C. Srinivasakannan, S. Guo, Textural characteristics of activated carbon by single step CO_2 activation from coconut shells, Journal of the Taiwan Institute of Chemical Engineers Volume 41 (2010) 367-372

82 W.M.A.W. Daud, W.S.W. Ali, M.Z. Sulaiman, The effects of carbonization temperature on pore development in palm-shell-based activated carbon, Carbon 38 (2000) 1925-1932

83 R.C. Bansal, M. Goyal, Carbon Adsorption, CRC Press 2005, ISBN: 978-0-8247-5344-3

84 V. Minkova, M. Razvigorova, E. Bjornbom, R. Zanzi, T. Budinova, N. Petrov, Effect of Water Vapour and Biomass Nature on the Yield and Quality of the Pyrolysis Products from Biomass, Fuel Processing Technology, 70 (2001) 51-63

85 D. Savova, E. Apak, E. Ekinci, F. Yardim, N. Petrov, D. Budinova, M. Razvigorova, V. Minkova, Biomass Bioenergy 21 (2001) 133

86 A-N.A. El-Hendawy, Surface and adsorptive properties of carbons prepared from biomass, Applied Surface Science 252 (2005) 287-295

87 T. Kopac, A. Toprak, Preparation of activated carbons from Zonguldak region coals by physical and chemical activations for hydrogen sorption, International Journal of Hydrogen Energy 32 (2007) 5005-5014

88 M. Molina-Sabio, M.T. Gonzalez, F. Rodriguez-Reinoso, A. Sepulveda-Escribano, Effect of steam and carbon dioxide activation in the micropore size distribution of activated carbon, Carbon 34 (1996) 505-509

89 R. Azargohar, A.K. Dalai, Steam and KOH activation of biochar: Experimental and modeling studies, Microporous and Mesoporous Materials 110 (2008) 413-421

90 R. Arriagada, R. Garcia, M. Molina-Sabio and F. Rodriguez-Reinoso, Effect of steam activation on the porosity and chemical nature of activated carbons from *Eucalyptus globulus* and peach stones, Microporous Materials 8 (1997) 123-130

91 M. Ahmedna, W.E. Marshall, R.M. Rao, Surface properties of granular activated carbons from agricultural by-products and their effects on raw sugar decolorization, Bioresource Technology 71 (2000) 103-112

92 K. Gergova, A. Galushko, N. Petrov, V. Minkova, Investigation of the porous structure of activated carbons prepared by pyrolysis of agricultural by-products in a stream of water vapor. Carbon 30 (1992) 721-727

93 A.A. Attia, B.S. Girgis, N.A. Fathy, Removal of methylene blue by carbons derived from peach stones by H_3PO_4 activation: Batch and column studies, Dyes and Pigments 76 (2008) 282-289

94 H. Benaddi, T.J. Bandosz, J. Jagiello, J.A. Schwarz, J.N. Rouzaud, D. Legrasc, F. Beguin, Surface functionality and porosity of activated carbons obtained from chemical activation of wood, Carbon 38 (2000) 669-674

95 W.K. Lafi, Production of activated carbon from acorns and olive seeds, Biomass and Bioenergy 20 (2001) 57-62

96 M. Jagtoyen, F. Derbyshire, Activated carbons from yellow poplar and white oak by H_3PO_4 activation, Carbon 36 (1998) 1085-1097

97 P.J.M. Carrott , M.M.L.R. Carrott, P.A.M. Mourao, Pore size control in activated carbons obtained by pyrolysis under different conditions of chemically impregnated cork, Journal of Analytical and Applied Pyrolysis 75 (2006) 120-127

98 L-Y. Hsu, H. Teng, Influence of different chemical reagents on the preparation of activated carbons from bituminous coal, Fuel Processing Technology 64 (2000) 155-166

99 C. Moreno-Castilla, F. Carrasco-Marin, M.V. Lopez-Ramon, M.A. Alvarez-Merino, Chemical and physical activation of olive-mill waste water to produce activated carbons, Carbon 39 (2001) 1415-1420

100 Y. Nakagawa, M. Molina-Sabio, F. Rodriguez-Reinoso, Modification of the porous structure along the preparation of activated carbon monoliths with H_3PO_4 and $ZnCl_2$, Microporous and Mesoporous Materials 103 (2007) 29-34

101 M.C. Baquero, L. Giraldo, J.C. Moreno, F. Suarez-Garcia, A. Martinez-Alonso, J.M.D. Tascon, Activated carbons by pyrolysis of coffee bean husks in presence of phosphoric acid, Journal of Analytical and Applied Pyrolysis 70 (2003) 779-784

102 L.S. Chan, W.H. Cheung, G. McKay, Adsorption of acid dyes by bamboo derived activated carbon, Desalination 218 (2008) 304-312

103 B. Corcho-Corral, M. Olivares-Marin, C. Fernandez-Gonzalez, V. Gomez-Serrano, A. Macias-Garcia, Preparation and textural characterisation of activated carbon from vine shoots (*Vitis vinifera*) by H_3PO_4—Chemical activation, Applied Surface Science 252 (2006) 5961-5966

104 Y. Diao, W.P. Walawender, L.T. Fan, Activated carbons prepared from phosphoric acid activation of grain sorghum, Bioresource Technology 81 (2002) 45-52

105 R. Yavuz, H. Akyildiz, N. Karatepe, E. Cetinkaya, Influence of preparation conditions on porous structures of olive stone activated by H_3PO_4, Fuel Processing Technology 91 (2010) 80-87

106 J-W. Kim, M-H Sohn, D-S. Kim, S-M. Sohn, Y-S. Kwon, Production of granular activated carbon from waste walnut shell and its adsorption characteristics for Cu^{2+} ion, Journal of Hazardous Materials 85 (2001) 301-315

107 H. Demiral, G. Gunduzoglu, Removal of nitrate from aqueous solutions by activated carbon prepared from sugar beet bagasse, Bioresource Technology 101 (2010) 1675-1680

108 T-H. Liou, Development of mesoporous structure and high adsorption capacity of biomass-based activated carbon by phosphoric acid and zinc chloride activation, Chemical Engineering Journal 167 (2011) 148-154

109 M.Z. Hussein, R.S.H. Tarmizi, Z. Zainal, R. Ibrahim, Preparation and characterization of active carbons from oil palm shells, Carbon 34 (1996) 1447-1454

110 Z. Hu, M.P. Srinivasan, Mesoporous high-surface-area activated carbon, Microporoous and mesoporous materials 43 (2001) 267-275

111 J.N. Sahu, J. Acharya, B.C. Meikap, Optimization of production conditions for activated carbons from Tamarind wood by zinc chloride using response surface methodology, Bioresource Technology 101 (2010) 1974-1982

112 F. Boudrahem, F. Aissani-Benissad, H. Ait-Amar, Batch sorption dynamics and equilibrium for the removal of lead ions from aqueous phase using activated carbon developed from coffee residue activated with zinc chloride, Journal of Environmental Management 90 (2009) 3031-3039

113 L.C.A. Oliveira, E. Pereira, I.R. Guimaraes, A. Vallone, M. Pereira, J.P. Mesquitac, K. Sapag, Preparation of activated carbons from coffee husks utilizing $FeCl_3$ and $ZnCl_2$ as activating agents, Journal of Hazardous Materials 165 (2009) 87-94

114 M. Zabihi, A.H. Asl, A. Ahmadpour, Studies on adsorption of mercury from aqueous solution on activated carbons prepared from walnut shell, Journal of Hazardous Materials 174 (2010) 251-256

115 A.C. Lua, T. Yang, Characteristics of activated carbon prepared from pistachio-nut shell by zinc chloride activation under nitrogen and vacuum conditions, Journal of Colloid and Interface Science 290 (2005) 505-513

116 Z. Hu, H. Guo, M.P. Srinivasan, N. Yaming, A simple method for developing mesoporosity in activated carbon, Separation and Purification Technology 31 (2003) 47-52

117 N.R. Khalili, M. Campbell, G. Sandi, J. Golas, Production of micro- and mesoporous activated carbon from paper mill sludge I. Effect of zinc chloride activation, Carbon 38 (2000) 1905-1915

118 F. Caturla, M. Molina-Sabio, F. Rodriguez-Reinoso, Preparation of activated carbon by chemical activation with $ZnCl_2$, Carbon 29 (1991) 999-1007

119 Y.A. Alhamed, H.S. Bamufleh, Sulfur removal from model diesel fuel using granular activated carbon from dates' stones activated by $ZnCl_2$, Fuel 88 (2009) 87-94

120 A-N.A. El-Hendawy, An insight into the KOH activation mechanism through the production of microporous activated carbon for the removal of Pb^{2+} cations, Applied Surface Science 255 (2009) 3723-3730

121 B.H. Hameed, I.A.W. Tan, A.L. Ahmad, Preparation of oil palm empty fruit bunch-based activated carbon for removal of 2,4,6-trichlorophenol: Optimization using response surface methodology, Journal of Hazardous Materials 164 (2009) 1316-1324

122 J. Guo, Y. Luo, A.C. Lua, R-A. Chi, Y-L. Chen, X-T. Bao, S-X. Xiang, Adsorption of hydrogen sulphide (H_2S) by activated carbons derived from oil-palm shell, Carbon 45 (2007) 330-336

123 K. Okada, N. Yamamoto, Y. Kameshima, A. Yasumori, Porous properties of activated carbons from waste newspaper prepared by chemical and physical activation, Journal of Colloid and Interface Science 262 (2003) 179-193

124 A.C. Lua, T. Yang, Effect of activation temperature on the textural and chemical properties of potassium hydroxide activated carbon prepared from pistachio-nut shell, Journal of Colloid and Interface Science 274 (2004) 594-601

125 D. Adinata, W.M.A.W. Daud, M.K. Aroua, Production of carbon molecular sieves from palm shell based activated carbon by pore sizes modification with benzene for methane selective separation, Fuel Processing Technology 88 (2007) 599-605

126 B.K. Hamad, A.M. Noor, A.R. Afida, M.N. Mohd Asri, High removal of 4-chloroguaiacol by high surface area of oil palm shell-activated carbon activated with NaOH from aqueous solution, Desalination 257 (2010) 1-7

127 J. Guo, A.C. Lua, Adsorption of sulphur dioxide onto activated carbon prepared from oil-palm shells with and without pre-impregnation, Separation and Purification Technology 30 (2003) 265-273

128 J. Guo, A.C. Lua, Textural and chemical characterisations of activated carbon prepared from oil-palm stone with H_2SO_4 and KOH impregnation, Microporous and Mesoporous Materials 32 (1999) 111-117

129 A.C. Lua, Q. Jia, Adsorption of phenol by oil-palm-shell activated carbons, Adsorption (2007) 13 129-137

130 J. Guo, A.C. Lua, Preparation of activated carbons from oil-palm-stone chars by microwave-induced carbon dioxide activation, Carbon 38 (2000) 1985-1993

131 A.C. Lua, J. Guo, Activated carbon prepared from oil palm stone by one-step CO activation for gaseous pollutant removal, Carbon 38 (2000) 1089-1097

132 J. Guo, A.C. Lua, Effect of surface chemistry on gas-phase adsorption by activated carbon prepared from oil-palm stone with pre-impregnation, Separation and Purification Technology 18 (2000) 47-55

133 J. Guo, A.C. Lua, Characterization of adsorbent prepared from oil-palm shell by CO_2 activation for removal of gaseous pollutants, Materials Letters 55 (2002) 334-339

134 J. Guo, A.C. Lua, Microporous Activated Carbons Prepared from Palm Shell by Thermal Activation and Their Application to Sulfur Dioxide Adsorption, Journal of Colloid and Interface Science 251 (2002) 242-247

135 Q. Jia, A.C. Lua, Effects of pyrolysis conditions on the physical characteristics of oil-palm-shell activated carbons used in aqueous phase phenol adsorption, Journal of Analytical and Applied Pyrolysis 83 (2008) 175-179

136 Q. Jia, A.C. Lua, Concentration-dependent branched pore kinetic model for aqueous phase adsorption, Chemical Engineering Journal 136 (2008) 227-235

137 W.M.A.W. Daud, M.A. Ahmad, M.K. Aroua, Carbon molecular sieves from palm shell: Effect of the benzene deposition times on gas separation properties, Separation and Purification Technology 57 (2007) 289-293

138 A.A. Ahmad, B.H. Hameed, Effect of preparation conditions of activated carbon from bamboo waste for real textile wastewater, Journal of Hazardous Materials 173 (2010) 487-493

139 M.A. Ahmad, R. Alrozi, Optimization of preparation conditions for mangosteen peel-based activated carbons for the removal of Remazol Brilliant Blue R using response surface methodology, Chemical Engineering Journal 165 (2010) 883-890

140 M.A. Ahmad, R. Alrozi, Optimization of rambutan peel based activated carbon preparation conditions for Remazol Brilliant Blue Removal, Chemical Engineering Journal 168 (2011) 280-285

141 A.A. Ahmad, B.H. Hameed, A.L. Ahmad, Removal of disperse dye from aqueous solution using waste-derived activated carbon: Optimization study, Journal of Hazardous Materials 170 (2009) 612-619

142 A. Bacaoui , A. Yaacoubi, A. Dahbi, C. Bennouna, R.P.T. Luu, F.J. Maldonado-Hodar, J. Rivera-Utrilla, C. Moreno-Castilla, Optimization of conditions for the preparation of activated carbons from olive-waste cakes, Carbon 39 (2001) 425-432

143 I.A.W. Tan, A.L. Ahmad, B.H. Hameed, Optimization of preparation conditions for activated carbons from coconut husk using response surface methodology, Chemical Engineering Journal 137 (2008) 462-470

144 I.A.W. Tan, A.L. Ahmad, B.H. Hameed, Preparation of activated carbon from coconut husk: Optimization study on removal of 2,4,6-trichlorophenol using response surface methodology, Journal of Hazardous Materials 153 (2008) 709-717

145 J.M. Salman, B.H. Hameed, Effect of preparation conditions of oil palm fronds activated carbon on adsorption of bentazon from aqueous solutions, Journal of Hazardous Materials 175 (2010) 133-137

146 J. Guo, A.C. Lua, Textural and Chemical Characterizations of Adsorbent Prepared from Palm Shell by Potassium Hydroxide Impregnation at Different Stages, Journal of Colloid and Interface Science 254 (2002) 227-233

147 S. Karagoz, T. Tay, S. Ucar, M. Erdem, Activated carbons from waste biomass by sulfuric acid activation and their use on methylene blue adsorption, Bioresource Technology 99 (2008) 6214-6222

148 K. Gergova, N. Petrov, S. Eser, Adsorption properties and microstructure of activated carbons produced from agricultural by products by steam pyrolysis. Carbon 32 (1994) 693-702

149 Y. Guo, D.A. Rockstraw, Physicochemical properties of carbons prepared from pecan shell by phosphoric acid activation, Bioresource Technology 98 (2007) 1513-1521

150 A.C. Deiana, M.F. Sardella, H. Silva, A. Amaya, N. Tancredi, Use of grape stalk, a waste of the viticulture industry, to obtain activated carbon, Journal of Hazardous Materials 172 (2009) 13-19

151 J. Hayashi, T. Horikawa, I. Takeda, K. Muroyama, F.N. Ani, Preparing activated carbon from various nutshells by chemical activation with K2CO3, Carbon 40 (2002) 2381-2386

152 D. Kalderis, S. Bethanis, P. Paraskeva, E. Diamadopoulos, Production of activated carbon from bagasse and rice husk by a single-stage chemical activation method at low retention times, Bioresource Technology 99 (2008) 6809-6816

153 J. Laine, A. Calafat, M. Labady, Preparation and characterization of activated carbons from coconut shell impregnated with phosphoric acid, Carbon 27 (1989) 191-195

154 A. Klijanienko, E. Lorenc-Grabowska, G. Gryglewicz, Development of mesoporosity during phosphoric acid activation of wood in steam atmosphere, Bioresource Technology 99 (2008) 7208-7214

155 A. Reffas, V. Bernardet, B. David, L. Reinert, M.B. Lehocine, M. Dubois, N. Batisse, L. Duclaux, Carbons prepared from coffee grounds by H_3PO_4 activation: Characterization and adsorption of methylene blue and Nylosan Red N-2RBL, Journal of Hazardous Materials 175 (2010) 779-788

156 T. Liou, S-J. Wu, Characteristics of microporous/mesoporous carbons prepared from rice husk under base- and acid-treated conditions, Journal of Hazardous Materials 171 (2009) 693-703

157 F. Suarez-Garcia, A. Martinez-Alonso, J.M.D. Tascon, Pyrolysis of apple pulp: chemical activation with phosphoric acid, Journal of Analytical and Applied Pyrolysis 63 (2002) 283-301

158 T. Tay, S. Ucar, S. Karagoz, Preparation and characterization of activated carbon from waste biomass, Journal of Hazardous. Materials 165 (2009) 481-485

159 M.S. Solum, R.J. Pugmire, M. Jagtoyen, F. Derbyshire, Evolution of carbon structure in chemically activated wood, Carbon 33 (1995) 1247-1254

160 C.A. Toles, W.E. Marshall, M.M. Johns, Surface functional groups on acid-activated nutshell carbons, Carbon 37 (1999) 1207-1214

161 F. Suarez-Garcia, A. Martinez-Alonso, J.M.D. Tascon, Nomex polyaramid as a precursor for activated carbon fibres by phosphoric acid activation. Temperature and time effects, Microporous and Mesoporous Materials 75 (2004) 73-80

162 C.A. Toles, W.E. Marshall & M.M. Johns, Phosphoric acid activation of nutshells for metals and organic remediation: Process optimization, Journal of Chemical Technology & Biotechnology 72 (1998) 255-263

163 Q. Hu, J. Pang, Z. Wu, Y. Lu, Tuning pore size of mesoporous carbon via confined activation process, Letters to the Editor Carbon 44 (2006) 1298-1352

164 S. Lei, J-I Miyamoto, H. Kanoh, Y. Nakahigashi, K. Kaneko, Enhancement of the methylene blue adsorption rate for ultramicroporous carbon fiber by addition of mesopores, Carbon 44 (2006) 1884-1890

165 L.D. Fiorentin, D.E.G. Trigueros, A.N. Modenes, F.R. Espinoza-Quinones, N.C. Pereira, S.T.D. Barros, O.A.A. Santos, Biosorption of reactive blue 5G dye onto drying orange bagasse in batch system: Kinetic and equilibrium modeling, Chemical Engineering Journal 163 (2010) 68-77

166 I.I. Salame, T.J. Bandosz, Role of surface chemistry in adsorption of phenol on activated carbons, Journal of Colloid and Interface Science 264 (2003) 307-312

167 I.I. Salame, T.J. Bandosz, Surface Chemistry of Activated Carbons: Combining the Results of Temperature-Programmed Desorption, Boehm, and Potentiometric Titrations, Journal of Colloid and Interface Science 240 (2001) 252-258

168 H.P. Boehm, Chemical identification of surface groups: In: Advances in catalysis, vol. 16 New York: Academic Press (1966) 179-274

169 J.A. Menendez, J. Phillips, B. Xia, L.R. Radovic, On the modification and characterization of chemical surface properties of activated carbon: In the search of carbon with stable basic properties, Langmuir 12 (1996) 4404-4410

170 A.M. Puziy, O.I. Poddubnaya, A. Martinez-Alonso, A. Castro-Muniz, F. Suarez-Garcia, J.M.D. Tascon, Oxygen and phosphorus enriched carbons from lignocellulosic material, Carbon 45 (2007) 1941–1950

171 V. Fierro, V. Torne-Fernandez, D. Montaneb, A. Celzard, Adsorption of phenol onto activated carbons having different textural and surface properties, Microporous and Mesoporous Materials 111 (2008) 276-284

172 A. Kongsuwan, P. Patnukao, P. Pavasant, Binary component sorption of Cu(II) and Pb(II) with activated carbon from *Eucalyptus camaldulensis Dehn* bark, Journal of Industrial and Engineering Chemistry 15 (2009) 465-470

173 S. Karaca, A. Gurses, R. Bayrak, Investigation of applicability of the various adsorption models of methylene blue adsorption onto lignite/water interface, Energy Conversion and Management 46 (2005) 33-46

174 L.J. Kennedy, J.J. Vijaya, K. Kayalvizhi, G. Sekaran, Adsorption of phenol from aqueous solutions using mesoporous carbon prepared by two-stage process, Chemical Engineering Journal 132 (2007) 279-287

175 S. Kuo, R. Bembenek, Sorption and desorption of chromate by wood shavings impregnated with iron or aluminum oxide, Bioresource Technology 99 (2008) 5617-5625

176 A.A. Ahmad, B.H. Hameed, N. Aziz, Adsorption of direct dye on palm ash: Kinetic and equilibrium modeling, Journal of Hazardous Materials 141 (2007) 70-76

177 M. Dogan, H. Abak, M. Alkan, Adsorption of methylene blue onto hazelnut shell: Kinetics, mechanism and activation parameters, Journal of Hazardous Materials 164 (2009) 172-181

178 A.E. Ofomaja, Kinetics and mechanism of methylene blue sorption onto palm kernel fibre, Process Biochemistry 42 (2007) 16-24

179 A.J. Fletcher, Y. Yuzak, K.M. Thomas, Adsorption and desorption kinetics for hydrophilic and hydrophobic vapors on activated carbon, Carbon 44 (2006) 989-1004

180 L.A. Langley a, D.H. Fairbrother, Effect of wet chemical treatments on the distribution of surface oxides on carbonaceous materials, Carbon 45 (2007) 47-54

181 M. Kuang, G-H Yang, W-J Chen, Z-X Zhang, Study on mercury desorption from silver-loaded activated carbon fibre and activated carbon fibre, Journal of Fuel Chemistry and Technology 36(4), 468-473

182 K-I. Hatano, S. Kikuchi, T. Miyakawa, M. Tanokura, K. Kubota, Separation and characterization of the colored material from sugarcane molasses, Chemosphere 71 (2008) 1730-1737

183 J. Sanchez-Martina, M. Gonzalez-Velasco, J. Beltran-Heredia, J. Gragera-Carvajala, J. Salguero-Fernandez, Novel tannin-based adsorbent in removing cationic dye (Methylene Blue) from aqueous solution. Kinetics and equilibrium studies, Journal of Hazardous Materials 174 (2010) 9-16

184 B.H. Hameed, A.L. Ahmad, K.N.A. Latiff, Adsorption of basic dye (methylene blue) onto activated carbon prepared from rattan sawdust, Dyes and Pigments 75 (2007) 143-149

185 F. Raposo, M.A.D. La Rubia, R. Borja, Methylene blue number as useful indicator to evaluate the adsorptive capacity of granular activated carbon in batch mode: Influence of adsorbate/adsorbent mass ratio and particle size, Journal of Hazardous Materials, 165 (2009) 291-299

186 N. Kannan, M.M. Sundaram, Kinetics and mechanism of removal of methylene blue by adsorption on various carbons-a comparative study, Dyes and Pigments 51 (2001) 25-40

187 S. Karaca, A. Gurses, M. Acikyildiz, M. Ejder, Adsorption of cationic dye from aqueous solutions by activated carbon, Microporous and Mesoporous Materials 115 (2008) 376-382

188 B.H. Hameed, M.I. El-Khaiary, Removal of basic dye from aqueous medium using a novel agricultural waste material: Pumpkin seed hull, Journal of Hazardous Materials 155 (2008) 601-609

189 C.Y. Yin, M.K. Aroua, W.M.A.W. Daud, Review of modifications of activated carbon for enhancing contaminant uptakes from aqueous solutions, Separation and Purification Technology 52 (2007) 403-415

190 Y. Zou, B-X Han, Preparation of Activated Carbons from Chinese Coal and Hydrolysis Lignin, Adsorption Science Technology 19 (2001) 59-72

191 S. Senthilkumaar, P.R. Varadarajan, K. Porkodi, C.V. Subbhuraam, Adsorption of methylene blue onto jute fiber carbon: kinetics and equilibrium studies, Journal of Colloid and Interface Science 284 (2005) 78-82

192 J. Yenera, T. Kopaca, G. Dogub, T. Dogu, Dynamic analysis of sorption of Methylene Blue dye on granular and powdered activated carbon, Chemical Engineering Journal 144 (2008) 400-406

193 I.A.W. Tan, A.L. Ahmad, B.H. Hameed, Adsorption of basic dye using activated carbon prepared from oil palm shell: batch and fixed bed studies, Desalination 225 (2008) 13-28

194 G. Vidal, A. Carvalho, R. Mendez, J.M. Lema, Influence of the content in fats and proteins on the anaerobic biodegradability of dairy wastewaters, Bioresource Technology 74 (2000) 231-239

195 B. Sarkar, P.P. Chakrabarti, A. Vijaykumar, V. Kale, Wastewater treatment in dairy industries - possibility of reuse, Desalination 195 (2006) 141-152

196 E.V. Ramasamy, S.A. Abbasi, Energy recovery from dairy waste-waters: impacts of biofilm support systems on anaerobic CST reactors, Applied Energy 65 (2000) 91-98

197 W. Janczukowicz, M. Zielinski, M. Debowski, Biodegradability evaluation of dairy effluents originated in selected sections of dairy production, Bioresource Technology 99 (2008) 4199-4205

198 M.R. Kosseva, C.A. Kent, D.R. Lloyd, Thermophilic bioremediation strategies for a dairy waste, Biochemical Engineering Journal 15 (2003) 125-130

199 B. Demirel, O. Yenigun, T.T. Onay, Anaerobic treatment of dairy wastewaters: a review, Process Biochemistry 40 (2005) 2583-2595

200 J.R. Banu, S. Anandan, S. Kaliappan, I-T. Yeom, Treatment of dairy wastewater using anaerobic and solar photocatalytic methods, Solar Energy 82 (2008) 812-819

201 J.P. Kushwaha, V.C. Srivastava, I.D. Mall, Treatment of dairy wastewater by commercial activated carbon and bagasse fly ash: Parametric, kinetic and equilibrium modelling, disposal studies, Bioresource Technology 101 (2010) 3474-3483

202 I.A. Sengil, M. Ozacar, Treatment of dairy wastewaters by electrocoagulation using mild steel electrodes, Journal of Hazardous Materials B137 (2006) 1197-1205

203 M. Frappart, O. Akoum, L.H. Ding, M.Y. Jaffrin, Treatment of dairy process waters modelled by diluted milk using dynamic nanofiltration with a rotating disk module, Journal of Membrane Science 282 (2006) 465-472

204 T. Jihen, B. Hassib, H. Moktar, N. Said, Improvement of dairy manufacture effluent anaerobic digestion with biological waste addition using a Chinese dome digester, Bioresource Technology 101 (2010) 3743-3746

205 L.J. Kennedy, K.M. Das, G. Sekaran, Integrated biological and catalytic oxidation of organics/inorganics in tannery wastewater by rice husk based mesoporous activated carbon—Bacillus sp., Carbon 42 (2004) 2399-2407

206 M.C.M.R. Leal, D.M.G. Freire, M.C. Cammarota, G.L. Sant'Anna Jr., Effect of enzymatic hydrolysis on anaerobic treatment of dairy wastewater, Process Biochemistry 41 (2006) 1173-1178

207 L. Loperena, M.D. Ferrari, A.L. Diaz, G. Ingold, L.V. Perez, F. Carvallo, D. Travers, R.J. Menes, C. Lareo, Isolation and selection of native microorganisms for the aerobic treatment of simulated dairy wastewaters, Bioresource Technology 100 (2009) 1762-1766

209 D. Mazumder, B. Roy, Low cost options for treatment and reuse of municipal wastewater. Indian Journal of Environmental Protection, 20 (2000) 529-532

210 R. Devi, R.P. Dahiya, COD and BOD removal from domestic wastewater generated in decentralised sectors, Bioresource Technology 99 (2008) 344-349

211 M.L. Hami, M.A. Al-Hashimi, M.M. Al-Doori, Effect of activated carbon on BOD and COD removal in a dissolved air flotation unit treating refinery wastewater, Desalination 216 (2007) 116-122

212 I.S. Arvanitoyannis, A. Kassaveti, Dairy Waste Management: Treatment Methods and potential Uses of Treated Waste, Waste Management for the Food Industries (2008) 569-628

213 C. Ng, J.N. Losso, W.E. Marshall, R.M. Rao, Freundlich adsorption isotherms of agricultural by-product-based powdered activated carbons in a geosmin-water system, Bioresource Technology 85 (2002) 131-135

214 I.A.W. Tan, A.L. Ahmad, B.H. Hameed, Adsorption of basic dye on high-surface-area activated carbon prepared from coconut husk: Equilibrium, kinetic and thermodynamic studies, Journal of Hazardous Materials 154 (2008) 337-346

215 S. Largegren, About the theory of so-called adsorption of soluble substances. Kungliga Suensk Vetenskapsakademiens Handlingar 241 (1898) 1-39

216 W.J. Weber Jr., J.C. Morris, Kinetics of adsorption on carbon from solution. Journal Sanitary Engineering Division, American Society of Civil Engineers 89 (1963) 31-59

217 A.C. Lua, J. Guo, Preparation and characterization of activated carbons from oil-palm stones for gas-phase adsorption, Colloids and Surfaces A: Physicochemical and Engineering Aspects 179 (2001) 151–162

218 M.A. Ahmad, W.M.A.W. Daud, M.K. Aroua, Synthesis of carbon molecular sieves from palm shell by carbon vapor deposition, Journal of Porous Materials 14 (2007) 393-399

219 I.A.W. Tan, A.L. Ahmad, B.H. Hameed, Adsorption of basic dye using activated carbon prepared from oil palm shell: batch and fixed bed studies, Desalination 225 (2008) 13-28

CHAPTER III

EXPERIMENT AND METHODOLOGY

3.1 Introduction

This section describes the materials, experimental methodology, statistical tool, textural characterization, adsorption and reagent recovery. It also describes the observations in the experiment.

3.2 Materials

3.2.1 Precursor

The precursor, palm shell generated from the process line of palm oil mill, provided by Nam Bee Oil Palm Estate Sdn Bhd, had been utilized for experiments. The palm shells were water washed and dried at 105 °C in a hot air oven until it is completely dry, which were then crushed, sieved to various sizes and stored in airtight containers for further experimentation.

Table 3.1(a) and (b) summarizes the various reports on proximate and ultimate analyses of palm shell, its char and PSAC. C and O are the most important element in raw palm shell, which constitute to more than 90% of total weight. The balance of weight is made of H, N and a trace amount of S. The ash content in palm shell is low, highlighting its suitability for production of activated carbon.

3.2.2 Chemical

Analytical grade H_3PO_4, supplied by Sigma-Aldrich (M) Sdn Bhd, was used without further purification as chemical reagent. The H_3PO_4 was diluted from original 85% (wt/wt) to 65% to be used as the standard concentration for the entire experiment. At 65%, H_3PO_4 is easier to handle as its viscosity is relatively lower. In addition, H_3PO_4 at such concentration has been reported to promote a higher adsorption into the precursor than at 85% [14].

Table 3.1 Reported (a) proximate analysis and (b) ultimate analysis of palm shell (on dry basis and value is in wt %).

a) Proximate analysis

Volatile matter	Fixed carbon	Ash	Ref
80.8	17.3	1.9	[1,2]
79.4	19.6	1.0	[3]
78.7	20.3	1.2	[4,5,6]
77.6	19.8	2.6	[6,7,8,9,10,11,12,13]

b) Ultimate analysis

C	H	O	N	Ref
53.7	5.6	40.5	0.2	[13]
50.1	6.8	41.2	1.9	[3]
50.0	6.9	41.0	1.9	[4,5,6]

3.2.3 Adsorbates

Analytical grade MB supplied by Sigma-Aldrich (M) Sdn Bhd, was used without further purification as dye adsorbate. The powdery form of MB was dissolved into distilled water before being used for adsorption investigation. A series of MB solution at different concentrations ranging from 1 mg/L to 10 mg/L were prepared and the concentration-adsorption calibration curve. 10 ml of each MB solution were placed in a standard optical-glass cells and the absorbance reading were determined using a UV-Visible spectrophotometer (Hach DR2800, Fig. 3.1) at a wavelength corresponding to the maximum

absorbance, 665 nm. A calibration graph was obtained by plotting the initial MB concentration, C_0 against absorbance reading (Appendices 1).

A standard dairy COD was prepared by dissolving milk based cream powder (Nestle creamer) in distilled water. Similar methods of making dairy COD were reported by several investigators [15,16,17,18,19]. The concentrations of dairy waste were measured in terms of COD value. The measurement of COD requires reaction between the adsorbate with specific reagent. For each measurement, 2.00 mL of samples were pipetted into the reagent vials. The mixture together with the vial was then heated at reactor (as shown in Fig. 3.2) at 150 °C for 120 min. The cooled vials were subsequently inserted into 16-mm cell holder in the spectrophotometer (Fig. 3.1). A wavelength of 620 nm was used to measure the COD concentration. Various concentration of dairy COD were subsequently obtained via dilution with appropriate portion of distilled water and these samples were maintained uniformly throughout the investigations in order to retain the feed characteristics.

Fig. 3.1. Spectrophotometer

Fig. 3.2. COD Reactor

3.3 Experiment methodology and procedure

3.3.1 Response surface methodology (RSM)

The Design of Experiment (DOE) method selected was the Response Surface Methodology (RSM) as this optimization tool allows the development of mathematical models that permits assessment of the relevance as well as statistical significance of the factor effects being studied. The tool also valuates the interaction effects between these factors [20]. The multivariate optimization schemes involve designs for which the levels of all the variables are changed simultaneously. During the multivariate optimization procedure, there are two types of variables: the responses and the factors. These responses are the dependent variables and their values depend on the levels of the factors. Amongst the various methods, Box-Behnken Design (BBD) was chosen over the more popular Central Composite Design method (CCD). BBD required less numbers of experiments relatively than CCD. Furthermore, due the range

selected in this research, it is physically impossible to conduct some experiments using CCD due to combinations of which all factors are simultaneously at their highest or lowest limit (for instance, activation time = -30 min). In addition, Ferreira et al. [21] has demonstrated that BBD is a more efficient method than CCD.

3.3.1.1 Box-Behnken Design

Box-Behnken designs (BBD), a class of rotatable or nearly rotatable second-order designs based on three-level incomplete factorial designs [22]. For 3 factors its graphical representation can be seen in two forms:

1. A cube that consists of the central point and the middle points of the edges, as can be observed in Fig. 3.3(a).
2. A figure of three interlocking 2^2 factorial designs and a central point, as shown in Fig. 3.3(b).

The number of experiments (N) required for the development of BBD is defined as $N=2k(k-1)+C_0$, (where k is number of factors and C_0 is the number of central points). For comparison, the number of experiments for a central composite design is $N=2k+2k+C_0$. A 2^3 factorial design, with 5 replicates at the centre point with total number of 17 trials were employed. The coded factor level for this Box-Behnken design was given in Table 3.2. 3 variables X_1 (impregnation ratio), X_2 (activation temperature) and X_3 (activation time), were selected and further optimized using Box–Behnken design in RSM to determine the exact optimal values of the individual factors that demonstrate desired yield-porosity quality. The coded and uncoded values of the variables at various levels are given in Table 3.3.

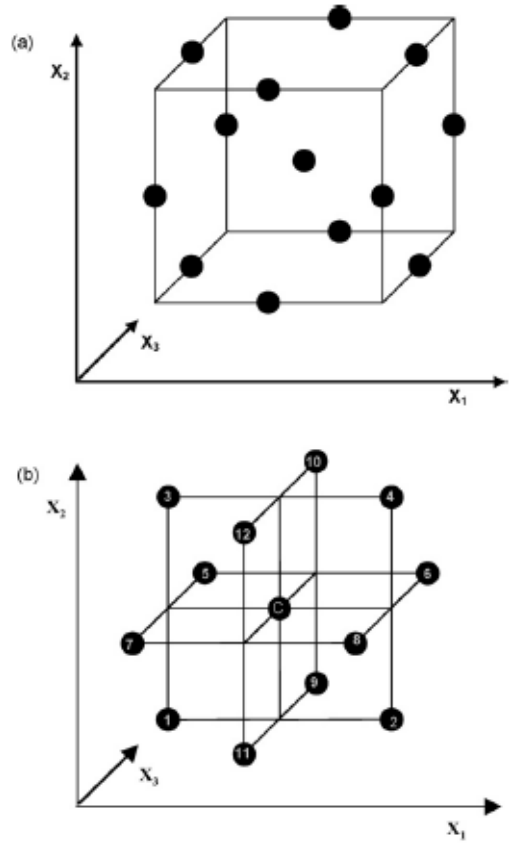

Fig. 3.3. (a) & (b) the cube and three interlocking 2^2 factorial design for Box-Behnken Design

Table 3.2 Coded factor levels for a Box Behnken Design of a three-variable system (with 5 replicas at centre)

No	X_1	X_2	X_3
1	-1	-1	0
2	1	-1	0
3	-1	1	0
4	1	1	0
5	-1	0	-1
6	1	0	-1
7	-1	0	1
8	1	0	1
9	0	-1	-1
10	0	1	-1
11	0	-1	1
12	0	1	1
C	0	0	0
C	0	0	0
C	0	0	0
C	0	0	0
C	0	0	0

Table 3.3 Coded and real concentration values of the independent variables

Coded value	Real value of variables		
	Impregnation ratio	Activation temperature	Activation time
(level)	wt H_3PO_4/wt PS	°C	min
-1	0.50	350	30
0	1.75	425	75
+1	3.00	500	120

The experimental results obtained in PSAC generation are presented in format as shown in Table 3.4. For statistical calculation, the relationships between the coded and actual values are described as following equation:

$$X_i = (A_i + A_o)/\Delta A_i$$

Where X_i is a coded value of the variables;

A_i the actual values of variables;

A_o the actual values of the A_i at the centre points;

ΔA the step change of variable

A non-linear computer-generated quadratic model as given in Eq. (3.1) was used for preliminary regression fits. Linear, interaction and quadratic effects of the factors were considered in this model. Coefficients of the respective effects were represented by β

$$Y = \beta_0 + \beta_1 x_1 + \beta_2 x_2 + \beta_3 x_3 + \beta_{11} x_1^2 + \beta_{22} x_2^2 + \beta_{33} x_3^2 + \beta_{12} x_1 x_2 + \beta_{13} x_1 x_3 + \beta_{23} x_2 x_3 \quad (3.1)$$

where Y is the predicted response, β_0 is a offset term, β_1 , β_2 *and* β_3 are linear offsets, β_{11} ,β_{22} *and* β_{33} are squared offset, β_{12} , β_{13} and β_{23} are interaction effect and x_i is dimensionless coded

value of X_i. Statistical software package Design-Expert (Version 6.0, State-Ease, USA) was used. Root Mean Square Error (RMSE) was calculated using the following formula, Eq. (3.2) [2]:

$$\mathrm{RMSE} = \sqrt{\frac{\sum_0^{\mathrm{N}}(\mathrm{Exp.}-\mathrm{Pred.})^2}{N}} \qquad (3.2)$$

Where Exp. is the experimental value, Pred. is the predicted value from model equations and *N* is the total number of experiments.

3.3.1.2 Analysis of variance (ANOVA)

Regression analysis and ANOVA has been utilized for fitting the model and examining the statistical significance of the model terms. The statistical tool is available in the mentioned software. The results of the second-order response surface model fitting were evaluated in the form of ANOVA. Subsequently, a mathematical regression model for responses of BET surface area (Y_1), pore volume (Y_2), average pore diameter (Y_3) and PASC yield (Y_4), could be calculated based on Eq. (3.1). The F-test, t-test, R^2, 3D response surface and 2D contour plots, etc. were examined to evaluate the model as well as to determine the optimum process conditions.

The *F*-value (the Fisher variance ratio) was used to statistically measure how well the factors describe the variation of the data about the mean. This analysis showed the discrepancy of the *F*-value from unity. The further the *F*-value was from unity, the more certain it was that the factors explain adequately the variation in the data about the mean, and the estimated factor effects are real. The analysis of each model term, was able to study the significance of the

linear effect (x_1, x_2, x_3), quadratic effects (x_1^2, x_2^2, x_3^2) and interaction effects ($x_1 x_2$, $x_1 x_3$, $x_2 x_3$) to the mathematical model generated.

The accuracy of the modeling was evaluated by the determination coefficient (R^2) and the adjusted determination coefficient R^2_{Adj}. In this context, a high value of R^2 would indicate the more the variability in the response could be explained by the model. In addition, a high value of R^2_{Adj} would also indicate a high level of significance for the model. A close R^2_{Adj} value is to unity is desired as it indicates the better the model fit the experimental data and hence, the smaller the difference between the predicted and observed values [23]

3.3.2 Palm shell activated carbon development

3.3.2.1 Impregnation of palm shell with H_3PO_4

Dried palm shell was impregnated with a predetermined amount of H_3PO_4 solution, 65 %(wt/wt) to achieve an desired IR. For example, 46.15 mL of 65% H_3PO_4 to 10 g palm shell for IR of 3. The H_3PO_4 soaked samples were left overnight and the excess water was evaporated in oven at 100 °C to ensure complete absorbance of the H_3PO_4 on to the palm shell particles.

Table 3.4 Box-Behnken Design: Experimental conditions

Run	Impregnation ratio		Activation temperature		Activation time		BET surface area	Pore volume	Average pore diameter
#	($wt_{H3PO4}/wt_{palm\ shell}$)		(°C)		(min)		Y_1 (m^2/g)	Y_2 (cm^3/g)	Y_3 (nm)
	X_1	Coded	X_2	Coded	X_3	Coded			
1	0.5	-1	425	0	120	1			
2	0.5	-1	500	1	75	0			
3	0.5	-1	425	0	30	-1			
4	0.5	-1	350	-1	75	0			
5	1.75	0	350	-1	30	-1			
6	1.75	0	500	1	120	1			
7	1.75	0	500	1	30	-1			
8	1.75	0	350	-1	120	1			
9	3	1	350	-1	75	0			
10	3	1	500	1	75	0			
11	3	1	425	0	120	1			
12*	3	1	425	0	30	-1			
13*	1.75	0	425	0	75	0			
14*	1.75	0	425	0	75	0			
15*	1.75	0	425	0	75	0			
16*	1.75	0	425	0	75	0			
17*	1.75	0	425	0	75	0			

*The centre point was replicated 5 times to estimate the experimental errors

3.3.2.2 Semi-carbonization

The acid soaked samples were semi-carbonised in a hot air oven (OSAW Industrial) at a preset furnace temperature of 170 °C for 1 h. This low temperature heat treatment method enables the partial release of volatile matter without the loss of carbon content.

3.3.2.3 Activation

The semi-carbonised material was activated in a muffle furnace (Protherm Furnace, PLF120/5) at a desirable activation temperature between 350 and 500 °C (for 30 to 120 min) under self-generated atmosphere. The feasibility and benefits of using 2-stage chemical activation method in a self-generated atmosphere are well documented in literature [24,25,26,27,28]. After activation, the samples were washed repetitively with distilled water

to remove residual acid. The completeness of washing process is confirmed with the conductivity of wash liquor less than 50 μS, using conductivity meter. The final product was air dried at 105 °C, before being manually ground to fine powder. Sieved to a size below 120 μm, these PSAC were utilized for product characterisation. Fig. 3.4 (a), (b) and (c) shows the physical states of palm shell, its char and PSAC.

Fig. 3.4. (a) Palm shell (b) semi-carbonised char and (c) palm shell activated carbon.

3.3.3 Characterisation methods

Palm shell, its chars and activated carbon was subjected to textural characterisation to study its chemical composition, surface area, pore volume, surface textural and pore characteristics.

3.3.3.1 BET surface area and pore structure analysis

Pore structure of the AC was characterized by N_2 adsorption at -196 °C with an accelerated surface area porosimetry system (Micromeritics, ASAP 2020). Prior to gas adsorption measurements, the carbon was degassed at 300 °C in a vacuum condition for a period of at least 2 h. N_2 adsorption isotherm is measured over a relative pressure (P/P_0) range from approximately 10^{-7} to 1. The BET surface area is calculated from the isotherms by using the Brunauer-Emmett-Teller (BET) equation [29]. The cross-sectional area of N_2 molecule is

assumed to be 0.162 nm. The Dubinin–Radushkevich (DR) method is used to calculate the micropore volume [30].

3.3.3.2 Particle size distribution analysis

The pore size distribution is ascertained by Non-local Density Functional Theory (NLDFT) [31] by minimising the grand potential as a function of the fluid density profile. The total pore volume [32] is estimated by converting the amount of N_2 gas adsorbed at a relative pressure of 0.99 to the equivalent liquid volume of the adsorbate (N_2). The mesopore volume is estimated by the subtracting the micropore volume from the total volume.

3.3.3.3 Thermogravimetric analysis (TGA)

Thermogravimetric analysis (TGA) was performed on palm shell, its chars and activated carbon with a thermogravimetric analyser (TA Instrument, Universal Analysis 2000 as shown in Fig. 3.5). In this analysis a sample is exposed to a temperature program (i.e. with a constant heating rate) while a balance detects weight changes [33]. All the samples were analysed at heating rate of 10 °C/min in an atmosphere of N_2 gas with a constant purge flow of 40 mL/min. Residual and derivative weight of the sample with respect to time and temperature were recorded.

3.3.3.4 Fourier transform infrared analysis (FT-IR)

The presence of surface functional groups and structure of palm shell, its char and PSAC were investigated using Fourier transform infrared (FT-IR) analyser (Thermo Scientific Nicolet iS10, shown in Fig. 3.6). The char and PSAC were ground in a mortar to fine powder (<100 um) before they were mixed with KBr by a weight ratio of 700:1. The disc containing

the mixture was then placed inside the analysis chamber and the IR spectrum is obtained over a frequency between 500 and 4000 cm^{-1}.

Fig. 3.5. Thermogravimetric analyser

Fig. 3.6. Fourier transform infrared spectroscope (FT-IR)

3.3.3.5 X-ray diffraction (XRD)

X-ray diffraction (XRD) analysis of samples was performed by using XRD facility at the COMBICAT Research centre of Universiti Malaya.

3.3.5.6 Scanning electron microscopy (SEM)

SEM analysis of samples was performed by using scanning electron microscope facility at the COMBICAT Research centre of Universiti Malaya.

3.4 Adsorption

Adsorption investigations were conducted on 2 different adsorbates, methylene blue (MB) and dairy COD. The selections of these materials were based on their significant presence in industrial wastewater in Malaysia. In addition, both species form large organic chain and could only be effectively remove by activated carbon with sizeable average pore diameter such as mesopores, a key research interest of PSAC produced in this work.

3.4.1 Adsorption isotherm

The adsorption isotherm experiments were conducted with a fixed amount of 0.2 g of PSAC mixed with 100 mL MB or dairy COD solutions of various concentrations ranging from 600 to 1400 mg/L for MB (200 to 2000 mg/L for dairy COD) in the isothermal shaker bath (Fig. 3.7) for 24 hours at constant temperature of 30, 40 and 50 °C without altering the pH of the adsorbate solution. Preliminary experiments were carried out to ensure that the adsorption process reached equilibrium within 24 hours. The amount of MB and dairy COD adsorbed by the PSAC is estimated based on the difference in the concentration of the adsorbates before and after completion of the experiment, with simple mass balance. The MB and dairy COD

concentrations were measured using a spectrophotometer at respectively wavelength as discussed in Section 3.2.3.

Fig. 3.7. Isothermal shaker bath

3.4.2 Effect of pH on adsorption isotherm

The effect of pH on MB and dairy COD adsorption was examined with the initial pH range of 1-14. The initial pH of the solution is adjusted by using 0.1N HCl or 0.1N NaOH. Dose of 0.2 g PSAC is added to 100 mL of solution having 1400 mg/L of MB and 800 mg/L dairy COD into 250-mL Erlenmeyer flasks. The flasks are then capped and constantly shaken in isothermal shaker at 100 Hz and 30 °C for 24 h. The pH is measured using a pH meter (Ecoscan, EUTECH Instruments).

3.4.3 Adsorption kinetics

The adsorption kinetics experiments were conducted with a fixed PSAC dose of 0.2 g at constant temperature and pH (30 °C and pH 7) with initial MB and dairy COD concentration of 600, 800 and 1200 mg/L. The change in concentration of the MB and dairy COD bath was monitored at intervals of time until no significant change in the concentration of the MB and dairy COD bath is observed. A significant variation in the concentration of the bath is observed until an adsorption time of only 120 min; the experiments were continued for duration of 240 min.

3.5 Reclaimed H_3PO_4 activation

H_3PO_4 were reclaimed and reused for successive activation in order to assess the effect of the reclaimed acid on the characteristics of the PSAC in the successive runs. The excess water in the reclaimed H_3PO_4 was removed by evaporation in oven (100 °C). Water fraction in the reclaimed reagent is slowly reduced by evaporating the H_3PO_4-water solution until it reached an original volume of 26.92 ml. H_3PO_4 recovery is calculated using below formula:

% H_3PO_4 recovery = (Weight of product of activation before washing - weight of dried product of activation after acid recovery)/ Weight of H_3PO_4 impregnated

The reclaimed H_3PO_4 was subsequently reused for palm shell activation. The IR in all the reclaimed runs were maintained constant at the desirable value of 1.75, by suitably reducing the weight of palm shells, in accordance with the reduction in loss of H_3PO_4 in the previous run. Experiments are carried out for 3 successive runs using the reclaimed reagents.

3.6 Observations

3.6.1 Palm shell activated carbon development

a) H_3PO_4 concentration: Investigations were conducted using the various H_3PO_4 concentrations for palm shell impregnation. At original concentration of 85% (wt/wt), H_3PO_4 is found to be high in viscosity and does not mixed thoroughly with palm shell especially for low IR of 0.5. At such, some palm shell particles were not "wetted" (as observed in changing to darker colour) and thoroughly impregnated by the reagent. Furthermore, substantiate with the disadvantages as highlighted in section 3.2.2, H_3PO_4 at 85% was not selected as the reagent preparation conditions. On the other hand, H_3PO_4 at 40% has relatively lower viscosity and mixed thoroughly with palm shell particles. It reacted well and produced PSAC with similar characterisation with of H_3PO_4 at 65% at a particular IR. Table 3.5 describes the BET surface areas of PSAC produced under various process conditions using H_3PO_4 at 65% and 45% concentration. As shown, the outcome of PSAC did not show much variation with the reagent concentration. It was observed that a much longer drying duration (at 100 °C in the oven) is required for H_3PO_4 at 45% due to the higher amount of water in the mixture. As such, the feasibility of using H_3PO_4 at 65% has been verified and was used for all PSAC preparation.

b) Palm shell particle size: The influence of palm shell particle size ranging between <1.0 mm to 4.0 mm were investigated at 2 different process conditions. The BET surface area, total pore volume and PSAC yield of these samples are shown in Table 3.6. Under similar process conditions, no appreciable differences observed on the BET surface are and total pore volume for PSAC prepared using palm shell particle between <1.0, 2.0-2.5 and 3.0-4.0 mm. This is in agreement with works by Lua and Guo in CO_2 activation of PSAC [1]. However, the PSAC yield is found to be lower for particle size <1.0 mm. This observation is more evident with the increase of activation temperature; due to the increase in oxidation from its

much larger unit surface area. Hence, palm shell with particle size fraction of 2.0-2.5 mm was selected for subsequent studies as preparation conditions for this work.

c) Impregnation ratio (IR): The influence of IR were assessed for range 0.5-4.0 and the results are presented in Fig. 3.8. The BET surface area increased with an increasing IR up to 2.5. However, the BET surface area started to decrease slightly at IR 3.0 before drop marginally at IR 4.0. It was observed from the mixing that amount of H_3PO_4 begins to be in excess upon IR 2.5. Excessive impregnation of H_3PO_4 as observed in IR 4.0 resulted in undesired oxidation and thus reduce the BET value and PSAC yield.

d) Activation temperature: H_3PO_4 has been associated with low temperature activation in comparison with other reagents such as KOH and $ZnCl_2$. Investigation on influence of temperature on PSAC were conducted for temperatures between 350, 400, 500 and 600 °C and the BET surface area and PSAC yield of the samples is shown as Fig. 3.9. It was observed that the BET surface area increased with temperature up to 500 °C before deteriorated significantly at 600 °C. PSAC yield was found to decrease slightly (between 350 and 500°) but reduced significantly at 600 °C. Hence, RSM analyses were made using 350 and 500 °C as the investigation limits.

Table 3.5 BET surface area of PSAC activated at different IR

Impregnation ratio (wt_{H3PO4}/wt_{PS})	H_3PO_4 concentration (%)	Temperature (°C)	Time (min)	BET surface area (m^2/g)
0.5	45	425	120	733
0.5	65	425	120	725
1.75	45	425	75	1521
1.75	65	425	75	1508
3.0	45	500	75	1562
3.0	65	500	75	1965

Table 3.6 BET surface area, total pore volume and yield of PSAC activated at various particle sizes of palm shell

Activation condition (IR/temperature/time)	Particle size (mm)	BET surface area (m^2/g)	Total pore volume (cm^3/g)	PSAC Yield (%)
0.50/425/120	<1.0	733	0.41	45
0.50/425/120	2.0-2.5	725	0.38	46
0.50/425/120	3.0-3.5	712	0.37	46
1.75/425/75	<1.0	1511	1.24	41
1.75/425/75	2.0-2.5	1508	1.25	48
1.75/425/75	3.0-3.5	1499	1.24	47
3.0/425/120	<1.0	1948	1.82	39
3.0/425/120	2.0-2.5	1965	1.91	45
3.0/425/120	3.0-3.5	1958	1.88	43

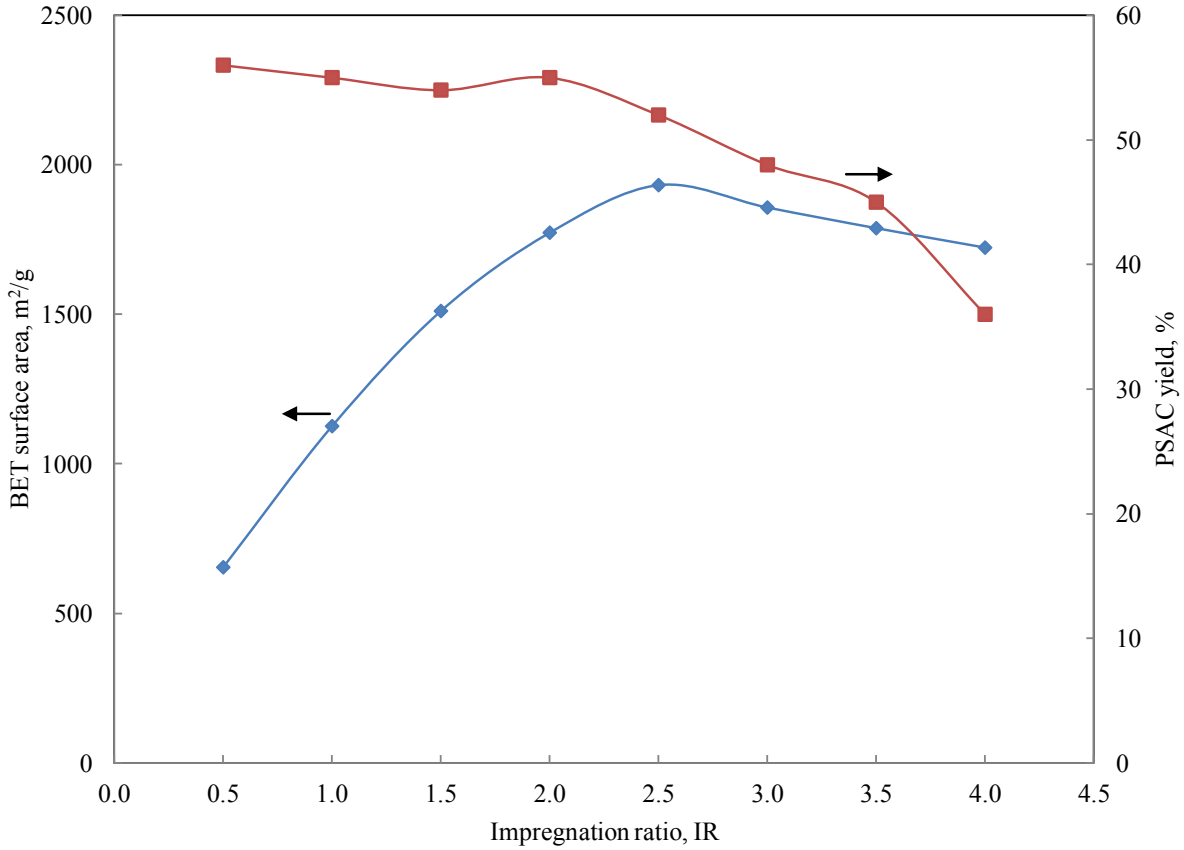

Fig. 3.8. BET surface area and yield of PSAC at IR 0.5-4.0

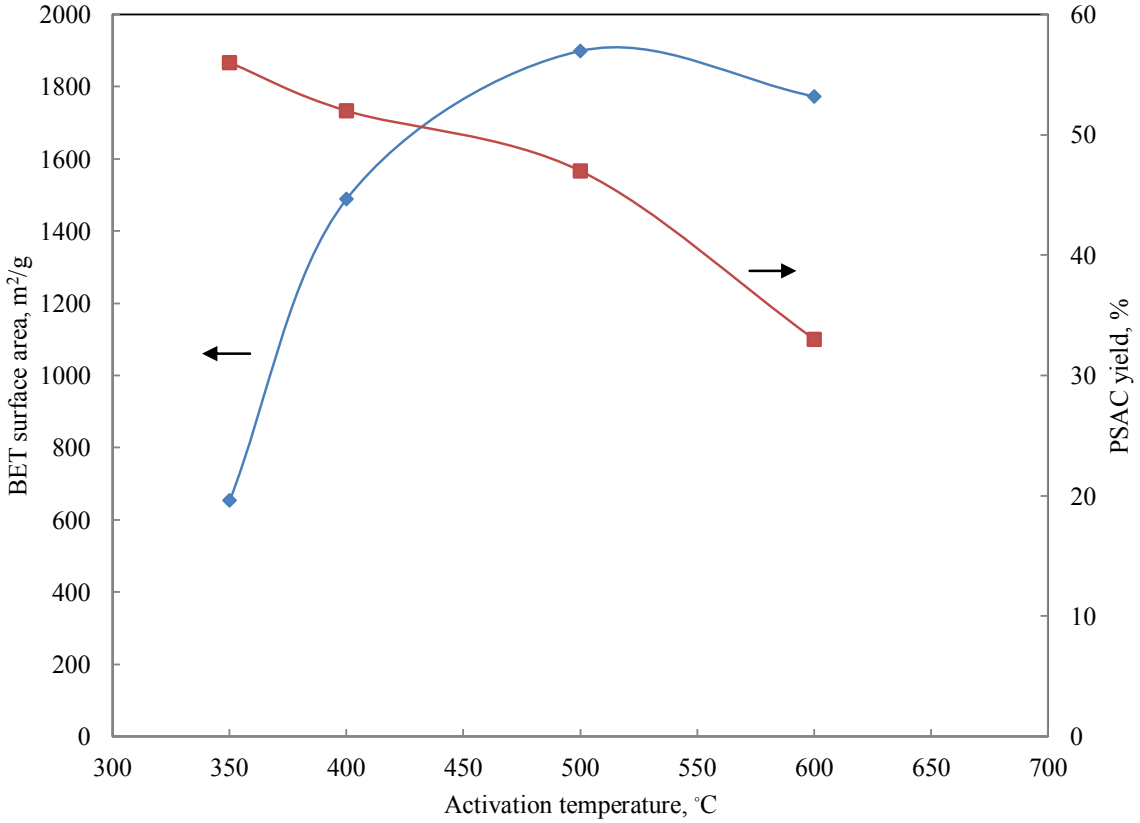

Fig. 3.9. BET surface area and yield of PSAC at activation temperature 350-600 °C

f) Semi-carbonization: The volume of palm shell-H_3PO_4 mixture was found to shrink upon semi-carbonization at 170 °C. Besides of the loss of residue moisture, these volumetric reductions are due to the release of primary volatile matters. The palm shell particle structure is found to be much weaker and could be crushed with light pressing, indicating that semi-carbonization result in reaction take place on the basic structure of palm shell. The effect is more significant with increase of activation temperature and IR.

g) Activation under self-generate atmosphere: White smoke was found to be released from the vent of the furnace immediately after the semi-carbonised palm shell-H_3PO_4 mixture were activated in muffle furnace. These white smokes consist of gaseous volatile matters from activation and the discharge is found to increase to a peak before decreasing gradually to a

stage no visible smoke being released. This signifies the release of most of the volatile matter and activation is focus on the pore generations.

h) Washing of activated complex: Water temperature was found to increase when the activated mixture is added with water. This is due to the exothermic process of H_3PO_4 hydrolysis. The conductivity of the liquor was found to increase significantly with pH reduced to extreme acidic zone (pH <1). These observations were due to the dissociation of the H_3PO_4 molecules in water to produce hydrogen ion and polyphosphates ions. The conductivity of the washed liquor was found to reduce gradually and showing a decay profile during the repeated batch washing. As such, vast amount of distilled water is required to get bring the low conductivity to final 50 µS/cm. This indicates that phosphorus component is strongly embedded on the carbon structure during activation.

3.6.2 Adsorption

In the batch adsorption experiment for MB and dairy COD, PSAC was found to distribute evenly among the adsorbate. Encouraged with mild agitation, PSAC particles suspended well (no sediments) throughout the experiment, a favourable characteristic for powdered activated carbon (PAC). Adsorption has resulted a higher density in PSAC-adsorbate complex; with tendency to settle as sediments when left idle (as seen in Fig. 3.10). This is a positive characteristic of PSAC as the time required for separation upon adsorption is reduced.

3.6.3 Reclaimed H_3PO_4 activation

Evaporation of excess water: A large amount of distilled water is needed to thoroughly wash H_3PO_4 from the produced PSAC. Intensive evaporation is required to get rid of the excess water in the reclaimed H_3PO_4. Heating the H_3PO_4 solution at higher temperature (150 °C)

was able to accelerate the process slightly as compared to heating at 100 °C. Heating under vacuum chamber is found to improve the evaporation significantly.

Fig. 3.10. Before and after adsorption of dairy COD at 2000 mg/L

3.7 References

1 A. C. Lua, J. Guo, Activated carbon prepared from oil palm stone by one-step CO activation for gaseous pollutant removal, Carbon 38 (2000) 1089–1097

2 J. Guo, A.C. Lua, Characterization of chars pyrolyzed from oil palm stones for the preparation of activated carbons, Journal of Analytical and Applied Pyrolysis 46 (1998) 113-125

3 S. Sumathi, S. Bhatia, K.T. Lee, A.R. Mohamed, Optimization of microporous palm shell activated carbon production for flue gas desulphurization: Experimental and statistical studies, Bioresource Technology 100 (2009) 1614-1621

4 W.M.A.W. Daud, W.S.W. Ali, Comparison on pore development of activated carbon produced from palm shell and coconut shell, Bioresource Technology 93 (2004) 63-69

5 W.M.A.W. Daud, W.S.W. Ali, M.Z. Sulaiman, The effects of carbonization temperature on pore development in palm-shell-based activated carbon, Carbon 38 (2000) 1925-1932

6 D. Adinata, W.M.A.W. Daud, M.K. Aroua, Production of carbon molecular sieves from palm shell based activated carbon by pore sizes modification with benzene for methane selective separation, Fuel Processing Technology 88 (2007) 599-605

7 J. Guo, A.C. Lua, Textural and chemical properties of adsorbent prepared from palm shell by phosphoric acid activation, Materials Chemistry and Physics 80 (2003) 114-119

8 A.C. Lua, J. Guo, Microporous Oil-Palm-Shell Activated Carbon Prepared by Physical Activation for Gas-Phase Adsorption, Langmuir 17 (2001) 7112-7117

9 J. Guo, A.C. Lua, Characterization of adsorbent prepared from oil-palm shell by CO2 activation for removal of gaseous pollutants, Materials Letters 55 (2002) 334-339

10 A.C. Lua, J. Guo, Preparation and characterization of activated carbons from oil-palm stones for gas-phase adsorption, Colloids and Surfaces A: Physicochemical and Engineering Aspects 179 (2001) 151-162

11 J. Guo, A.C. Lua, Kinetic study on pyrolytic process of oil-palm solid waste using two-step consecutive reaction model, Biomass and Bioenergy 20 (2001) 223-233

12 J. Guo, A.C. Lua, Textural and Chemical Characterizations of Adsorbent Prepared from Palm Shell by Potassium Hydroxide Impregnation at Different Stages, Journal of Colloid and Interface Science 254 (2002) 227-233

13 J. Guo, W.S. Xu, Y.L. Chen, A.C. Lua, Adsorption of NH3 onto activated carbon prepared from palm shells impregnated with H2SO4, Journal of Colloid and Interface Science 281 (2005) 285-290

14 R. Baccar, J. Bouzid, M. Feki, A. Montiel, Preparation of activated carbon from Tunisian olive-waste cakes and its application for adsorption of heavy metal ions, Journal of Hazardous Materials 162 (2009) 1522-1529

15 J.P. Kushwaha, V.C. Srivastava, I.D. Mall, Treatment of dairy wastewater by commercial activated carbon and bagasse fly ash: Parametric, kinetic and equilibrium modelling, disposal studies, Bioresource Technology 101 (2010) 3474-3483

16 Z. Laszlo, S. Kertesz, S. Beszedes, Z. Hovorka-Horvath, G. Szabo, C. Hodur, Effect of preozonation on the filterability of model dairy waste water in nanofiltration, Desalination 240 (2009) 170-177

17 M.C.M.R. Leal, D.M.G. Freire, M.C. Cammarota, G.L. Sant'Anna Jr, Effect of enzymatic hydrolysis on anaerobic treatment of dairy wastewater, Process Biochemistry 41 (2006) 1173-1178

18 E.V. Ramasamy, S.A. Abbasi, Energy recovery from dairy waste-waters: impacts of biofilm support systems on anaerobic CST reactors, Applied Energy 65 (2000) 91-98

19 E.V. Ramasamy, S. Gajalakshmi, R. Sanjeevi, M.N. Jithesh, S.A. Abbasi, Feasibility studies on the treatment of dairy wastewaters with upflow anaerobic sludge blanket reactors, Bioresource Technology 93 (2004) 209-212

20 Y. Han, Z. Li, X. Miao, F. Zhang, Statistical optimization of medium components to improve the chitinase activity of Streptomyces sp. Da11 associated with the South China Sea sponge Craniella australiensis, Process Biochemistry 43 (2008) 1088-1093

21 S.L.C. Ferreira, R.E. Bruns, H.S. Ferreira, G.D. Matos, J.M. David, G.C. Brandao, E.G.P. da Silva, L.A. Portugal, P.S. dos Reis, A.S. Souza, W.N.L. dos Santos, Box-Behnken design: An alternative for the optimization of analytical methods, Analytica Chimica Acta 597 (2007) 179-186

22 S.L.C. Ferreira, R. E. Bruns, E.G.P. da Silva, W.N.L. dos Santos, C.M. Quintella, J. M. David, J. B. de Andrade, M. C. Breitkreitz, I.C.S.F. Jardim, B.B. Neto, Statistical designs and response surface techniques for the optimization of chromatographic systems, Journal of Chromatography A, 1158 (2007) 2-14

23 Y. Tao, Y. Wang, S. Yan, L. Ye, Optimization of omethoate degradation conditions and a kinetics model, International Biodeterioration & Biodegradation 62 (2008) 239-243

24 C. Srinivasakannan, M.Z. Abu Bakar, Production of activated carbon from rubber wood sawdust, Biomass & Bioenergy 27 (2004) 89-96

25 C.A. Toles, W.E. Marshall, M.M. Johns, Phosphoric acid activation of nutshells from metal and organic remediation: process optimization, Journal of Chemical Technology and Biotechnology 72 (1998) 255-63

26 B.S. Girgis, M.K. Ishak, Activated carbon from cotton stalk by impregnation with phosphoric acid, Material Letters 39 (1999) 107-14

27 T. Vernersson, P.R. Bonelli, E.G. Carrella, A.L. Cukierman, Arundo donax cane as a precursor for activated carbon preparation by phosphoric acid activation, Bioresource Technology 83 (2002) 95-104

28 S.A. Dastgheib, D.A. Rockstraw, Pecan shell activated carbon: synthesis, characterization and application for the removal of copper from aqueous solution, Carbon 39 (2001) 1849-1855

29 S.J. Gregg, K.S.W. Sing, Adsorption, Surface Area and Porosity, second ed., Academic Press, London, 1982

30 M.M. Dubinin, Progress in Surface and Membrane, vol. 9, Academic Press, New York, 1975

31 C. Lastoskie, K.E. Gubbins, N. Quirke, Characterization of porous solids. Studies in surface science and catalysis, vol. 87, Elsevier, New York, 1994

32 R. Arriagada, R. Garcia, M. Molina-Sabio, F. Rodriguez-Reinoso, Effect of steam activation on the porosity and chemical nature of activated carbons from Eucalyptus globulus and peach stones, Microporous. Materials 8 (1997) 123-130

33 A.G. Barneto, J.A. Carmona, J.E.M. Alfonso, R. S. Serrano, Simulation of the thermogravimetry analysis of three non-wood pulps, Bioresource Technology 101 (2010) 3220-3229

CHAPTER IV

PALM SHELL ACTIVATED CARBON DEVELOPMENT

4.1 Introduction

Many researchers have investigated the development of palm shell activated carbon (PSAC) using various chemical and physical activation methods. The process conditions adopted have been thoroughly assessed and textural characteristics of produced PSAC have been reviewed (section 2.8). These process conditions were found to be far from comprehensive. For instance, carbon yield, a key factor of process economy has not been well investigated and reported. Also, usage of continuous inert gas during activation, even though widely practiced, has not been justified. In this chapter, investigations were conducted on PSAC development using non-conventional H_3PO_4 activation, with the aims to achieve high carbon yield and well developed porosity simultaneously. Additional step of a semi-carbonization and activation under self-generate atmosphere, are the variations in the process as compared to conventional H_3PO_4 activation. Response Surface Methodology (RSM), a process optimization tool, has been adopted to assess as well as to optimize the development of key textural characteristics, i.e. surface area, pore volume, average pore diameter and carbon yield.

4.2 Model development

The optimum level of the key factors and the effect of their interactions on PSAC surface area development were determined by the Box–Behnken Design (BBD) of RSM. A total 17

experiments were conducted and the regression equation was developed to analyse factor interactions by identifying the significant factors contributing to the regression model and to determine the optimal values. All the 3 variables X_1, X_2 and X_3 (IR, $wt_{H3PO4}/wt_{\text{ palm shell}}$, activating temperature, °C and activating time, min) are shown in both coded and uncoded (actual) form in Table 4.1. Code values for the variable parameters were used to facilitate regression with -1 as the minimum level and +1 as the maximum level. The centre runs (0, 0, and 0) were repeated 5 times to determine the experimental error.

4.3 The effects of activation parameters on the BET surface area

The coefficients of empirical model and their statistical analyses were evaluated using the Design Expert 6.0.6 Software. The complete design matrixes together with the response values obtained from the experimental results for BET Surface area of PSAC are given in Table 4.1. The response of the centre point (IR: 1.75, activation temperature: 425 °C, and activation time: 75 min) was 1527 m^2/g. Eq. (4.1) is the quadratic regression model for the BET surface area (Y_1), an attempt to fit the data by least-squares, involving all the terms regardless of their significance.

$$\text{BET surface area, } Y_1 = 1526.60 + 500.25*X_1 + 454.63*X_2 + 48.38*X_3 - 244.30*X_1^2 - 254.05*X_2^2 - 82.05*X_3^2 + 115.75*X_1X_2 + 168.25*X_1X_3 - 252.50*X_2X_3 \quad (4.1)$$

The quality of the model developed was evaluated based on the correlation coefficient R-squared (R^2), standard deviation values and R^2 adjusted are presented in Table 4.2.

Table 4.1 The Box-Behnken experimental design: BET surface area, pore volume and average pore diameter

Sample	Impregnation ratio, $wt_{H3PO4}/wt_{palm\ shell}$		Temperature, °C		Time, min		BET surface area	Pore volume	Average pore diameter
	X_1	Coded	X_2	Coded	X_3	Coded	Y_1, m^2/g	Y_2, cm^2/g	Y_3, nm
1	0.5	-1	425	0	120	+1	729	0.38	2.06
2	0.5	-1	500	+1	75	0	663	0.34	2.06
3	0.5	-1	425	0	30	-1	734	0.39	2.11
4	0.5	-1	350	-1	75	0	330	0.14	2.43
5	1.75	0	350	-1	30	-1	380	0.11	2.34
6	1.75	0	500	+1	120	+1	1496	1.07	2.86
7	1.75	0	500	+1	30	-1	2139	1.45	2.78
8	1.75	0	350	-1	120	+1	747	0.41	2.19
9	3.0	+1	350	-1	75	0	1162	0.49	2.44
10	3.0	+1	500	+1	75	0	1958	1.90	3.27
11	3.0	+1	425	0	120	+1	2003	2.13	3.53
12*	3.0	+1	425	0	30	-1	1335	1.09	2.94
13*	1.75	0	425	0	75	0	1540	1.25	2.71
14*	1.75	0	425	0	75	0	1488	1.28	2.73
15*	1.75	0	425	0	75	0	1632	1.31	2.66
16*	1.75	0	425	0	75	0	1429	1.29	2.47
17*	1.75	0	425	0	75	0	1544	1.29	2.65

*The centre point was replicated 5 times to estimate the experimental errors

Table 4.2 Statistical parameters obtained from the ANOVA for the reduced models of BET surface area

Variables	BET surface area, m^2/g
Standard deviation, SD	232.52
Mean	1253.47
R^2	0.9255
R^2 adjusted	0.8296
Adequate precision	10.709

The coefficient of determination R^2 of 0.9255 for Eq. (4.1) indicating that 92.55% of the total variation in the BET surface area was attributed to the experimental variables studied. The R^2 value close to unity is an indication of good agreement between the experimental and the predicted surface area development from this model. The value of the adjusted coefficient of determination (R^2 adjusted), is found to be reasonably high (82.96%) asserting all the three variables studied to have synergistic effects on BET surface area and significant to the model [1,2]. For this model, the predicted R^2 is in reasonable agreement with the adjusted-R^2 as they are within 0.20 of each other. It is better to use adjusted-R^2 instead of R^2, because R^2 increases by addition of variables, but the adjusted R^2 does not always increase as variables are added to the model [4,5]. The value of adequate precision (signal to noise ratio) of 10.709 is high, indicates adequacy of the model to navigate the design space.

The analysis of variance (ANOVA) to test the significance and adequacy of the quadratic model for BET surface area development is listed in Table 4.3. The test of lack-of-fit (LOF) is a special diagnostic test to determine whether discrepancies between measured and expected values can be attributed to random or systematic error. *F*-value, calculated as the ratio between the lack of fit mean square and the pure error mean square, is the statistical parameter used to determine whether the LOF is significant or not, at the significance level. If "Prob> *F*" value for LOF is less than 0.05, there is statistically significant LOF at the 95% confidence level. The ANOVA for response surface quadratic model indicate that *F*-value was 9.66 for BET surface area, implies that the model was significant because model terms has value of "Prob> *F*" less than 0.05. The Prob>F less than 0.05 are consider to be significant while higher than 0.1 are insignificant. In this case, X_1 and X_2 were significant model terms whereas X_3, X_1^2, X_2^2, X_3^2, X_1X_2, X_1X_3 and X_2X_3 were insignificant to the

response. The Prob> *F* of LOF for the BET surface area (Y_1), models were smaller than 0.05 indicating an undesirable significant LOF.

The fitted regression equation showed good fit of the model and was successful in capturing the correlation between the process variables and the response variable. From the ANOVA analysis, the model was found to be adequate for predicting the optimized production of high surface area PSAC within the range of the preparation variables studied.

Table 4.3 ANOVA for response surface quadratic model on BET surface area development

Source	Sum of squares	Deg. of freedom	Mean square	F value	Prob > F
Model	4699129	9	522125	9.66	0.003
X_1	2002001	1	2002001	37.03	0.0005
X_2	1653471	1	1653471	30.58	0.0009
X_3	18721	1	18721	0.35	0.5747
X_1^2	251295	1	251295	4.65	0.068
X_2^2	271753	1	271753	5.03	0.0599
X_3^2	28346	1	28346	0.52	0.4925
X_1X_2	53592	1	53592	0.99	0.3526
X_1X_3	113232	1	113232	2.09	0.1911
X_2X_3	255025	1	255025	4.72	0.0664
Residual	378465	7	54066		
Lack of Fit	355858	3	118619	20.99	0.0066
Pure Error	22607	4	5652		

To establish the ideal BET surface area, the three-dimensional response surface curves and contour plots were drawn using statistically significant model to understand the interaction of the parameters. Fig. 4.1 is the three-dimensional response surface which was based the most important two variables (activation temperature and IR) on BET surface area of PSAC. The activation time was fixed at centre level (t = 75 min). As can be seen from Fig. 4.1, the plot are approximately symmetrical in shape with semi-circular contour. It is found that at

activation time of 75 min, BET surface area is found to increase with activation temperature and IR before reaching a plateau at 500 °C and IR of 3. The highest BET value of 2099 m^2/g was obtained within the range of both variables studied (500 °C and 3.0 IR). Similar pattern were observed on the two-dimensional representation. The contour plot of the response on the temperature and IR plane (Fig. 4.2) show semi-concentric curve with the maximum points of the variables.

Fig. 4.3 is a 3D plot of BET surface area model for IR of 3.0. According to this prediction, the increase in activation temperature or duration, the surface area increases. Also can be inferred from the figure, the BET surface area stop to increase a certain limit of activation temperature, indicating optimum point for all the 3 variables within the range studied. The maximum predicted surface area for PSAC is indicated by the surface for temperature from 463 to 500 °C, disregard the activation time (Fig. 4.4).

The highest BET surface areas obtained in this work is 2139 m^2/g is slightly lower than highest BET value reported at 2247 m^2/g by Hamad et al. [6]. However it should be noted that the mentioned PSAC were produced using a much more complex chemical-physical process. Palm shells were washed and neutralized upon 24 h treatment with NaOH at 85-90 °C. The material is then dried in oven before being activated at 800 °C for 2 h. This was followed by a second stage of activation using CO_2 gas at 800 °C for 1.5 h. This process is technically more complex for up-scaling as compared to the method utilized in this work. Furthermore, due to the extensive treatment under much higher temperature, the resulted PSAC yield is 30% which is lower than PSAC yield achieved in this work. These adverse process conditions and outcome means the process is less economically attractive.

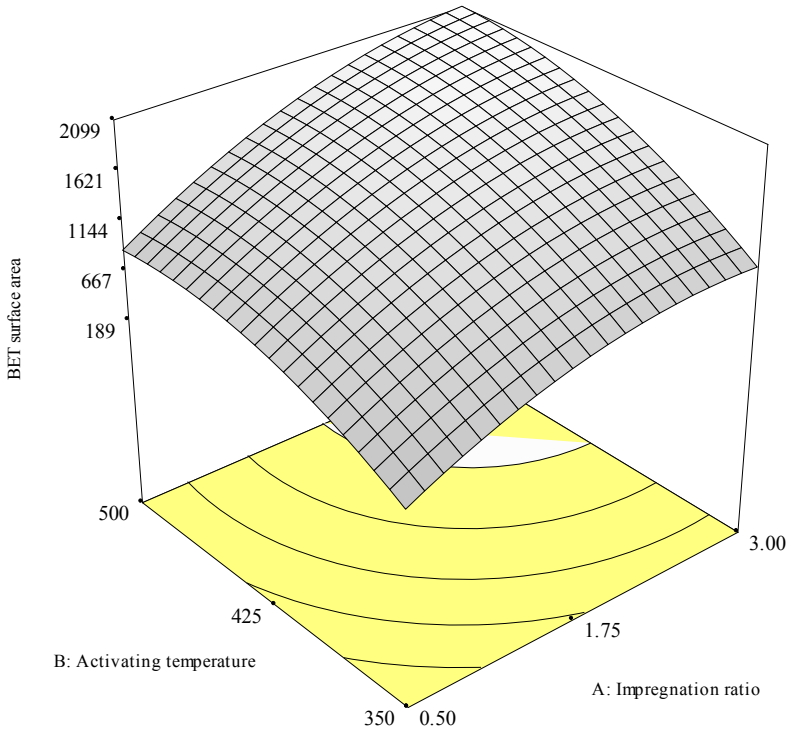

Fig. 4.1. Response surface plot (3D) of BET surface area (t= 75 min)

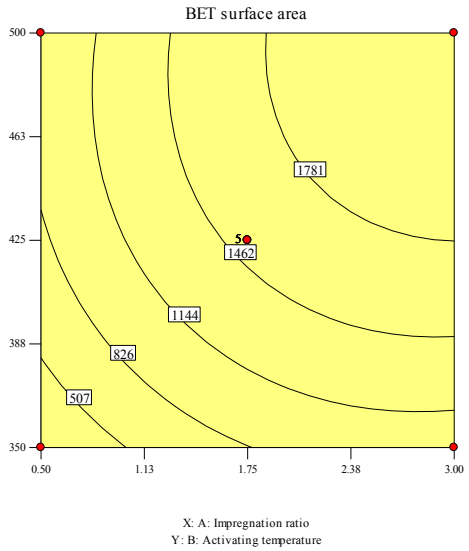

Fig. 4.2. Contour plot (2D) of BET surface area (t= 75 min)

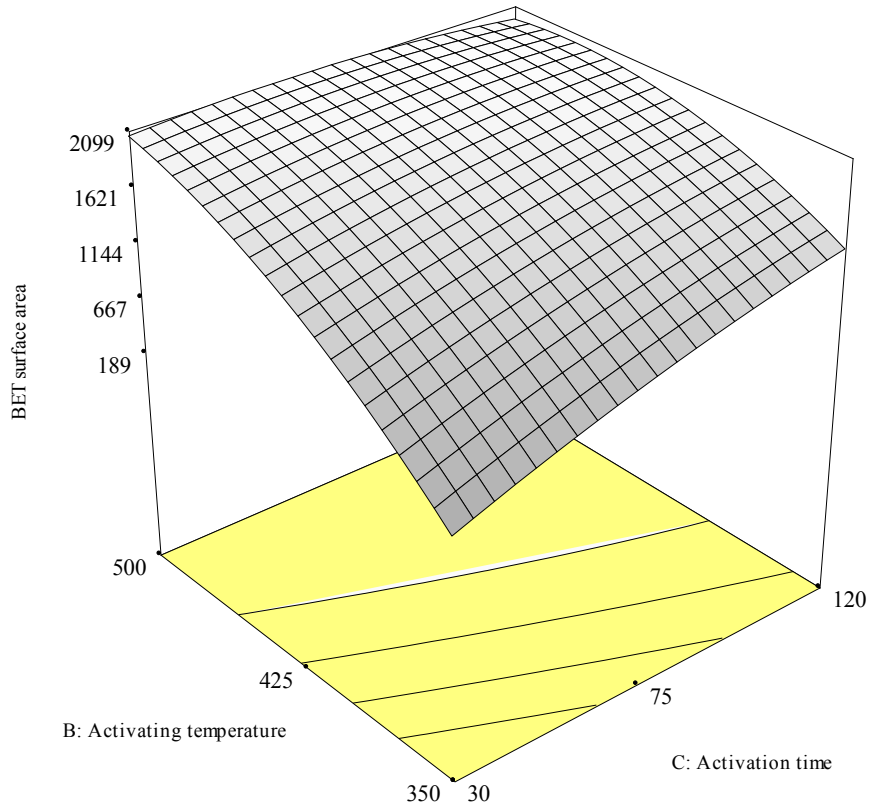

Fig. 4.3. Response surface plot (3D) of BET surface area (IR= 3.0)

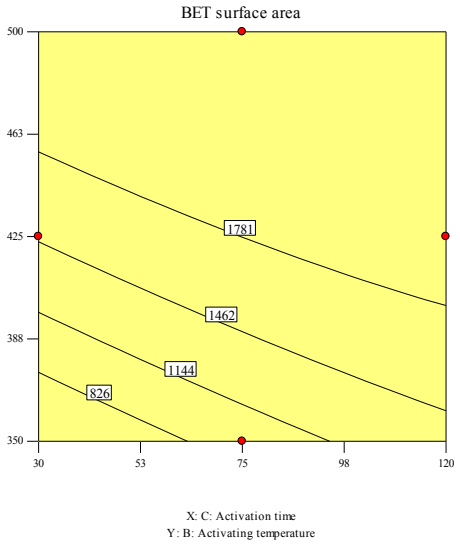

Fig. 4.4. Contour plot (2D) of BET surface area (IR= 3.0)

The feasibility and benefits of using 2-step chemical activation method in a self-generated atmosphere are documented in literature and are due to Srinivasakannan & Abu Bakar [7], Toles et al. [8], Girgis et al. [9], Vernersson et al. [10], Dastgheib & Rockstraw [11]. However, the mechanism of such activation has not been thoroughly investigated. It has been reported that porosity development in this stage is ascribed to the phosphoric oxides formed at the carbonization temperatures, which act as local oxidizing agents performing controlled gasification and the process actually requires the presence of a small amount of air (O_2) [12]. While most activation applied an inert gas (mainly N_2) to minimise potential of O_2 oxidation; the significance of presence of trace amount of O_2 has been overlooked.

The presence of small quantity of O_2 during activation has also been attributed to promoting porosity development. According to Klasson et al. [13], O_2 possibly reacts with the carbon in the shells and generate volatile (combustible) gases from the heating of the materials. The reaction of a combustible gas (as CH_4 equivalents) with O_2 to create CO and CO_2 is shown in Eq. (4.2) and (4.3):

$$CH_4 \text{ (equivalents)} + 1.5O_2 \rightarrow CO + 2H_2O \quad (4.2)$$

$$CH_4 \text{ (equivalents)} + 2O_2 \rightarrow CO_2 + 2H_2O \quad (4.3)$$

The findings in this work (well developed surface area) correspond well with the work by Molina-Sabio et al. [13] who found that the atmosphere (N_2 or air) did not affect the pore structure when sufficient H_3PO_4 was used for the impregnation (as seen in samples with IR of 1.75 or 3.0). Thus we could conclude that the atmosphere used in this study, SGA responds well to the need of pore development. Activation under SGA could be viewed as *pseudo-physiochemical activation* of which 2 reagents, H_3PO_4 and O_2 (trace amount) activate the

palm shell simultaneously. This finding provides an important alternative to conventional H_3PO_4 method by eliminating the needs of a continuous inert gas flow.

4.4 The effect of activation parameters on the pore volume and pore diameter

The effect of the 3 variables on the pore volume and average pore diameter of PSAC were also investigated by RSM using three-dimensional plots and contour plots. An ideal PSAC for adsorption should have a large pore volume while PSAC with average pore diameter in the mesoporous region provides good adsorption of macromolecular adsorbates such as dye and organic waste. Using the coefficients determined, the predicted model in terms of actual factors for PSAC pore volume and average pore diameter are as shown in Eq. (4.4) and (4.5).

$$\text{Pore volume, } Y_2 = 1.28 + 0.54*X_1 + 0.45*X_2 + 0.12*X_3 - 0.16*X_1^2 - 0.40*X_2^2 - 0.12*X_3^2 + 0.30*X_1X_2 + 0.26*X_1X_3 - 0.17*X_2X_3 \quad (4.4)$$

$$\text{Average pore diameter, } Y_3 = 2.64 + 0.44*X_1 + 0.20*X_2 + 0.059*X_3 + 0.012*X_1^2 - 0.11*X_2^2 - 0.00425*X_3^2 + 0.30*X_1X_2 + 0.16*X_1X_3 + 0.058*X_2X_3 \quad (4.5)$$

The value of the coefficient of determination, R^2 for pore volume is found to be high (96.48%, as shown in Table 4.6), asserting all the 3 variables studied to have synergistic effects on pore volume. It also indicates a high significance of the model. The R^2 value for average pore diameter is however slightly lower at 89.33%. ANOVA for pore volume and average pore diameter indicated that the *F*-value was 21.34 and 6.51 respectively, which implies that both models were significant.

Table 4.4 and 4.5 show the ANOVA for regression model equations and coefficients for PSAC pore volume and average pore diameter while Table 4.6 and 4.7 summarised the

statistical parameters obtained from the ANOVA. From the analysis, all the 3 process variables are found to be influencing the development of pore volume while only IR and activation temperature are significant to average pore diameter. The analysis of *F*-value found IR to be the most significant factor on outcome of both pore volume and average pore diameter. Certain interactions between the process parameters have also shown considerable effects on both models while activation time has only a minor influence. Figs. 4.5 to 4.12 show the interactions between the variables in response surface plot and contour plot for PSAC pore volume and average pore diameter using actual values for the entire axis. As observed, Figs. 4.5 to 4.8 are in agreement with ANOVA; i.e. pore volume is seen to increase with all 3 variables. One the other hand, no significant changes in average pore diameter were observed when IR is low (such as 0.5), regardless of the activation temperature (Fig. 4.9 and 4.11). When the IR is higher, the increase in temperature result is larger average pore diameter. The result implies a minimum impregnation is required for large pore size PSAC to develop. On the other hand, Fig. 4.10 and 4.12 highlights activation time average pore diameter is the least significant when the shells are sufficiently impregnated.

At sufficient activation time (t= 75 min), pore volume could increase 100 times from 0.02 to 2.0 cm^3/g, correspond to the change in activation condition from 350 °C at 0.5 IR to 500 °C at 3.0 IR (Fig. 4.5 & 4.7). On the other hand, when palm shell is sufficiently impregnated, pore volume was found to increase with activation temperature (Fig. 4.6). A total pore volume of 1.9 cm^3/g (or higher) for PSAC generated in this study is found to be higher than those reported in available literature. A compilation of porous characteristics of the activated carbon from palm shells has been discussed in section 2.8, which clearly indicates the ranges of pore volumes using palm shells. It can be observed from the compilation that a pore volume of 1.27 cm^3/g has only been reported by Guo & Lua [14], with the corresponding surface area being 1837 m^2/g for palm shells.

Table 4.4 ANOVA for response surface quadratic model on pore volume

Source	Sum of squares	Deg. of freedom	Mean square	F value	Prob > F
Model	5.80	9	0.64	21.34	0.0003
X_1	2.38	1	2.38	78.68	< 0.0001
X_2	1.63	1	1.63	53.94	0.0002
X_3	0.11	1	0.11	3.74	0.0945
X_1^2	0.11	1	0.11	3.77	0.0932
X_2^2	0.68	1	0.68	22.53	0.0021
X_3^2	0.06	1	0.06	2.08	0.1929
X_1X_2	0.37	1	0.37	12.12	0.0102
X_1X_3	0.28	1	0.28	9.13	0.0194
X_2X_3	0.12	1	0.12	3.83	0.0913
Residual	0.21	7	0.03		
Lack of Fit	0.21	3	0.07	145.47	0.0002
Pure Error	0.0019	4	0.00		

Table 4.5 ANOVA for response surface quadratic model on average pore diameter

Source	Sum of squares	Deg. of freedom	Mean square	F value	Prob > F
Model	2.41	9	0.27	6.51	0.0109
X_1	1.55	1	1.55	37.72	0.0005
X_2	0.31	1	0.31	7.5	0.0290
X_3	0.028	1	0.028	0.67	0.4392
X_1^2	0.0005813	1	0.0005813	0.014	0.9086
X_2^2	0.047	1	0.047	1.15	0.0319
X_3^2	0.00007605	1	0.00007605	0.00185	0.9669
X_1X_2	0.36	1	0.36	8.77	0.0211
X_1X_3	0.10	1	0.10	2.49	0.1583
X_2X_3	0.013	1	0.013	0.32	0.5881
Residual	0.29	7	0.041		
Lack of Fit	0.25	3	0.082	7.72	0.0386
Pure Error	0.042	4	0.011		

Table 4.6 Statistical parameters for pore volume obtained from the ANOVA for the reduced models

Variables	Pore volume, cm^3/g
Standard deviation, SD	0.17
Mean	0.96
R^2	0.9648
R^2 adjusted	0.9196

Table 4.7 Statistical parameters for average pore diameter obtained from the ANOVA for the reduced models

Variables	Average pore diameter, nm
Standard deviation, SD	0.20
Mean	2.60
R^2	0.8933
R^2 adjusted	0.7562

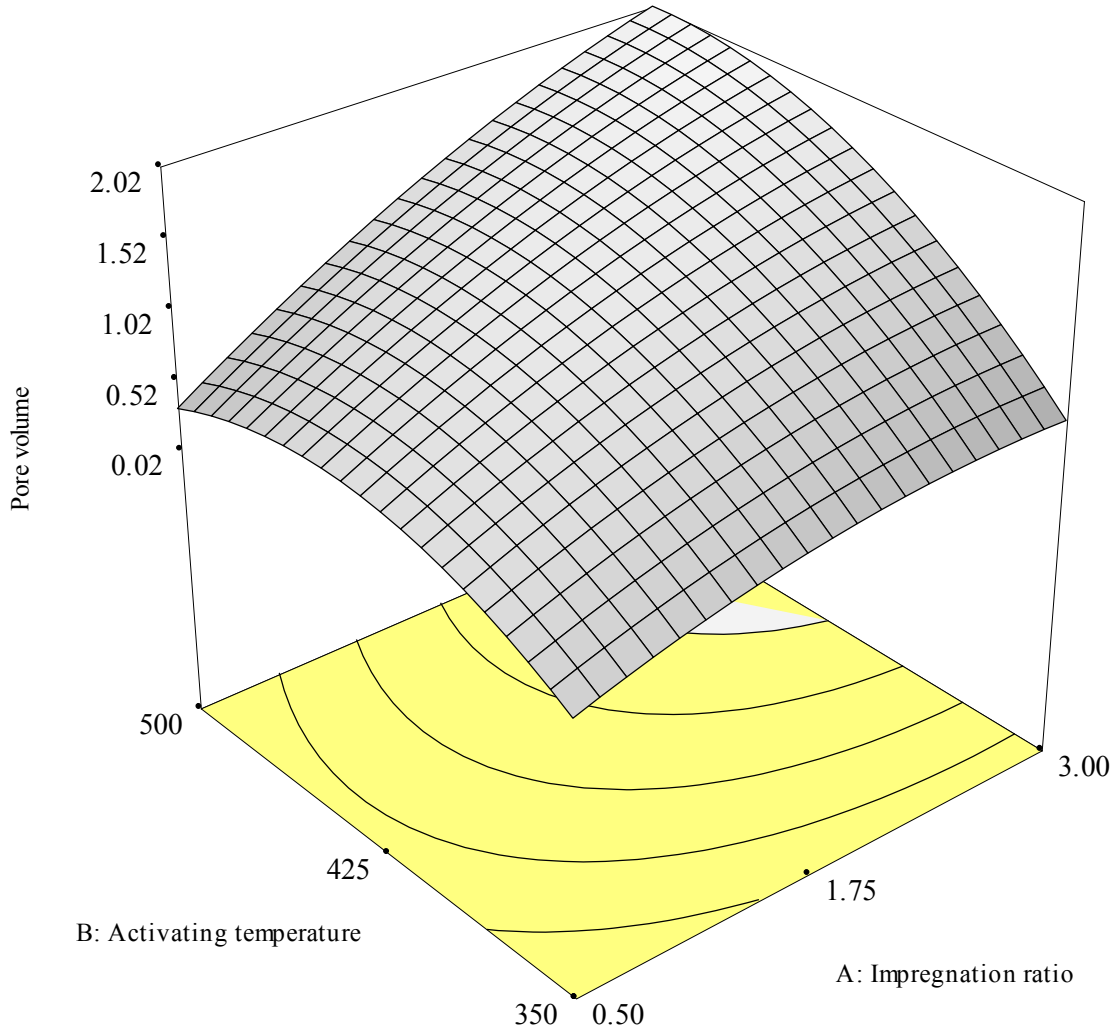

Fig. 4.5. Response surface plot (3D) of pore volume (t= 75 min)

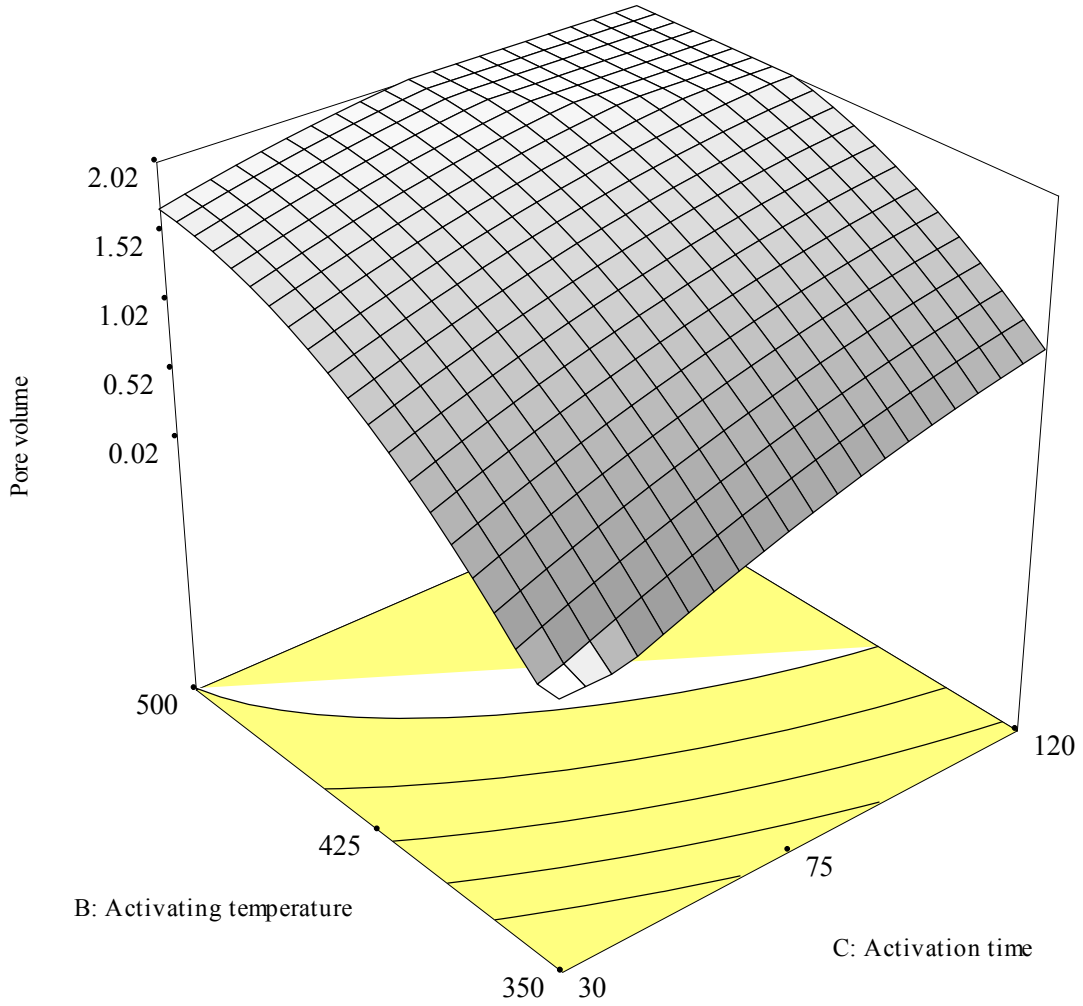

Fig. 4.6. Response surface plot (3D) of pore volume (IR=1.75)

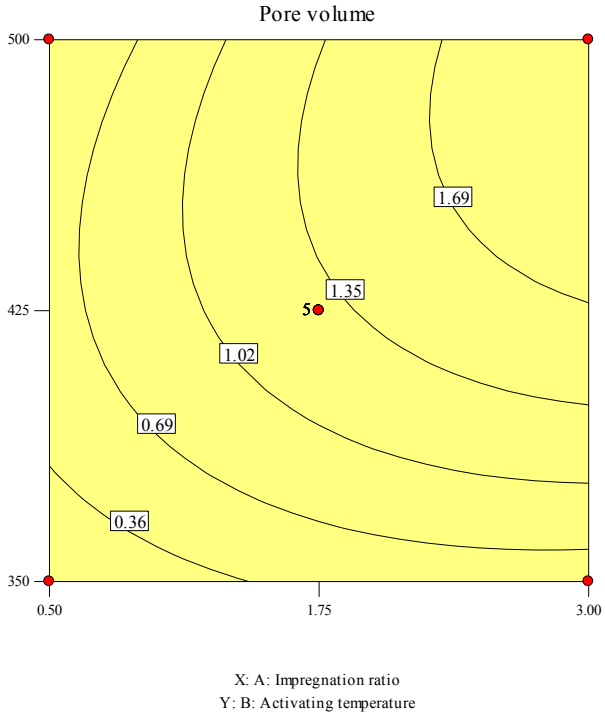

Fig. 4.7. Contour plot (2D) of pore volume (t= 75 min)

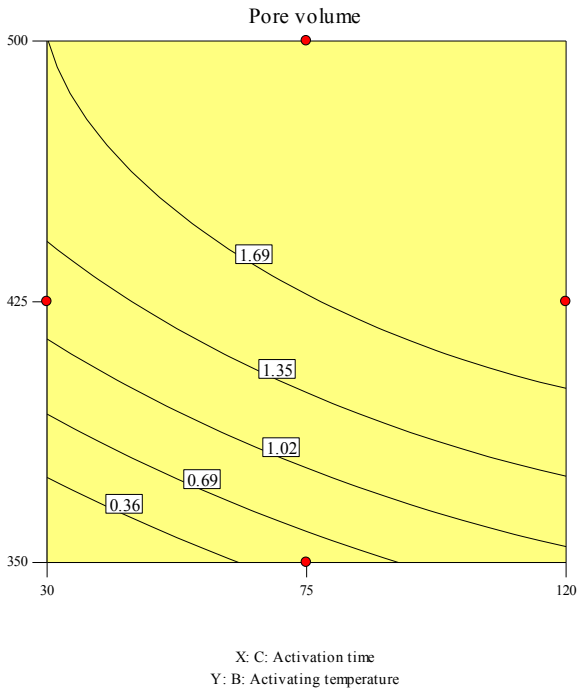

Fig. 4.8. Contour plot (2D) of pore volume (IR=1.75)

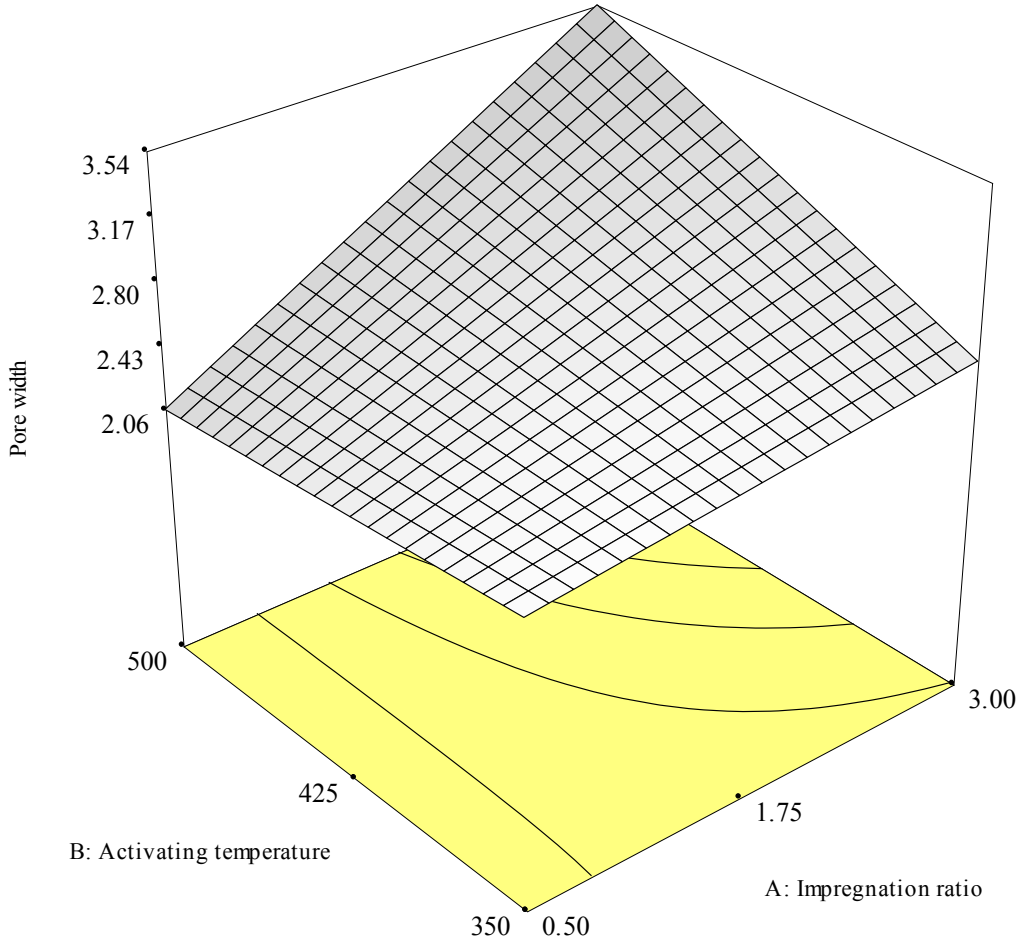

Fig. 4.9. Response surface plot (3D) of average pore diameter (t= 75 min)

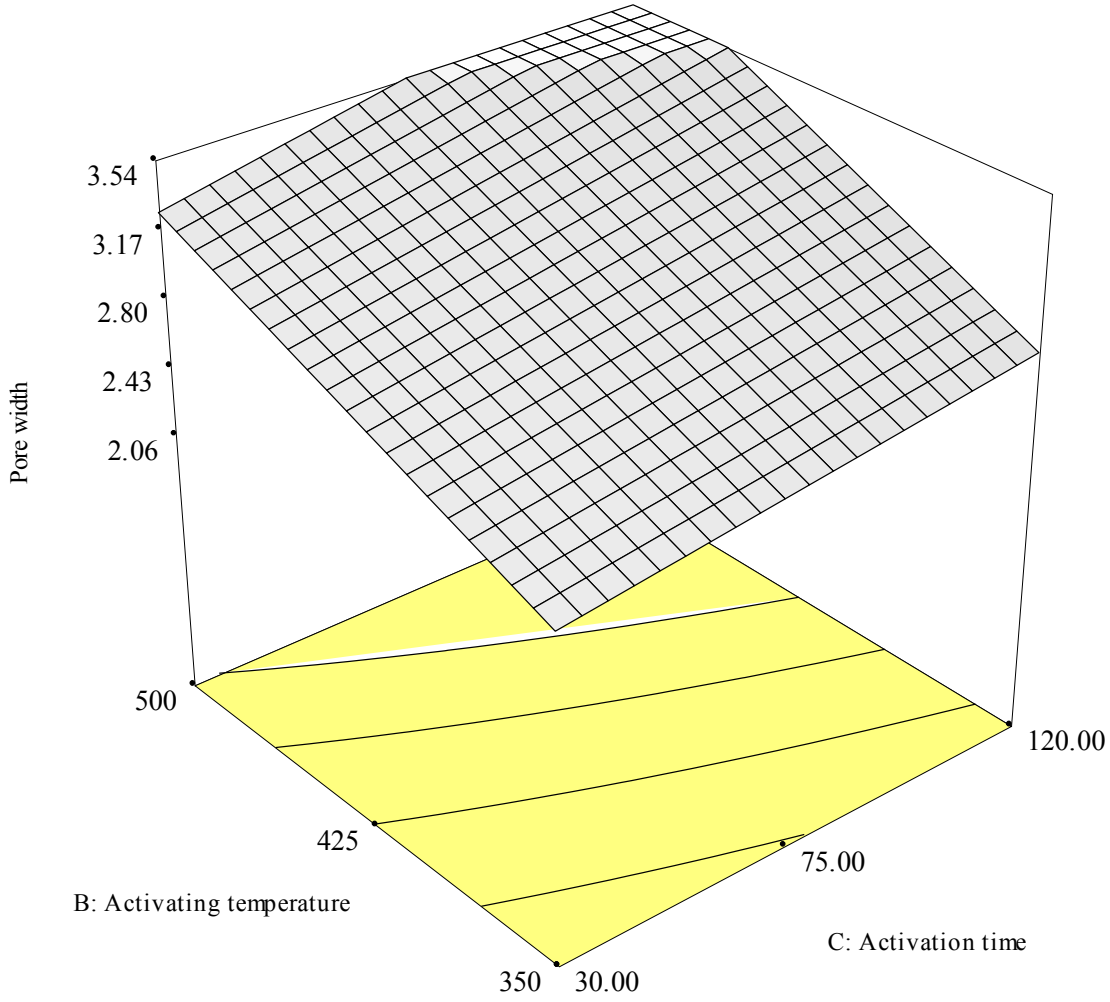

Fig. 4.10. Response surface plot (3D) of average pore diameter (IR= 1.75)

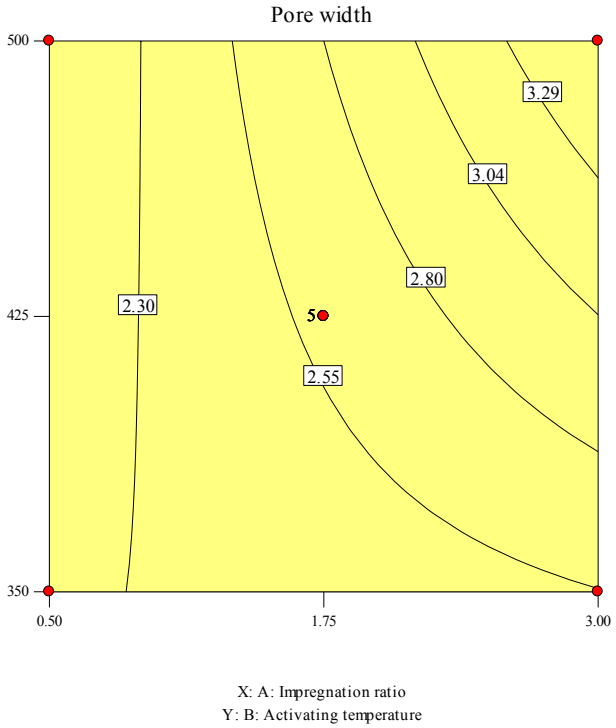

Fig. 4.11. Contour plot (2D) of average pore diameter (t= 75 min)

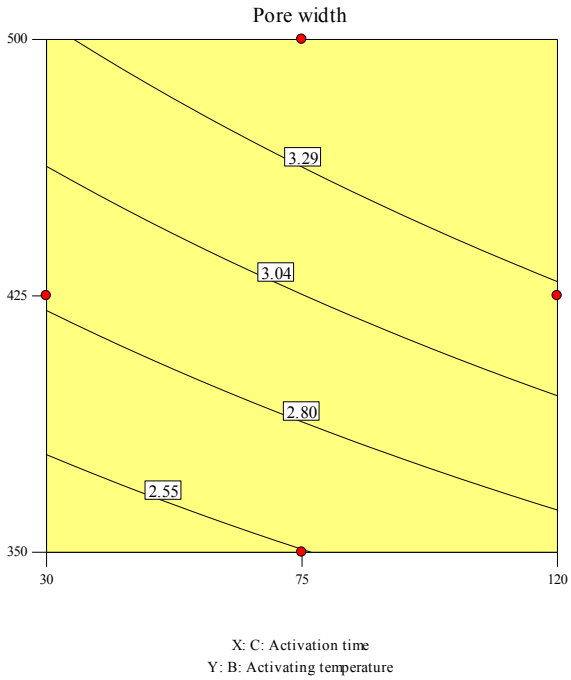

Fig. 4.12. Contour plot (2D) of average pore diameter (IR= 1.75)

Mesoporous AC is regularly associated with low surface area. Although the developed PSAC in this work are of mesopore rich, the total surface area were found to be high and unaffected (with average pore diameter and BET surface area are in excess of 2.5 nm and 1950 m^2/g respectively). This accomplishment could be attributed to the high pore volume in PSAC. While transformation of micropores into mesopores sees the collapse of micropores wall (that leads to lower surface area); the relatively larger volume in the PSAC contributed to the large surface area and compensated to the surface area loss. The unique nature of the porous carbon prepared in the present study, is expected to facilitate adsorption of large quantum of high molecular weight compounds with ease, owing to the pore size and the surface area.

The pore size distribution (PSD) along with cumulative pore size distribution of the PSAC sample activated at 500 °C, 3 IR and 75 min is shown in Figs. 4.13 & 4.14. As shown in PSD, 3 peaks with the first peak in the ultra-micropore range with pore size less than 1 nm, while the second peak within the range of 1 to 2 nm and the third one with a peak in the range of 2 to 4 nm. The presence of significant amounts of pores in the size range in excess of 2 nm is well evidenced from the figure, with the contribution of mesopores being 76.7% of the total surface area.

Fig. 4.15 shows adsorption-desorption isotherms of N_2 at -196 °C on PSAC activated at 500 °C. Between samples 2 and 7, a transition from *narrow* mesopores to large mesopores is noticeable, inline with the change from a horizontal plateau adsorption pattern to a more open knees and steep branches, corresponds to the difference between unfavourable to favourable impregnation condition (IR for sample 2 and 7 is 0.5 and 1.75). Such transition is also seen in the significant increase in surface area development (from 663 to 2139 m^2/g). This observation signify the important of impregnation in AC development.

Also seen in Fig. 4.15, PSAC samples 6 and 7 were prepared at adequate impregnation and activated temperature (1.5 IR and 500°C) but activated at different duration. The volume adsorped by sample 7 (activation time of 60 min) is significantly higher than sample 6 (activation time of 120 min) corresponds to the difference in N_2 volume adsorbed. Prolong exposure to thermal treatment, coupled with high IR and activation temperature, would result in excessive reactions on the carbon surface which collapse the pore wall and reduce PSAC surface area. The difference in activation duration is seen in BET surface area and pore volume; 1496 m^2/g and 1.07 cm^3/g for sample 7 as compared to 2139 m^2/g and 1.45 cm^3/g for sample 6.

The influence of activation temperature on adsorption-desorption isotherms are depicted in Fig. 4.16. All PSAC were impregnated with IR of 0.5 to assess the influence of activation temperature. Almost all samples exhibits isotherms horizontal to P/P_o axis with little hysteresis observed due to low impregnation. PSAC sample 4, for instance was prepared under low activation temperature (350 °C), exhibit minimum gas volume adsorbed, correspond to low textural development (BET surface area and Pore volume: 330 m^2/g and 0.14 cm^3/g). Increase in activation temperature assist in development of porosity as seen with multifold increase in gas volume adsorbed (Sample 1,2 and 3). However, the textural quality is still low (Sample 1: 729 m^2/g, 0.38 cm^3/g; Sample 2: 663 m^2/g and 0.34 cm^3/g).

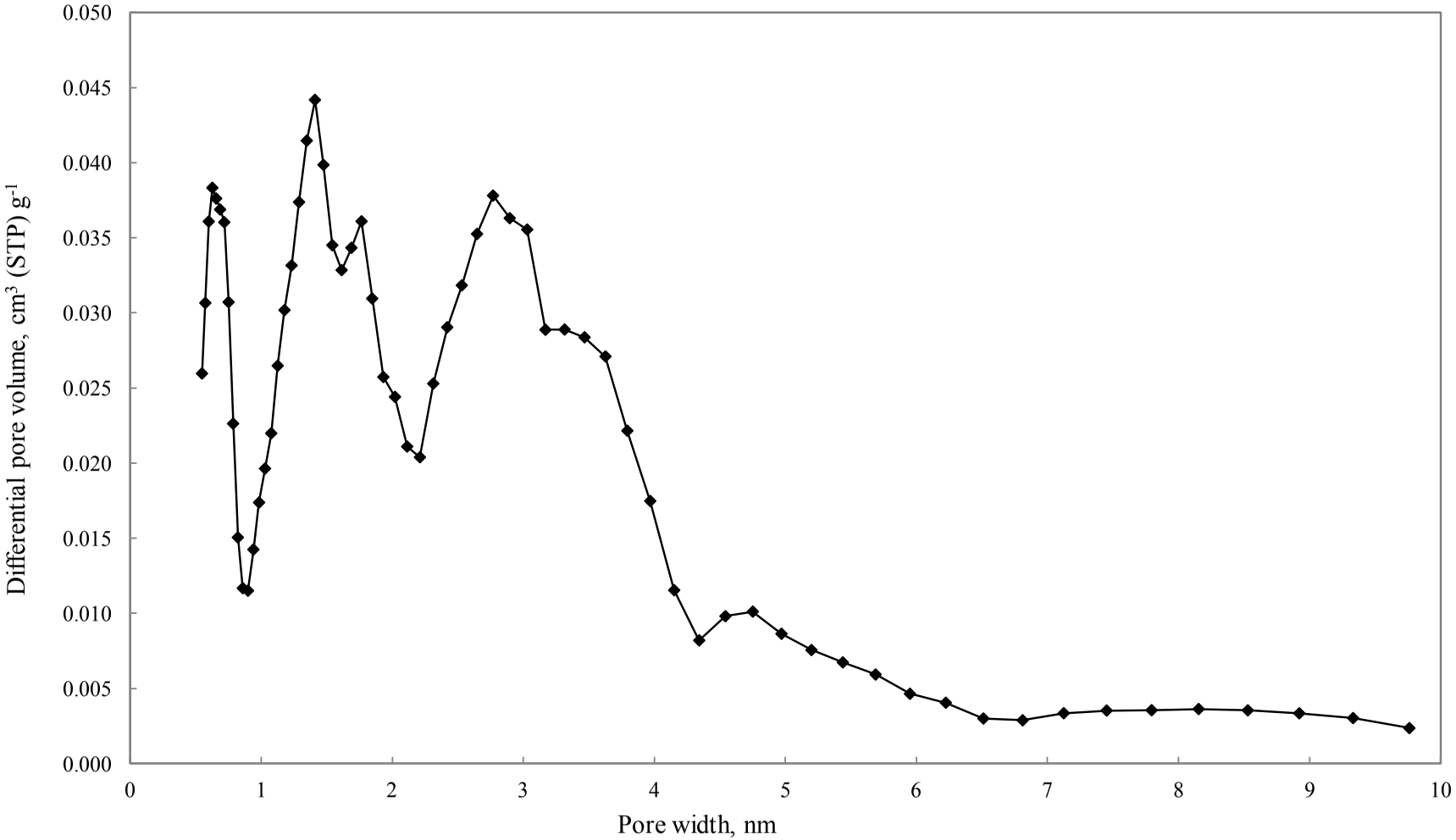

Fig. 4.13. Pore size distribution of H_3PO_4-PSAC (IR= 3.0, T= 500 ºC and t=75 min)

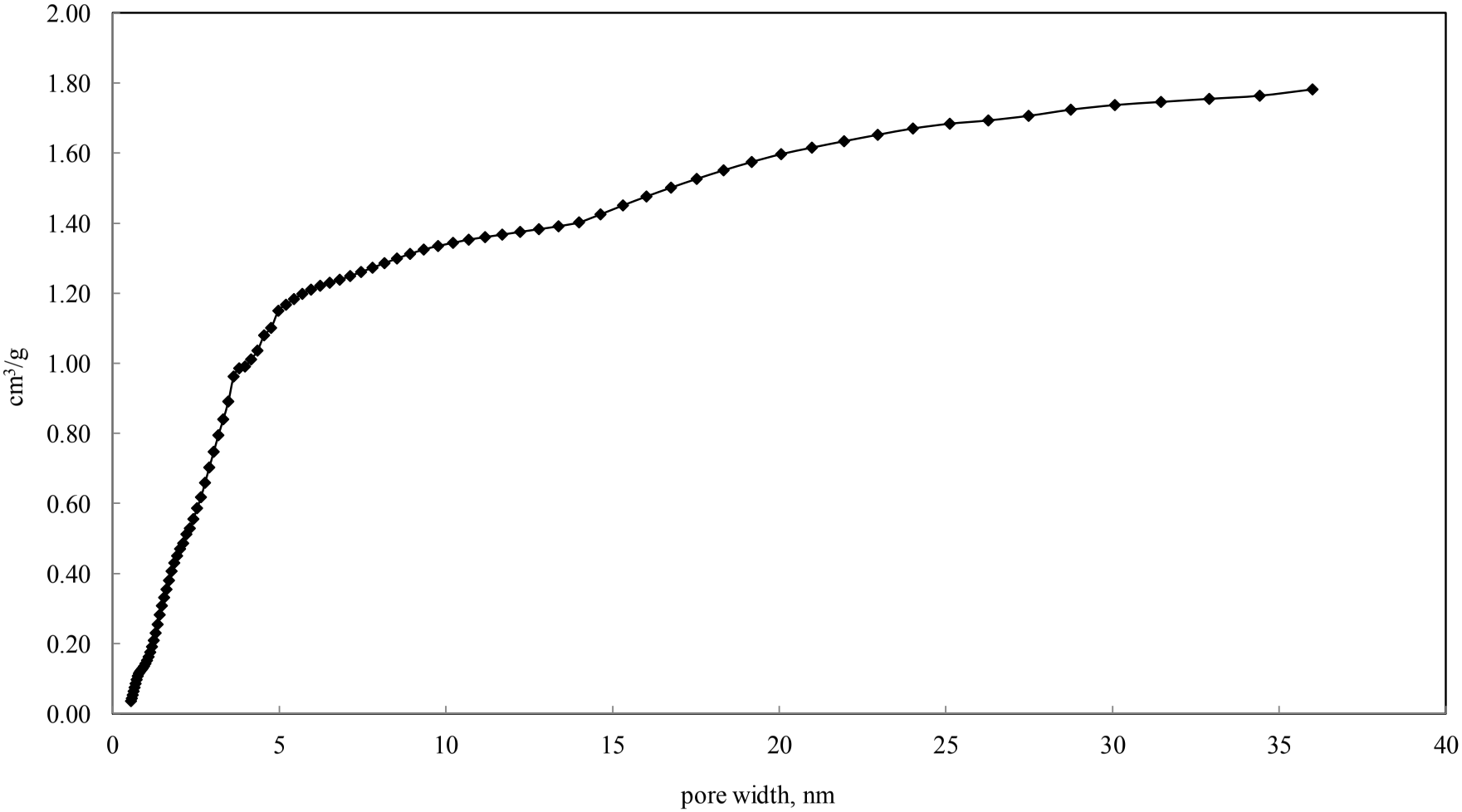

Fig. 4.14. DFT/ Monte- Carlo cumulative pore volume plot of H_3PO_4-PSAC (IR= 3.0, T= 500 ºC and t=75 min)

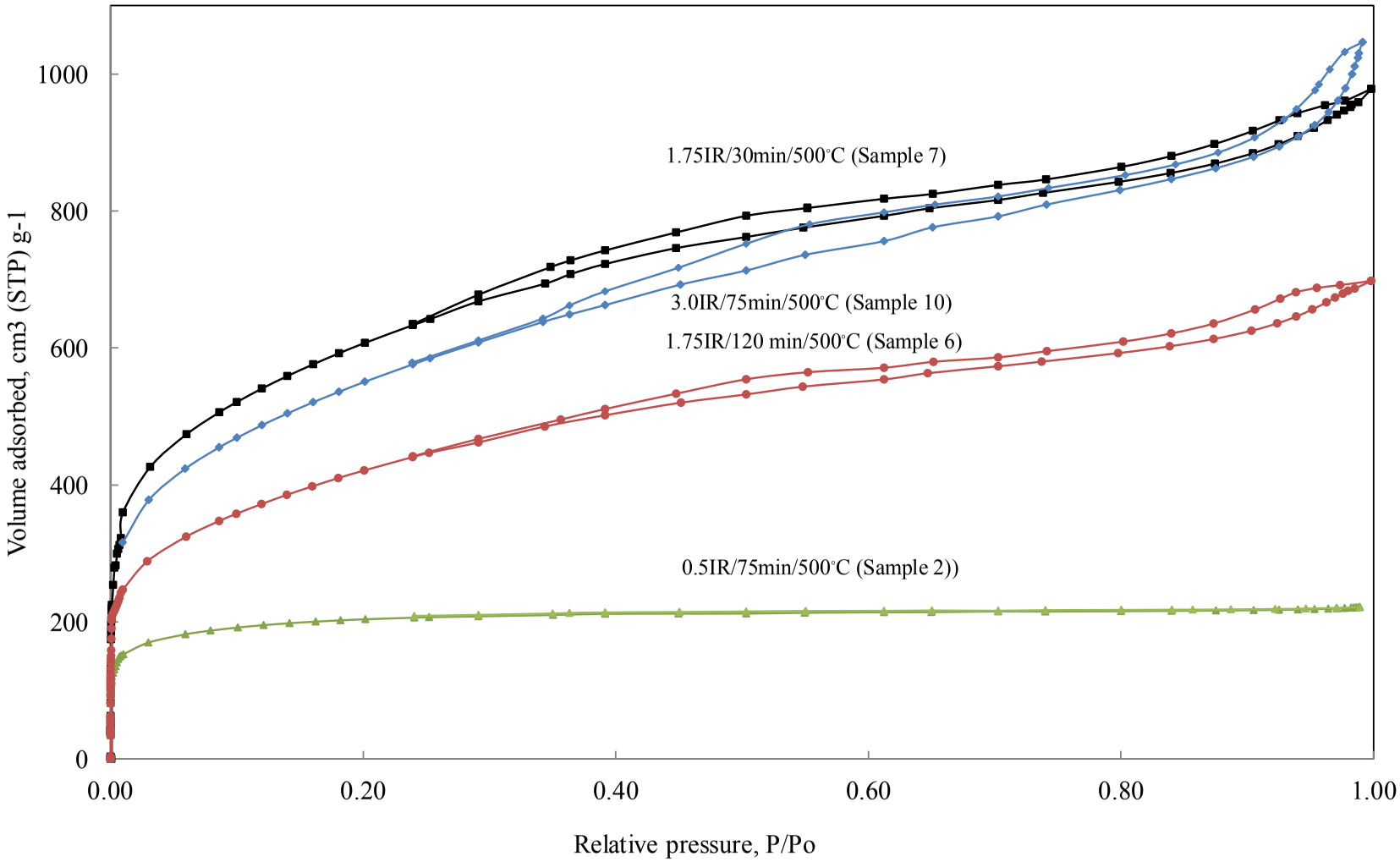

Fig. 4.15. N_2 adsorption of PSAC (T= 500 ºC)

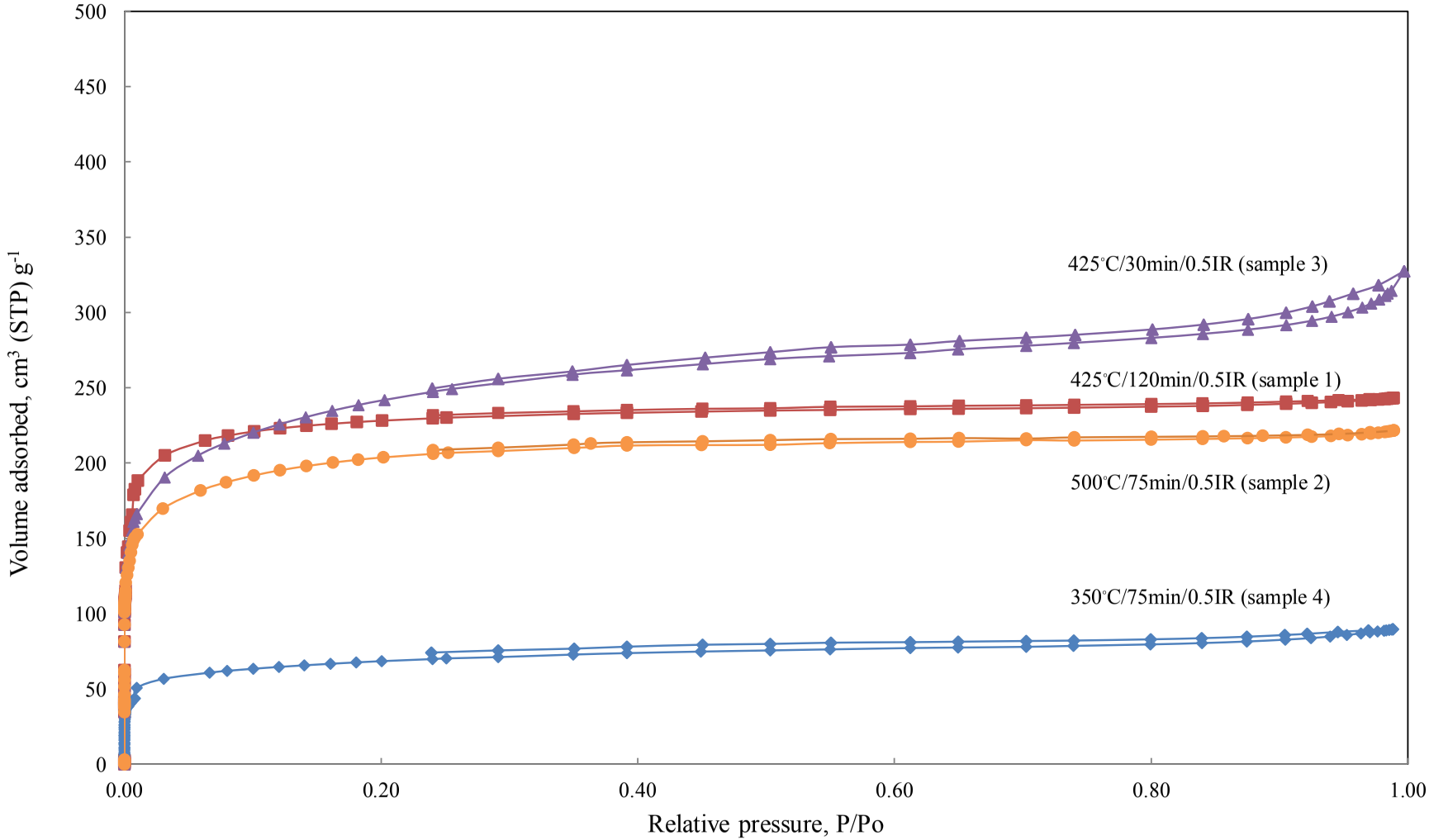

Fig. 4.16. N_2 adsorption of PSAC (IR= 0.5)

4.5 The effects of activation parameters on the PSAC yield

The complete experimental results of PSAC yield as well as the second-order response surface model fitting in the form of analysis of variance (ANOVA) are given in Tables 4.8 and 4.9 respectively. The response surface models were derived for the PSAC yield from the 17 experiments after discarding the insignificant effects. The quadratic regression model for the yield of PSAC in terms of actual factors is given by Eq. (4.6):

$$\text{PSAC yield, } Y_4 = 48.00 - 0.37*X_1 - 3.38*X_2 - 2.00*X_3 - 0.13*X_1^2 - 0.13*X_2^2 + 0.63*X_3^2 + 0.25*X_1X_2 + 0.00*X_1X_3 + 0.50*X_2X_3 \quad (4.6)$$

The coefficient of determination R^2 of 0.8930 for Eq. (4.6) indicating that 89.3% of the PSAC yield was attributed to the experimental variables studied. From the ANOVA of the response surface quadratic model for PSAC yield (Table 4.9), the model F-value of 6.49 implied that the model was significant. Unlike the observation in responses for BET surface area and pore characteristics, IR is the least influential variable in comparison with activation temperature and time. It is further evident from Prob >*F* value, indicate that only X_2 and X_3 are significant while the rest of the terms are not.

As expected, the PSAC yield is found to decrease from 54% to 43% with temperature. This observation is in agreement with most of AC investigations. High activation temperature could increase the volatility and rate of reaction between H_3PO_4 and precursor. Figs. 4.17 and 4.19 show a weak interaction between activation temperature and IR. PSAC yield is almost solely determined by activation temperature. On the other hand, a stronger interaction between activation temperature and activation time was observed. Fig. 4.18 and 4.20 revealed PSAC yield decrease gradually with both factors.

Table 4.8 The Box-Behnken experimental design: PSAC yield

Run #	Impregnation ratio ($wt_{H3PO4}/wt_{palm\ shell}$)		Temperature (°C)		Time (min)		PSAC yield Y_4 (% wt/wt)
	X_1	Coded	X_2	Coded	X_3	Coded	
1	0.5	-1	425	0	120	+1	46
2	0.5	-1	500	+1	75	0	46
3	0.5	-1	425	0	30	-1	51
4	0.5	-1	350	-1	75	0	51
5	1.75	0	350	-1	30	-1	55
6	1.75	0	500	+1	120	+1	43
7	1.75	0	500	+1	30	-1	45
8	1.75	0	350	-1	120	+1	51
9	3.0	+1	350	-1	75	0	49
10	3.0	+1	500	+1	75	0	45
11	3.0	+1	425	0	120	+1	46
12*	3.0	+1	425	0	30	-1	51
13*	1.75	0	425	0	75	0	48
14*	1.75	0	425	0	75	0	47
15*	1.75	0	425	0	75	0	48
16*	1.75	0	425	0	75	0	49
17*	1.75	0	425	0	75	0	48

Table 4.9 Statistical parameters obtained from the ANOVA for the reduced models for PSAC yield

Variables	PSAC yield, %
Standard deviation, SD	1.48
Mean	48.18
R^2	0.8930
R^2 adjusted	0.7553

Table 4.10 ANOVA for response surface quadratic model on PSAC yield

Source	Sum of squares	Deg. Of freedom	Mean square	F value	Prob > F
Model	127.2	9	14.14	6.49	< 0.0110
X_1	1.13	1	1.13	0.52	0.4957
X_2	91.12	1	91.12	41.83	0.0003
X_3	32.0	1	32.00	14.69	0.0064
X_1^2	0.066	1	0.066	0.030	0.8670
X_2^2	0.066	1	0.066	0.030	0.8670
X_3^2	1.64	1	1.64	0.75	0.4137
$X_1 X_2$	0.25	1	0.25	0.11	0.7447
$X_1 X_3$	0.00	1	0.00	0.00	1.000
$X_2 X_3$	1.00	1	1.00	0.46	0.5198
Residual	15.25	7	2.18		
Lack of Fit	13.23	3	4.42	3.60	0.0308
Pure Error	2.0	4	0.50		

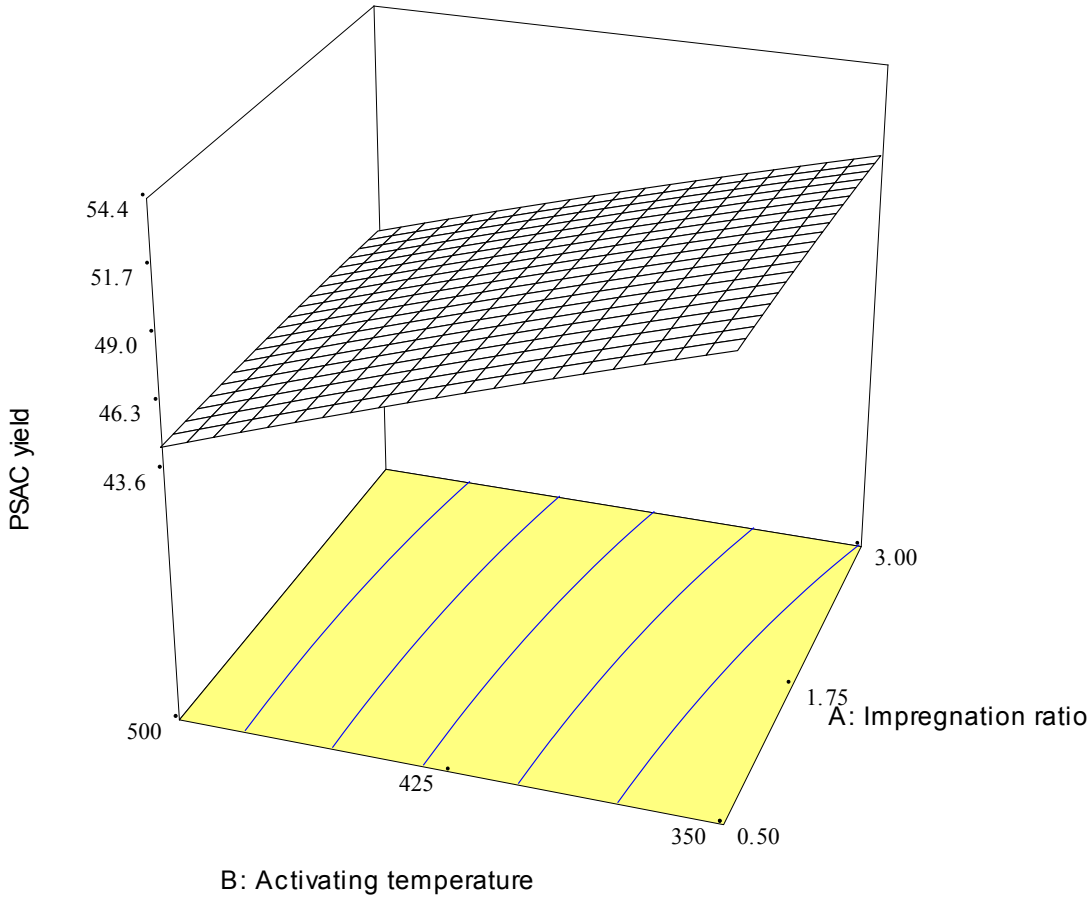

Fig. 4.17. Response surface plot (3D) of carbon yield (t= 75 min)

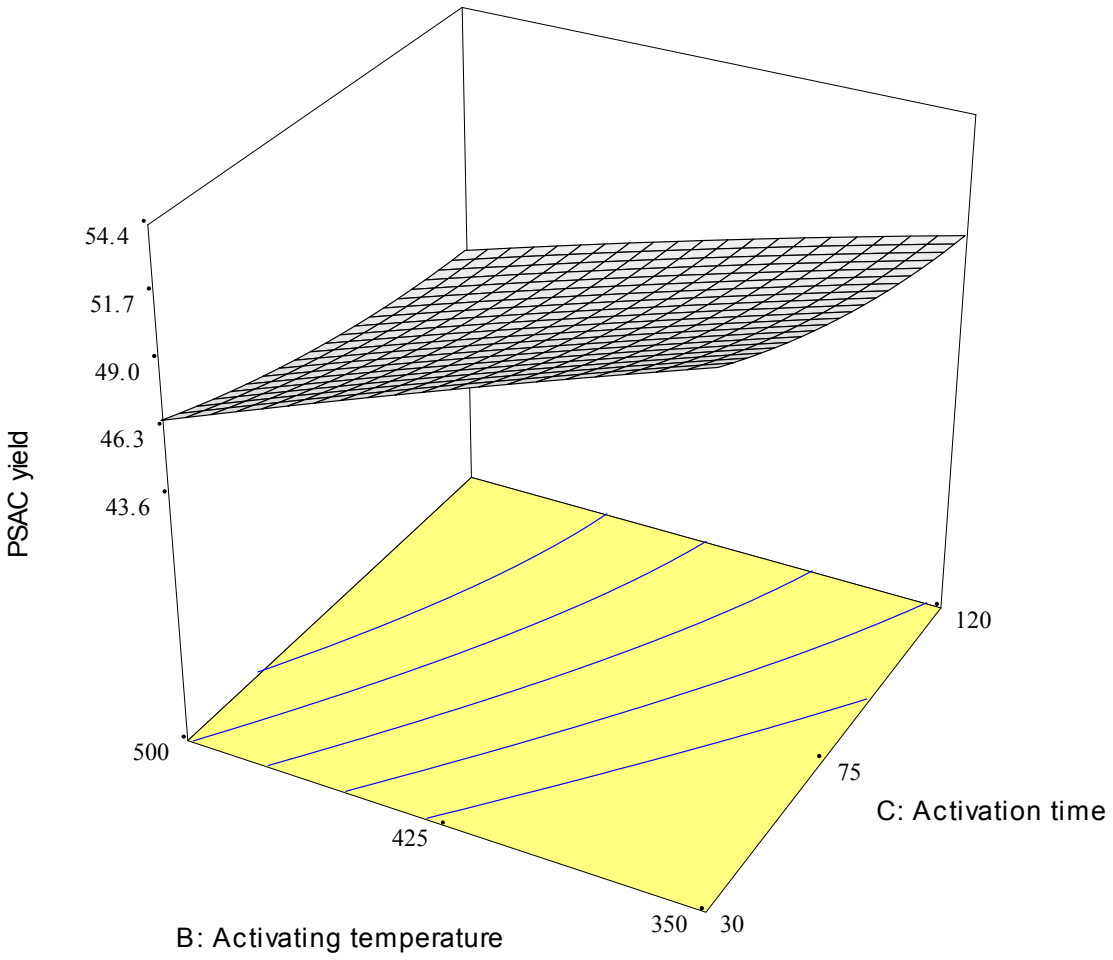

Fig. 4.18. Response surface plot (3D) of carbon yield (IR= 1.75)

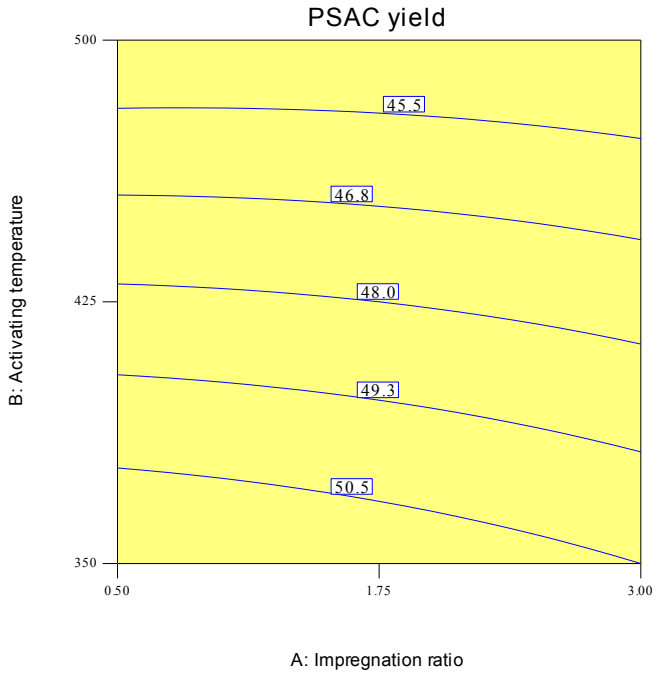

Fig. 4.19. Contour plot (2D) of carbon yield (t= 75 min)

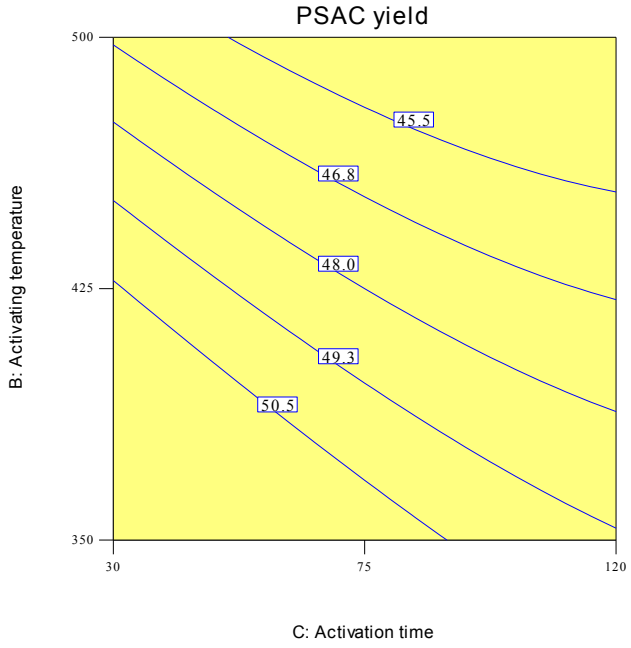

Fig. 4.20. Contour plot (2D) of carbon yield (IR= 1.75)

From RSM analysis, activation temperature is found to have the biggest influence on the PSAC yield among the 3 investigated variables. The yield was found to decrease gradually with activation temperature (Fig. 4.17 & 4.18). Also observed, the PSAC yield is almost independent from IR when sufficient activation time is allocated (Fig. 4.19). Similar observation was reported by Prahas et al. on H_3PO_4 activated jackfruit peel, with the yield was found to remain constant for IR 1-4 within the activation temperature range of 350 °C to 550 °C [17]. The variation in PSAC yield, however is small as compares to surface area and pore parameters.

In addition to the porous nature of the AC, the yield is a desirable parameter to assess effectiveness of the activation process, as it relates to process economics. As shown in Table 2.1 of the PSAC yields using different activation processes, the yield of PSAC utilizing present process is 48.1%, which is the highest of yield reported for palm shell based precursor. Guo and Lua [18] have reported a yield of 40%, while Hu et al. [19] have reported a yield of 37% with the activation using a combined physical-chemical activation using CO_2-$ZnCl_2$. However, both the above work reported a surface area less than 1200 m^2/g, substantially lower than the surface area and the pore volume generated in the present process.

During thermal decomposition of lignocellulosic precursors, the presence of H_3PO_4 in the interior of precursor restricts the formation of tar as well as other liquids such as acetic acid and methanol by formation of cross-links, and inhibits the shrinkage of the precursor particle by occupying certain substantial volumes [18,20]. The H_3PO_4 forms a layer of linkage such as phosphate and polyphosphate esters, which could protect the internal pore structure and thus prevent the adsorbent from excessive burn-off. As the pore evolution for chemical

process commence at much lower temperatures, a higher yield is desirable than the thermal process where excessive burn-off is encountered at higher temperature.

AC with high surface area (BET >2000 m^2/g) and carbon yield (approximately 50%) have not been reported in open literature. This work provides the direct evidence that surface area development is not necessarily associate with excessive burn-off (which is seen in low AC yield). This observation highlights the significance of semi-carbonization. Such additional charring process to chemical activation provides a platform for early reactivity between reagent and palm shell that results in effective release of volatiles matters at low temperature, while leaving the carbon structure intact. Meanwhile, activated under self-generate atmosphere has significantly promote the phosphate reactions and generate a vast amount of pores.

The gap between the ceramic door and muffle furnace wall is not completely air tight and air (O_2) are drawn into the combustion chamber during activation. The variance in the amount of O_2 drawn into the oven could have contributed to a moderate coefficient of determination (R^2= 0.8930). On the other hand, the variety of polyphosphoric acids (with general formula of $H_{n+2}P_nO_{3n+1}$) in H_3PO_4 solution [21] may have some influence on the PSAC yield.

4.6 Conclusions

In this study, palm shells were activated by H_3PO_4 using non-conventional chemical activation method. 3 parameters: activation temperature, impregnation ratio and activation time, selected as significant based on literature research, were further optimized by DOE numerical optimization tool, applying Box-Behnken Design (BBD) to calculate the optimum conditions to produce PASC with desired characteristics. The quadratic models were developed for BET surface area, pore volume, average pore diameter and PSAC yield using Design-Expert software. The statistical tests including test of significance, Lack-of-fit statistics and R-squared statistics approve that models can adequately represent the data. The following conclusions could be derived based on the present work:

1. The DOE model and statistical analysis (ANOVA) were found to be reliable for optimization development of PSAC with high surface area and desirable porosity. The second-order polynomial models developed indicated that the optimum process conditions for BET surface area, porosity and PSAC yield.
2. PSAC with favourable textural characteristics has been developed using H_3PO_4 activation under self-generate atmosphere. IR and activation temperature was found to be significant to surface area development while activation time (if >30 min) is less significant. The PSAC developed at 500 °C for 30 min (IR 1.75) has the highest porous properties (BET surface area of 2139 $m^{2/}g$).
3. All 3 experiment variables were found to be significant to pore volume development. Pore volume could increase 100 times from 0.02 to 2.0 cm^3/g, correspond to the change in process variables from lower to upper limits.
4. Average pore diameter was found to be influenced by all 3 variables and increase from 2.06 to 3.54 with the increase in process variables.

5. The PSAC yield is high as compares to other H_3PO_4-PSAC or chemical activation methods. IR was found to be less significant as compared to activation temperature and time on PSAC yield.

4.7 References

1 A.A. Ahmad, B.H. Hameed, Effect of preparation conditions of activated carbon from bamboo waste for real textile wastewater, Journal of Hazardous Materials 173 (2010) 487-493

2 M.Z. Alam, E.S. Ameem, S.A. Muyibi, N.A. Kabbashi, The factors affecting the performance of activated carbon prepared from oil palm empty fruit bunches for adsorption of phenol, Chemical Engineering Journal 155 (2009) 191-198

3 M.N. Bari, M.Z. Alam, S.A. Muyibi, P. Jamal, A. Al-Mamun, Improvement of production of citric acid from oil palm empty fruit bunches: Optimization of media by statistical experimental designs, Bioresource Technology 100 (2009) 3113-3120

4 D.C. Montgomery, Design and Analysis of Experiments, fourth ed., John Wiley & Sons, USA, 1997, Chapter 13.

5 R. Azargohar, A.K. Dalai, Steam and KOH activation of biochar: Experimental and modeling studies, Microporous and Mesoporous Materials 110 (2008) 413-421

6 B.K. Hamad, A.M. Noor, A.R. Afida, M.N. Mohd Asri, High removal of 4-chloroguaiacol by high surface area of oil palm shell-activated carbon activated with NaOH from aqueous solution, Desalination 257 (2010) 1-7

7 C. Srinivasakannan, M.Z. Abu Bakar, Production of activated carbon from rubber wood sawdust, Biomass & Bioenergy 27 (2004) 89-96

8 C.A. Toles, W.E. Marshall & M.M. Johns, Phosphoric acid activation of nutshells for metals and organic remediation: Process optimization, Journal of Chemical Technology & Biotechnology 72 (1998) 255-263

9 B.S. Girgis, S.S. Yunis, A.M. Soliman, Characteristics of activated carbon from peanut hulls in relation to conditions of preparation, Materials Letters 57 (2002) 164-172

10 T. Vernersson, P.R. Bonelli, E.G. Carrella, A.L. Cukierman, Arundo donax cane as a precursor for activated carbon preparation by phosphoric acid activation. Bioresource Technology 83 (2002) 95-104

11 S.A. Dastgheib, D.A.Rockstraw, Pecan shell activated carbon: synthesis, characterization and application for the removal of copper from aqueous solution, Carbon 39 (2001) 1849-55

12 B.S. Girgis, A.N.A. El-Hendawy, Porosity development in activated carbons obtained from date pits under chemical activation with phosphoric acid, Micropor. Mesopor. Mater. 52 (2002) 105-117

13 K.T. Klasson, L.H. Wartelle, J.E. Rodgers III, I.M. Lima, Copper(II) adsorption by activated carbons from pecan shells: Effect of oxygen level during activation, Industrial Crops and Products 30 (2009) 72-77

14 J. Guo, A.C. Lua, Effect of surface chemistry on gas-phase adsorption by activated carbon prepared from oil-palm stone with pre-impregnation, Separation and Purification Technology 18 (2000) 47-55

15 M.C. Baquero, L. Giraldo, J.C. Moreno, F. Suarez-Garcia, A. Martinez-Alonso, J.M.D. Tascon, Activated carbons by pyrolysis of coffee bean husks in presence of phosphoric acid, Journal of Analytical and Applied Pyrolysis 70 (2003) 779-784

16 R.C. Bansal, M. Goyal, Carbon Adsorption, CRC Press 2005, ISBN: 978-0-8247-5344-3

17 D. Prahas, Y. Kartika, N. Indraswati, S. Ismadji, Activated carbon from jackfruit peel waste by H3PO4 chemical activation: Pore structure and surface chemistry characterization, Chemical Engineering Journal 140 (2008) 32-42

18 J. Guo, A.C. Lua, Textural and chemical properties of adsorbent prepared from palm shell by phosphoric acid activation. Materials Chemistry and Physics 80 (2003) 114-119

19 Z. Hu, H. Guo, M.P. Srinivasan, N. Yaming, A simple method for developing mesoporosity in activated carbon, Separation and Purification Technology 31 (2003) 47-52

20 M. Jagtoyen, J. Groppo, F. Derbyshire, Activated carbons from bituminous coals by reaction with H_3PO_4: The influence of coal cleaning, Fuel Processing Technology 34 (1993) 85-96

21 H. Marsh, F. Rodriguez-Reinoso, Activated carbon, First ed., Elsevier Ltd., Oxford, 2006

22 A. Klijanienko, E. Lorenc-Grabowska, G. Gryglewicz, Development of mesoporosity during phosphoric acid activation of wood in steam atmosphere, Bioresource Technology 99 (2008) 7208-7214

CHAPTER V

CHARACTERISATION AND ADSORPTION

5.1 Introduction

This chapter presents the development of palm shell activated carbon using thermogravimetric analysis (TGA) covering different process conditions. The changes on surface chemistry were assessed using Fourier transfer infrared (FT-IR) and scanning electrons microscopy (SEM) analysis. The equilibrium adsorption capacity of the activated carbon with respect to methylene blue and dairy COD was measured to assess the effectiveness of PSAC. The equilibrium adsorption data was utilized to identify an appropriate adsorption isotherm theory, by fitting the data with various adsorption isotherm models.

5.2 Thermogravimetric analysis (TGA)

5.2.1 TGA of palm shell

The kinetic study of pyrolysis is essential to understand the degradation mechanism of biomass. Carbonization of untreated palm shell, H_3PO_4 treated char and AC were carried out under N_2 atmosphere at a heating rate of 10 °C/min and the volatile evolution was monitored using TGA. The derivative thermogravimetric (DTG) curves were plotted against temperature in the same plot in order to understand the kinetics (Fig. 5.1). The carbonization process of the untreated palm shell can be approximately described by a strong evolution of

moisture and volatile that show three stages of weight loss, accounting for a total loss of 74.2%.

The first stage of weight loss of the palm shell occurs at 30-110 °C, contributes to 7.8% weight loss, could be attributed to the removal of water and light volatile compounds in palm shell (hydrogen, light hydrocarbons and tar). It is expected to show some variation depending on the nature of palm shell, moisture content and residual oil content. The second weight loss occurs over a wider temperature range (110 to 450 °C) accounting for highest weight loss of approximately 60%, could be attributed to decomposition of two main lignocellulosic groups, hemicellulose and cellulose. At the temperature range between 450 and 800 °C, the palm shell residual weight reduced from 33.7% to 25.8%, (weight loss of 7.9%) mainly attributed to the decomposition of remaining lignin.

Two distinct peaks were observed between 230-450 °C, with the first peak at 280 °C could be attributed to the thermal decomposition of hemicelluloses, while second peak at 350 °C was due to the decay of with cellulose and lignin. This is in good agreement with observation by Luangkiattikhun et al. [1] and Yang et al. [2] but different with Guo & Lua [3] who have reported a higher peak temperature of 325 °C and 470 °C.

It is generally agreed that the thermal decomposition of hemicellulose, contributs to the first peak, as it is the easiest of component to decompose, while the second sharper peak is due to degradation of cellulose, which has high thermal stability as compared to hemicellulose. Lignin decomposition, however, take place over a wider temperature interval and it overlaps with the decomposition of hemicellulose and cellulose.

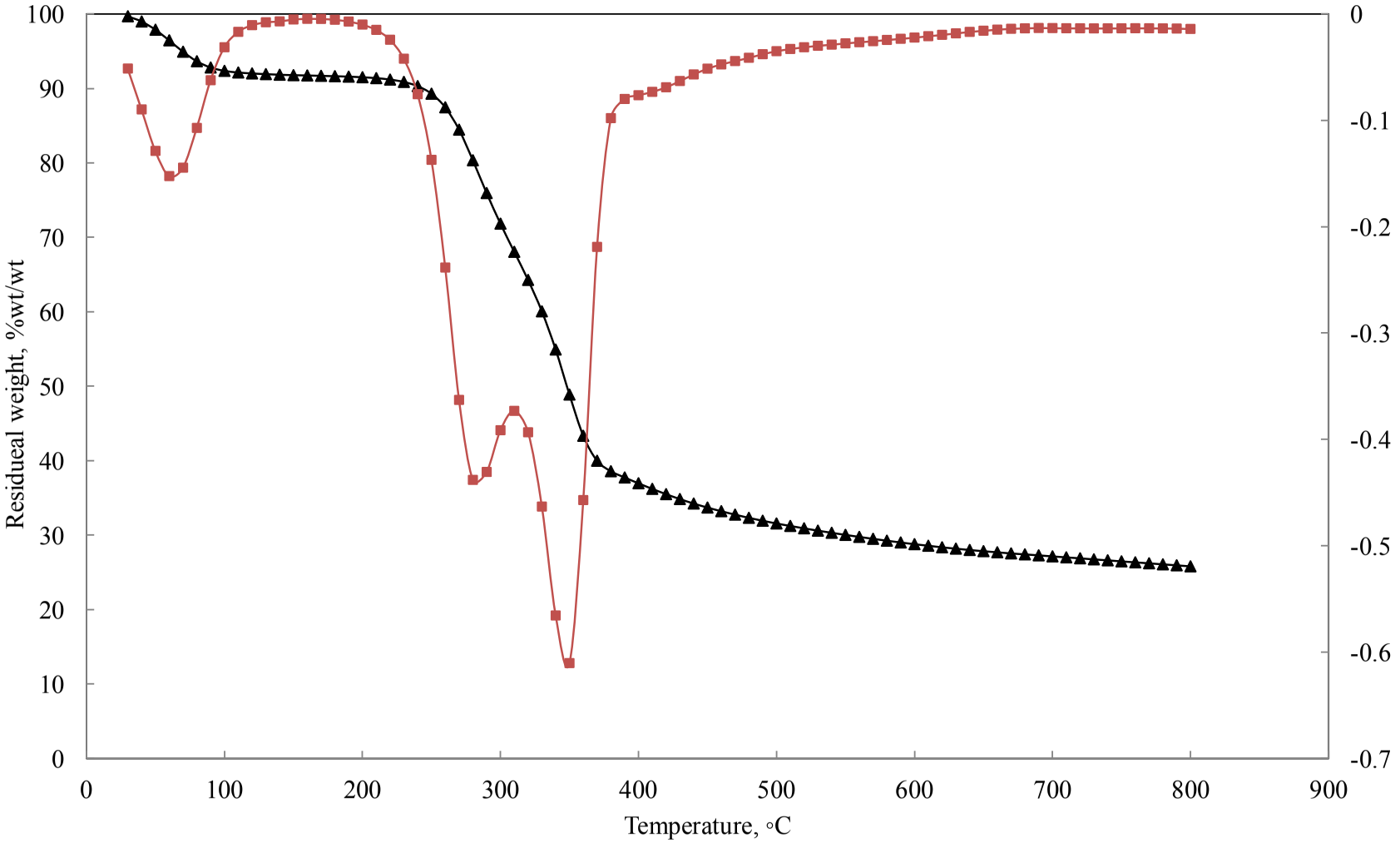

Fig. 5.1. TG (▲) and DTG (■) of palm shell pyrolysed at heating rate 10 ℃/min.

These observations are in good agreement with works on various lignocellulosic materials as summarized in Table 5.1. Font et al. [4] observed two weight-loss steps in almond shell between 210-330 °C and between 330-400 °C, corresponding to hemicellulose and cellulose decomposition, with respective maximum weight-loss rates at 293 °C and 360 °C. Similarly, Chen & Wu [5] studied the pyrolysis of rice husks, and observed that hemicellulose and cellulose decomposes zone between 150-350 °C and 275-350 °C with maximum weight-loss rate at 360°C . The difference in peaks could be attributed to the lignocelluloses composition of the materials. As shown in Table 5.2, palm shell has higher lignin as compared to apple pulp and rice husk, in line with its relatively lower peak temperatures (1^{st} and 2^{nd} peaks).

5.2.2 Effect of semi-carbonization for H_3PO_4 activation

The volatile evolution during carbonization of the H_3PO_4 treated samples (Char and PAC) were monitored by TGA and the results were compared to those of untreated palm shell. TGA has been used widely in literature for process development as well as to understand the mechanism of AC development. Danish et al. [6] used TGA to investigate the influence of reagents, CaO and KOH on thermal stability of *Acacia Mangium* wood AC while Teng et al. [7] employed TGA to understand carbonization process in AC development. Similar methods were utilized by Cuhadaroglu & Uygun [8] to evaluate the ability of KOH and NaOH in suppressing volatile matters release. Kriaa et al. [9] conducted TGA on lignin-AC and observed a strong evolution of volatiles occurring before 200 °C. Similar investigations have been reported on AC cloth and fiber [10]. To the author's knowledge, utilization of TGA to characterize palm shell char or PSAC has not been reported in open literature. As AC preparation in this work is different from conventional chemical activation, with additional step of semi-carbonization and activation under self-generate atmosphere, TGA could provide an insight on the non-conventional activation method using H_3PO_4.

Table 5.1 Summary for temperature of the peak maxima obtained on different materials

Reference	Material	Peak Temperature, °C	
		1st	2nd
This work	Palm Shell	283	348
Luangkiatikhun [1]	Palm Shell	295	365
Yang [2]	Palm shell	250	340
Guo & Lua [3]	Palm Shell	325	470
Hayashi [40]	Palm Shell	270	350
R. Font [4]	Almond Shell	310	368
Elizalde-Gonzalez [41]	Mango Pit	296	367
Suarez-Garcia [42]	Apple pulp	233	328
Chen & Wu [5]	Rice Husk	217	316

Table 5.2 Lignocellulosic composition of biomass

Biomass	Lignin	Peak Temperature, °C	
	(%)	1st	2nd
Palm Shell	53.4	283	348
Apple pulp	17.3	233	328
Rice Husk	21.4	217	316

Fig. 5.2 shows a comparison of the carbonization behavior of palm shell, palm shell chars and AC, up to 800 °C [Note: All samples were thoroughly washed to remove H_3PO_4]. The similarity in weight loss trends in all three samples (30-250 °C) seems to be due to the loss of moisture content and a small fraction of light volatile compound. Subsequent mass loss trends for the char and PSAC are different from the original biomass. While the majority of weight loss for untreated palm shell occurred rapidly between 250 °C and 400 °C, a slower gradual trend being observed in palm shell char and AC. At the final temperature of 800 °C, only a small percentage weight loss was observed for PSAC (14%) as compares to char and untreated palm shell (44% and 74% respectively).

Fig. 5.3 highlights the weight loss rate (DTG) vs the temperature for palm shell char and PSAC. While the pyrolysis of untreated palm shell consists of two distinct kinetic schemes (Fig. 5.1), only one-step scheme is observed for the char. The disappearance of those sharp peaks (which is due to the release of predominantly tars from untreated palm shell) at 250-400 °C indicates the significant change in chemical composition in char. Even though semi-carbonization was carried out at a relatively low temperature (170 °C), substantial release of volatilities has resulted in a carbon rich residual that exhibit higher thermal stability. H_3PO_4 accelerates the bond cleavage reactions, leading to the early evolution of volatiles. This observation of early reactivity due to H_3PO_4 activation is in line with the reports due to Jagtoyen & Derbyshire [11]. TGA analysis on the effect of semi-carbonization, has not been reported in open literature, as only a very few earlier work utilized similar activation method. The semi-carbonization treatment could be seen as a mechanism to encourage the release of non-carbon elements (mainly N and O) as primary volatiles to leave behind a structure favorable for activation. This could possibly provide favorable AC preparation condition such

as low activation temperature and short activation time and high AC yield with well developed textural characteristics.

On the other hand, no kinetic scheme was observed for PSAC. The first significant weight loss occurred only at 600 °C, indicating a thermally stable structure of PSAC. H_3PO_4 activation has resulted in a highly cross linked structure in PSAC which is less prone to volatile loss. The observation highlights the capability of H_3PO_4 in suppressing volatilities during pyrolysis, which are in agreement with observation due to Teng et al. [7] and Kriaa et al. [9].

The effectiveness of semi-carbonization is applicable only to H_3PO_4 activation (not with other reagents). H_3PO_4 is known for the ability to catalyze reaction at low temperature, as evident from the initiation of hydrolysis reactions upon mixing with precursor at room temperature [12]. Carbonization at 170 °C would further enhance the chemical reactivity, seen from the evolution of volatile matters that provide the right condition towards pore development. As indicated in Fig. 5.3, the minimum weight loss rate implies that PSAC becomes stabilized during H_3PO_4 activation. The weight loss was probably due to the release of CO and CO_2 that may have remained unburned or partially burned during activation. Hence, it can be deduced from this study that the PSAC developed has high stability up to 600 °C. The low weight loss rate of PSAC implies that the H_3PO_4 activation method suppress the release of volatile matters during pyrolysis. This is in agreement with well developed surface area of PSAC reported in chapter IV.

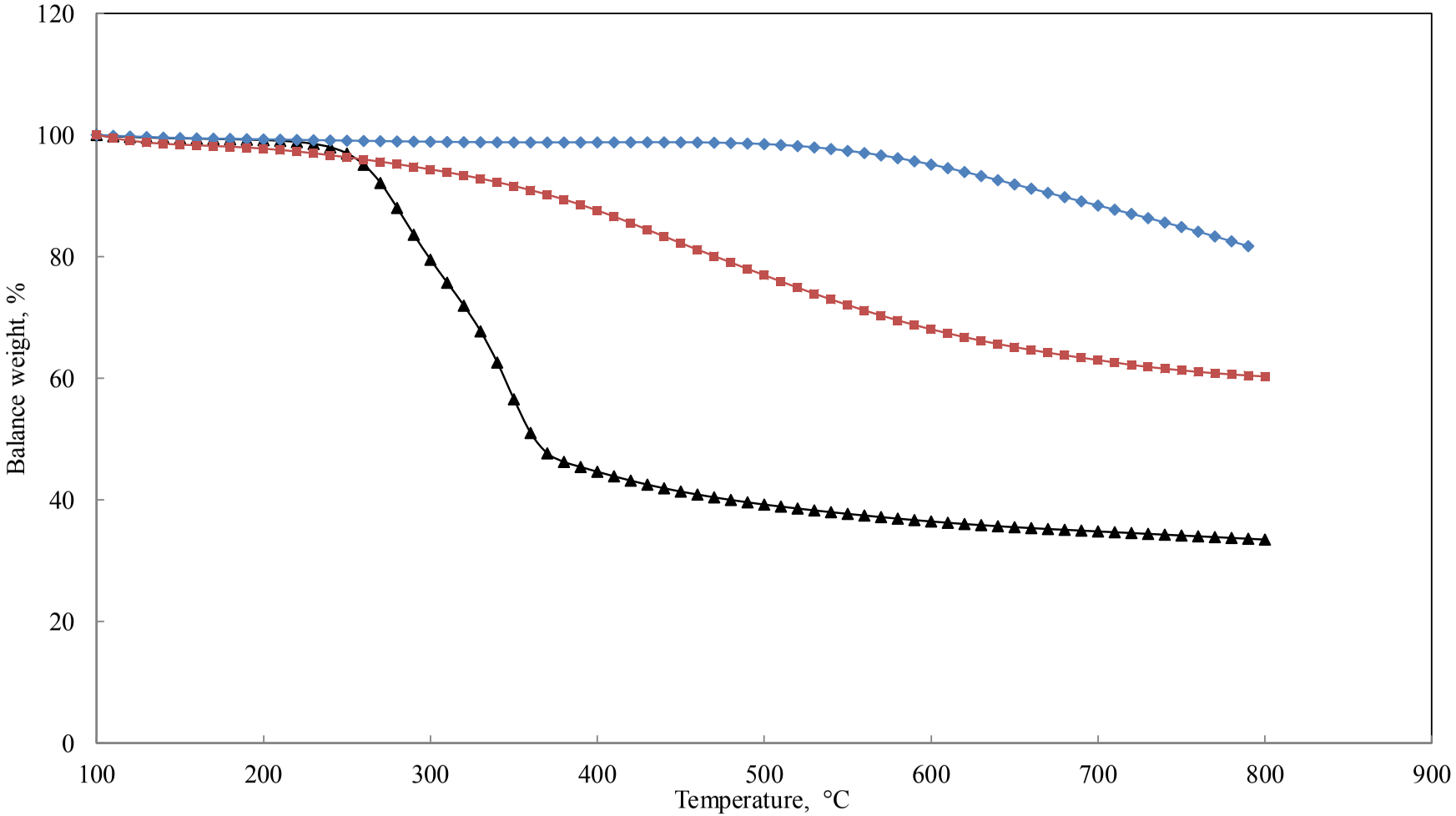

Fig 5.2. TG of raw palm shell (▲), char (■) and PSAC (♦) prepared at 500 °C of activation temperature

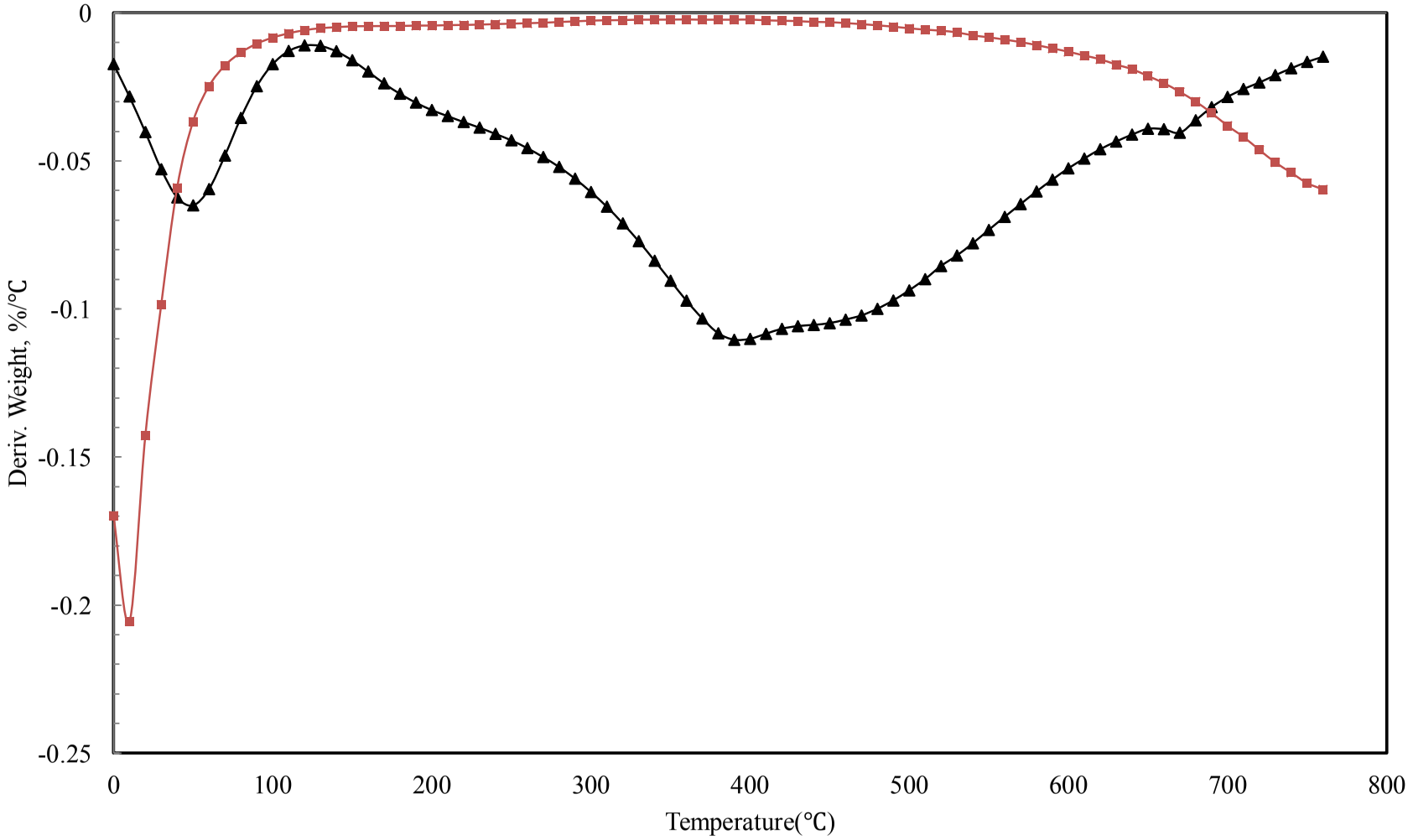

Fig. 5.3. DTG of palm shell char (▲) and PSAC (■)

5.2.3 Effect of activation temperature

The volatile evolution of PSAC developed at 400 (PSAC-400), 500 (PSAC-500) and 600 °C (PSAC-600) during pyrolysis was monitored by TGA and the weight loss curve is show in Fig 5.4. In general, TGA curves of all PSAC samples are quite similar, with almost no loss up to 500 °C. This is followed by a zone with a marked drop in weight for temperature between 500-800 °C.

The weight loss for PSAC activated at 600 °C is the lowest at 14% while it is almost twice at 23% for the other 2 samples. Activation at 600 °C not only provides the activation for most effective volatiles evolution, but also develops a highly cross-linked structure as seen in a thermally stable carbon. This is further evident in plots of weight loss rate vs temperature (DTG) (Fig. 5.5.). For temperature 150-600 °C, PSAC-400 exhibits the highest rate of weight loss followed by PSAC-500. One can observe that the rate of volatility of PSAC-600 is almost zero up to 500 °C, indicate a thermally stable structure.

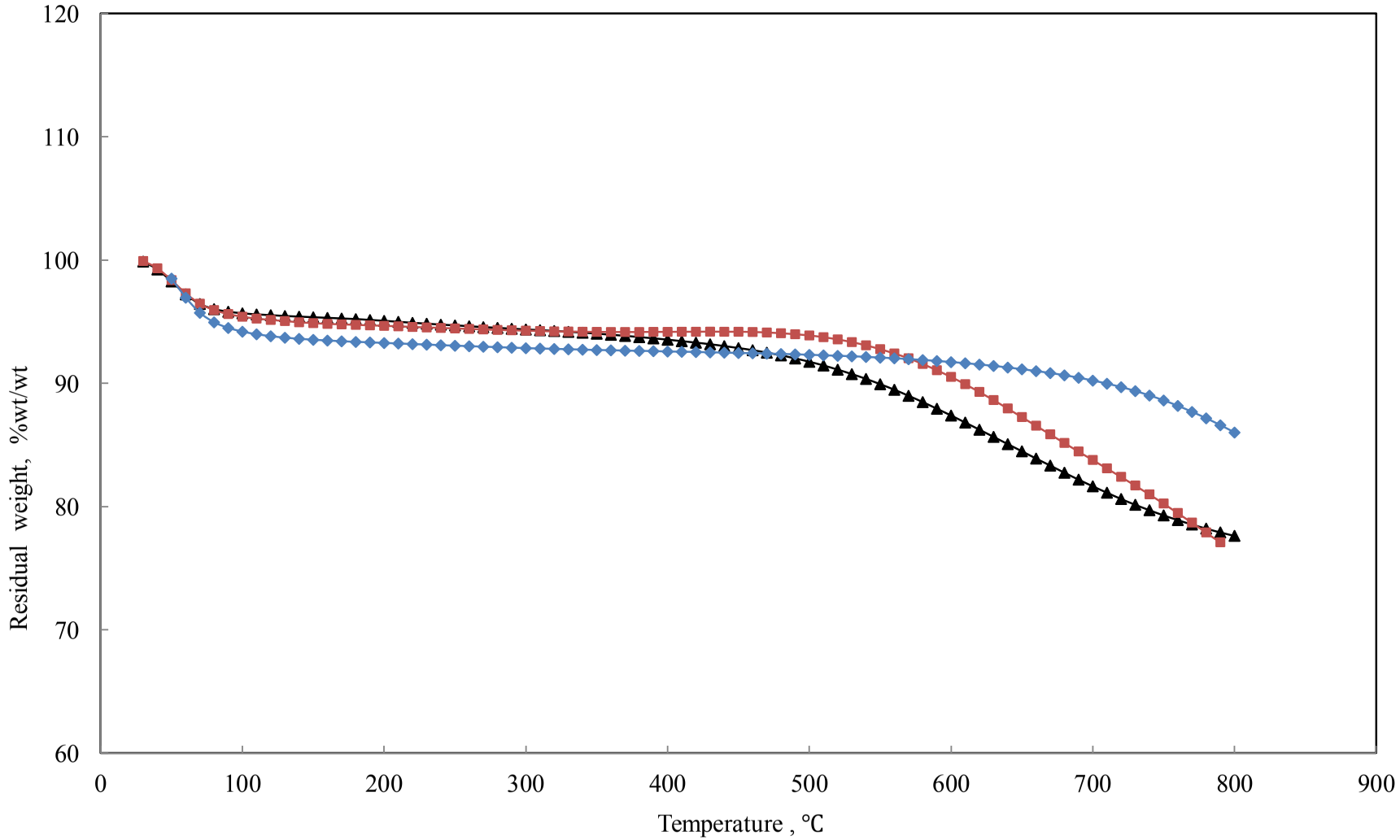

Fig. 5.4. TG of PSAC [T= 400 (▲), 500 (■) and 600 (♦) °C]

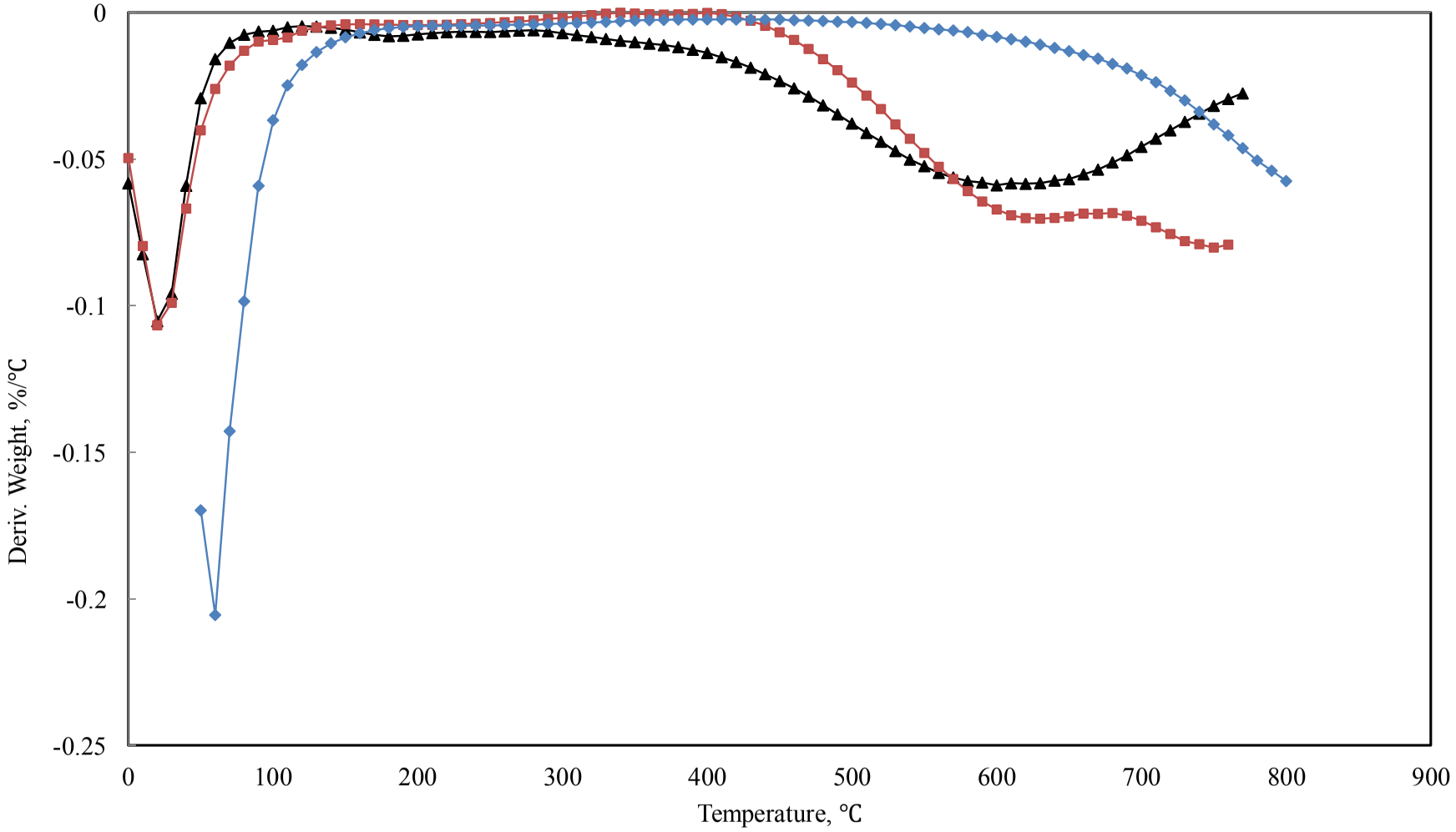

Fig 5.5. DTG of PSAC [T= 400 (▲), 500 (■) and 600 (♦) °C]

5.2.4 Effect of impregnation ratio

The RSM investigation has indicated the influence of IR on PSAC (discussed in Chapter IV). The TGA behavior of PSAC with IR between 0.5 and 3.0 (activated at 500 °C and 75 min) is as shown in Fig. 5.6. Due to treatment with same reagent, all PSAC samples exhibits almost similar weight loss profile.

The PSAC weight loss decreases with increase in IR (from 0.5 up to 2.0, except for PSAC with IR 3.0). The increase of the reagent concentration is likely to promote more efficient H_3PO_4 reactions. Thus, under these conditions, the release of tarry materials would be minimized as seen in higher residue weight. On the other hand, excessively high IR of 3.0 may be due to aggressive alteration by H_3PO_4 groups on the carbon surface resulting in PSAC with weaker carbon structure or mechanical strength, which is prone to thermal degradation. The PSAC prepared with 0.5 IR, could possibly have significant residual amount of volatile matters that are yet to be effectively removed. Its removal during TGA could possibly be attributed for the weight loss. However the weight loss trend for all IR looks similar, indicating the effectiveness of H_3PO_4 activation on palm shell.

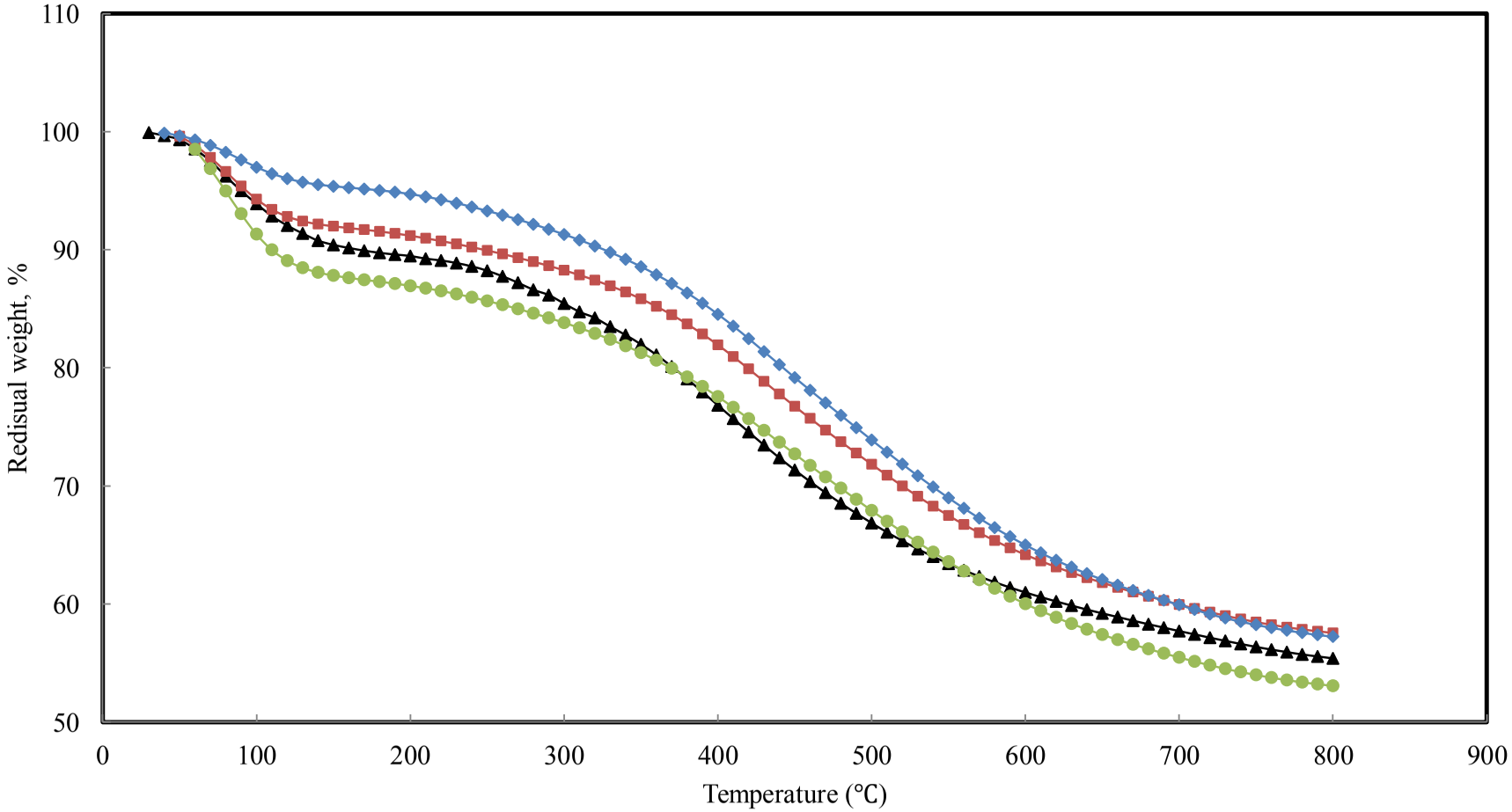

Fig 5.6. TG of palm shell chars at different IR, (▲: 0.5, ■:1.0 ♦: 2.0, ●:3.

5.3 Fourier transform infrared (FT-IR) analysis

Surface functional groups on the palm shell, its char and H_3PO_4 activated carbon were detected by Fourier transform infrared spectrometry (FTIR) for adsorption band 4000-500 cm^{-1}. Table 5.1 (a) to (c) summarize the wavenumbers and assignments of the main bands for all 3 samples.

Table 5.1 (a) FT-IR adsorption band of palm shell

Adsorption band	Assignments
3595 and 3340 cm^{-1}:	O-H stretching in acid and methanol
1720 and 1508 cm^{-1}:	C=O stretching in ketone and carbonyl
1605 cm^{-1}:	C=O stretching in quinones and carboxylic anhydrides
1242 cm^{-1}:	C-O-C stretching in alkyl aryl ethers
1033 cm^{-1}:	C-O stretching in $–CH_2OH$

Table 5.1 (b) FT-IR adsorption band of palm shell char

Adsorption band	Assignments
3381 cm^{-1}:	O–H stretching in hydroxyl functional groups
2359 cm^{-1}:	C=O stretching in ketone, quinone and aromatic rings
1601 cm^{-1}:	C=C stretching in alkyl aryl ethers
1224 cm^{-1}:	C-O-C stretching in ethers

Table 5.1 (c) FT-IR adsorption band of PSAC

Adsorption band	Assignments
3375 cm^{-1}:	O–H stretching in hydroxyl functional groups
2360 and 2343cm^{-1}:	C=O stretching in ketone, quinone and aromatic rings
1559 cm^{-1}:	C=O stretching in quinones, carboxylic anhydrides
1507 cm^{-1}:	C=C stretch in aromatic rings;
1384 cm^{-1}:	C-H bending in alkanes ; and
1180 cm^{-1}:	O-C stretching in P-O-C or P=OOH or P=O stretching in phosphate ester,
668 cm^{-1}:	O–H bending in phenol, ester, ether and aromatic

From the FT-IR spectrum, the main surface functional groups in palm shell are carbonyl groups (ketone, quinone) and ethers. Similar observations on palm shell were reported in other works [13,14]. The bands at 1750–1150 cm^{-1} which peak at 1163 cm^{-1} are likely due to methoxyl–O–CH_3, C–O–C stretching and C=C stretching of aromatic rings. These are functional groups associated with the lignin, which is the main component of palm shell [2]. Upon semi-carbonization, the char displayed the surface functional groups of ketone, quinone and aromatic rings with the band attributed to C=O stretching vibrations at 2360 cm^{-1}.

Phenols, carboxylic anhydrides and carbonyl groups are acidic functional groups [15] found in H_3PO_4-activated PSAC. Similar observations were reported on other works on H_3PO_4-activated PSAC [16,17]. These groups provide the acidic characteristic to the PSAC. In addition, a unique band attributed to C=O stretching vibrations at 2360 cm^{-1} could be found, which has not been reported in the previous PSAC studies. The presence of ketone is due to the incorporation of oxygen atoms at the edge of the aromatic sheet or within the carbon matrix during the activation process. In this case, oxygen atoms are from self-generated atmosphere that enriched carbon dioxide atmosphere. The appearance of a broad band between 1300 and 1100 cm^{-1} with a maximum at 1220-1180 cm^{-1} is observed in the spectra suggests significant alteration by H_3PO_4 activation. According to Puziy et al. [18], the band around 1220-1180 cm^{-1} is due to the stretching of hydrogen-bonded P=O in the phosphate ester, O–C bond in P–O–C linkage, or P=OOH bond. This observation indicates the incorporation of phosphates onto the carbon surface during H_3PO_4 activation. Such observation on PSAC has not been reported. As observed, chemical activation of a palm shell with H_3PO_4 results in significant change on surface chemistry of the PSAC having strong acidic surface groups.

The spectrum of FT-IR of H_3PO_4 activated PSAC at 0.5, 1.75 and 3.0 IR are shown in Fig. 5.8. Overall, the spectrum of PSAC prepared at 0.5 IR is similar to samples prepared at IR of 1.75 and 3.0, except for the stronger peaks in the spectrum, suggesting higher intensities in the oxygen functional groups. The surface functional groups of ketone, quinone and aromatic rings with the band attributed to C≡O stretching vibrations at 2360 cm^{-1} is found to increase with IR.

The influence of activation on PSAC surface characteristics has been assessed with FT-IR and spectrum is shown in Fig. 5.9. There are no conspicuous differences between the spectra, which obtained for PSAC developed at 300, 425 and 500 °C. The only detectable difference is in the small increase in intensity of 2360 cm^{-1} adsorption band with activation temperature. The growth of this band signify the increase in ketone, quinone and aromatic rings in PSAC. One can conclude this is could be due to the increase of oxygen atoms incorporation into carbon matrix with increase in activation temperature.

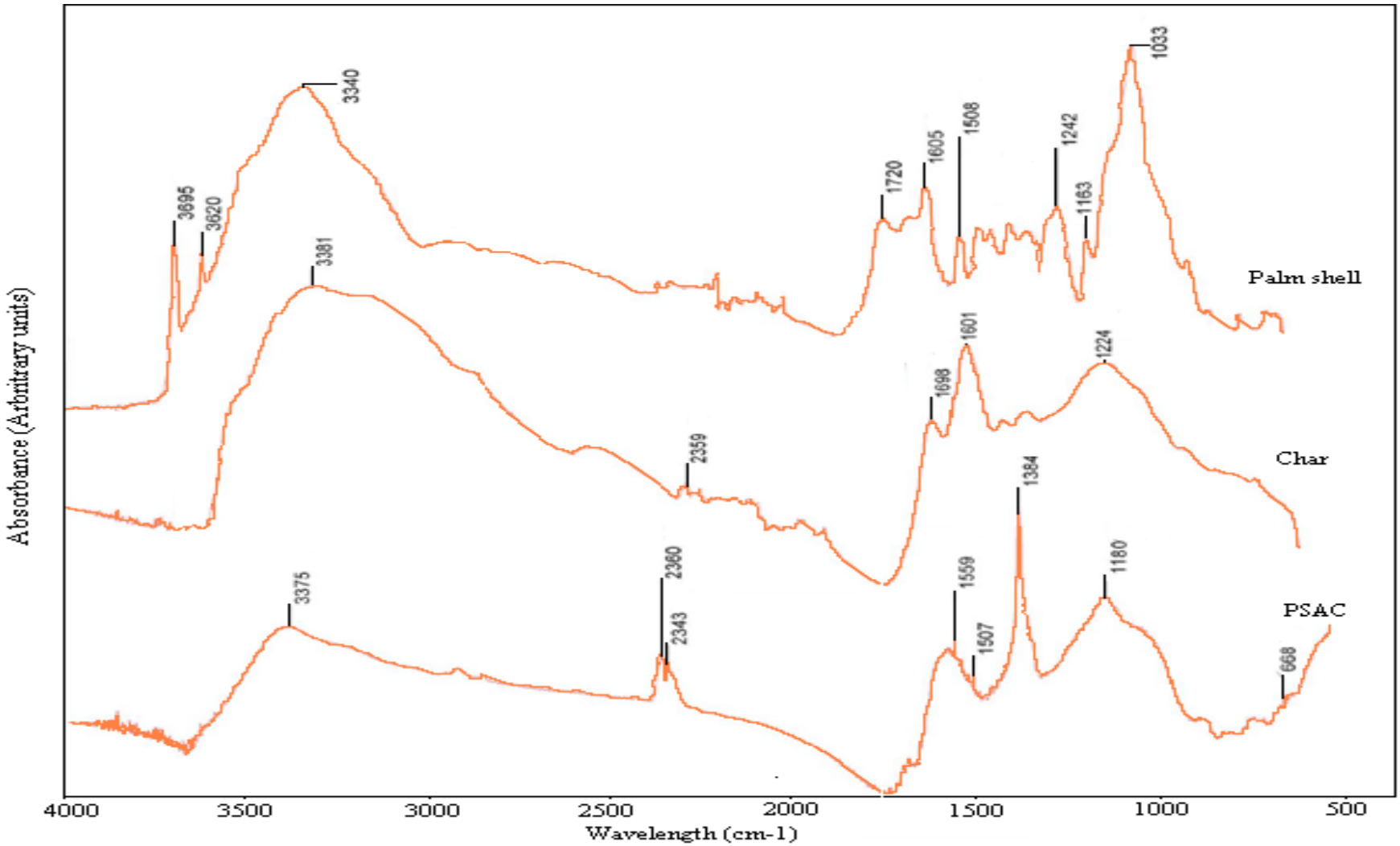

Fig 5.7. FT-IR spectra of palm shell, char and PSAC (T= 425 °C, IR= 1.75, t= 75 min)

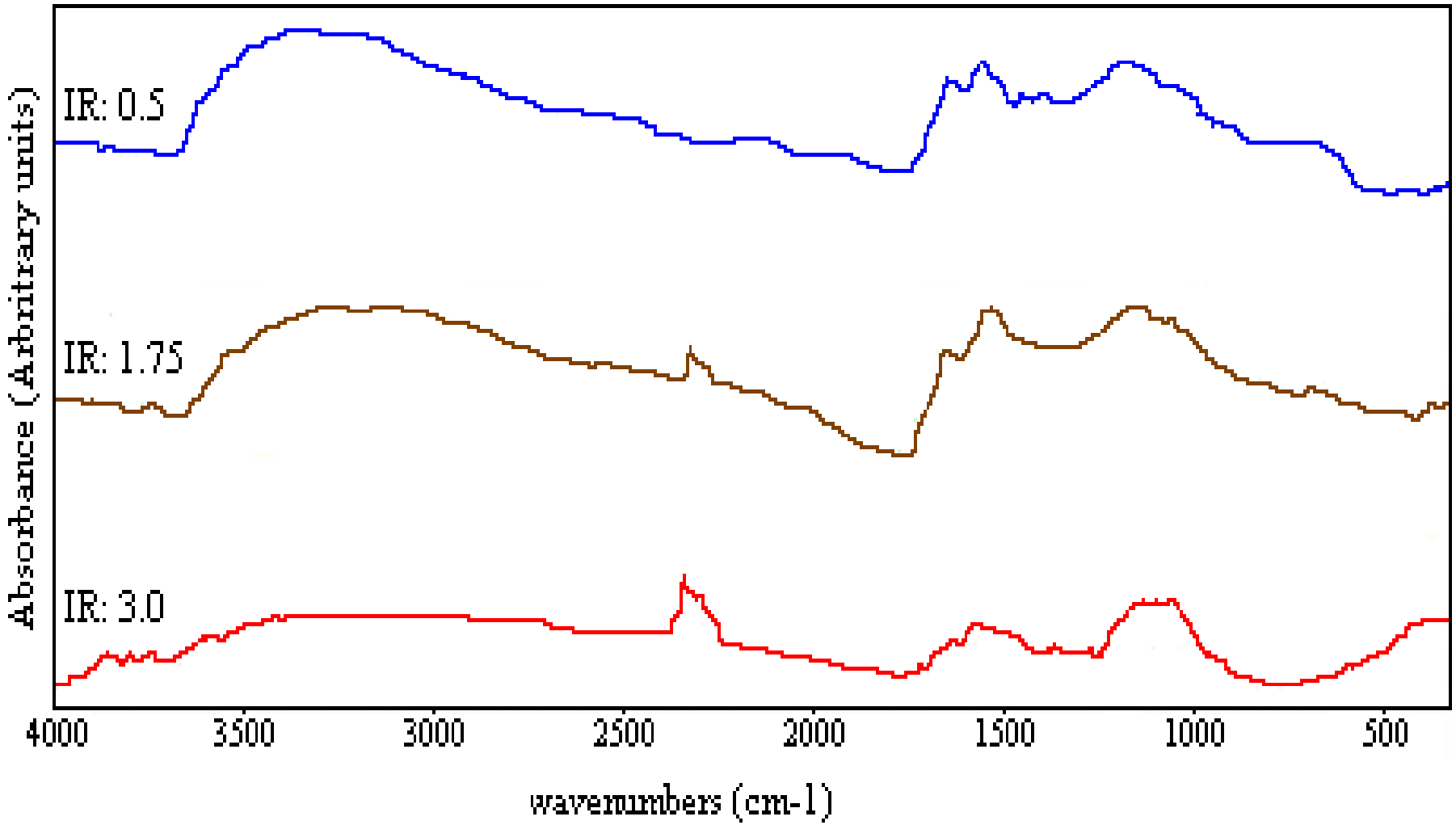

Fig. 5.8. FT-IR spectra of PSAC developed with different IR

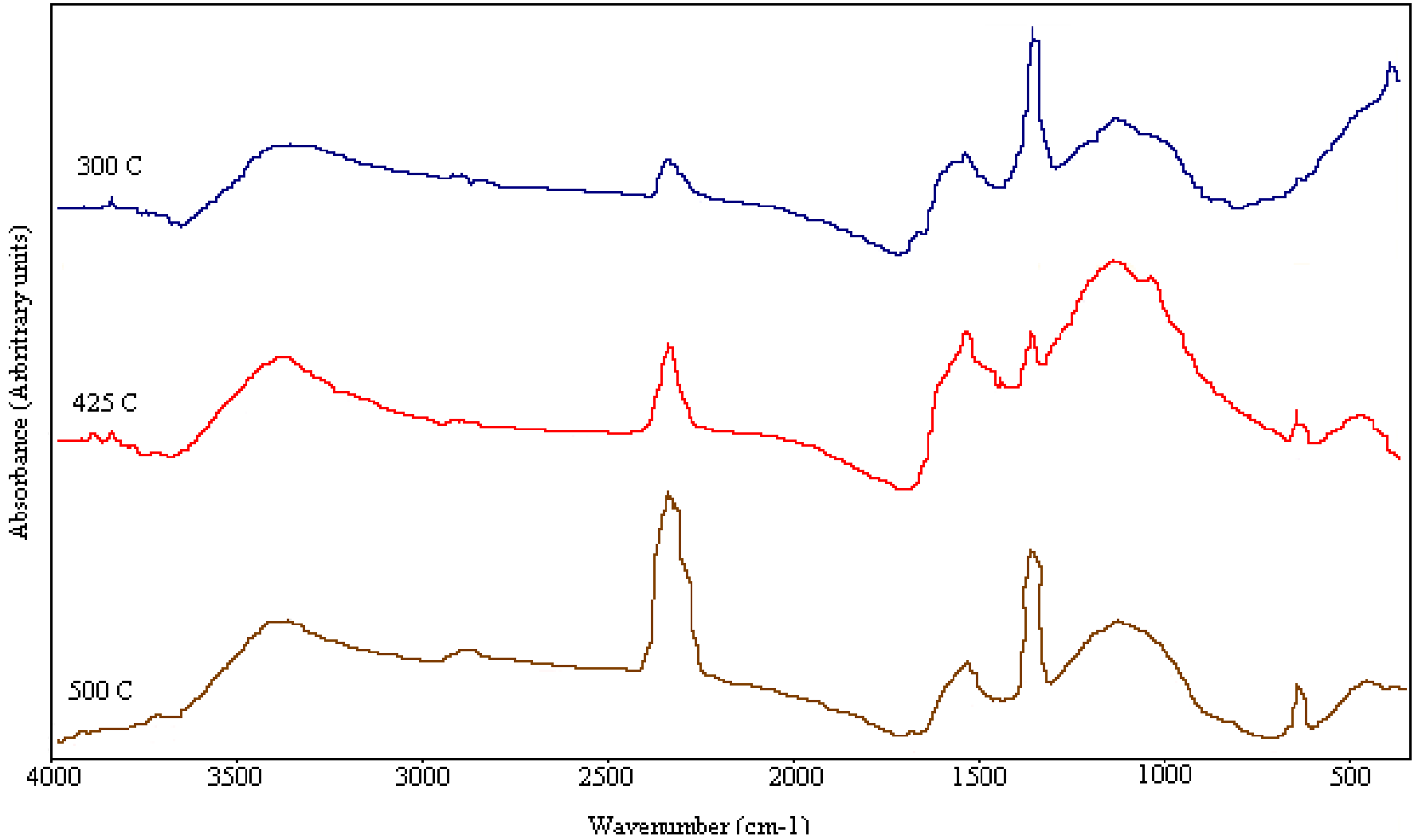

Fig. 5.9. FT-IR spectra of PSAC developed with different activation temperature

5.4 Scanning electron microscopy (SEM) analysis

From the SEM micrograph, the development of cavities as a result of H_3PO_4 activation is clearly visible on the external surface of all PSAC samples, especially for PSAC activated under favorable condition [Fig. 5.10 (c) & (d)]. Low IR would result in PSAC with lower number of pores on carbon surface as shown in Fig. 5.10 (a) even though activated at favorable temperature and adequate activation time. On the other hand, Fig. 5.10 (b) shows the pore development under very unfavorable condition (300 °C, 0.5IR, 30 min); it is visible that the pores developed are smaller and highly irregular in nature. The "nodule-like" structures in the interior of PSAC particles [Fig. 5.10 (d)] indicates phosphoric acid activation results in pore development inside the particle due to activation.

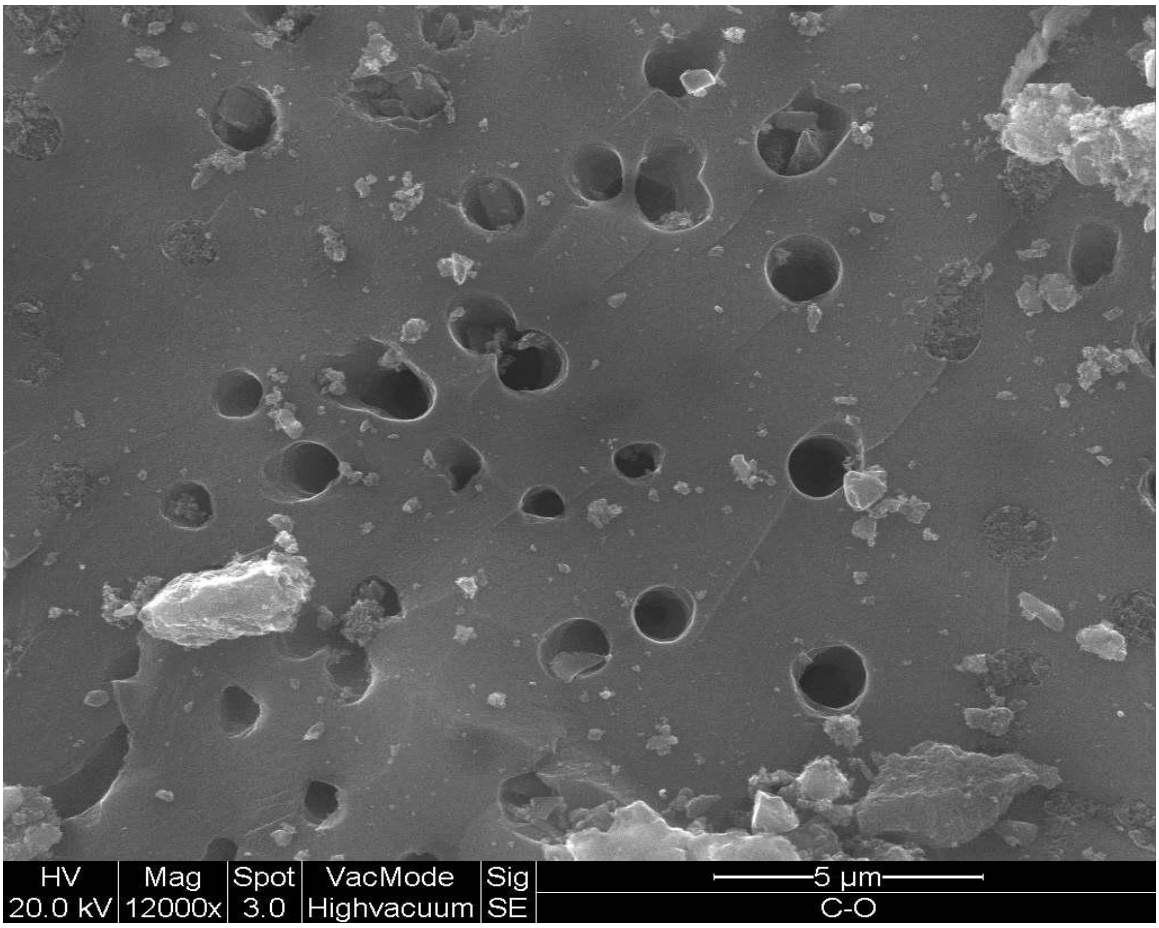

Fig. 5.10. (a) SEM image of PSAC surface (T= 425 °C, IR= 0.50 and t= 30 min)..

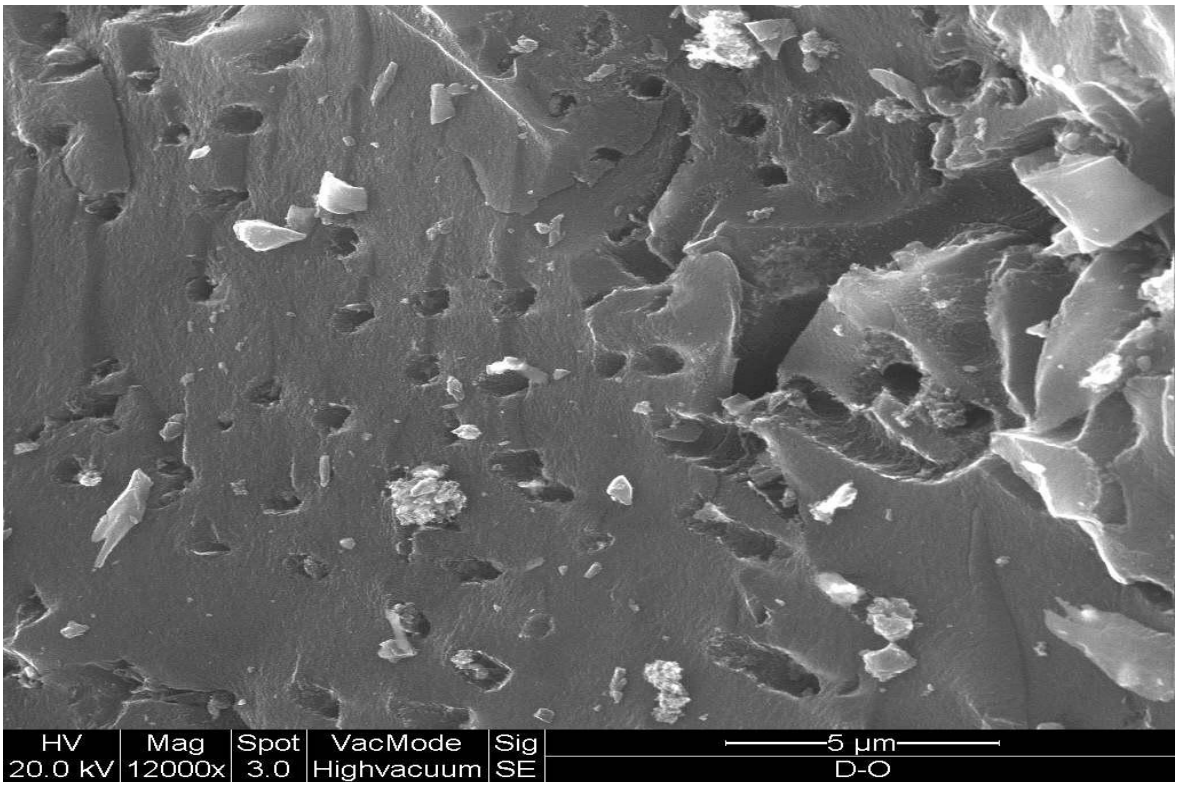

Fig. 5.10. (b) SEM image of PSAC surface (T= 300 °C, IR= 0.50 and t= 30 min)

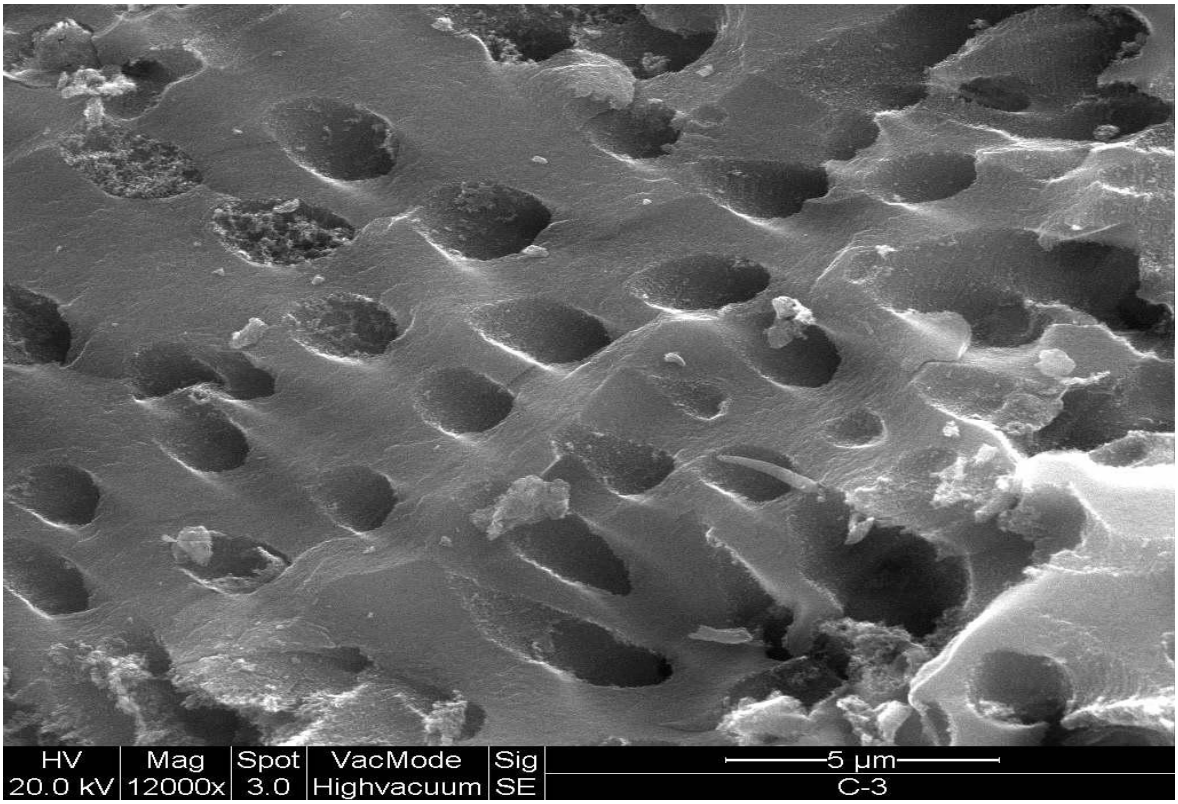

Fig. 5.10. (c) SEM image of PSAC surface (T= 500 °C, IR= 1.75 and t= 30 min)

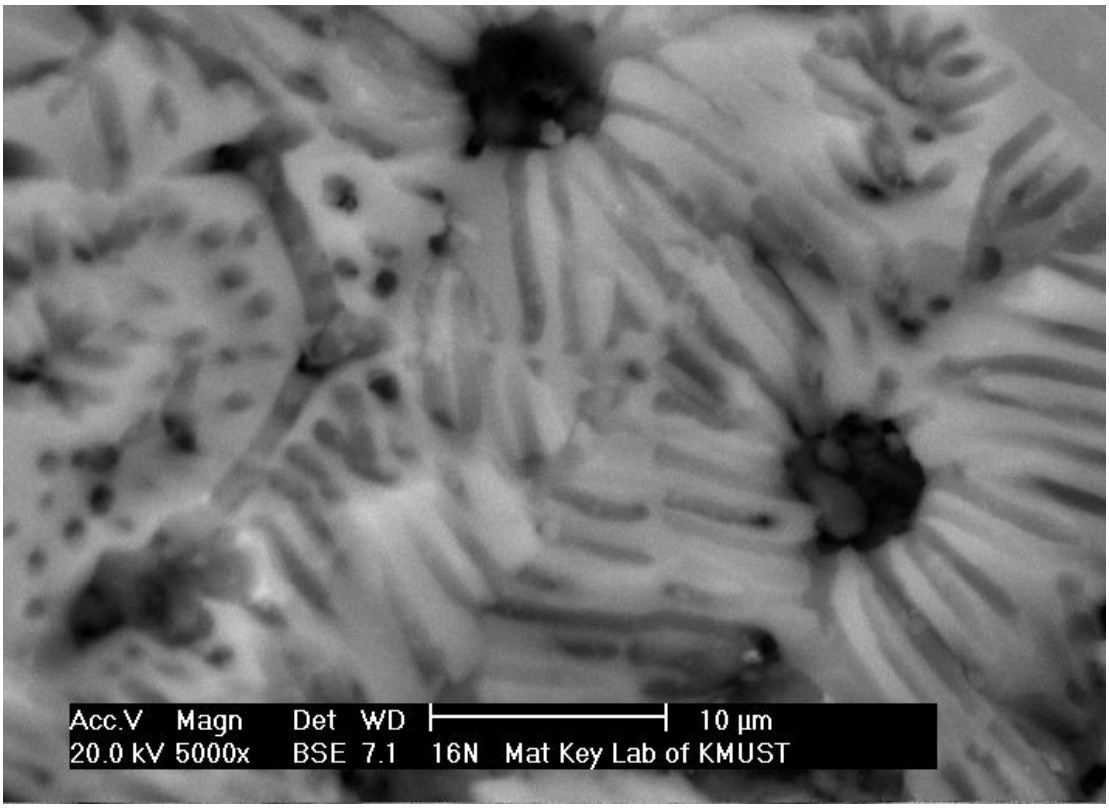

Fig. 5.10. (d) SEM image of PSAC surface (T= 500 °C, IR= 1.75 and t= 30 min)

5.5 Palm shell activated carbon adsorption

AC adsorption has been extensively used in the tertiary water treatment processes. The adsorption of macromolecules using AC has not been properly addressed in the available literature. In this chapter, PSAC samples with high fraction of mesopores are used in conjunction with the basic characteristics of macromolecules. Adsorption studies using PSAC have been conducted using MB dye and diary waste. The MB is a single molecule while the diary waste has high in molecular heterogeneity, tested based on the variation in COD.

5.5.1 Adsorption equilibrium

The influence of temperature on the MB and dairy COD adsorption rate and equilibrium on PSAC were investigated at three different temperatures of 30, 40 and 50 °C at an initial concentration of 1200 mg/L for MB (30, 35 and 40 °C at an initial concentration of 1400

mg/L for dairy COD). The developed PSAC is with a total pore volume and BET surface area of 1.9 cm^3/g and 1958 m^2/g respectively. The average pore diameter is larger than 3.2 nm, with the ratio of the mesopore to the total surface area in excess of 75%. Fig. 5.11 is a typical plot of the equilibrium adsorption of MB in the solid phase corresponding to the MB concentration in the liquid phase, showing the effect of temperature. A sharp rise in the equilibrium adsorption capacity at low concentration of MB in the liquid is observed, which reaches an asymptote at higher liquid phase MB concentration. It is further evident the increase in the equilibrium adsorption capacity of the PSAC with temperature of the adsorption process. As detailed in the experimental section, the solid and the liquid phase are maintained in contact at stable conditions over 24 hours to establish the equilibrium adsorption isotherm.

An increase in the equilibrium adsorption capacity with increase in temperature indicates adsorption process being endothermic. The increasing temperature aids increasing the number of MB molecules to acquire sufficient energy to penetrate the external boundary layer of PSAC particles to enable the interaction with active site at the surface. In addition, Hameed et al. [19] reported an increase in temperature may produce a swelling effect within the internal structure of the adsorbent that enabling large dye to penetrate further. Meanwhile, Dogan et al. [20] suggested a possible mechanism of interaction is the reaction between the chromophere groups such as alcoholic, carboxylic and phenolic of the adsorbent surface and the cationic group in the dye molecule; such reactions could be favorable at higher temperatures. Also known, the increasing temperature would result in increase of the diffusion rate of adsorbate molecules across the external film layer and into the internal pores of the adsorbent particle [21,22]. Furthermore, an increase in temperature would also result in the shift of adsorption equilibrium due to Le- Chatelier Principle.

On the other hand, the PSAC adsorption characteristics on macromolecular adsorbate were investigated using dairy COD under similar process condition except temperature which is at 30, 35 and 40 °C. The typical plot of the equilibrium adsorption of dairy COD waste corresponding to the various concentration in the liquid phase is shown as in Fig. 5.12. Unlike MB adsorption, the equilibrium adsorption capacity is found to rise gradually throughout the dairy COD concentration without a clear asymptote reached, even at initial SD concentration at as high as 1800 mg/l. It is also evident that dairy COD adsorption is less influenced by process temperature with adsorption value almost similar for all initial concentration applied. dairy COD is make up of various types of organics such as fats, proteins, carbohydrate and minerals, with each component may behave differently towards changes of temperature. As such, dairy COD adsorption by PSAC is highly heterogeneity in nature and the influence of temperature could not be clearly identified.

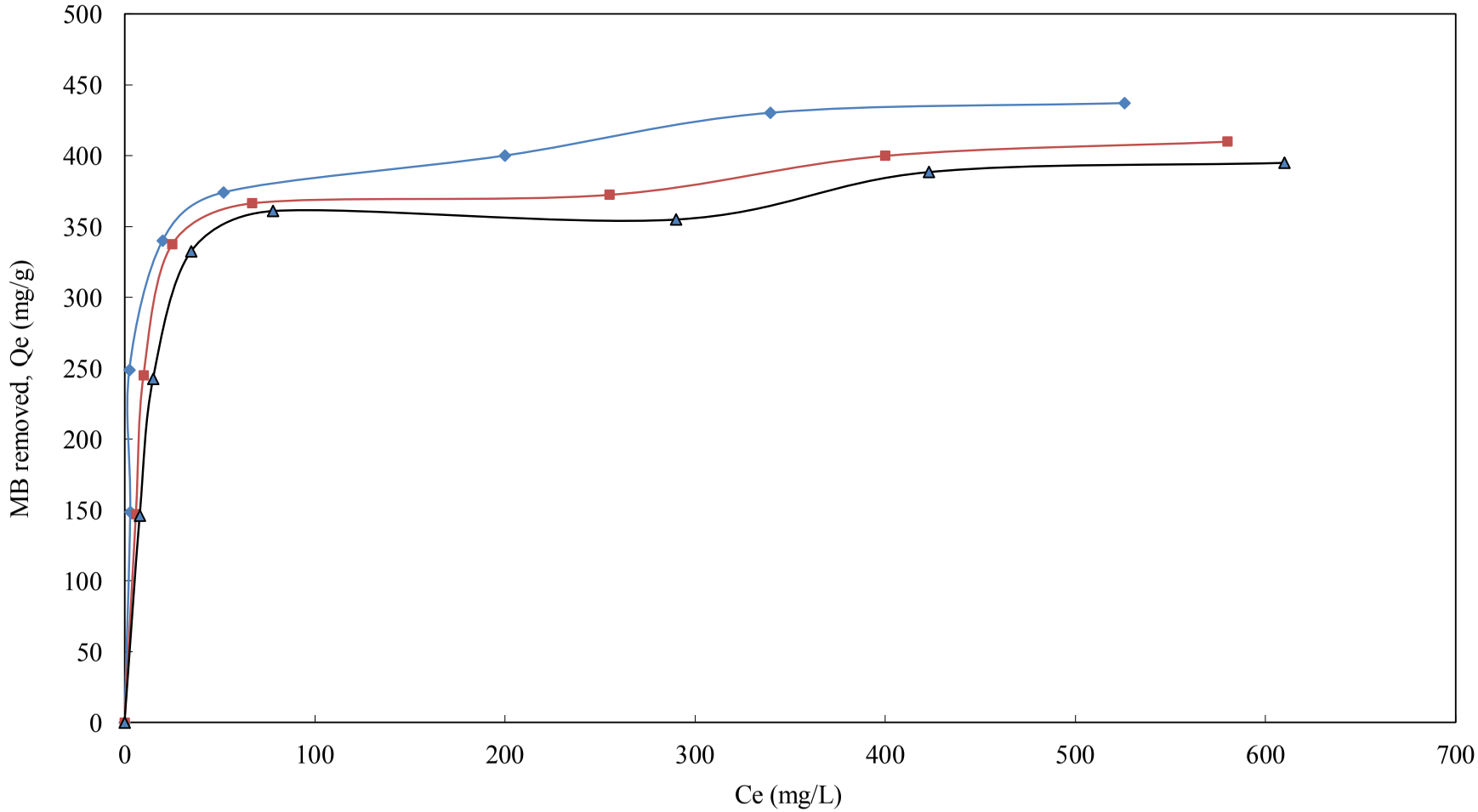

Fig. 5.11. Effect of temperature on the MB adsorption onto PSAC (▲: 30 ºC; ■: 40 ºC; ♦: 50 ºC)

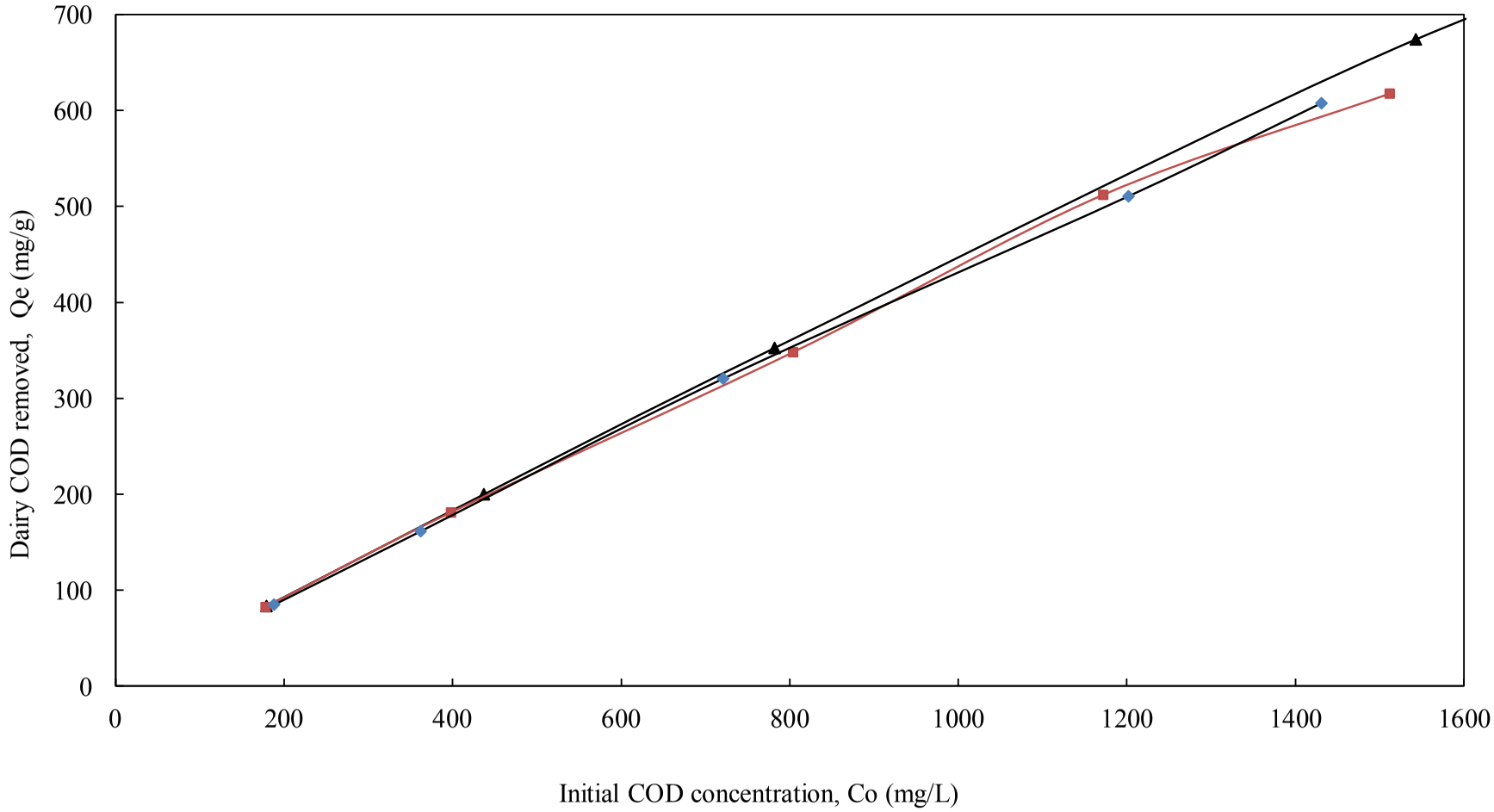

Fig 5.12. Effect of temperature on the dairy COD adsorption onto PSAC (▲: 30 ºC; ■: 35 ºC; ♦: 40 ºC)

The quantity of MB dye or dairy COD uptake by PSAC is found to be influenced by initial concentration and the temperature at different degree [23]. The adsorption isotherms generated at different temperature for the PSAC are tested with popular adsorption isotherm models to identify appropriate mechanism of adsorption. The experimental outcomes are fitted with the Langmuir, Freundlich and Temkin isotherm models to evaluate the model parameters by minimizing error between the experimental data and the model equation. The correlation coefficients, R^2, served as an indicator to check the appropriateness of the model. The evaluated model parameters are listed in Table 5.3.

5.5.1.1 Langmuir isotherm

From section 2.2, the Langmuir equation, which is applicable to homogeneous sorption, can be described by the linearised form:

$C_e/Q_e = 1/Q_0b + C_e(1/Q_0)$

The Langmuir constants Q_0 (mg/g) and b (L/mg) are determined from the slope and intercept of the plot of specific adsorption, C_e/Q_e against the equilibrium concentration, C_e as presented in Fig. 5.13 & 5.14 The close proximity of the experimental data with the model equation evidenced from the R^2 value (Table 5.3) of 0.9998 and 0.9877 respectively for MB and dairy COD adsorption, demonstrates suitability of the Langmuir isotherm model.

5.5.1.2 Freundlich isotherm

From Section 2.13.1(b), the logarithmic form of Freundlich isotherm is given by the following equation:

$\log Q_e = \log K_F + (1/n)\log C_e$

where K_F (mg/g)(L/mg)$^{1/n}$ and n are the Freundlich adsorption constant. $1/n$ is the heterogeneity factor that measure of the adsorption intensity as well as its favorability. The linearised Freundlich plot of logQ_e versus logC_e is shown in Fig. 5.15 & 5.16 along with Freundlich constants K_F and $1/n$. The R^2 value is shown in Table 5.3, and it corresponds to 0.9694 and 0.9838 for MB and dairy COD adsorption respectively, demonstrating the magnitude of variation between the experimental data and the model equation.

Table 5.3 Langmuir, Freundlich and Temkin isotherm constants for MB and dairy COD adsorption onto PSAC

Isotherm	Methylene blue (MB)	Dairy COD
Langmuir	Q_0= 434.7 mg/g b= 0.1729 L/mg R^2= 0.9998	Q_0= 1250 mg/g b= 3.970 L/mg R^2= 0.9877
Freundlich	K_F= 227 (mg/g)(L/mg)$^{1/n}$ $1/n$= 0.1097 R^2= 0.9694	K_F= 166.3 (mg/g)(L/mg)$^{1/n}$ $1/n$= 0.6774 R^2= 0.9838
Temkin	A= 336.97 L/g B= 36.859 R^2= 0.9868	A= 11.11 L/g B= 219.05 R^2= 0.9557

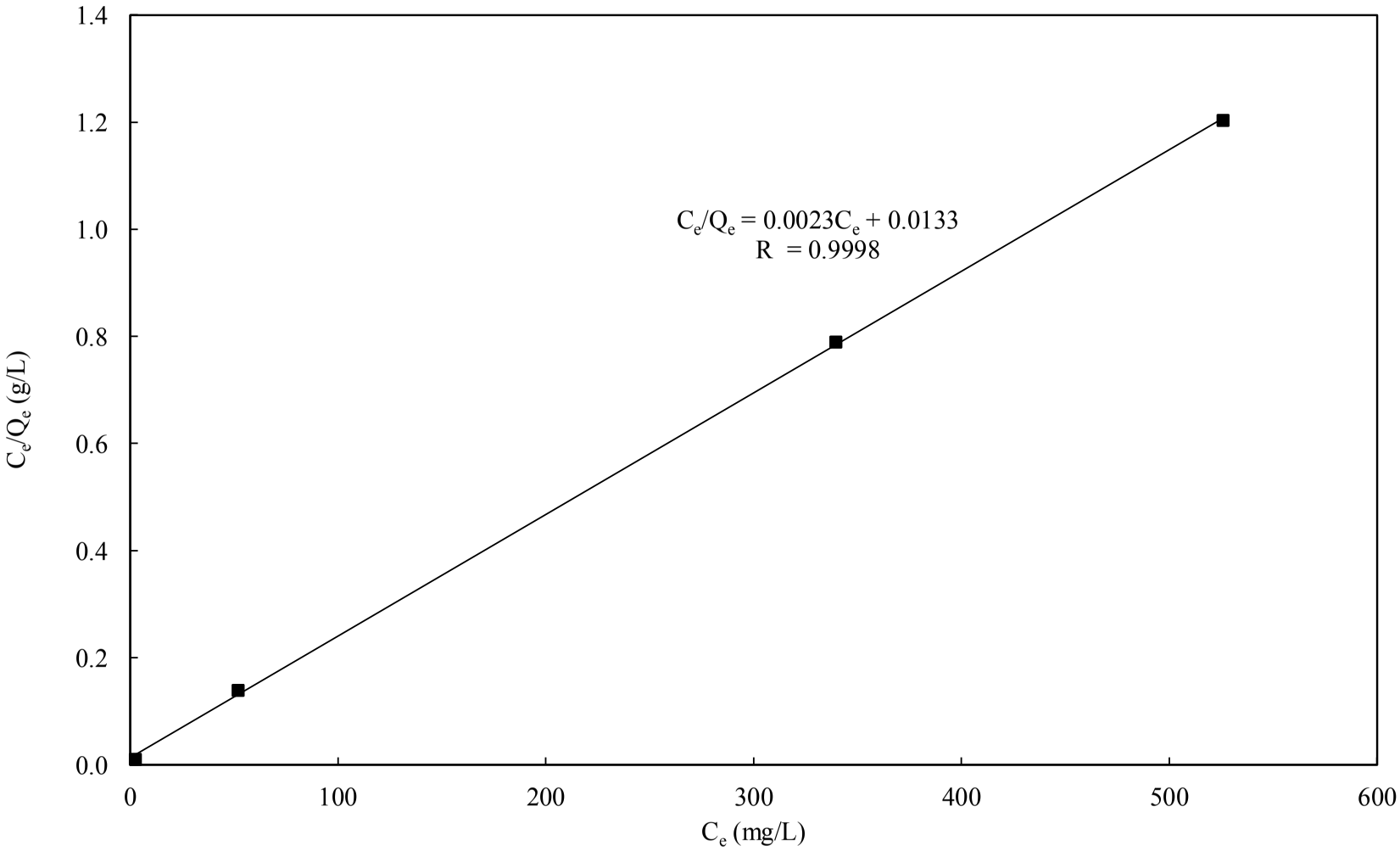

Fig. 5.13. Langmuir isotherm for MB adsorption onto PSAC

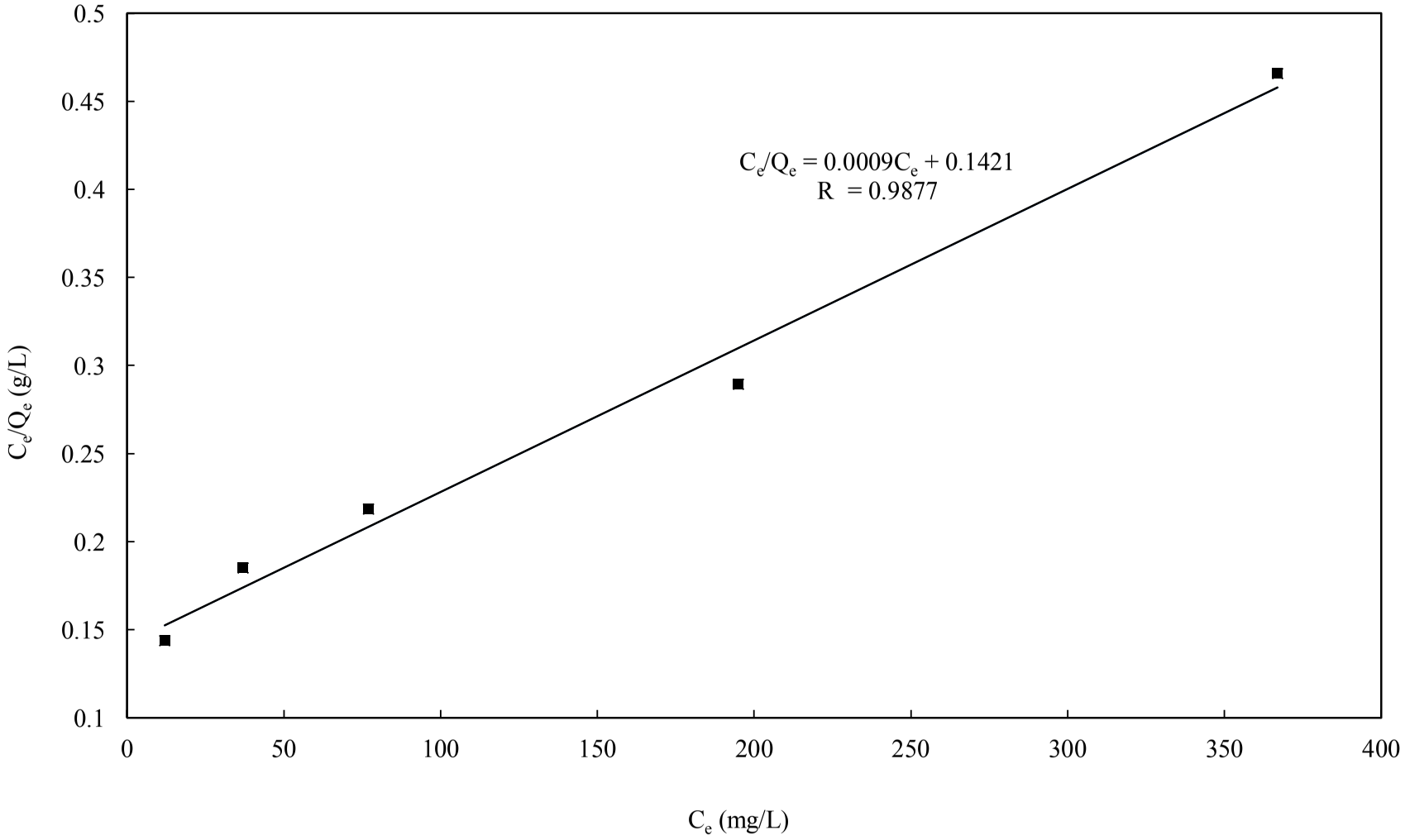

Fig. 5.14. Langmuir isotherm for dairy COD adsorption onto PSAC

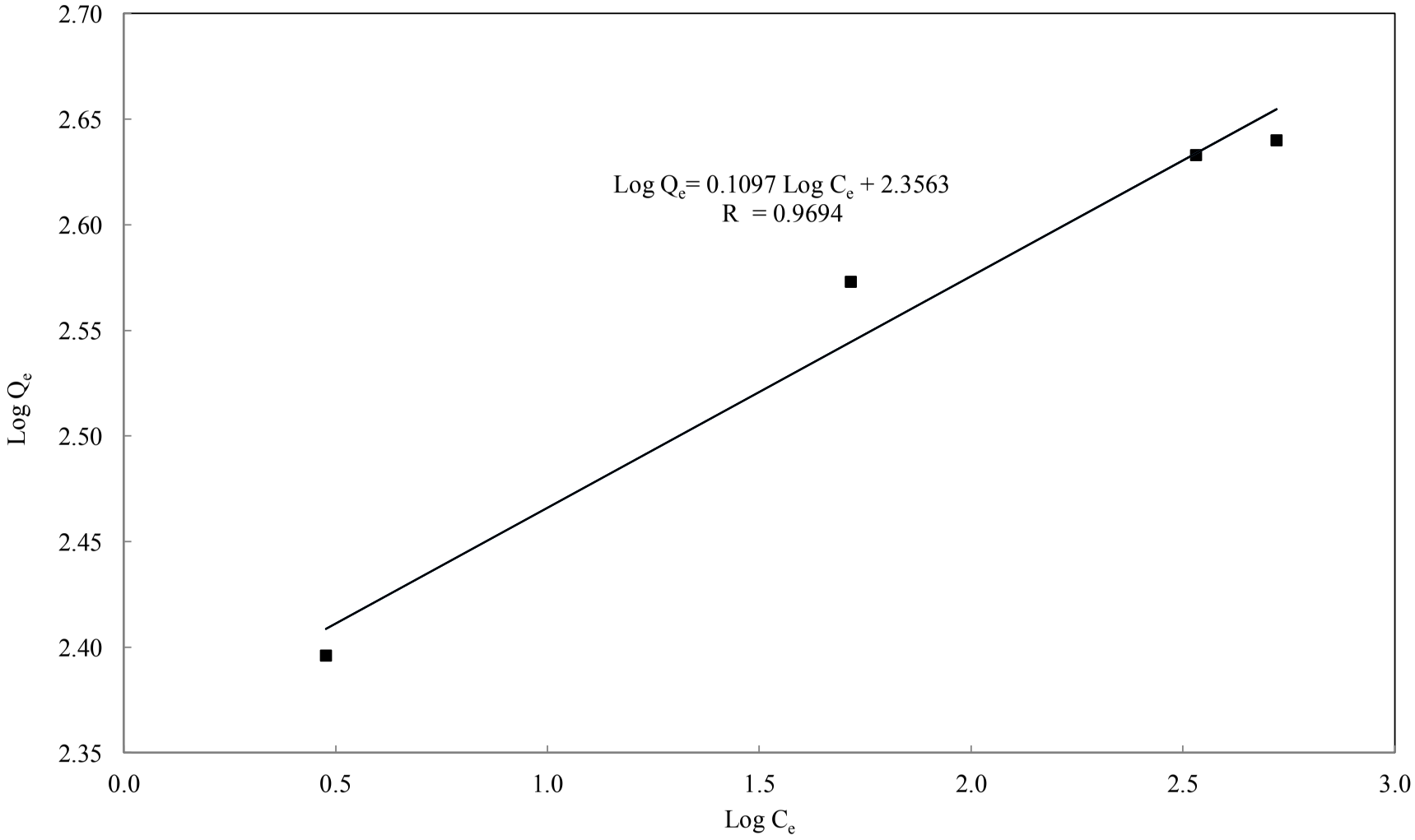

Fig. 5.15. Freundlich isotherm for MB adsorption onto PSAC

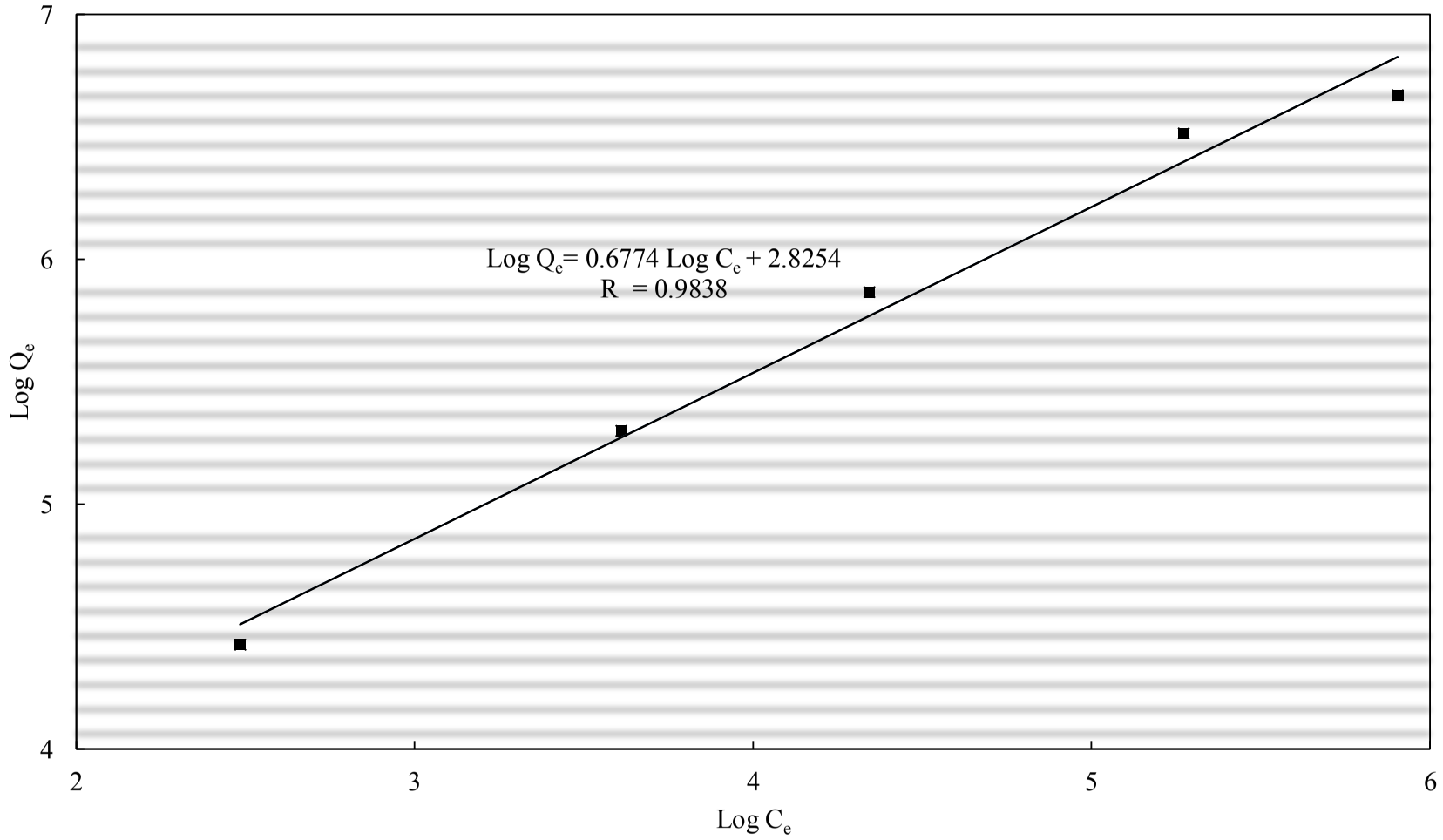

Fig. 5.16. Freundlich isotherm for dairy COD adsorption onto PSAC

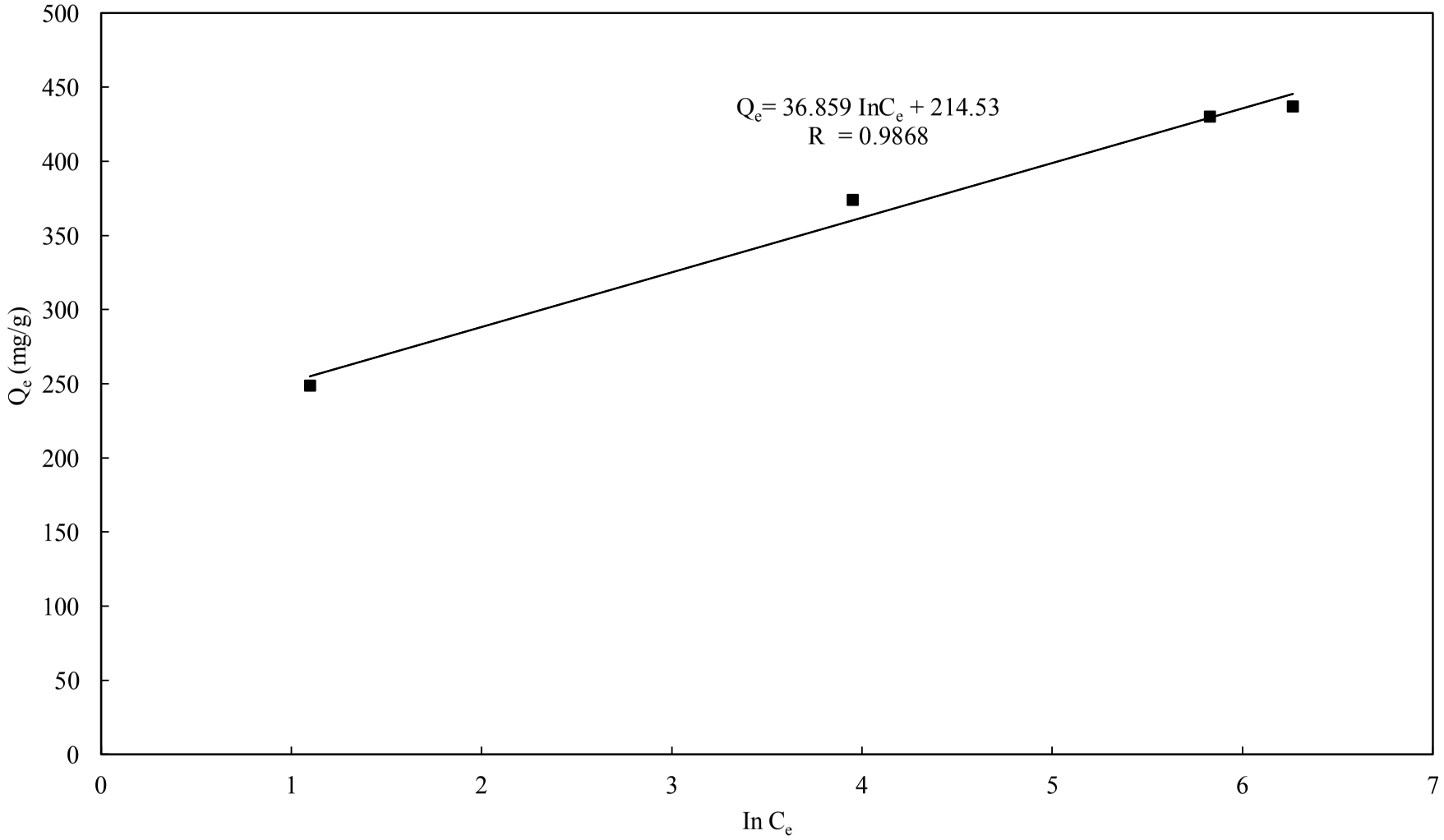

Fig.5.17. Temkin isotherm for MB adsorption onto PSAC

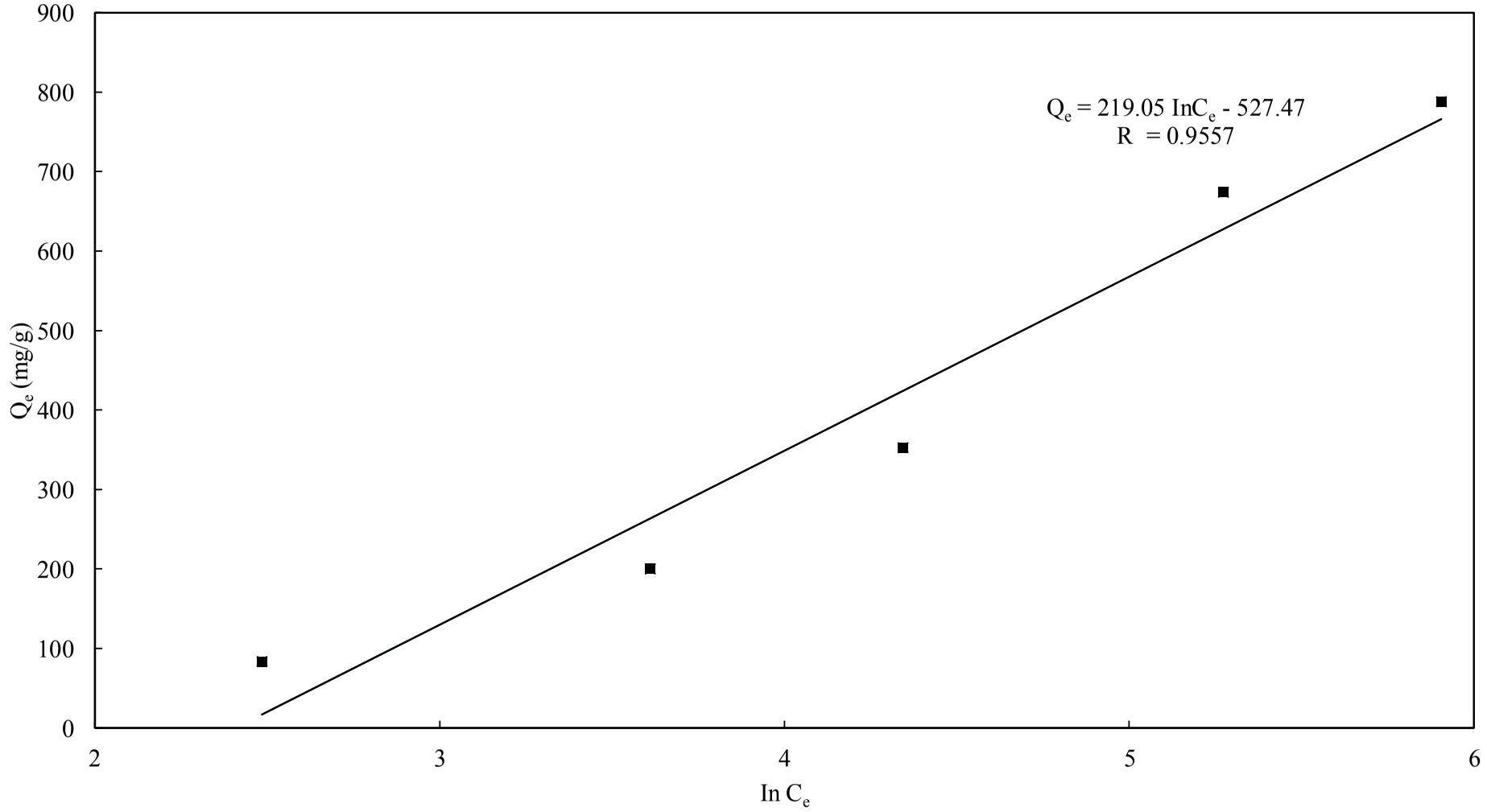

Fig. 5.18. Temkin isotherm for dairy COD adsorption onto PSAC

5.5.1.3 Temkin isotherm

From section 2.13.1(c) the linearised form of Temkin isotherm is expressed as:

$Q_e = (RT/b)\text{In}(A) + (RT/b)\text{In}C_e$

where A (L/g) is the equilibrium binding constant corresponding to the maximum binding energy and B (= RT/b), is the Temkin constant related to heat of sorption. R (8.314 J/mol K) is the universal gas constant and T (K) is the absolute solution temperature. The plot of the above equation is shown in Fig. 5.17 (MB) and 5.18 (dairy COD) along with the Temkin isotherm constants A and B. *The* R^2 value of the Temkin model is presented in Table 5.3 and it corresponds to 0.9868 and 0.9557 for MB and dairy COD respectively

From Table 5.3, the highest R^2 values correspond to Langmuir model with a R^2 value of 0.9998 and 0.9877, while the lowest value for MB adsorption corresponds to Freundlich isotherm model. The well fit of the experimental data with the Langmuir isotherm model indicate the adsorption behavior to observe predominantly a monolayer adsorption, involving chemical and physical adsorption. This observation is in agreement with literature on MB adsorption onto activated carbon prepared from palm shell [24], palm fiber, coconut husk [25], jute fiber [26] and sunflower oil cake [27]. No comparison could be made on dairy COD isotherms due to the absence of such works in available literatures.

5.5.2 Effect of solution pH

The pH affects the surface charge of the adsorbents as well as the degree of ionization of different pollutants which may cause a shift in the equilibrium values of the adsorption process. As shown in Fig. 5.19, it is evident that pH does effect the MB adsorption onto PSAC significantly beyond a pH of 7, while its affect up to a pH of 7 is insignificant, although the figure shows a qualitative increase. On the other hand, it is observed pH

influenced dairy COD adsorption differently. The adsorption isotherm increase from pH 1 to optimum pH 3 before decrease gradually to pH 14. Phosphoric or polyphosphoric acids react with the carbonaceous precursor to form phosphate or polyphosphate esters resulting carbon adsorbents with strongly acidic surface groups [18]. The acid surface of H_3PO_4 activated carbons is obviously due to phosphorus and oxygen-containing species such as phosphate or polyphosphate esters, along with carboxylic and phenolic groups.

At lower pH, the excess H^+ ions deter the electrostatic attractions between positively charged MB cations and positively charged acidic surface site, resulting in a net ionic repulsion effect. As the pH increases, the availability of OH^- ions increases the electrostatic attractions with the acidic surface sites of the PSAC. These transitions enhance electrostatic interaction with MB cations and hence increase the dye uptake. This is in agreement with observation due to Senthilkumaar et al. [26], using carbon from H_3PO_4 activated jute fiber (*corchorus capsularis*),who have reported a significant increase in MB adsorption in the pH range from 7 to 10.

Tan et al. [28], using adsorbent from HCl-treated palm shell, reported a significant increase in MB adsorption from pH 7 onwards. While Karagoz et al. [27] found a significant increase in MB adsorption with pH only until pH 6 (after which MB adsorption became constant) for adsorbent from H_2SO_4 activated sunflower oil cake. Similar trend were reported by Hameed on untreated garlic peel. On the other hand Lata et al. [29] reported an insignificant influence of pH, for carbon produced from H_3PO_4 activated biomass, (*Parthenium hysterophorus)* and Garg et al. [30] with untreated rosewood sawdust. These observations highlighted the complexity of AC adsorption with regards to surface chemistry and pore characteristics, in which is strongly depending on the nature of precursor and activation method.

5.5.3 Adsorption kinetics

Adsorption kinetics is known to vary with the concentration of the adsorbent, agitation rate, the adsorption temperature, the pH of the solution and size of the adsorbent. At low agitation rate the resistance for mass transfer will be significant, which reduces with the increase in agitation rate. The agitation rate is chosen in the present study such that the mass transfer limitations are absent, evidenced from the preliminary experiments. The present study attempts to assess the effect of initial concentration of the MB dye and dairy COD, at a constant bath temperature of 30 $^{\circ}$C, pH of 7, with the size of the adsorbent being less than 120 μm.

Fig. 5.21 shows an increase in the rate of adsorption with increase in the initial concentration of MB from 600 to 1200 mg/L with the maximum adsorption corresponding to 306 to 421 mg/g. It is found the removal of MB is rapid during the initial period while the uptake slowdown with increase in time. The reduction in the rate of adsorption with no significant variation in the concentration of the solution indicates the existence of saturation adsorption condition, which could be achieved approximately around 70 min. No significant changes in the MB dye uptake are observed with further increase of contact time up to 24 hours. Similar observations have been reported in the literature for the removal of dyes such as MB [31], malachite green [32] and methyl violet [33].

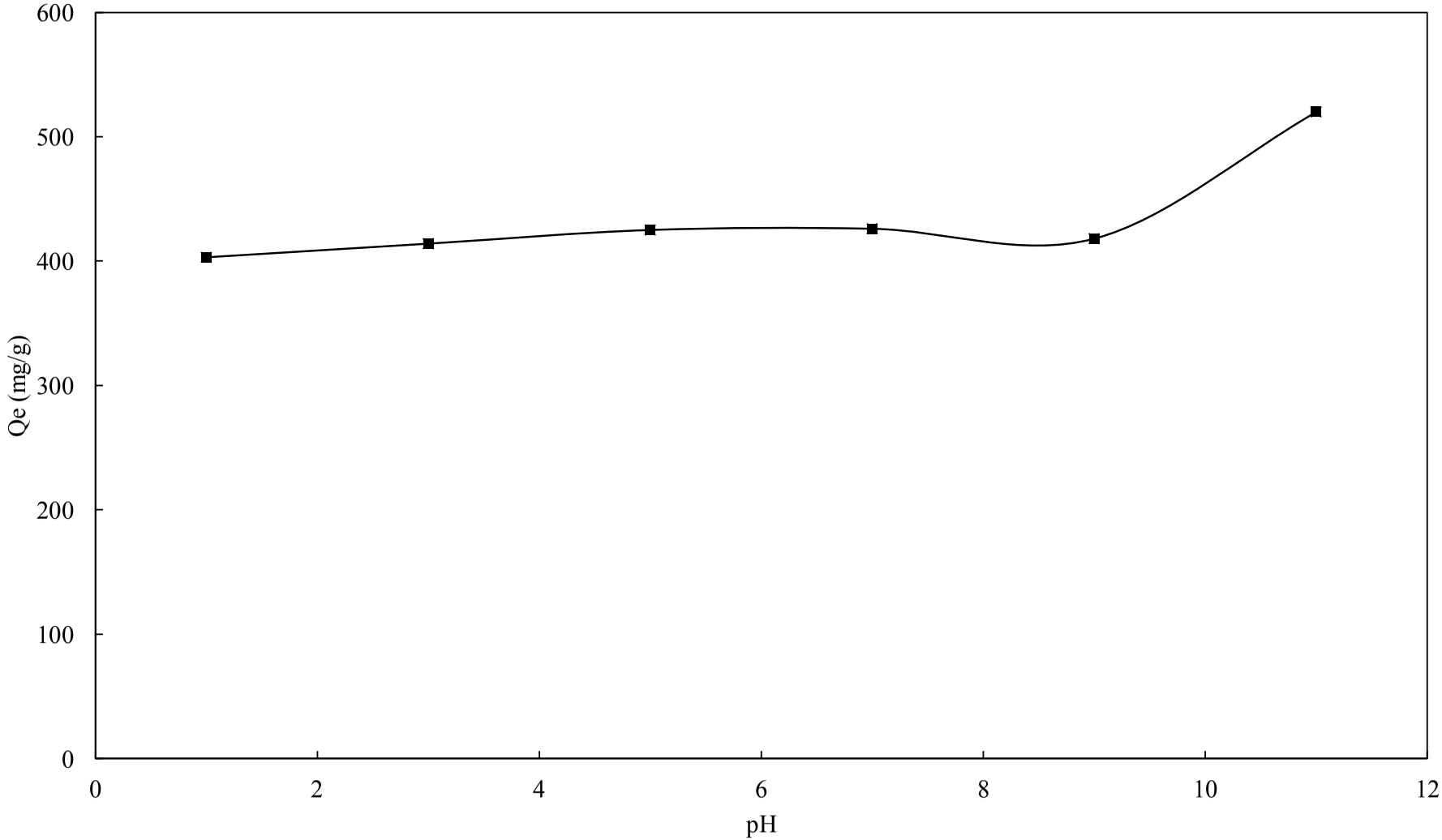

Fig. 5.19. Effect of pH on MB adsorption onto PSAC (MB concentration: 1400mg/L; PSAC dose: 2 g/L)

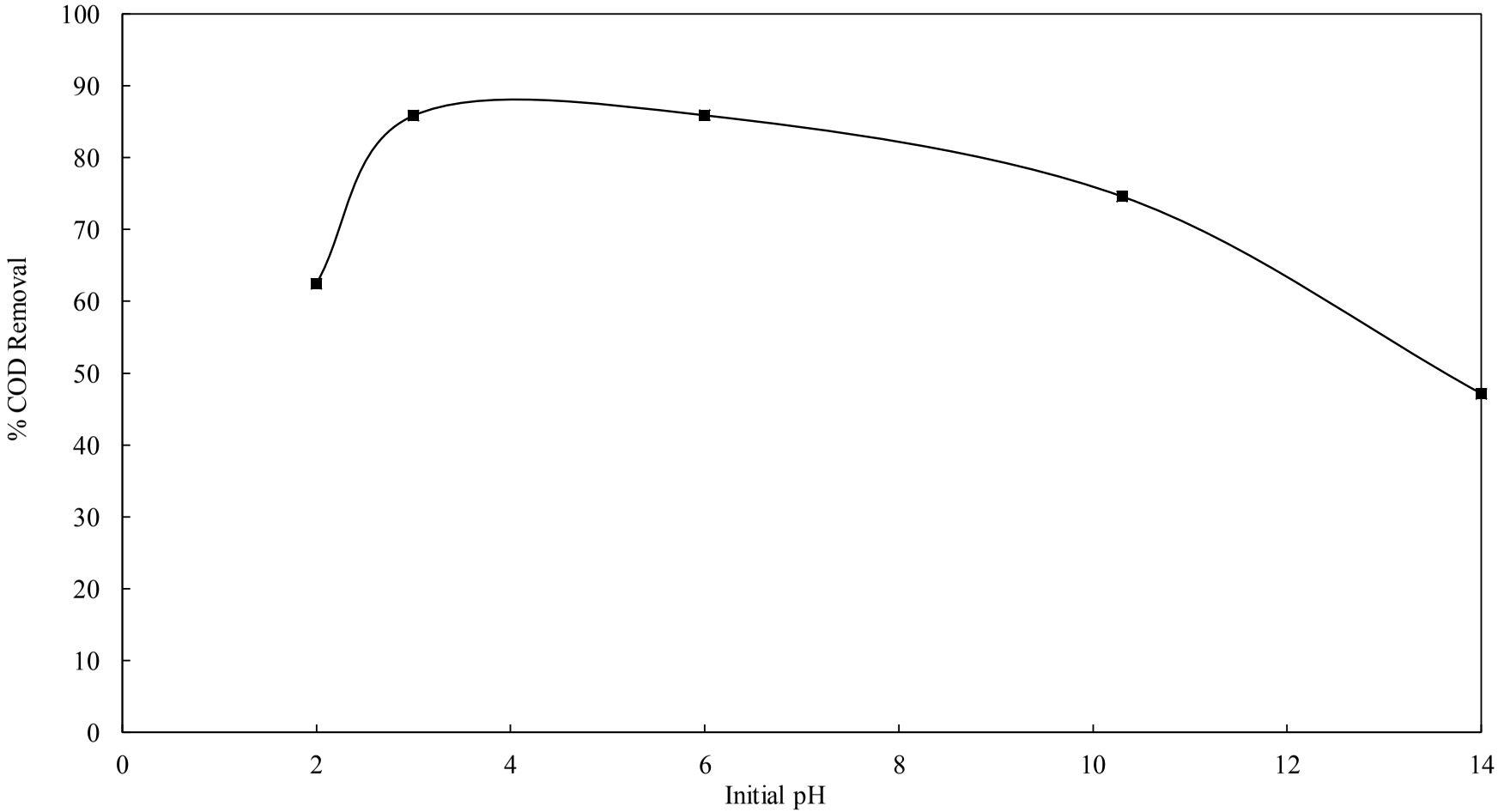

Fig. 5.20. Effect of pH on dairy COD adsorption onto PSAC (dairy COD concentration: 1400mg/L; PSAC dose: 2 g/L)

In batch adsorption systems, a monolayer of adsorbate is normally formed on the surface of the adsorbent, and the rate of removal of adsorbate species from aqueous solution is controlled primarily by the rate of transport of the adsorbate species from the exterior/outer sites to the interior site of the adsorbent particles [31,32]. An increase in the initial MB concentration increases the mass transfer driving force to overcome all mass transfer resistances of molecules between the aqueous and solid phases [20]. Similar observation on dairy COD with maximum adsorption increase from 375 to 532 mg/g for initial concentration from 850 to 1250 mg/g. The same duration (70 min) in achieving saturation, indicating dairy COD adsorption may be via similar mechanism as MB.

5.5.3.1 The pseudo-first-order kinetic model

The pseudo-first-order kinetic Lagergren equation [34] is derived as:

$\log(Q_e - Q_t) = \log Q_e - (k_1/2.303)t$

where Q_e and Q_t are the amounts of MB adsorbed (mg/g) at equilibrium and at time t (min), respectively, and k_1 (min^{-1}) is the adsorption rate constant of pseudo-first-order adsorption. The validity of the model can be checked by linearised plot of $\log(Q_e - Q_t)$ versus t. Fig. 5.23 & 5.24 shows the linear plot of $\log(Q_e - Q_t)$ versus t, while Table 5.3 & 5.4 summarizes the model constants k_1 and Q_e along with R^2 values. The R^2 values which evidence the acceptability of the model in representing the experimental data is found to vary from 0.887 to 0.9855 for MB concentration of 600-1200 mg/L while it is 0.8938 to 0.9341 for dairy COD for concentration of 850-1250 mg/L.

5.5.3.2 The pseudo-second-order kinetic model

The second-order kinetic model is conveniently expressed in the linearised form as:

$t/Q_t = 1/k_2Q_e^2 + t/Q_e$

where Q_e and Q_t are the amounts of MB adsorbed (mg/g) at equilibrium and at time t (min), respectively, and k_2 is the rate constant (min^{-1}).

The linear plots of t/Q_t against t are shown in Fig. 5.25 & 5.26. It is found, from Table 5.3 & 5.4, there is a good agreement between the experimental and the calculated adsorption $Q_{e,exp}$ and $Q_{e,cal}$. This is further supported by the correlation coefficient values for the second-order kinetic model which is almost equal to unity (R^2=1) for all MB concentrations, highlighting the suitability of pseudo-second-order kinetic model to describe the MB as well as dairy COD adsorption dynamics.

5.5.3.3 Intraparticle diffusion model

The intraparticle diffusion equation [35] can be described as:

$$Q_t = K_p t^{1/2} + C$$

Where C is the intercept and k_p is the intraparticle diffusion rate constant ($mg.g^{-1}min^{-1/2}$), which can be evaluated from the slope of linear plot of Q_t versus $t^{1/2}$. The linearised plot of the intraparticle model equation is shown in Figs. 5.27 & 5.28. The R^2 values for the Intraparticle diffusion is found to vary between 0.9561 to 0.9765 and is shown in Table 5.3 & 5.4.

For all MB concentration the R^2 values is more than 0.99 for pseudo-second-order kinetic model, which is higher than that of the pseudo-first-order kinetic model and intraparticle diffusion model. The high values of correlation coefficients show that the data conformed well to the pseudo-second-order rate kinetic model. This is in agreement with the literature reports on the adsorption of MB using activated carbons from various biomasses [25-27,37-38].

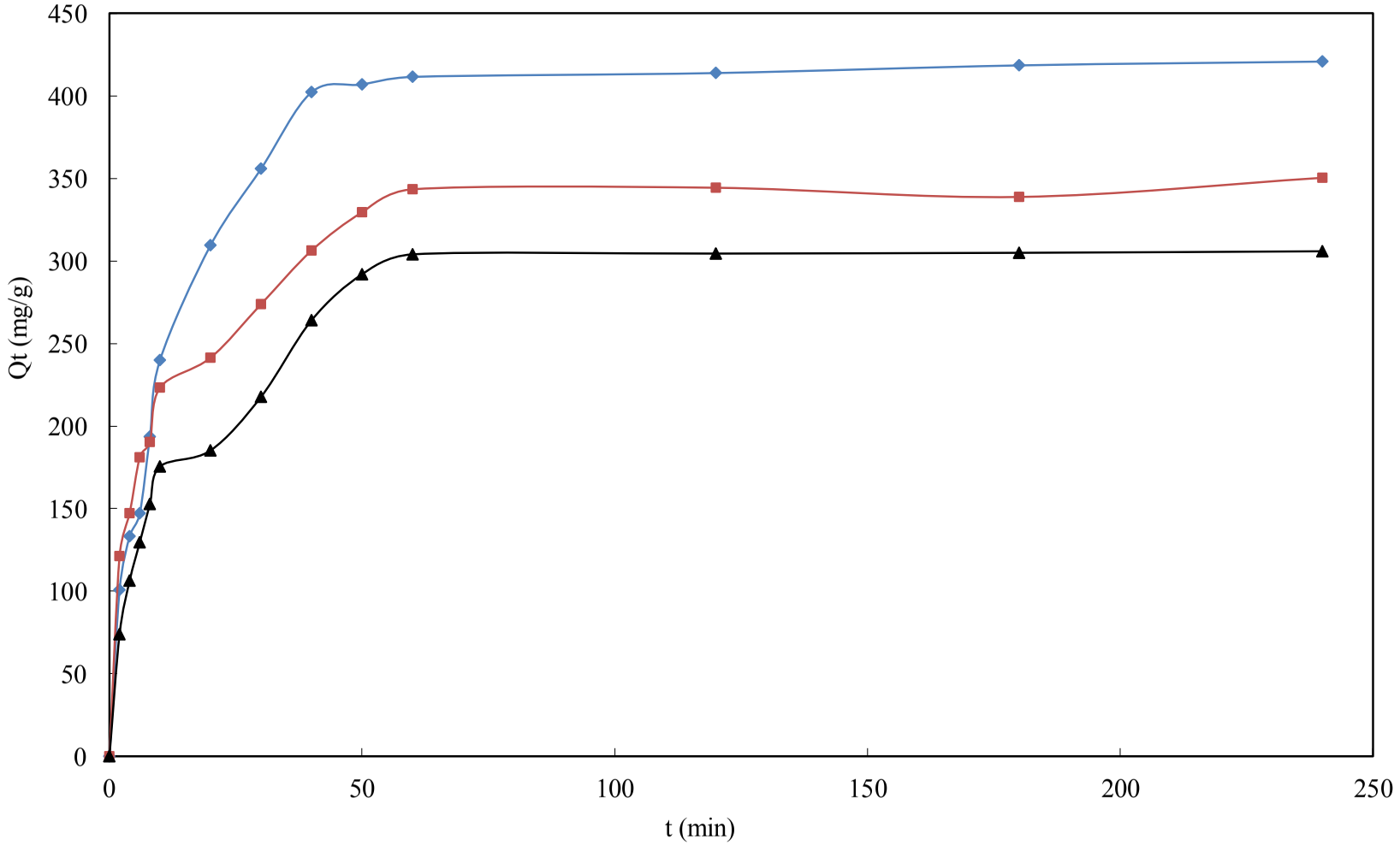

Fig. 5.21. Effect of initial concentration on MB adsorption rate onto PSAC (▲: 600mg/L; ■: 800mg/L; ♦:1200mg/L)

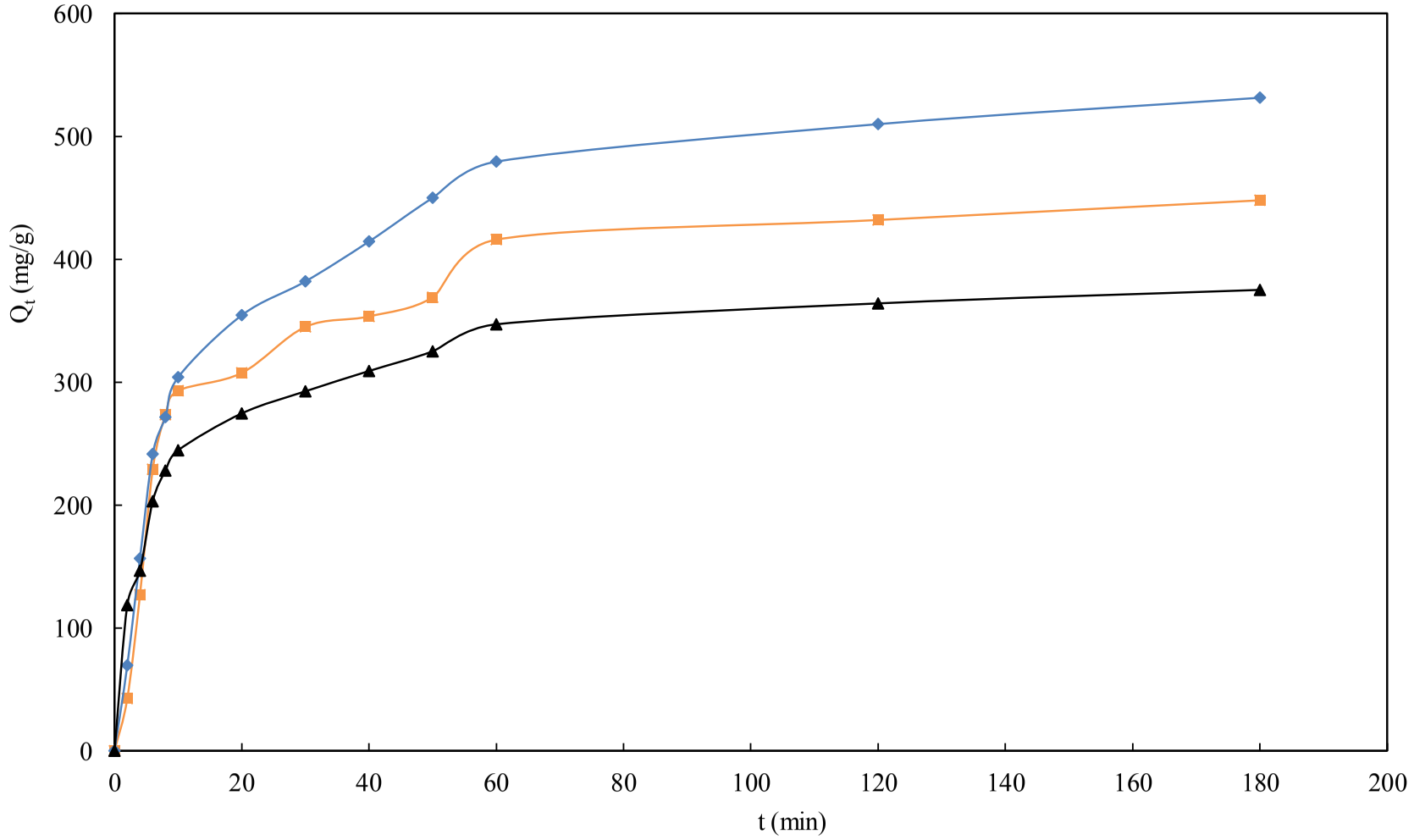

Fig. 5.22. Effect of initial concentration on COD adsorption rate onto PSAC (▲: 850mg/L; ■: 1000mg/L; ♦:1250mg/L)

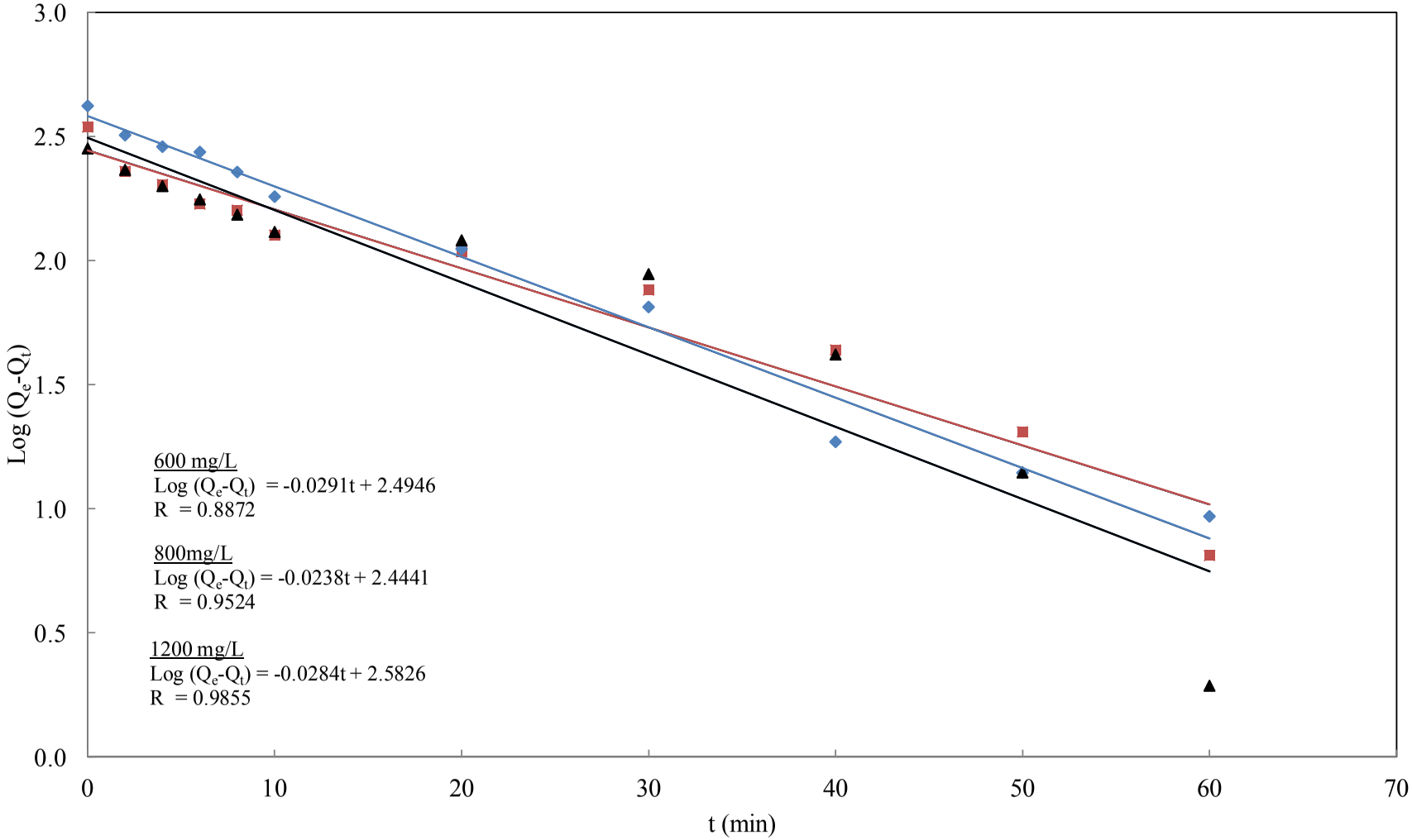

Fig. 5.23. Pseudo-first-order plots for different initial MB concentrations (▲: 600 mg/L; ■: 800 mg/L; ♦: 1200 mg/L)

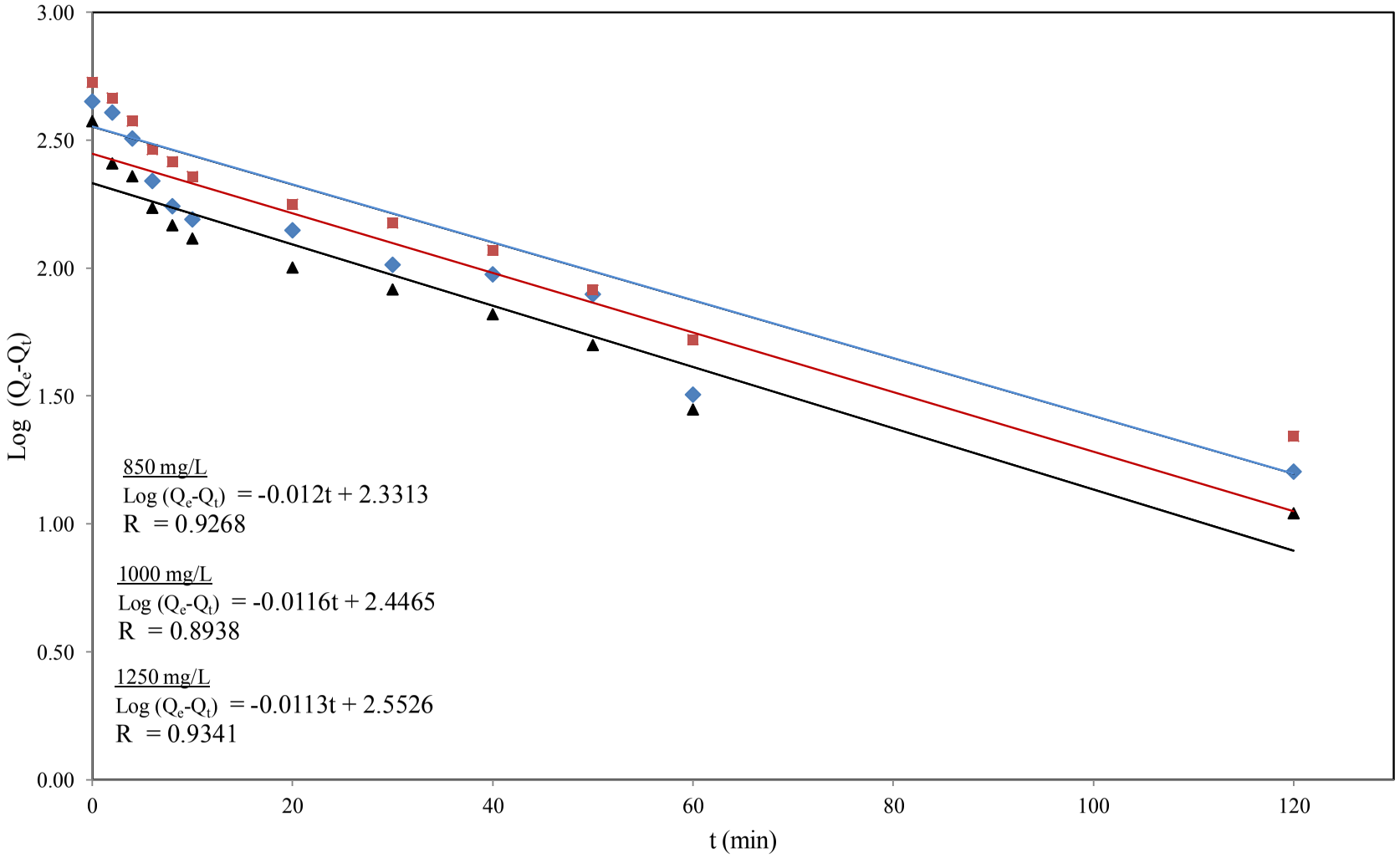

Fig.

Fig. 5.24. Pseudo-first-order plots for different initial dairy COD concentrations (▲: 850 mg/L; ■: 1000 mg/L; ♦: 1250 mg/L)

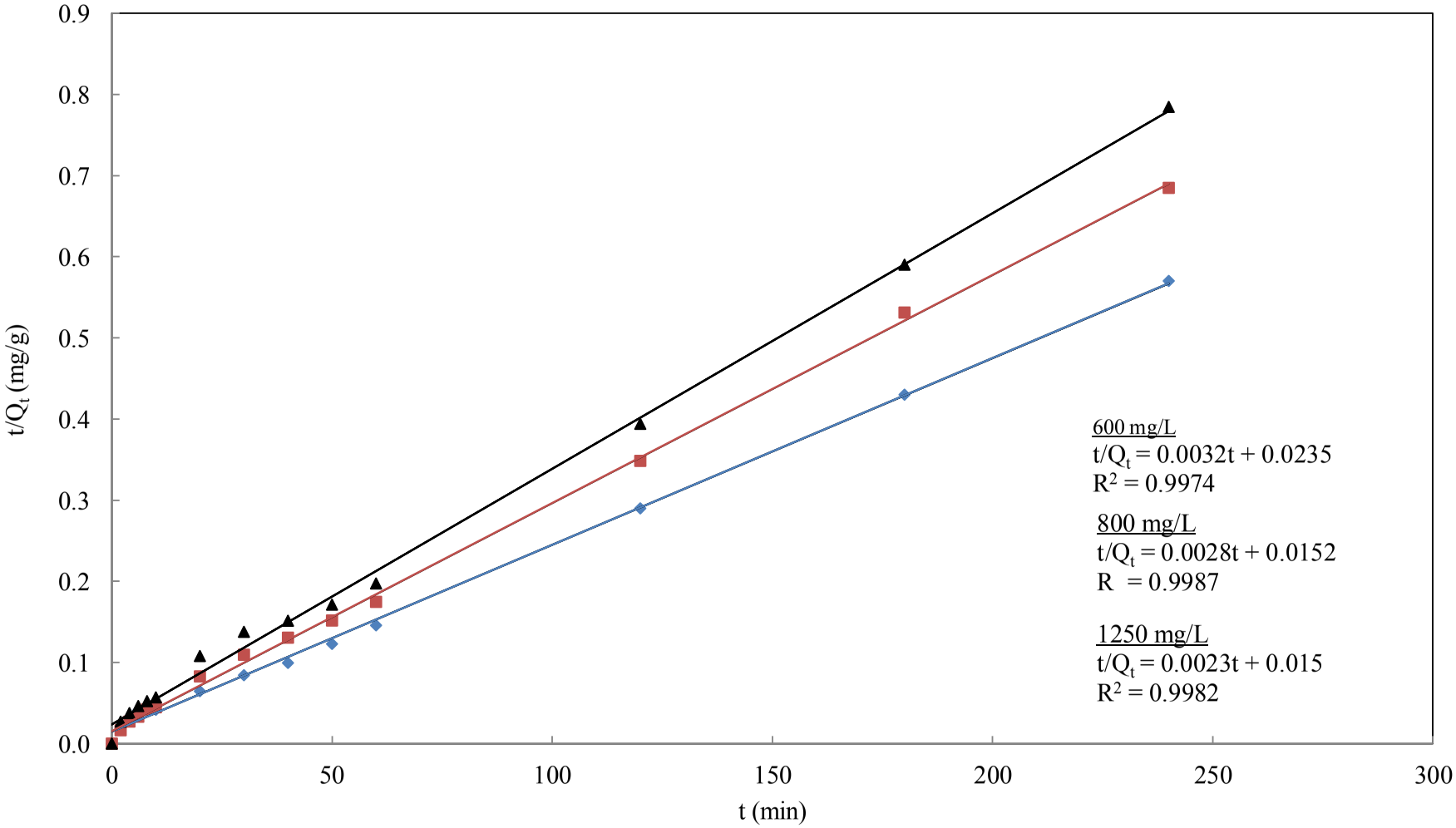

Fig. 5.25. Pseudo-second-order plots for different initial MB concentrations (▲: 600 mg/L; ■: 800 mg/L; ♦: 1200 mg/L)

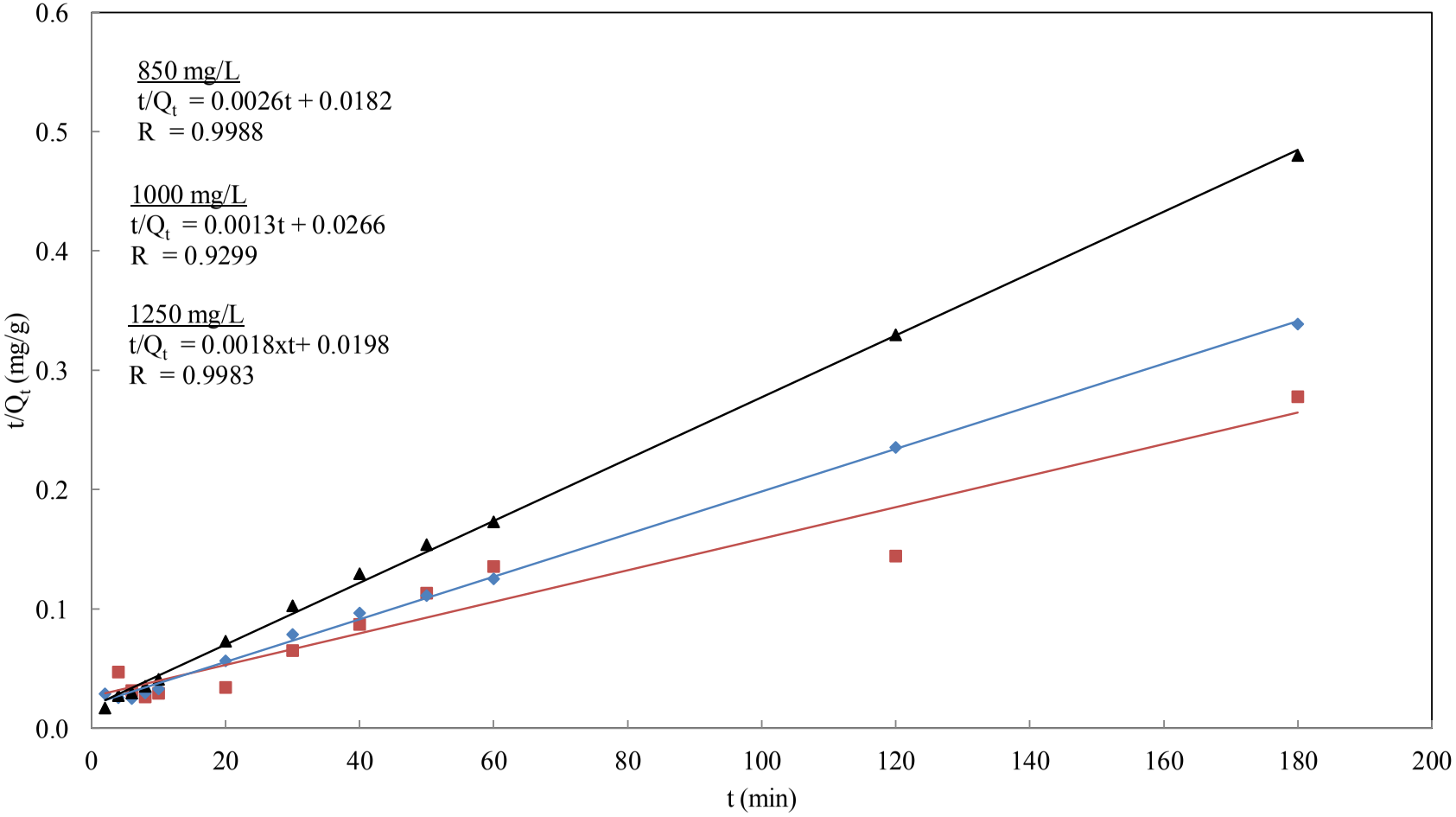

Fig. 5.26. Pseudo-second-order plots for different initial dairy COD concentrations (▲: 850 mg/L; ■: 1000 mg/L; ♦: 1250 mg/L)

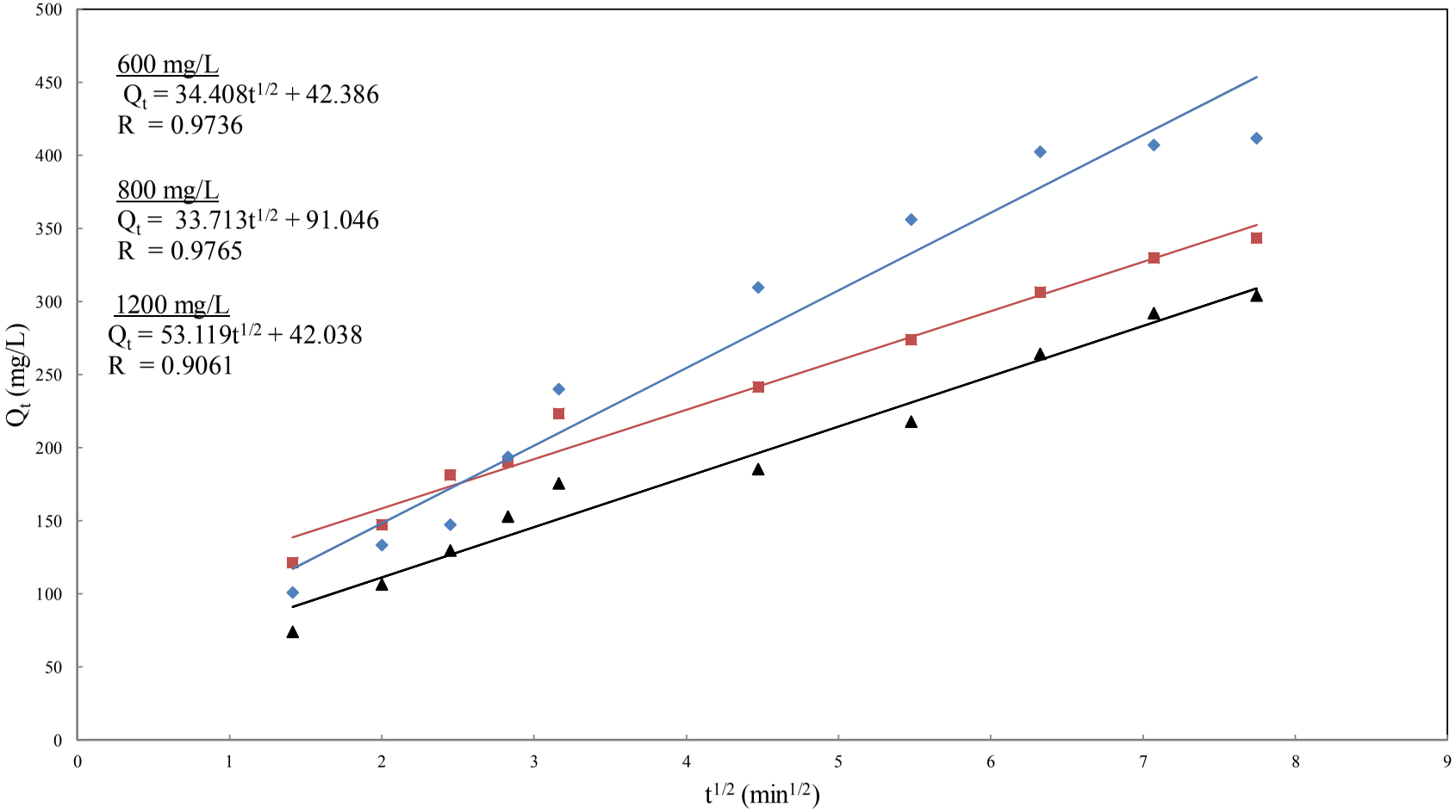

Fig. 5.27. Intraparticle diffusion plots for different initial MB concentrations (▲: 600 mg/L; ■: 800 mg/L; ♦: 1200 mg/L)

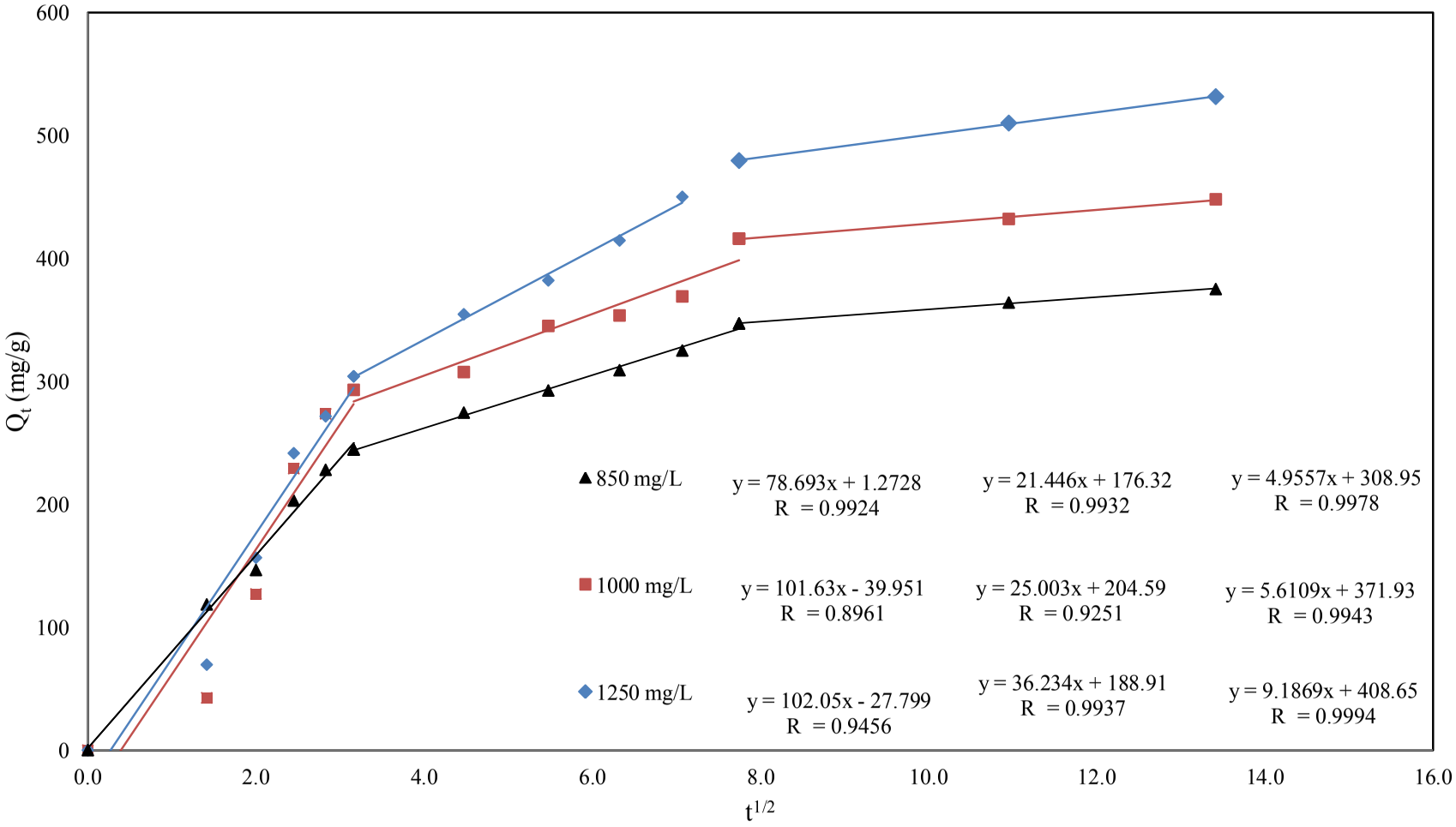

Fig. 5.28. Intraparticle diffusion plots for different initial dairy COD concentrations (▲: 850 mg/L; ■: 1000 mg/L; ♦: 1250 mg/L)

Table 5.4 Non-linear kinetics parameters calculated for MB adsorption onto PSAC

MB: Adsorption kinetic	Initial Concentration, C_o (mg/L)		
	600	800	1200
Pseudo-first-order kinetic model			
$Q_{e,\,exp}$ (mg/g)	306	350	421
$Q_{e,\,cal}$ (mg/g)	312	278	382
k_1 (min^{-1})	0.06702	0.05481	0.06541
R^2	0.8872	0.9524	0.9855
Pseudo-second-order kinetic model			
$Q_{e,\,cal}$ (mg/g)	312.5	357.1	434.8
k_2 x10^{-4} (min^{-1})	4.357	5.158	3.527
R^2	0.9974	0.9987	0.9982
Intraparticle diffusive model			
k_P ($mg.g^{-1}min^{-1/2}$)	34.408	33.713	53.119
C	43.386	91.046	42.038
R^2	0.9736	0.9765	0.9561

Table 5.5 Non-linear kinetics parameters calculated for dairy COD adsorption onto PSAC

Dairy COD: Adsorption kinetic	Initial Concentration, C_o (mg/L)		
	850	1000	1250
Pseudo-first-order kinetic model			
$Q_{e,\,exp}$ (mg/g)	375	448	532
$Q_{e,\,cal}$ (mg/g)	214.44	279.58	356.94
k_1 (min^{-1})	-0.12	-0.0116	-0.0113
R^2	0.9268	0.8938	0.9341
Pseudo-second-order kinetic model			
$Q_{e,\,cal}$ (mg/g)	384.62	769.23	555.56
h (g/mg.min)	54.95	37.59	50.51
k_2 (min^{-1})	0.1429	0.0489	0.0909
R^2	0.9988	0.9299	0.9983
Intraparticle diffusive model			
k_P ($mg.g^{-1}min^{-1/2}$)	49.9	44.08	49.16
C			
	0.9924	0.8961	0.9456
	0.9932	0.9251	0.9937
R^2	0.9978	0.9943	0.9994

5.5.4 Comparison of MB uptake by PSAC with other biomass based AC

Table 5.6 shows the compilation of the various maximum MB adsorption capacities reported in literature for different biomass precursors. The maximum MB adsorption capacity of the activated carbon produced in the present study is well among the highest reported owing to the high pore volume and the surface area with appropriate pore diameter. Among the different published literature only the report due to Hameed et al. [39], shows an MB adsorption capacity of 454.2 mg/g, for the bamboo precursor using combined physical-chemical activation. However it should be noted that the bamboo-activated carbon were produced from a much more complex process i.e. carbonization at 700 °C for 1 h under N_2 atmosphere followed by KOH (1:1 impregnation ratio) with activation temperature of 850 °C for 2 h. Tan et al. [24] with the palm shell precursor using KOH activation have reported only 244 mg/g but at higher activation temperature of 850 °C. In general the majority of the literature reports a lower MB adsorption capacity with the activation temperatures and time being significantly higher than that utilized in the present study. The higher adsorption capacity coupled with simplified experimental conditions of activation in a self-generated atmosphere, lower activation time and temperature, with significantly higher yield well augurs the present process commercially favorable, in comparison with the existing processes.

Table 5.6 Comparison of the maximum adsorption of MB on various biomass based AC and the adsorption models

Reference	Precursor	Reagent	Temp, °C	Time, min	Q_e, mg/g	Adsorption model	
						Isotherm	Kinetics
This work	Palm Shell	H_3PO_4	500	75	438	Langmuir	Pseudo-second-order
[36]	Bamboo	CO_2/KOH	850	120	454	Langmuir	Pseudo-second-order
[22]	Coconut husk	CO_2KOH	850	120	435	Langmuir	Pseudo-second-order
[40]	Vetiver roots	H_3PO_4	600	60	423	Redlich– Peterson	BWS equation
[41]	Oil palm fibre	CO_2/KOH	862	60	204	Langmuir	
[21]	Palm shell	CO_2/KOH	850	120	244	Langmuir	Pseudo-second-order
[23]	Jut Fiber	H_3PO_4			226	Langmuir	Intraparticle diffusion
[42]	Apricot stone	H_2SO_4	250	1440	221	Langmuir, Freundlich	Intraparticle diffusion

5.6 Conclusions

Thermal decomposition of palm shell, its char and PSAC were studied by TGA analysis. Effect of semi-carbonization and the non-conventional H_3PO_4 activation method (under self-generate atmosphere) were investigated. The surface chemistry of the PSAC were assessed by FT-IR and SEM. This study also investigates the use of PSAC for the removal of MB and dairy COD before modelled based on developed adsorption isotherm and kinetics models. The following conclusions could be derived based on the characterisation and adsorption study pertaining to the developed PSAC:

1. Based on the TGA analysis, pyrolysis process of palm shell consist of two distinct kinetic schemes, while only single step was observed for the char, indicating the significant contribution by semi-carbonization towards textural development. No kinetic scheme observed on PSAC signifies its low volatility and correspond to well-developed textural characteristics.
2. Chemical activation with H_3PO_4 results in significant change on palm shell surface chemistry and produced PSAC with strongly acidic surface groups. However no observable variation in surface functional groups on PSAC prepared with different IR and activation temperature.
3. The pore characteristics of the PSAC are highly favourable for adsorption of high molecular weight compounds. The PSAC exhibits a high MB equilibrium adsorption capacity of 438 mg/g with the adsorption isotherm increasing with the adsorption temperature. Similar trend was observed in dairy COD uptake by PSAC with maximum adsorption could be higher than 1000 mg/g at high initial concentration.
4. Among the various adsorption isotherm models, the Langmuir model is able to explain the adsorption process well, evidenced by the proximity of the model with the

experimental data while among the different kinetic models tested with the experimental kinetic data, a pseudo-second-order model is found to fit the experimental data with close proximity. This finding is applicable for MB as well as dairy COD adsorption by PSAC.

5.7 References

1 P. Luangkiattikhun, C. Tangsathitkulchai, M. Tangsathitkulchai, Non-isothermal thermogravimetric analysis of oil-palm solid wastes, Bioresource Technology 99 (2008) 986-997

2 H. Yang, R. Yan, D.T. Liang, H. Chen, C. Zheng, Pyrolysis of Palm Oil Wastes for Biofuel Production, Asian Journal on Energy and Environment 7 (2006) 315-323

3 J. Guo , A.C. Lua, Kinetic study on pyrolytic process of oil-palm solid waste using two-step consecutive reaction model, Biomass and Bioenergy 20 (2001) 223-233

4 R. Font, A. Marcilla, E. Verdti, J. Devesa, Thermogravimetric kinetic study of the pyrolysis of almond shells and almond shells impregnated with $CoCl_2$, JournaI of Analytical and Applied Pyrolysis 21(1991) 249-264

5 W-H Chen, J-S Wu, An evaluation on rice husks and pulverized coal blends using a drop tube furnace and a thermogravimetric analyzer for application to a blast furnace, Energy 34 (2009) 1458–1466

6 M. Danish, R. Hashim, M.N.M. Ibrahim, M. Rafatullah, T. Ahmad, O. Sulaiman, Characterization of Acacia Mangium wood based activated carbons prepared in the presence of basic activating agents, Bioresources 6 (2011) 3019-3033

7 G. Teng, T-S. Yeh, L-Y. Hsu, Preparation of activated carbon from bituminous coal with phosphoric acid activation, Carbon 36 (1998) 1387-1395

8 D. Cuhadaroglu, O. A. Uygun, Production and characterization of activated carbon from a bituminous coal by chemical activation, African Journal of Biotechnology 7 (2008) 3703-3710

9 A. Kriaa, N. Hamdi, E. Srasra,Removal of Cu (II) from water pollutant with Tunisian activated lignin prepared by phosphoric acid activation, Desalination 250 (2010) 179-187

10 G.E. Shter, Y. Shindler, Y. Matatov-Meytal, G.S. G.M. Sheintuch, Thermal behavior of the phenol–Pd–ACC system, Carbon 40 (2002) 2547-2557

11 M. Jagtoyen, F. Derbyshire, Activated carbons from yellow poplar and white oak by H_3PO_4 activation, Carbon 36 (1998) 1085-1097

12 C. Moreno-Castilla, F. Carrasco-Marin, M.V. Lopez-Ramon, M.A. Alvarez-Merino, Chemical and physical activation of olive-mill waste water to produce activated carbons, Carbon 39 (2001) 1415-1420

13 J. Guo, A.C. Lua, Characterization of adsorbent prepared from oil-palm shell by CO_2 activation for removal of gaseous pollutants, Materials Letters 55 (2002) 334-339

14 J. Guo, A.C. Lua, Textural and chemical properties of adsorbent prepared from palm shell by phosphoric acid activation, Materials Chemistry and Physics 80 (2003) 114-119

15 R.C. Bansal, M. Goyal, Carbon Adsorption, CRC Press 2005, ISBN: 978-0-8247-5344-3

16 J. Guo & A.C. Lua, Surface Functional groups on oil-palm-shell adsorbents prepared by H3PO4 and KOH activation and their effects on the adsorptive capacity, Institution of Chemical Engineers, Trans IChemE, Part A, 81 (2003) 585-590

17 J. Guo, A.C. Lua, Adsorption of sulphur dioxide onto activated carbon prepared from oil-palm shells with and without pre-impregnation, Separation and Purification Technology 30 (2003) 265-273

18 A.M. Puziy, O.I. Poddubnaya, A. Martinez-Alonso, F. Suarez-Garcia, J.M.D. Tascon, Surface chemistry of phosphorus-containing carbons of lignocellulosic origin, Carbon 43 (2005) 2857-2868

19 B.H. Hameed, A.A. Ahmad, Batch adsorption of methylene blue from aqueous solution by garlic peel, an agricultural waste biomass, Journal of Hazardous Materials 164 (2009) 870-875

20 M. Dogan, H. Abak, M. Alkan, Adsorption of methylene blue onto hazelnut shell: Kinetics, mechanism and activation parameters, Journal of Hazardous Materials 164 (2009) 172-181

21 I.A.W. Tan, A.L. Hameed, B.H. Hameed, Adsorption isotherms, kinetics, thermodynamics and desorption studies of 2,4,6-trichlorophenol on oil palm empty fruit bunch-based activated carbon 164 (2009) 473-482

22 S. Karaca, A. Gurses, M. Acikyildiz, M. Ejder, Adsorption of cationic dye from aqueous solutions by activated carbon, Microporous and Mesoporous Materials 115 (2008) 376-382

23 T. Thinakaran, P. Panneerselvam, P. Baskaralingam, D. Elango, S. Sivanesan, Equilibrium and kinetic studies on the removal of Acid Red 114 from aqueous solutions using activated carbons prepared from seed shells, Journal of Hazardous Materials 158 (2008) 142-150

24 I.A.W. Tan, A.L. Ahmad, B.H. Hameed, Adsorption of basic dye using activated carbon prepared from oil palm shell: batch and fixed bed studies, Desalination 225 (2008) 13–28

25 I.A.W. Tan, A.L. Ahmad, B.H. Hameed, Adsorption of basic dye on high-surface-area activated carbon prepared from coconut husk: Equilibrium, kinetic and thermodynamic studies, Journal of Hazardous Materials 154 (2008) 337-346

26 S. Senthilkumaar, P.R. Varadarajan, K. Porkodi, C.V. Subbhuraam, Adsorption of methylene blue onto jute fiber carbon: kinetics and equilibrium studies, Journal of Colloid and Interface Science 284 (2005) 78-82

27 S. Karagoz, T. Tay, S. Ucar, M. Erdem, Activated carbons from waste biomass by sulfuric acid activation and their use on methylene blue adsorption, Bioresource Technology 99 (2008) 6214-6222

28 Tan, I.A.W.; Ahmad, A.L.; Hameed, B.H. (2008) Enhancement of basic dye adsorption uptake from aqueous solutions using chemically modified oil palm shell activated carbon. Colloid Surf., A 318: 88–96.

29 H. Lata, V.K. Garg, R.K. Gupta, Removal of a basic dye from aqueous solution by adsorption using Parthenium hysterophorus: An agricultural waste, Dyes Pigments 74 (2007) 653-658

30 V.K. Garg, M. Amita, R. Kumar, R. Gupta, Basic dye (methylene blue) removal from simulated wastewater by adsorption using Indian Rosewood sawdust: a timber industry waste, Dyes Pigments, 63 (2004) 243-250

31 N. Kannan, M.M. Sundaram, Kinetics and mechanism of removal of methylene blue by adsorption on various carbons- a comparative study, Dyes Pigments, 51 (2001) 25-40

32 R. Malik, D.S. Ramteke, S.R. Wate, Adsorption of malachite green on groundnut shell waste based powdered activated carbon. Waste Manage. (Oxford), 27 (2007) 1129-1138

33 Ho, Y.S.; McKay, G. (1999) Pseudo-second order model for sorption processes. Proc. Biochem., 34: 451–465.

34 S. Largegren, S. About the theory of so-called adsorption of soluble substances. *Kungliga Suensk Vetenskapsakademiens Handlingar*, 241: 1–39.

35 Weber Jr., W.J.; Morris, J.C. (1963) Kinetics of adsorption on carbon from solution. J. Sanit. Eng. Div. Am. Soc. Civil Eng., 89 (1898) 31-59

36 M.A. Al-Ghouti, M.A.M. Khraishehb, M.N.M. Ahmad, S. Allen, Adsorption behaviour of methylene blue onto Jordanian diatomite: A kinetic study, Journal of Hazardous Materials, 165 (2009)589-598

37 Y.S. Ho, G. McKay, Sorption of dye from aqueous solution by peat, Chemical Engineering Journal 70 (1998) 115-124

38 Y.S. Ho, G. McKay, The kinetics of sorption of divalent metal ions onto sphagnum moss peat, Water Research 34 (2000) 735-742

39 B.H. Hameed, A.T.M. Din, A.L. Ahmad, Adsorption of methylene blue onto bamboo-based activated carbon: Kinetics and equilibrium studies. *J. Hazard. Mater.*, 141(2007) 819-825

40 J. Hayashi, T. Horikawa, I. Takeda, K. Muroyama, F.N. Ani, Preparing activated carbon from various nutshells by chemical activation with K2CO3, Carbon 40 (2002) 2381-2386

41 M.P. Elizalde-Gonzalez* , V. Hernandez-Montoya, Characterization of mango pit as raw material in the preparation of activated carbon for wastewater treatment, Biochemical Engineering Journal 36 (2007) 230-238

42 F. Suarez-Garcia, A. Martinez-Alonso, J.M.D. Tascon, Pyrolysis of apple pulp: chemical activation with phosphoric acid, Journal of Analytical and Applied Pyrolysis 63 (2002) 283-301

43 S. Altenor, B. Carene, E. Emmanuel, J. Lambert, J-J. Ehrhardt, S. Gaspard, Adsorption studies of methylene blue and phenol onto vetiver roots activated carbon prepared by chemical activation, Journal of Hazardous Materials 165 (2009) 1029-1039

44 B.H. Hameed, I.A.W. Tan, A.L. Ahmad, Optimization of basic dye removal by oil palm fibre-based activated carbon using response surface methodology, Journal of Hazardous Materials 158 (2008) 324-332

45 A. Demirbas, Agricultural based activated carbons for the removal of dyes from aqueous solutions: A review, Journal of Hazardous Materials 167 (2009) 1-9

CHAPTER VI

RECEOVERY AND REUSABILITY OF REAGENT

6.1 Introduction

This chapter reports the investigation on the influence of activation temperature on the recovery of H_3PO_4 and activation efficiency of the reclaimed acid with the focus on textural characteristics of the PSAC produced. H_3PO_4 is reclaimed and reused for successive palm shell activation in order to assess the effect of the reclaimed acid on the characteristics of the activated carbon in the successive runs. The impregnation ratio in all the reclaimed runs are maintained constant at the desirable value of 1.75, by suitably reducing the weight of palm shells, in accordance with the reduction in loss of H_3PO_4 in the previous run. SEM analysis we conducted and the presence of surface functional groups and structure of palm shell, its char and activated carbon were investigated using Fourier transform infrared (FT-IR) and X-ray diffraction (XRD) analyser.

6.2 H_3PO_4 recovery

Fig. 6.1 shows the recovery of H_3PO_4 for 3 successive runs using reclaimed H_3PO_4 at an activation temperature range of 375-525 °C. It is found that more than half of the H_3PO_4 is lost upon 3 successive runs at all activation temperatures. Activation at 375 °C is found to have the highest residual acid of 46% (wt/wt) while the lowest is recorded for 525 °C at 30%.

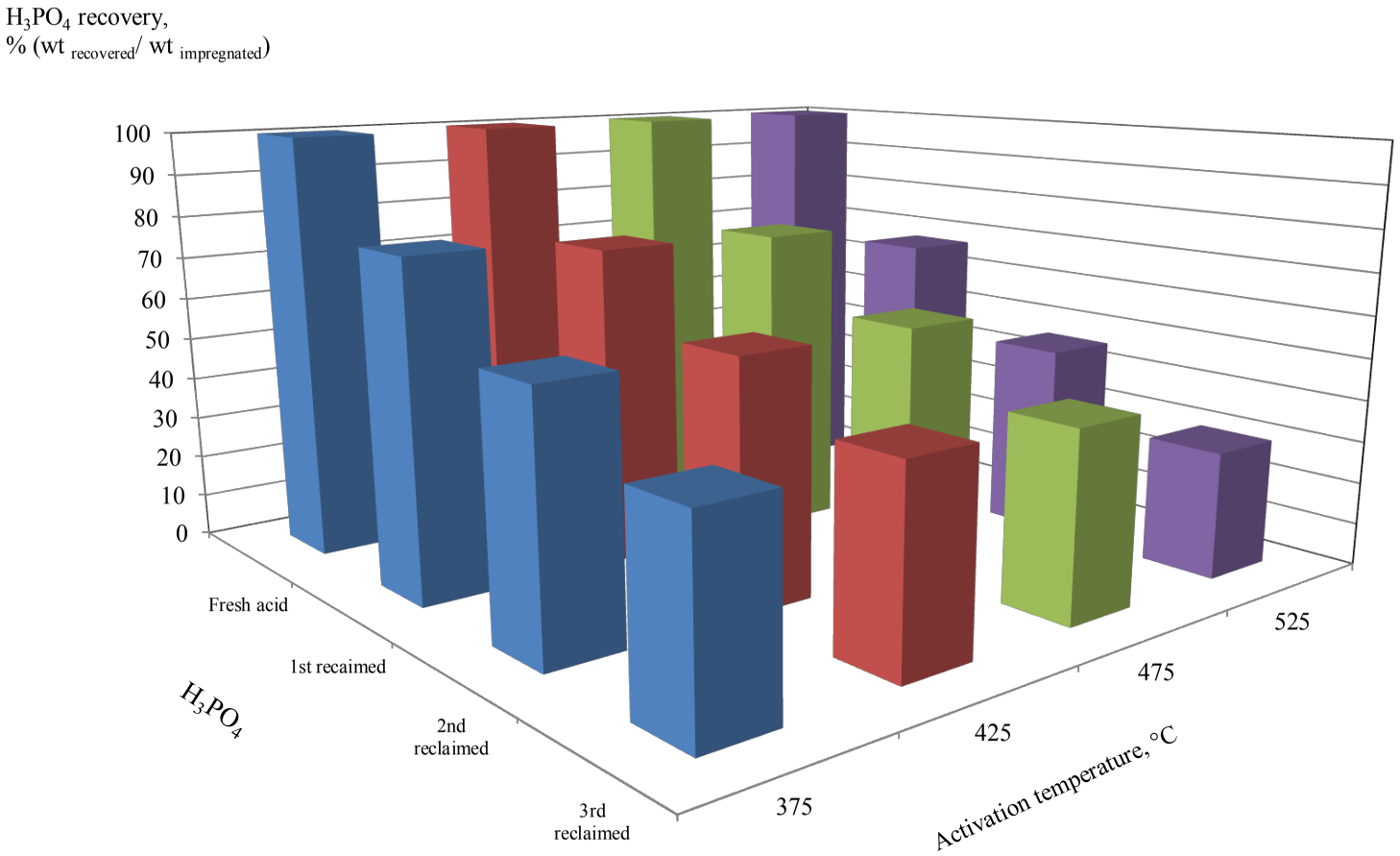

Fig. 6.1. Reagent H_3PO_4 recovery rate in 3 reclaimed activation at 375-525 °C

Activation at temperature range 375-475 °C have little effect on the recovery of H_3PO_4 as the recovery is found to be approximately 45%.

For each activation temperature, the fraction of reagent lost in reclamation starting with fresh H_3PO_4 and 3 subsequent activations using the reclaimed H_3PO_4 are shown in Fig. 6.2. A fraction of H_3PO_4 is found to be unrecoverable upon activation using fresh acid. The percentage loss is found to be in the range of 21-26% irrespective of whether the activation is performed with fresh H_3PO_4 or with reclaimed acid for activation temperature in the range of 375–475 °C. However the loss is found to be higher in the range of 31 to 35% at the activation temperature of 525 °C.

The data presented in Fig. 6.1 & 6.2 clearly indicate the inability of the process to fully recover the H_3PO_4 upon activation irrespective of the activation temperature. The loss of reagent could be attributed to a fraction lost during handling, which is a minor factor and uniform in all experiments, considering the consistency of procedure followed in the recovery process. Apart from the handling loss the process loss could be due to the introduction of phosphorus into the carbon matrix which is fixed in some chemically bonded forms, such as -C-P- bonds or -C-O-P bonds [1,2,3,4]. The addition or insertion of phosphate groups drives the process of dilation that after removal of the acid leaves the matrix in an expanded state with an accessible pore structure. Washing the carbon after activation would not remove all the phosphorus and therefore fail to expose the complete pore structure of the carbon, resulting in some of the pores being closed. Presence of chemically bonded phosphorus compound in H_3PO_4 activated carbon is well documented and further evidence indicate high stability of the phosphorus compounds fixed at higher temperatures in excess of 500 °C [3], which explain the higher proportional loss of the reagent at 525 °C

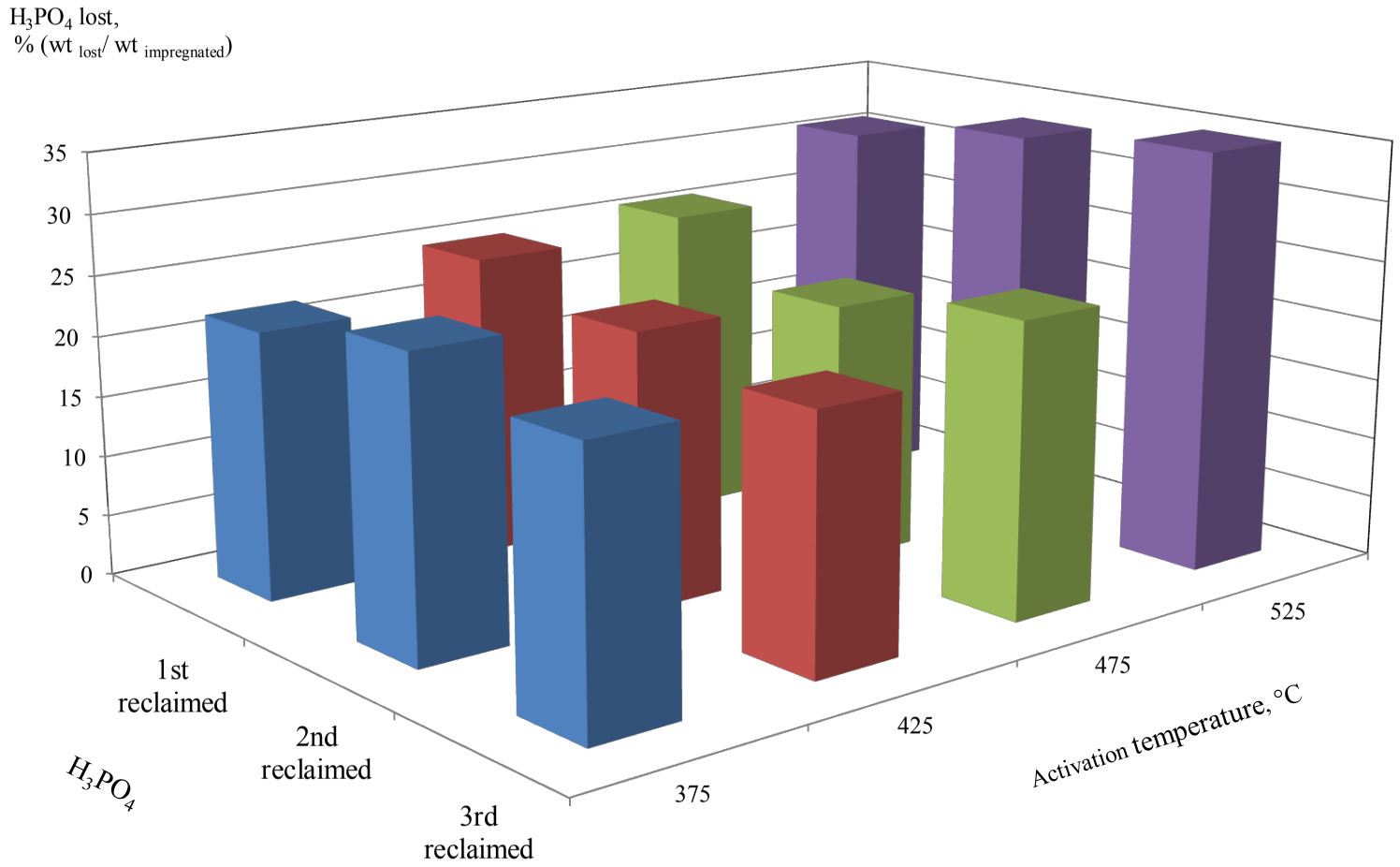

Fig. 6.2. Reagent H_3PO_4 lost rate in 3 reclaimed activation at 375-525 °C

The reagent recovery in the present study is lower as compared to other activating agents such as KOH, with the percentage recovery reported as high as 97% [5]. KOH is not a dehydrating agent and is strictly restricted to the external surface. It doesn't form chemical linkages or embed into pore cavity, rather remains as solid upon activation. This is evident from the textural characteristics of the carbons produced using KOH with high narrow-micro porosity [6]. Also, these basic agents react only after the precursor has been at least partially carbonised at higher temperatures [7,8,9]. This reduces the potential of permanent chemical bonding with surface structure. Even at high impregnation ratios, no significant visual change such as swelling of mixture or formation of tar is observed [6]. Absence of such physical changes in swelling or contraction further reduces entrapment potential of KOH molecules which result in higher reagent recovery. Reaction between the KOH and the precursor leads to the formation of volatile or soluble products (removed during the final washing of the product), such as K_2CO_3 [10] as compared to insoluble phosphate esters. The high activation temperature for KOH activation process results in relatively lower carbon yields which are reported to be for PSAC: 27.4% [11]; oil palm fibre: 22.5% [12]; oil palm fronds: 21.6% [13]; corn cob: 22% [14]; coconut shell: 13.2% [15]; peanut hull: 32% [16] and pistachio-nut shell: 22% [17].

Chemical activation mechanism of $ZnCl_2$ is rather similar to H_3PO_4 activation as both activating agents involve cross-linking reactions resulting in aromatisation in the carbon structure and tar product yield [18]. H_3PO_4 is a Bronstead acid and strong dehydrating agent, thus being more effective to induce bond cleavage than $ZnCl_2$. The small size of the $ZnCl_2$ molecule encourages reagent recovery while H_3PO_4 is a mixture of multiple types of molecules from the small H_3PO_4 and $H_4P_2O_5$ to larger size of $H_{13}P_{11}O_{34}$ [6] resulting a higher possibility of entrapment of the molecule and more difficult to leach out using similar

washing method. The ash content produced by H_3PO_4, chemical activation is also significantly higher as compared to $ZnCl_2$ [18].

6.3 Activated carbon yield

Activation temperature plays an important role on the yield of activated carbon. The yields of PSAC in this study is found between 45 and 55% for activation at temperature range 375-475 °C. Dehydration of palm shell by H_3PO_4 occurs before palm shell pyrolysis, resulting in a well developed porous texture and good yields. In addition, it is the dehydrogenation properties of H_3PO_4 that inhibit formation of tar and reduce the production of other volatile products during pyrolysis. High yield of lignocellulosic activated carbon are well documented, for other precursors activated with H_3PO_4: peach stones: 42–44% [19], woods: 45% [20], bamboo: 46% [21], coconut shells: 49–52% [22], vetivers root: 47–49% [23-56] and olive-waste cakes: 43% [24].

The variation of the heat treatment temperature below 475 °C does not exert any remarkable effect on the yield of PSAC. This is in agreement with findings of Gomez-Tamayo et al. [25] on H_3PO_4 activated evergreen oak. A qualitative trend in the yield reduction of activated carbon with increase in temperature of activation can be observed from Fig. 6.3, with the effect being more pronounced at a higher activation temperature of 525 °C. An increase in the activation temperature indicates the increase in rate of reaction between the precursor and the H_3PO_4, evidenced from the reduction in the yield. At high temperature, the weight loss rate of carbon is higher, primarily due to the initial large amount of volatiles (which can be easily released) as well as the loss of moisture to a lesser extent. This is in agreement with works by Liou & Wu [26] stating a visible declined of yield after 500 °C in H_3PO_4 activated rice husk.

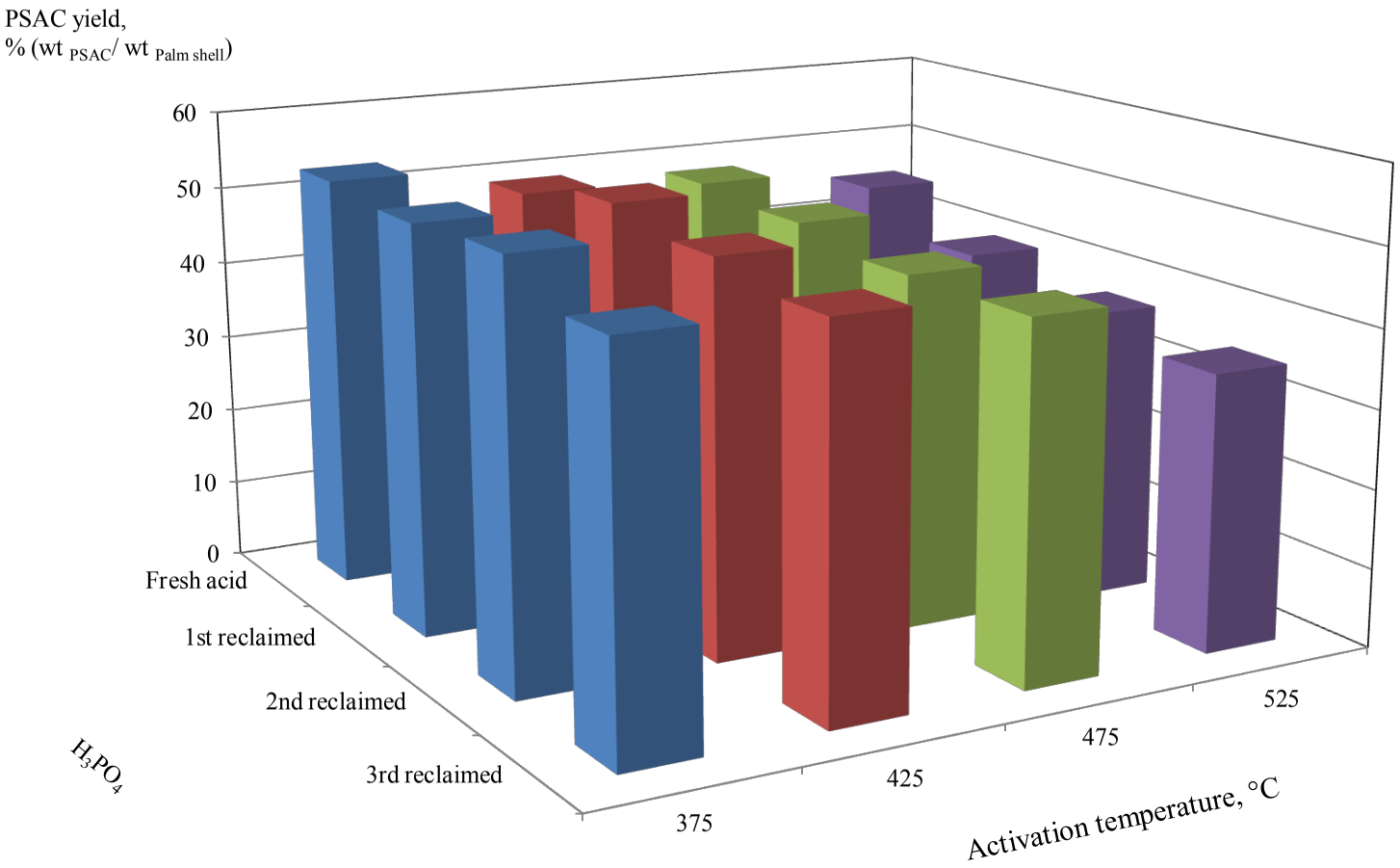

Fig. 6.3. PSAC yield in fresh and reclaimed H_3PO_4 activation at 375-525 °C

All the experiments including both fresh as well as reclaimed H_3PO_4 activations are fixed at constant impregnation ratio of 1.75. As shown in Fig. 6.3, negligible decline in PSAC yield is observed using reclaimed H_3PO_4 at activation temperature range 375–525 °C, asserting the reclaimed reagent is not influenced by the numbers of successive runs with reclaimed acid.

6.4 BET surface area analysis

Fig. 6.4 shows the BET specific surface area of PSAC at different activation temperatures using fresh and reclaimed H_3PO_4. The BET specific surface area increases in accordance to the activation temperature of 375 to 525 °C, with the maximum BET surface area of 2153 m^2/g at an activation temperature of 525 °C with fresh H_3PO_4 acid. As can be observed from the figure although the highest surface area carbon is produced at 525 °C, the utilization of reclaimed acid for successive activation significantly reduces the textural characteristics of the carbon. However at temperature range of 375-475 °C, PSAC produced using reclaimed H_3PO_4 possess an extensive surface area, provided activation is at constant impregnation ratio. PSAC from reclaimed H_3PO_4 exhibited BET surface areas almost similar with the PSAC produced using fresh H_3PO_4, asserting the functionality of reclaimed acid is still intact and not deteriorated with the number of reuse in impregnation-activation. A significant increase in the surface area is observed with increase in the activation temperature up to an activation temperature of 475 °C, with all the subsequent reclaimed runs as well confirming the repeatability of the surface area. The surface area seems to reach a plateau at 475 °C indicating the optimum conditions around 475 °C. Hence the optimum conditions for activation has been identified to be an activation temperature of 475 °C, with an impregnation ratio of 1.75, at an activation time of 75 min.

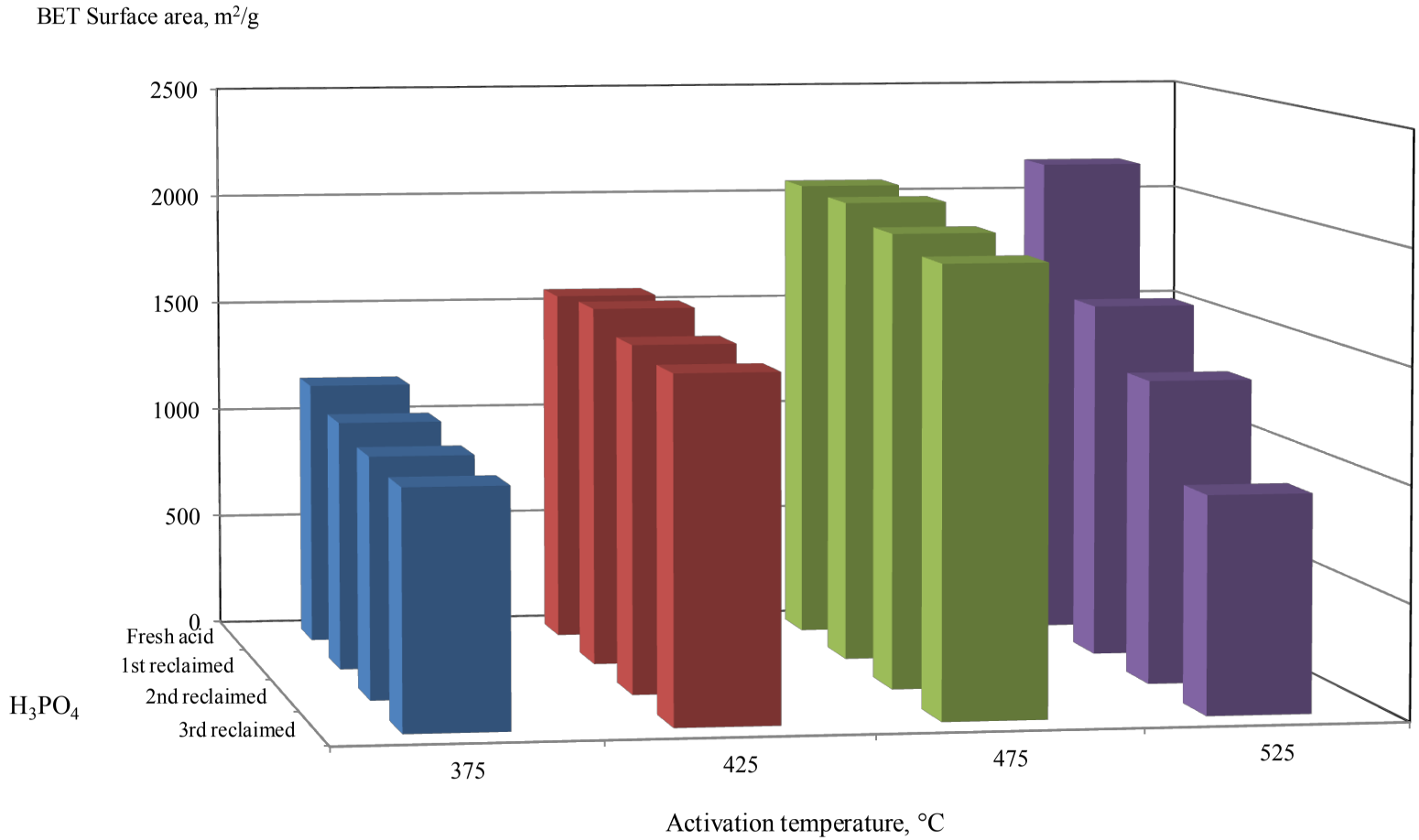

Fig. 6.4. BET surface area of PSAC activated by fresh and reclaimed H_3PO_4 activation at 375-525 °C

On the aspects of reuse of H_3PO_4 for activation Guo & Lua [27] and Toles et al. [28] have reported a sharp decline in the BET surface area. Reclaimed reagent activation in both works were based on assumption H_3PO_4 could be recovered wholly and available for all subsequent activation. H_3PO_4 recovery ratio were not measured or reported. In view of the significant portion of unrecoverable in H_3PO_4, activation with reclaimed H_3PO_4 in those works was likely to be at lower impregnation ratio. It is well known that the impregnation ratio is one of the significant parameters that greatly influence the porosity development. This indicates that each successive run using reclaimed acid, was conducted at a lower impregnation ratio, which sufficiently explains the contradicting behaviour of results reported in literature as compare to the present study. The reported drastic decrease in surface area with the reclaimed H_3PO_4 could be due to low impregnation ratio in spite of the report of silicate pollution from glassware that inhibits surface area development.

When activated at 525 °C, BET surface area prepared using reclaimed H_3PO_4 decline drastically as compared to PSAC prepared using fresh acid. The BET surface area of PSAC reduced from 1575 m^2/g in 1st reclaimed activation run to 941 m^2/g in 3rd reclaimed activation run. It appears that activation temperature of 525 °C has severe effect on the functionality of reclaimed H_3PO_4, even though the successive activation runs are at constant impregnation ratio. Pore volume of PSAC increase with activation temperature up to 475 °C as shown in Fig. 6.5, with the largest pore volume being 1.3 cm^3/g. As a case of comparison with other activating agents, Hu et al. recorded a pore volume of 0.9 cm^3/g for coconut based activated carbon with BET surface area of 2309 m^2/g [15] while Zuo & Han has recorded a BET surface area of 2400 m^2/g and a pore volume of 1.4 cm^3/g for coal based activation carbon [29].

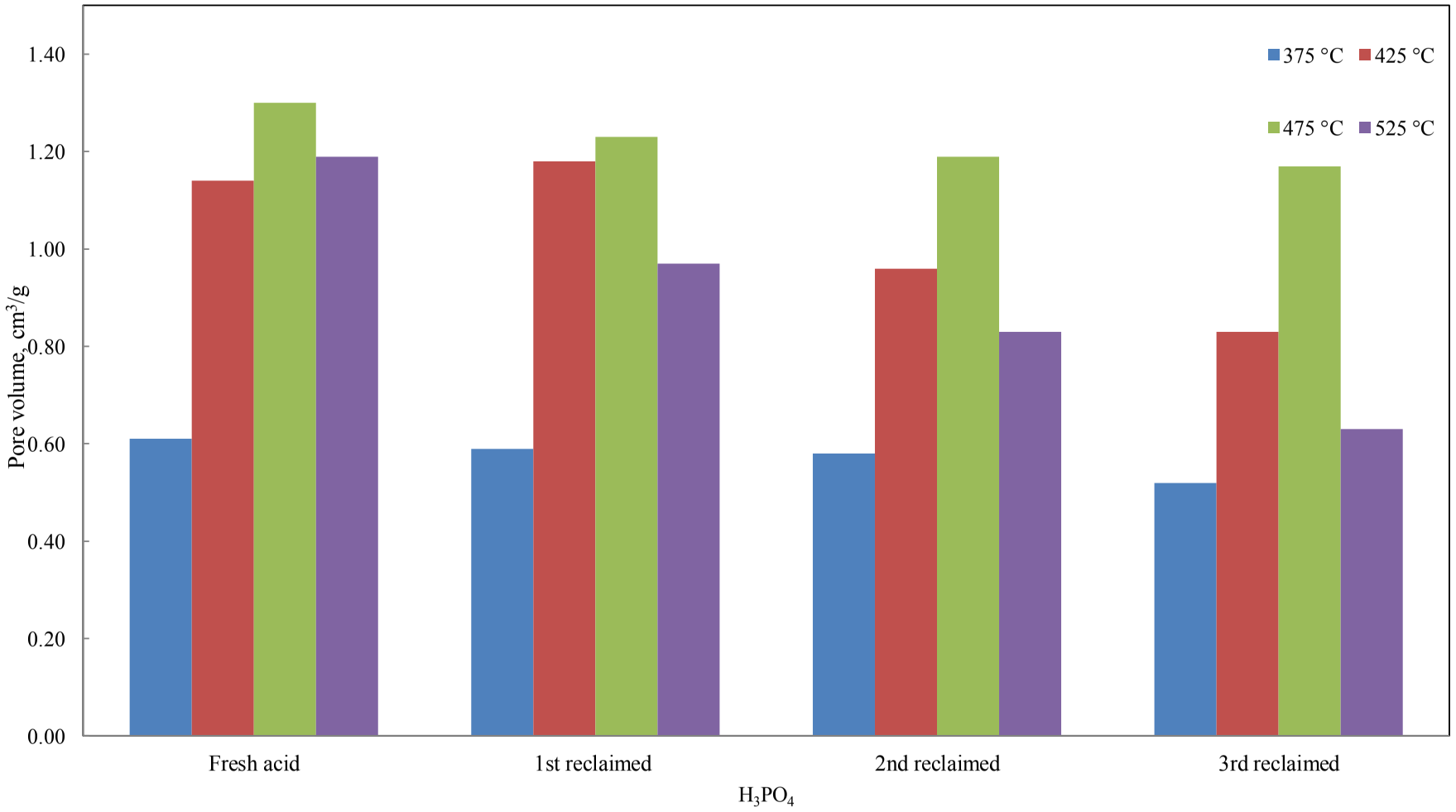

Fig. 6.5. Pore volume of PSAC activated by fresh and reclaimed H_3PO_4 activation at 375-525 °C

A drastic reduction in pore volume at an activation temperature of 500 °C with H_3PO_4 has been reported by Carrott et al. [30] which is in agreement with the present results. At temperatures above 500 °C, the phosphate and polyphosphate bridges become thermally unstable and the decrease in surface area/pore volume is the result of an increase in the size of aromatic units and shrinkage in the material [27,31]. Such observation have been reported in H_3PO_4 activation on various biomass precursors such as cork respectively [30], apple pulp [31] and white oak & yellow poplar woods [32].

6.5 SEM analysis

Fig. 6.6 (a) indicates PSAC surface with incomplete washing (PSAC sample which collected when wash liquor show conductivity of 700 uS/cm). The rod like white salt of phosphate is found to be firmly inhibiting a significant numbers of the developed pore. The process of diffusion of phosphorous compounds from the inner porous net work to the surface of the carbon is a slow diffusion process which demands long duration/repeated washing for maximizing removal of H_3PO_4 from activated carbon. Fig. 6.6 (b) on the other hand, shows the quality of pore on complete washing (conductivity of wash liquor less than 50 μS/cm). Such macro-size pores would provide the porous network leading to meso and micropores. Although the surface looks devoid of phophorous compounds as seen in Fig. 6.6a, the probablity presence of minor amounts of phophorous compounds inside the porous net work cannot be eliminated, which accounts for the loss of H_3PO_4 on activation. Fig. 6.6 (c) on the other hand, shows the surface structure of PSAC produced using 3rd reclaimed H_3PO_4 at 525 °C. The pore development is seen to be shallow and limited to the surface, with a high fraction of them fail to make full surface penetration, leading to a possibly lower available porous network in the carbon. This observation is in agreement with the low BET surface area and pore volume recorded at activation temperature of 525 °C.

6.6 FT-IR analysis

FT-IR transmission spectra of the palm shell, its chars and PSAC have been obtained, in order to qualitatively characterise the functional group, as shown in Fig. 6.7 & 6.8 The appearance of a broad band between 1300 and 1100 cm^{-1} with a maximum at 1220-1180 cm^{-1} is observed in the spectra in PSAC suggests significant alteration by H_3PO_4 activation. According to Puziy et al. [33], the band around 1220-1180 cm^{-1} is due to the stretching of hydrogen-bonded P=O in a phosphate ester, O–C bond in P–O–C linkage, or P=OOH bond. This observation is generally attributed to phosphorous and phosphor carbonaceous compounds [24,34], suggesting that H_3PO_4 produces char oxidation, introducing oxygenated functionalities in the PSAC. The peak at 1450 cm^{-1} is due to C-H asymmetrical bending while peak at 1720 cm^{-1} is assigned to C=O stretching vibrations in ketone, aldehydes, and aromatic esters. The broad peaks at 2300-2400cm^{-1} could be ascribed to the presences of –COOH functional groups and the broad band at 3500-3300 cm^{-1} could be attributed to hydroxyl (O-H) groups such or adsorbed water.

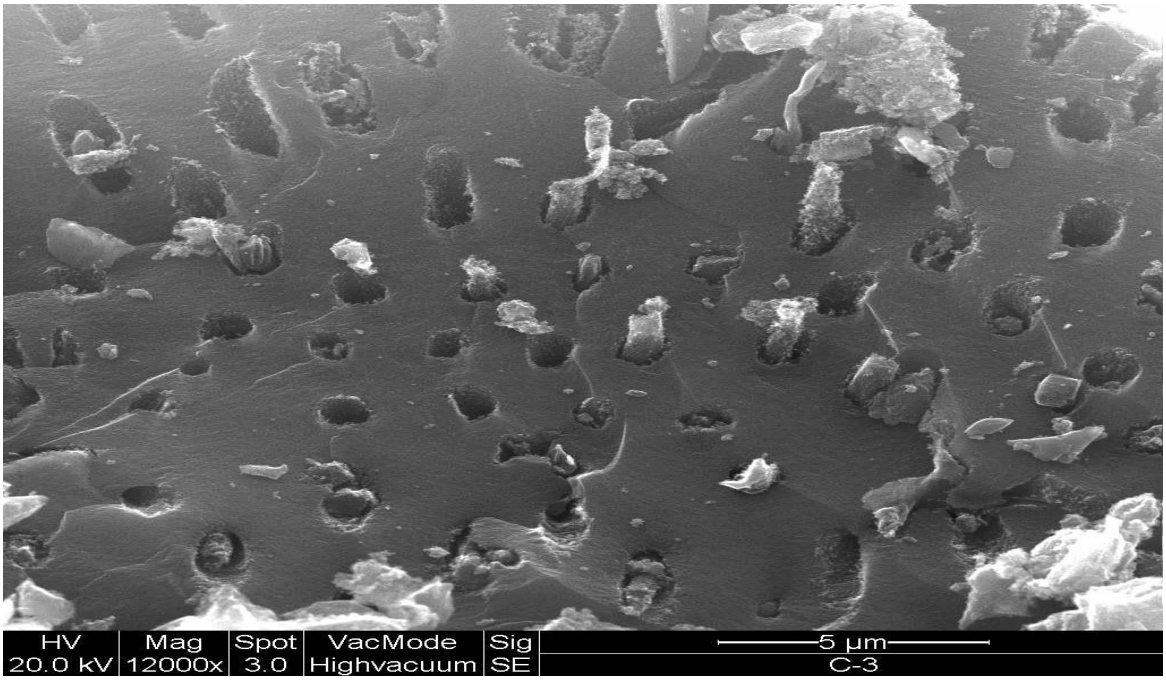

Fig. 6.6. (a) SEM image of PSAC surface (incomplete washed)

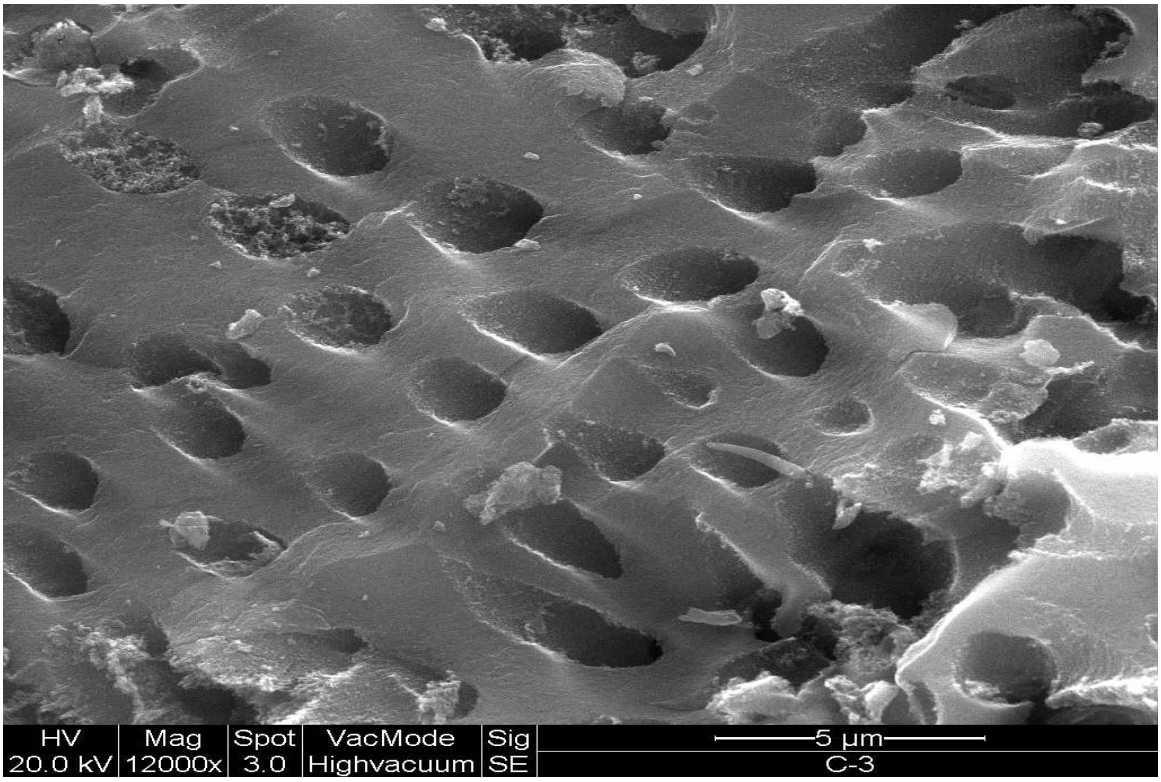

Fig. 6.6. (b) SEM image of PSAC surface (complete washed)

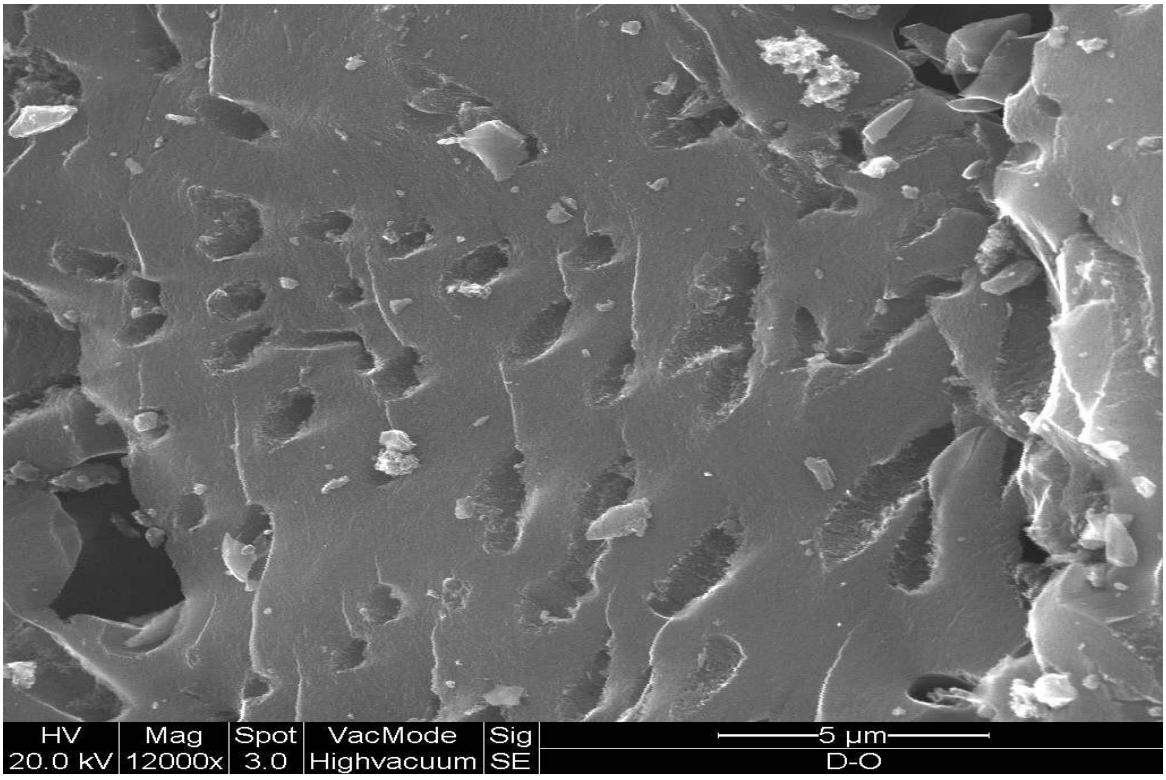

Fig. 6.6. (c) SEM image of PSAC surface (activated using 3rd reclaimed H_3PO_4 at 525 °C)

An increase in the intensities of bands corresponding to O- and/or P-containing groups as highlighted in the chars confirms reaction between H_3PO_4 and palm shell beginning during impregnation and drying stage, resulting in phosphate linkages on palm shell surface. Some of these bands can also involve P-containing groups; for instance, bands at 1120–1080 cm^{-1} have been ascribed to P-O symmetrical stretching in polyphosphates [1-7]. This suggests that oxidation of palm shell char occurs via introduction of oxygenated functionalities in the carbonaceous materials.

Fig. 6.8 shows no conspicuous difference between FT-IR spectra for PSAC obtained from fresh or among reclaimed H_3PO_4. It can be confirmed that there are no additional bands formed due to the usage of reclaimed acid. This confirms the similarity of the surface functional groups of the PSAC prepared using reclaimed acid with the one prepared using fresh acid

6.7 XRD analysis

Fig. 6.9 shows the characteristic of phosphate content in various the PSAC samples prepared using fresh H_3PO_4 and activated at temperature ranging 375-525 °C. The characteristic diffraction peak around $2\theta = 22.5°$ indicating the presence of phosphates on the washed PSAC surface. It is observed that the peak intensity for PSAC prepared at 525 °C is significantly higher than PSAC below 500 °C, such intense diffraction confirm a much higher concentrated presence of phosphate on the carbon surface. This observation validates the highest H_3PO_4 loss upon activation.

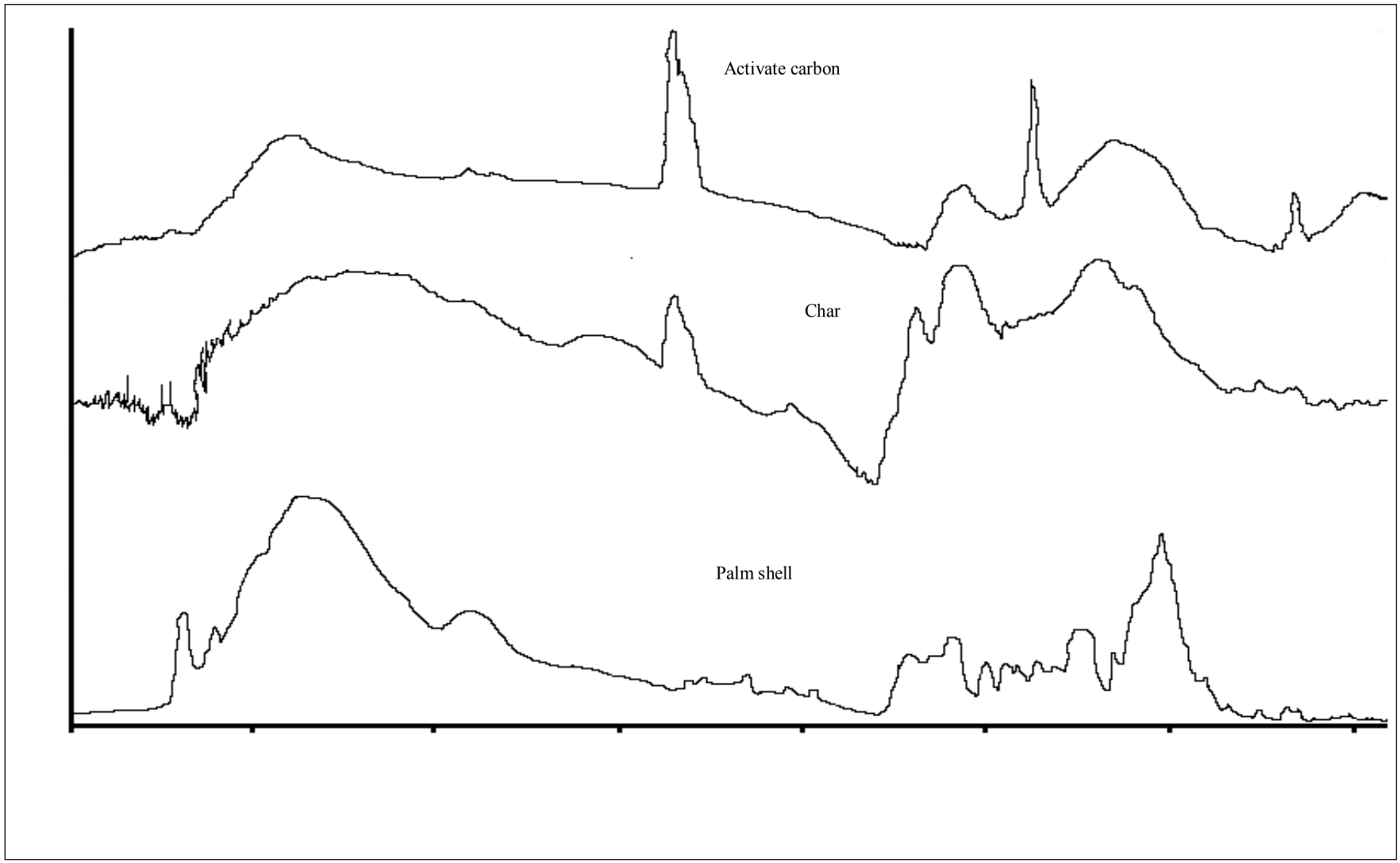

Fig. 6.7. FT-IR spectra of palm shell, its char and PSAC

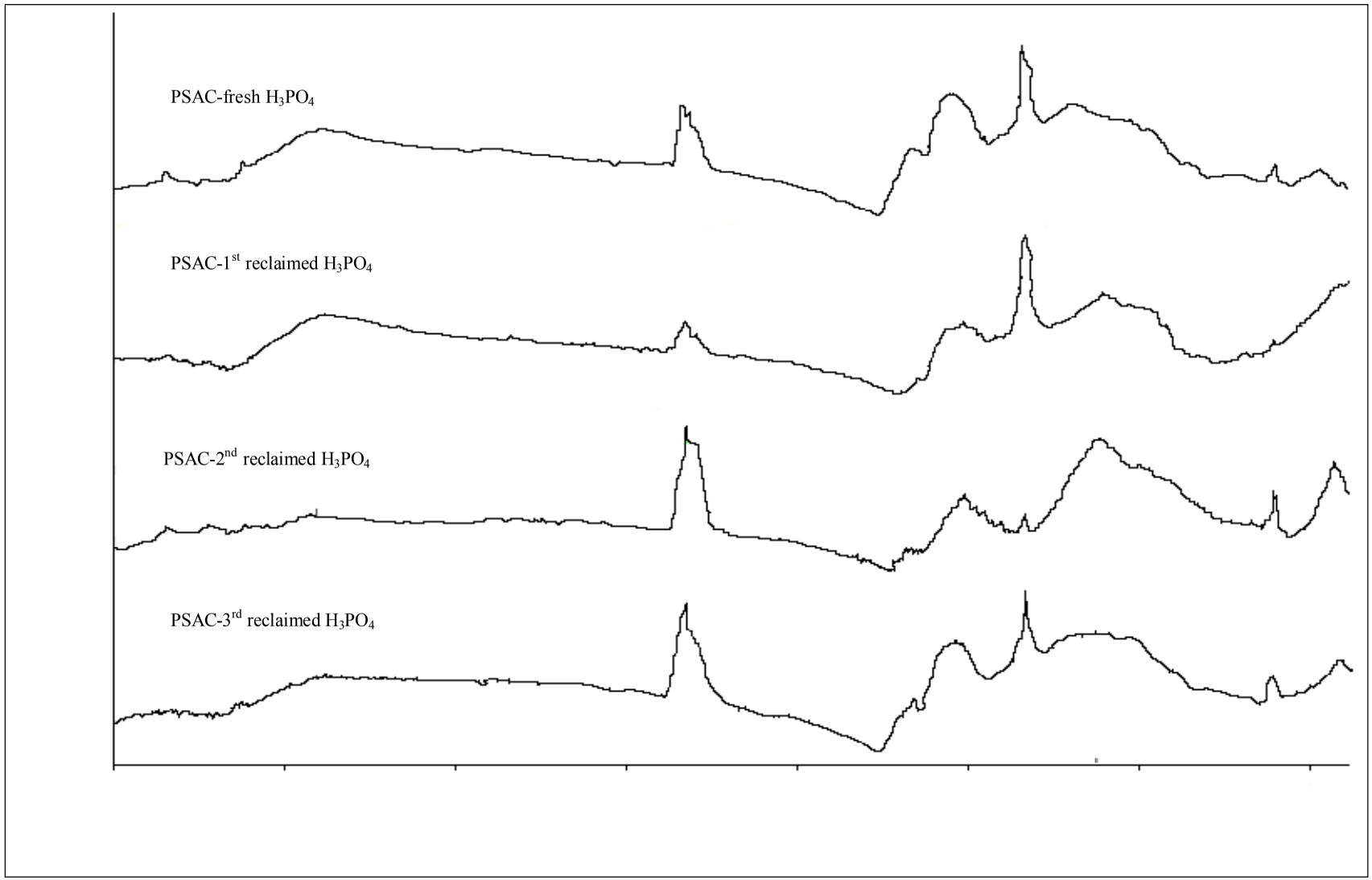

Fig. 6.8. FT-IR spectra of PSAC (activated with fresh and reclaimed H_3PO_4)

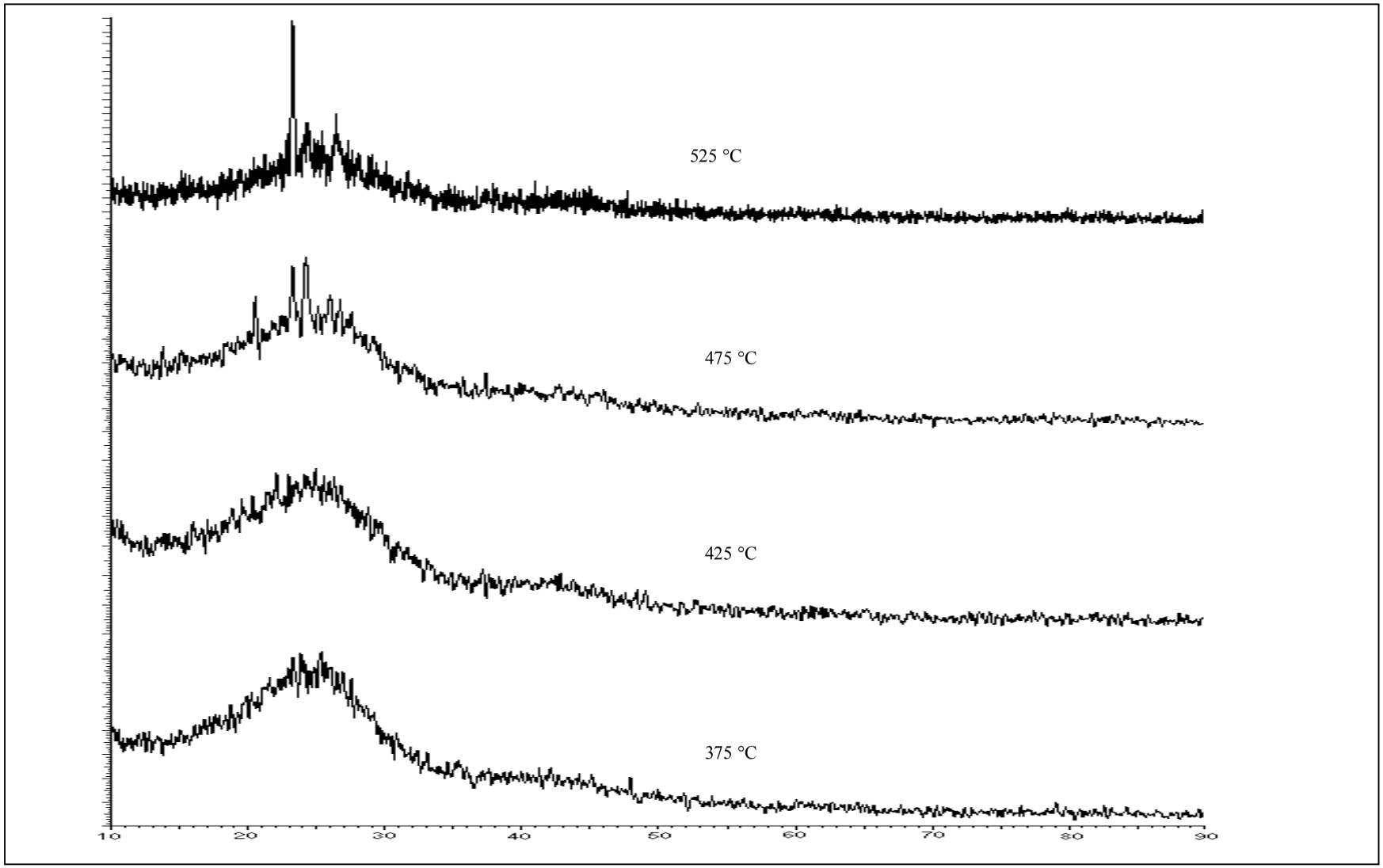

Fig. 6.9. XRD pattern of PSAC (activated at 375-525 °C)

6.8 Conclusions

An in-depth attempt to understand the recovery and reusability of H_3PO_4, one of the popular acting agents. The followings are the conclusion of present study:

1. The activation process results in a weight loss of 20-25% in H_3PO_4 for the activation temperature range of 325 to 475 °C, while it is 30-35% at 525 °C. The trend is consistent in activation with fresh or reclaimed H_3PO_4.
2. With fresh H_3PO_4, the yield of activated carbon reduces marginally from 52% to 45% with increase in activation temperature from 325 to 475 °C. The usage of reclaimed H_3PO_4 for successive activation doesn't show any significant effect on the yield. Also, the yield from reclaimed H_3PO_4 activation closely adhering to the fresh reagent. However at 525 °C and using reclaimed H_3PO_4, the carbon yield continues to decrease in successive runs with the yield of 35% at the 3rd recycle run.
3. The BET surface area of palm shell activated carbon is found to increase significantly with activation temperature up to 475 °C (approaching a plateau), indicating the reach of optimum activation temperature. The surface area with reclaimed H_3PO_4 in the successive runs doesn't show any variation as compared with fresh H_3PO_4. However there is a drastic reduction when activation with reclaimed H_3PO_4 at 525 °C.
4. The pore volume is found to increase with activation temperature up to 475 °C before decreasing at a higher temperature, with the same trend reflected in activation with the reclaimed H_3PO_4.
5. The present study highlights the successful reuse of reclaimed H_3PO_4 as reagent, guarantying same textural characteristics of palm shell activated carbon, provided the impregnation ratio is maintained at similar level.

6.9 References

1 F. Suarez-Garcia, A. Martinez-Alonso, J.M.D. Tascon, Nomex polyaramid as a precursor for activated carbon fibres by phosphoric acid activation. Temperature and time effects, Microporous and Mesoporous Materials 75 (2004) 73-80

2 Y. Guo, D.A. Rockstraw, Physical and chemical properties of carbons synthesized from xylan, cellulose, and Kraft lignin by H3PO4 activation, Carbon 44 (2006) 1464-1475

3 D. Prahas, Y. Kartika, N. Indraswati, S. Ismadji, Activated carbon from jackfruit peel waste by H_3PO_4 chemical activation: Pore structure and surface chemistry characterization, Chemical Engineering Journal 140 (2008) 32-42

4 M. Jagtoyen, M. Thwaites, J. Stencel, B. McEnaney, F. Derbishire, Adsorbent carbon synthesis from coals by phosphoric acid activation, Carbon 30 (1992) 1089-1096

5 T. Tay, S. Ucar, S. Karagoz, Preparation and characterization of activated carbon from waste biomass, Journal of Hazardous. Materials 165 (2009) 481-485

6 H. Marsh, F. Rodriguez-Reinoso, Activated carbon, First ed., Elsevier Ltd., Oxford, 2006

7 K. Okada, N. Yamamoto, Y. Kameshima, A. Yasumori, Porous properties of activated carbons from waste newspaper prepared by chemical and physical activation, Journal of Colloid and Interface Science 262 (2003) 179-193

8 L-Y. Hsu, H. Teng, Influence of different chemical reagents on the preparation of activated carbons from bituminous coal, Fuel Processing Technology 64 (2000) 155-166

9 M.A. Lillo-Rodenas, D. Cazorla-Amoros, A. Linares-Solano, Understanding chemical reactions between carbons and NaOH and KOH: an insight into the chemical activation mechanism, Carbon 41(2003) 267-275

10 M.A. Lillo-Rodenas, J. Juan-Juan, D. Cazorla-Amoros, A. Linares-Solano, About reactions occurring during chemical activation with hydroxides, Carbon 42 (2004) 1371-1375

11 J. Guo, A.C. Lua, Textural and Chemical Characterizations of Adsorbent Prepared from Palm Shell by Potassium Hydroxide Impregnation at Different Stages, Journal of Colloid and Interface Science 254 (2002) 227-233

12 B.H. Hameed, I.A.W. Tan, A.L. Ahmad, Optimization of basic dye removal by oil palm fibre-based activated carbon using response surface methodology, Journal of Hazardous Materials 158 (2008) 324-332

13 J.M. Salman, B.H. Hameed, Effect of preparation conditions of oil palm fronds activated carbon on adsorption of bentazon from aqueous solutions, Journal of Hazardous Materials 175 (2010) 133-137

14 Q. Cao, K-C. Xie, Y-K. Lv, W-R. Bao, Process effects on activated carbon with large specific surface area from corn cob, Bioresource Technology 97 (2006) 110-115

15 Z. Hu, H. Guo, M.P. Srinivasan, N. Yaming, A simple method for developing mesoporosity in activated carbon, Separation and Purification Technology 31 (2003) 47-52

16 B.S. Girgis, S.S. Yunis, A.M. Soliman, Characteristics of activated carbon from peanut hulls in relation to conditions of preparation, Materials Letters 57 (2002) 164-172

17 A.C. Lua, T. Yang, Effect of activation temperature on the textural and chemical properties of potassium hydroxide activated carbon prepared from pistachio-nut shell, Journal of Colloid and Interface Science 274 (2004) 594-601

18 P.T. Williams, A.R. Reed, High grade activated carbon matting derived from the chemical activation and pyrolysis of natural fibre textile waste, Journal of Analytical and Applied Pyrolysis 71 (2004) 971-986

19 M. Molina-Sabio, F. Rodriguez-Reinoso, F. Caturla, M.J. Selles, Porosity in granular carbons activated with phosphoric acid, Carbon 33 (1995) 1105-1103

20 H. Benaddi, D. Legras, J.N. Rouzaud, F. Beguin, Influence of the atmosphere in the chemical activation of wood by phosphoric acid, Carbon 38 (1998) 306-309

21 A.W.M. Ip, J.P. Barford, G. McKay, Production and comparison of high surface area bamboo derived active carbons, Bioresource Technology 99 (2008) 8909-8916

22 M.K.B. Gratuito, T. Panyathanmaporn, R.A. Chumnanklang, N. Sirinuntawittaya, A. Dutta, Production of activated carbon from coconut shell: Optimization using response surface methodology. Bioresource Technology 99 (2008) 4887-4895

23 S. Altenor, B. Carene, E. Emmanuel, J. Lambert, J-J. Ehrhardt, S. Gaspard, Adsorption studies of methylene blue and phenol onto vetiver roots activated carbon prepared by chemical activation, Journal of Hazardous Materials 165 (2009) 1029-1039

24 R. Baccar, J. Bouzid, M. Feki, A. Montiel, Preparation of activated carbon from Tunisian olive-waste cakes and its application for adsorption of heavy metal ions, Journal of Hazardous Materials 162 (2009) 1522-1529

25 M.D.M. Gomez-Tamayo, A. Macias-Garcia, M.A.D. Diez, E.M. Cuerda-Correa, Adsorption of Zn(II) in aqueous solution by activated carbons prepared from evergreen oak (*Quercus rotundifolia L.),* Journal of Hazardous Materials 153 (2008) 28-36

26 T.-H. Liou, S-J. Wu, Characteristics of microporous/mesoporous carbons prepared from rice husk under base- and acid-treated conditions, Journal of Hazardous Materials 171 (2009) 693-703

27 J. Guo, A.C. Lua, Textural and chemical properties of adsorbent prepared from palm shell by phosphoric acid activation. Materials Chemistry and Physics 80 (2003) 114-119

28 C.A. Toles, W.E. Marshall & M.M. Johns, Phosphoric acid activation of nutshells for metals and organic remediation: Process optimization, Journal of Chemical Technology & Biotechnology 72 (1998) 255-263

29 Y. Zou, B.X. Han, High-surface-area activated carbon from Chinese coal, Energy Fuels 15 (2001) 1383-1386

30 P.J.M. Carrott, M.M.L. Ribeiro Carrott, P.A.M. Mourao, Pore size control in activated carbons obtained by pyrolysis under different conditions of chemically impregnated cork, Journal of Analytical and Applied Pyrolysis 75 (2006) 120-127

31 F. Suarez-Garcia, A. Martinez-Alonso, J.M.D. Tascon, Pyrolysis of apple pulp: chemical activation with phosphoric acid, Journal of Analytical and Applied Pyrolysis 63 (2002) 283-301

32 M. Jagtoyen, F. Derbyshire, Activated carbons from yellow poplar and white oak by H_3PO_4 activation, Carbon 36 (1998) 1085-1097

33 A.M. Puziy, O.I. Poddubnaya, A. Martinez-Alonso, F. Suarez-Garcia, J.M.D. Tasco, Surface chemistry of phosphorus-containing carbons of lignocellulosic origin, Carbon 43 (2005) 2857-2868

34 Y. Guo, D.A. Rockstraw, Activated carbons prepared from rice hull by one-step phosphoric acid activation, Microporous and Mesoporous Materials 100 (2007) 12-19

CHAPTER VII

CONCLUSIONS AND RECOMMENDATIONS

7.1 Conclusions

This work is in relation to a systematic study of producing activated carbon (AC) from palm shell, a solid waste produced from palm oil mills in many tropical countries. The investigation began with literature survey to identify the factors that influence AC development. The areas looked into are activation methods, characteristics of AC particularly for PSAC and the recovery and reusability of the activation reagent. The quantitative effect of activation temperature, impregnation ratio and activation time were investigated via process optimization by using optimisation tool, Box-Behnken Design (BBD) of Response Surface Methodology (RSM). The PSAC process development begins with semi-carbonization of H_3PO_4-impregnated palm shell at 170 °C before activation under self-generated atmosphere at 350-500 °C. Four quadratic models were developed for BET surface area, pore volume, pore width and PSAC yield using statistical software. Statistical tests such as test of significance, Lack-of-fit statistics and R-squared statistics were conducted to assess the adequacy of the models in representing the data.

The developed PSAC were characterised for its thermal decomposition behaviour by TGA analysis to assess the effects of semi-carbonization and activation under self-generated atmosphere. Surface characteristics of the PSAC were also being evaluated by FT-IR, TGA,

SEM and XRD. Suitability of the PSAC for adsorption on macromolecules in particular to methylene blue (MB) and dairy COD were investigated and the adsorption isotherm and kinetics for both adsorbates were established. Lastly, the recovery and reusability of H_3PO_4, a popular reagent for chemical activation were thoroughly investigated.

Optimization by RSM of the conditions for PSAC development has proved to be useful and effective while the response surface and contour plots were able to graphically illustrate the optimum set of operating variables. The statistical analysis based on BBD showed that palm shell activated at 500 for 30 min (IR= 1.75) produced PSAC with the highest surface area (2193 m^2/g). The model also predicted the pore volume would vary significantly, that is between 0.02 to 2.0 cm^3/g depending on the changes in the process conditions. The pores were found to be in mesopore range, with pore width between 2.06 and 3.53 nm, a unique characteristic of the PSAC. The PSAC yield, ranging 43 to 55% are among the highest reported for chemical activation of biomass. Activation temperature was found significantly influence PSAC yield, while IR didn't show any effect on yield.

Despite the simplifications, mechanism of palm shell char and PSAC pyrolysis using TGA facilitated understanding the significance of semi-carbonization and activation under self-generate atmosphere. Semi-carbonization has produced a char that is low in non-carbon elements, as demonstrated in its high thermal stability. The developed PSAC has demonstrated excellent thermal stability even though activated at relatively low temperature, highlighting the effectiveness of self-generate atmosphere in releasing volatile matters. FT-IR analysis shows the surface functional groups in PSAC are acidic, a characteristics of H_3PO_4 activation while SEM images of PSAC developed under favourable conditions clearly shows network of accessible pores.

The pore characteristics of the PSAC are highly favourable for adsorption of high molecular weight compounds. The PSAC exhibits a high MB adsorption capacity of 438 mg/g with the adsorption isotherm increases with temperature. Similar trend were observed in dairy COD uptake with maximum adsorption higher than 1000 mg/g. The adsorption pattern could be explained based on the Langmuir isotherm model evidenced from the highest correlation coefficient as compared to other models. Among the different kinetic models tested, a pseudo-second-order model is found to fit the experimental data with close proximity.

The activation process results in a weight loss of more than 20 % in H_3PO_4 for the activation temperature range of 325 to 475 °C, irrespective of activation either with fresh or reclaimed H_3PO_4. The loss reagent is even higher at high temperatures. The surface area for samples using reclaimed H_3PO_4 does not show any variation as compared with fresh H_3PO_4. However there is a drastic reduction with reclaimed H_3PO_4 at 525 °C due to unfavourable activation conditions.

7.2 Recommendations for Future Work

The work presented in this thesis has the potential to generate future works that will further the AC development, adsorption and reagent recovery. The outline of some of the potential future research (but not limited to) could be as follows:

1. As demonstrated in Chapter 4, H_3PO_4 activation under self-generation atmosphere is effective in development of AC with well-developed textural characteristics. The comprehensive activation mechanism was however, not explicitly presented and this could be further explored in the future. The gasification of amorphous carbon is complex due to its highly disorganised structure. It would be interesting to see the development of a carbon activation model that is capable of predicting basic porous

properties of AC and as such, verify the significance of the mentioned non-conventional activation.

2. The potential of the developed PSAC has not been fully explored. For instance, the significant of this mesoporous AC in conjunction to membrane bioreactor as a hybrid treatment system could contribute to advanced treatment system for high organic wastewater. The mesoporous characteristics could also be explored in areas that has been dominated by synthetic mesoporous carbons such as recovery of enzymes, vitamins and proteins.
3. H_3PO_4 recovery upon activation is an effort consuming process as observed in the exponential-decay profile of washed liquor conductivity. Effective reagent recovery from AC-H_3PO_4 complex results in a large amount of water, which demands large amount of energy for evaporation prior to subsequent impregnation. Ultrasonic assisted extraction method- a technique that has showed significant improvement in AC regeneration, could be utilized as an enhancement to conventional washing. The ultrasonic waves and associated micro-disturbances of cavitation bubbles may reduce the mass transfer boundary layer could possibly improve the efficiency of H_3PO_4 recovery.

APPENDIX

MB calibration curve

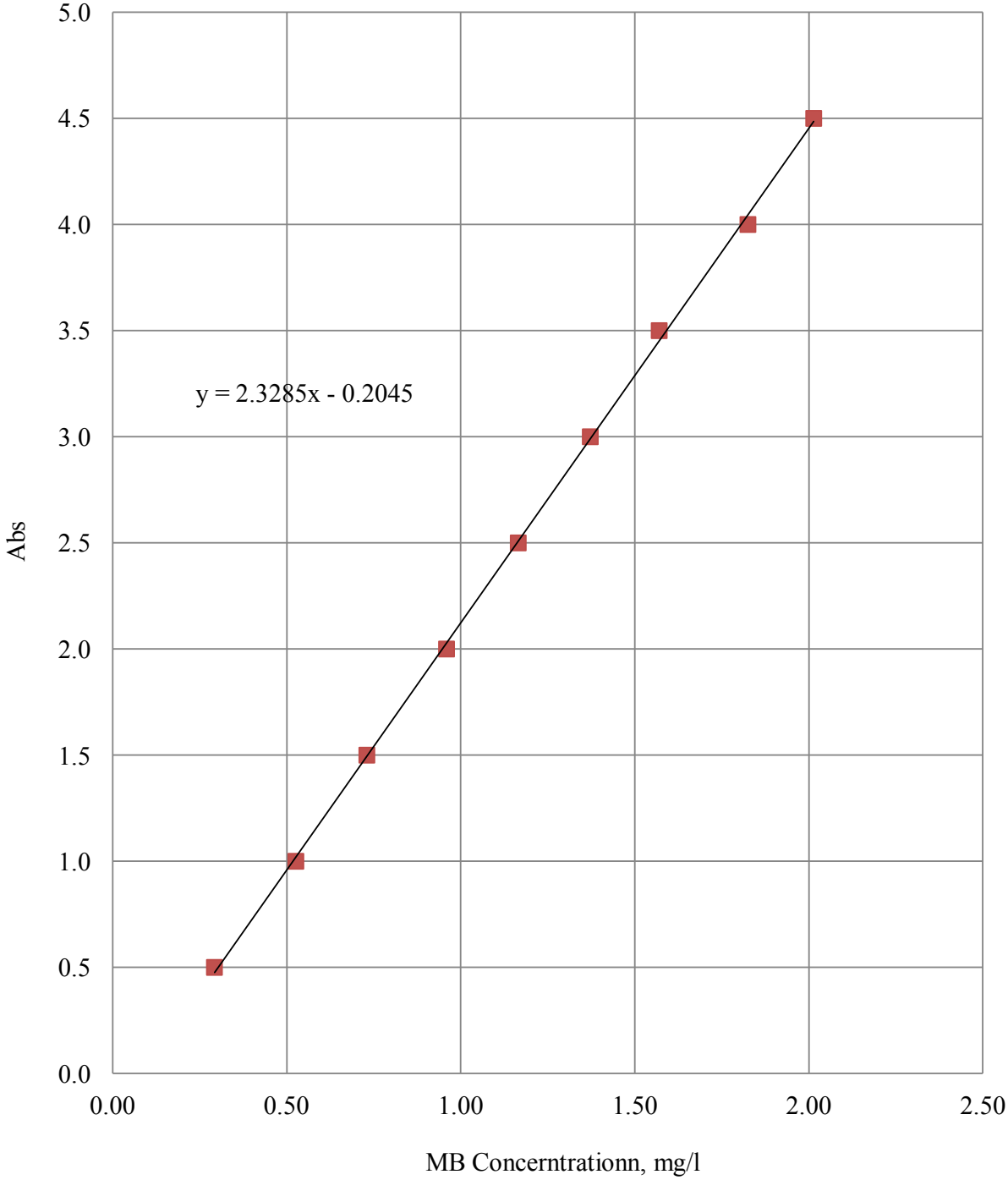

Journal of Analytical and Applied Pyrolysis 88 (2010) 181–186

Contents lists available at ScienceDirect

Journal of Analytical and Applied Pyrolysis

journal homepage: www.elsevier.com/locate/jaap

Activation of palm shells by phosphoric acid impregnation for high yielding activated carbon

W.C. Lim, C. Srinivasakannan*, N. Balasubramanian

Monash University, Sunway Campus, Selangor, Malaysia

ARTICLE INFO

Article history:
Received 19 October 2009
Accepted 2 April 2010

Keywords:
Activated carbon
Phosphoric acid
High yield
Iodine number
BET surface area

ABSTRACT

A compilation of the yield of activated carbons corresponding to good textural characteristics (BET surface area > 1000 m^2/g) derived from palm shells, irrespective of the activation process has revealed a yield lower than 30%. Having known the ability of chemical activation methods to produce high yielding activated carbons, the present study utilizes a two stage activation process in a self-generated atmosphere to prepare activated carbon. A low activation temperature (425 °C) and activation time (30 min) has been utilized, while varying the impregnation ratio of phosphoric acid from 0.5 to 3. The yield of activated carbon is not found to vary with the impregnation ratio and is found to be around 50%. The textural characteristics are found to improve with increase in the impregnation ratio, up to an optimal value of 2, while found to decrease beyond. The BET surface area of activated carbon corresponding to an impregnation ratio of 3, with an iodine number of 1035 mg/g is found to be 1109 m^2/g with a pore volume of 0.903 cm^3/g and an average pore diameter of 3.2 nm. The textural characteristics of activated carbon reveal that the pore size is widely distributed with the contribution of micropores around 50%.

1. Introduction

Utilization of biomass for the production of porous carbons is well established industrially, as the demand is abundant due to varied industrial application. Activated carbons with highly developed surface area are widely used in a variety of industries for applications which include separation/purification of liquids and gases, removal of toxic substances, as catalysts and catalyst support [1–5]. With the development of technology, the applications of activated carbons keep expanding, with newer application such as super-capacitors, electrodes, gas storage, and so on [6–8]. The importance of activated carbon as a popular adsorbent can also be realized from the quantum of the carbon related research which revolves around activated carbons.

Activated carbons have been traditionally produced by the partial gasification of the char either with steam or CO_2 or a combination of both. Usually the physical activation is a two-step process which involves the carbonization of a carbonaceous material followed by the activation of the resulting char at elevated temperature in the presence of suitable oxidizing gases such as carbon dioxide, steam, or their mixtures. The gasification reaction results in removal of carbon atoms and in the process simultaneously produce a wide range of pores (predominantly micropores), resulting in porous activated carbon. Physical activation process is widely adopted industrially for commercial production owing to the simplicity of process and the ability to produce activated carbons with well-developed microporosity and desirable physical characteristics such as the good physical strength.

In chemical activation process the precursors are impregnated with dehydrating chemicals such as H_3PO_4, $ZnCl_2$, K_2CO_3, NaOH or KOH and carbonized at desired conditions in a single step. Chemical activation offers several advantages which include single step activation, low activation temperatures, low activation time, higher yields and better porous structure. The chemical agents used are substances with dehydrogenation properties that inhibit the formation of tar and reduce the production of other volatile products. The disadvantage of chemical activation process is the need for an important washing step, which is time consuming due to number of washings required to completely remove the activation agent from the carbon. Of the several activating agents reported the most important and commonly used activating agents are phosphoric acid, zinc chloride and alkaline metal compounds. Phosphoric acid and zinc chloride are used for the activation of lignocellulosic materials that have not been carbonized previously; whereas metal compounds such as KOH are commonly used for the activation of coal precursors or chars [9]. As compared to zinc chlo-

* Corresponding author at: The Petroleum Institute, Abudhabi, UAE.
E-mail address: csrinivasakannan@pi.ac.ae (C. Srinivasakannan).

0165-2370/$ – see front matter © 2010 Elsevier B.V. All rights reserved.
doi:10.1016/j.jaap.2010.04.004

Table 1
Process conditions and properties of palm shell activated carbon.

Activating agent	Carbonization conditions (°C, h)	Optimum activation conditions (°C, h)	Inert/activating gas flowrate (l/h)	BET surface area (m^2/g)	Total pore volume (cm^3/g)	Yields (% wt. activated carbon/wt. dried palm shell)	Additional information	Ref.
Chemical and physical activation method								
$ZnCl_2$ & CO_2	500/3	500/1	N_2 & CO_2	1500			Impregnation ratio (IR): 1.0–4.0	[33]
$ZnCl_2$ & CO_2	600/2	800/1	N_2 (9) & CO_2 (6)	1837	1.27	30	Sample washed before carbonization	[34]
$ZnCl_2$ & CO_2	800	800/2–3	N_2 & CO_2	2492	1.4	23.5	No cooling on the char and CO_2 replace N_2	[15]
$ZnCl_2$ & CO_2	800	800/2	N_2 (5); CO_2 (20)	1291	0.79	37	IR 1.0, no cooling on the char and CO_2 replace N_2	[35]
H_3PO_4 & CO_2	600/2	800/1	N_2 (9) & CO_2 (6)	1563	1.03	28	Sample washed before carbonization	[34]
H_3PO_4 & CO_2	600/2	800/1	CO_2	1563			Sample were pretreated with H_3PO_4	[36]
KOH & CO_2	600/2	800/1	N_2 (9) & CO_2 (6)	1408	0.77	25	Sample washed before carbonization	[34]
KOH & CO_2	600/2	800/1	CO_2	1408	0.72		Sample were pretreated with KOH	[36]
KOH & CO_2	700/2	850/2	N_2 (9) & CO_2	596	0.34		Impregnation on char at 1:1	[37]
KOH & CO_2	600/2	800/1	N_2 (9) & CO_2 (6)	1562	0.75		Sample washed before carbonization	[38]
H_2SO_4 & CO_2	600/2	800/1	N_2 (9) & CO_2 (6)	1408	0.72		Sample washed before carbonization	[38]
Chemical activation method								
H_3PO_4		500/2	N_2 (9)	1135		40	IR used is 8.0	[16]
H_2SO_4		700/2	N_2 (9)	1014			IR used is 8.0	[39]
KOH		700/2	N_2 (9)	1148			IR used is 6.0	[39]
H_2SO_4		700/2	N_2 (9)	1250			IR used is 6.0	[11]
K_2CO_3		800/1	N2	1200	0.5		One stage activation	[40]
K_2CO_3		800/2	N_2 (15)	1170		18.9	IR 1.0	[10]
Physical activation method								
CO_2	600/3	850/2	N_2 (9) & CO_2 (6)	1410	0.71		One stage activation	[41]
CO_2	600/3	900/0.5	N_2 (9) & CO_2 (6)	1366			Two stages activation	[42]
CO_2		800/2	CO_2 (6)	1062		17	One stage activation	[16]
CO_2	600/3	900/0.5	CO_2 (6)	1366	0.69	10.2	Two stages activation	[43]
CO_2	500/3	900/0.5	N_2 (9) & CO_2 (6)	1366	0.48	10.3	Two stages activation	[44]
CO_2		1100/1.5	N_2 (30) & CO_2 (30)	1052	0.76		Two stages activation	[45]
CO_2	300–700/2	900/2	N_2 (9) & CO_2 (6)	1062			Two stages activation	[11]
CO_2	600/2	800/1	CO_2	1366			Two stages activation	[36]
CO_2	850	850/1	N_2 (9) &CO_2				Two stages activation	[46]
CO_2	600/2	900/0.5	N_2 (9) & CO_2 (6)	1366	0.6	10	Two stages activation	[47]
CO_2		900/2	CO_2 (6)	1062			One stage activation	[39]
Steam	400	900/1	Vacuum & steam/N_2	1183	0.69		Carbonization under vacuum	[48]
Steam	675/2	900/1	Vacuum & steam	998			Carbonization under vacuum	[49]
Steam	500–900	500–900/1	N_2 (9) & steam/N_2				Two stages activation	[50]
Steam	900/1	900/7	N_2 & steam	1319	0.73		Two stages activation	[51]

ride the phosphoric acid is most preferred due to environmental problems associated with zinc chloride [10,11]. Further activated carbons prepared using phosphoric acid has better acceptance in food, fine chemical and pharmaceutical applications due to its non-contaminating nature.

The rapid growth of Malaysia palm industries has ranked her the world's biggest exporter of quality palm oil with revenue of RM65 billion in year of 2008. For every 2.5 kg of crude palm oil produced, about 80 kg of palm shells are generated and thus are posing disposal issues. The global production of palm oil is reported to be around 48 million tons [12], which corresponds to a palm shell generation of 1500 million tons. The availability of palm shells, far exceed the total demand for activated carbon, which is estimated to be only around 1.2 million tons [13]. The palm shell has no specific technical use and only a small portion is used as fuel to generate process steam in the palm-processing mill [2,14]. However, its high density, relatively high carbon content and low ash content are desirable properties of a suitable precursor for the preparation of high-grade activated carbon. These renewable agricultural wastes are cost-effective alternatives to more expensive and polluting precursors like coal for the production of activated carbon [4].

Activated carbon with suitable pore structure having high surface area has good value realization, commercial acceptance and hence it is imperative to utilize processes that maximize the yield with good pore characteristics. Majority of the study reports only the pore structure and pore characteristics of the activated carbon, without the due mention to the yield of activated carbon. The yield as well as the pore structure of the activated carbon is widely reported to be influence by the activation temperature [10,15,16], activation time [15] and the impregnation ratio [10,15,17,18]. Generally the yield of activated carbon decreases with increase in activation temperature, activation time and impregnation ratio, while the pore characteristic improves with increase in the above stated parameters, mostly to an optimum value and decreases beyond [10,16].

Table 1 summarizes the number of studies pertaining to the preparation of activated carbon using palm shells utilizing physical, chemical and combination of physical and chemical activation methods as well as the properties of the resulting PSAC. It can be observed that majority of the work reports only about the pore characteristics without mentioning the corresponding yield. Among the reported literature the yield of activated carbon using physical activation methods is found to be less than 17%, with the activation temperatures around 900 °C. While the combination of physical/chemical activation methods reports yield less than 30% with the activation temperatures of around 800 °C, with an exception of $ZnCl_2/CO_2$ activation resulting in a yield of 37%. Among the chemical activation methods the K_2CO_3 activation produced a very low yield of 19%, while the phosphoric acid activation at 500 °C resulted in a yield of 40%, which is significantly higher than the other activation methods and activating agents. It can be observed that the yield of activated carbon varied widely depending upon the processing methods. Induced by the result due to Guo and Lua [16], and the advantages of phosphoric based activation methods due to Srinivasakannan and Bakar [19] the present study attempts to explore further into the low temperature activation using phosphoric acid for the conversion of palm shells into activated carbon. Toward this experimental methods due to Srinivasakannan and Bakar [19] is adopted, utilizing a two stage activation process in a self-generated atmosphere, at an activation temperature of 425 °C, with the activation time of 30 min, by varying the impregnation ratio of 0.5–3. The choice of low activation temperature and time is aimed at improving the process economics based on the recent report due to Gratuito et al. [20].

Table 2
Reported proximate analyses and ultimate analyses of oil palm shell (on dry basis and value is in wt.%).

Volatile matter	Fixed carbon	Ash	Ref.
(*a*) *Proximate analyses*			
80.8	17.3	1.9	[41,52]
79.4	19.6	1	[45]
78.7	20.3	1.2	[46,50,53]
77.6	19.8	2.6	[16,42,43,47,53–56]
76.7	21.2	2.1	Present study

C	H	O	N	Ref.
(*b*) *Ultimate analyses*				
53.7	5.6	40.5	0.2	[11]
50.1	6.8	41.2	1.9	[45]
50	6.9	41	1.9	[46,50,53]
49.5	6.3	43.6	0.5	Present study

2. Experimental methods

2.1. Materials

Wet shells generated from the process line of palm oil mill, provided by Nam Bee Oil Palm Estate Sdn Bhd, has been utilized for experiments. The palm shells are water washed to remove dirt and fibers. The cleaned shells are dried at 105 °C in a hot air oven until it is completely dry, which are then crushed, sieved to obtain particle with size range 1–2 mm and stored in airtight containers for further experimentation. Table 2 presents the elemental composition and ultimate analysis of oil palm shells, reported by various authors, along with the results of the analysis due to the present study.

2.2. Methods

The experimental samples are prepared by mixing 20 g of predried palm shells with phosphoric acid based on impregnation ratio between 0.5 and 3. The impregnation ratio is defined as the ratio of weight of 100% phosphoric acid utilized for impregnation to the weight of the dry palm shells. A 65% phosphoric acid is utilized for soaking so as to promote the adsorption of reagents into the sample. The phosphoric acid soaked sample is left overnight in ambient environment and the excess water was evaporated in oven (100 °C) to ensure complete absorbance of the phosphoric acid on to the palm shell powder. The acid soaked samples are semi-carbonized in a hot air oven (Universal Hot Air Oven, OSAW Industrial Products) at a preset furnace temperature of 170 °C for 1 h. The semi-carbonized material is activated in a muffle furnace (Protherm Furnace, PLF120/5) for desirable activation condition at 425 °C and 30 min. All activations are carried out by exposing the samples directly to 425 °C without the flow of inert gas. The advantage of this specific method of activation has been discussed in detail by Srinivasakannan and Bakar [19]. After activation, the activated carbon is immediately quenched in distilled water before being manually grinded to fine powder. The samples are subsequently washed repetitively with distilled water to remove residual acid. The completeness of washing process is confirmed with the conductivity of wash liquor less than 50 μS, using conductivity meter. A conductivity of wash liquid corresponding to 50 μS may be equated to a phosphoric acid concentration less than 0.01 g/l. Based on the concentration vs. conductivity chart, it is possible to estimate the total quantity of phosphoric acid extracted from the samples, with simple material balance. The product is finally air dried at 105 °C, which are utilized for product characterization. The desirability of such experimental conditions with reference to process scale up has been analyzed and is due to Srinivasakannan and Bakar [19].

2.3. Product characterization

The activated carbon is characterized, for yield and iodine adsorption capacity and pore characteristics for the selected sample. Yield is defined as the ratio of weight activated carbon produced to the dry weight of precursor. Iodine number is defined as milligrams of iodine adsorbed by a gram of carbon, using the procedure as stated in ASTM [D4607-94(2006)]. Iodine number is commonly used in industries as a measure of adsorption capacity, reflecting the amount of micropores in the carbon. Iodine number approximates the internal surface area of activated carbon and measure availability of pores greater than 1.0 nm in diameter [19]. The relationship between the iodine number and internal surface area in terms of m^2/g of activated carbon has been well established in the literature for various precursors. The most recent studies by Mianowski et al. [21], Bestani et al. [22] and Noszko et al. [23] have established equivalence of iodine number with BET surface area with in acceptable errors valid up to a BET surface area of 1000 m^2/g. At surface areas higher than 1000 m^2/g the surface areas are found to be higher than the iodine number [21].

2.3.1. Textural characteristics

Pore structure of the selected sample is characterized by nitrogen adsorption at 77 K with an accelerated surface area porosimetry system (Autosorb-1-C, Quantachrome). Prior to gas adsorption measurements, the carbon is degassed at 300 °C in a vacuum condition for a period of at least 2 h. Nitrogen adsorption isotherm is measured over a relative pressure (P/P_0) range from approximately 10^{-7} to 1. The BET surface area is calculated from the isotherms using the Brunauer–Emmett–Teller (BET) equation [24]. The cross-sectional area of nitrogen molecule is assumed to be 0.162 nm. The Dubinin–Radushkevich (DR) method is used to calculate the micropore volume [25]. The pore size distribution is ascertained by Non-local Density Functional Theory (NLDFT) [24,26] by minimizing the grand potential as a function of the fluid density profile. The total pore volume [27] is estimated by converting the amount of nitrogen gas adsorbed at a relative pressure of 0.95 to the equivalent liquid volume of the adsorbate (nitrogen). The mesopore volume is estimated by the subtracting the micropore volume from the total volume.

2.4. Selection of process parameters

The activation process of biomass is widely understood to be influenced by the activation temperature, activation time and impregnation ratio. The major advantage of phosphoric acid based activation process as compared to other impregnation agents is the low activation temperature. Although there are several reports of activation temperatures ranging up to 800 °C (Table 1) with different chemical activation methods, the optimum temperatures have been identified to be temperatures below 500 °C for different precursors [17,18,29,30]. The recent report due to Gratuito et al. [20] for process optimization of coconut shell using phosphoric acid activation, utilizing the experimental conditions due to Srinivasakannan and Bakar [19] has reported an optimum activation temperature of 416 °C. Since the process economics largely depends on the activation temperature, a lower activation temperature is desirable and hence an activation temperature of 425 °C is selected.

The optimum activation time is reported to vary between 30 and 120 min depending upon the activation method and the activating agent. However in general the activation time is significantly lower using phosphoric acid activation method and have been reported to be less than 45 min by Srinivasakannan and Bakar [19]. A lower activation time is desirable as it improves the process economics and increases the product yield. Gratuito et al. [20] have recently reported an optimum temperature of less than 30 min for coconut shell activation using phosphoric acid. As the objective of the present work is to produce activated carbon with high yields and good textural characteristics an activation time of 30 min is selected. The impregnation ratio is a significant parameter that has effect on yield and textural characteristics of the activated carbon. Several studies have reported improvement in textural characteristics with increase in the impregnation ratio [17,29,30,31], with an optimum impregnation ratio. The impregnation ratio is varied from 0.5 to 3 to assess the yield and the textural characteristics of the activated carbon.

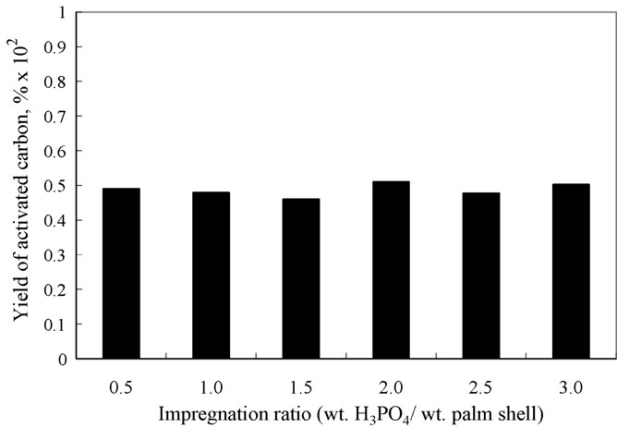

Fig. 1. Yields of PSAC with H_3PO_4 impregnation ratio at an activation temperature of 425 °C and activation time of 30 min.

3. Results and discussion

The activation temperature and activation time is fixed at the lowest possible values supported by the literature evidence, due to the process economic benefits. The impregnation ratio has been varied to assess its effect on the yield and textural characteristics of the activated carbon. Fig. 1 shows the effect of impregnation ratio on the yield of activated carbon while Fig. 2 shows the effect of impregnation ratio on the iodine adsorption capacity of the activated carbon. An increase in the impregnation ratio does not show any tangible effect on the yield of activated carbon and the yield is found to be approximately around 50% for all the impregnation ratios. This indicates that the impregnation ratio does not alter the kinetics of the reaction between the carbon and the phosphoric acid. Similar study due to Guo and Lua [16] reported a decrease of yield with increase in activation temperature, while the effect of impregnation ratio was not reported. However it should be noted

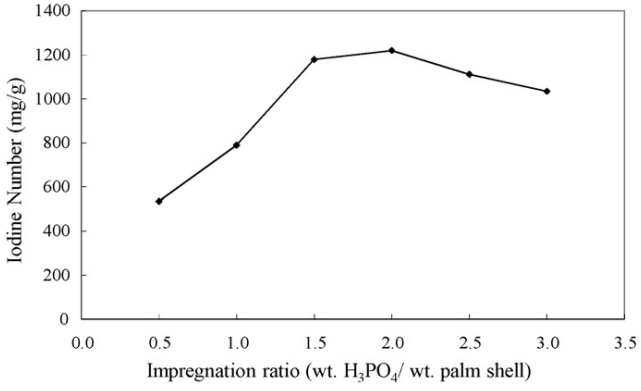

Fig. 2. Iodine number of PSAC with H_3PO_4 impregnation ratio at an activating temperature of 425 °C and activation time of 30 min.

that they reported a yield of around 40% at an activation temperature of 500 °C, with good textural characteristics of the activated carbon. Taking into consideration the trend reported by Guo and Lua [16], a yield of 50% is well justified although the experimental methods are different. It should be noted that Guo and Lua [16] have conducted experiments in an inert medium. In physical activation methods using steam or carbon dioxide as the activating agent the yield significantly decreases with increase in the concentration of the activating agent, as the rate of reaction significantly increase with the concentration of the activating agent. Although steam is generated during the process of dehydration of phosphoric acid, it does not alter the kinetics of the gasification reaction ($C + H_2O \rightarrow CO + H_2$) due to low activation temperatures. Hence an increase in the concentration of phosphoric acid does not decrease the yield of activated carbon. During thermal decomposition of lignocellulosic precursors, the presence of phosphoric acid in the interior of precursor restricts the formation of tar as well as other liquids such as acetic acid and methanol by the formation of cross-links, and inhibits the shrinkage of the precursor particle by occupying certain substantial volumes [16]. The phosphoric acid forms a layer of linkage such as phosphate and polyphosphate esters, which could protect the internal pore structure and thus prevent the adsorbent from excessive burn-off. As the pore evolution for chemical process commence at much lower temperatures a higher yield is expected than the thermal process where excessive burn-off is encountered at higher temperature.

Fig. 2 shows an increase in iodine number with increase in the impregnation ratio, with the highest iodine number of 1210 mg/g corresponding to an optimum impregnation ratio of 2. An increase in impregnation ratio beyond the optimum results in a decrease in iodine number. Iodine number approximates the internal surface area of activated carbon and measures availability of pores greater than 1.0 nm in diameter [19]. The relationship between the iodine number and internal surface area in terms of m^2/g of activated carbon has been well established in the literature for various precursors. The increase in iodine absorption capacity well reflects the increase in porosity of the activated carbon with increase in the impregnation ratio. This could be due to the minimization of the formation of tars and other liquids, which could otherwise clog up the pores and inhibit the development of pore structures. In addition, the phosphoric acid dehydrates during activation and remains as salts of phosphoric acid well inside the porous structure of the activated carbon occupying substantial volumes. Once they are released by intense washing after preparation, a large amount of microporosity is created. Increase in surface area of the activated carbon with increase in impregnation ratio is well documented in the literature and the optimum impregnation ratio is reported to range from 1 to 4 depending on the kind of precursor. Girgis and Ishak [18] and Girgis et al. [28] reported an increase in the surface area until an impregnation ratio of 1.6 for cotton stalk, whereas until an impregnation ratio of 1 for peanut hull. In both cases the increase in pore volume was observed with impregnation ratio until the optimum impregnation ratio and to decrease beyond. Vernersson et al. [32] reported an increase in pore volume until an impregnation ratio of 2, although the maximum surface area corresponds to an impregnation ratio of 1.5. Guo and Lua [16] have also reported an increase in pore surface area with increase in impregnation ratio with a maximum surface area of 1135 m^2/g. However the correct impregnation ratio is not evident from the study as the excess amount of phosphoric acid was filtered prior to drying the samples. A similar study due to Adinata et al. [10] on the activation of palm shells using K_2CO_3, reports an increase in surface area of the activated carbon with increase in impregnation ratio until an impregnation ratio of 1 with a sharp rise in surface area at an impregnation ratio of 1 and a drastic decrease beyond.

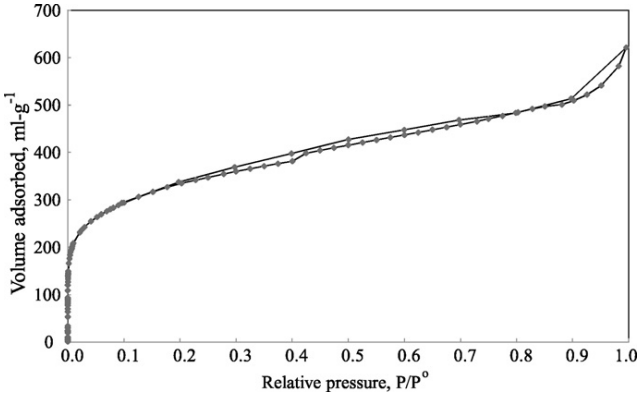

Fig. 3. Adsorption isotherms of N_2 at −196 °C on activated carbon prepared at an impregnation ratio of 3, activation temperature of 425 °C and activation time of 30 min.

As the objective of present to study is to evidence the ability of the phosphoric acid activation process to produce high yielding activated carbon with good textural characteristics, the BET surface area analysis of the sample corresponding to an impregnation ratio of 3 with an iodine number of 1035 mg/g was performed using a BET surface area analyzer. This sample was chosen as the relation between surface area and the iodine number is well established up to an iodine number of 1000 mg/g. The BET surface area corresponding to the iodine number of 1035 mg/g is estimated to be 1109 m^2/g, with the pore volume is 0.903 cm^3/g. Although the pore volume is significantly higher than that reported in the literature, the surface area is comparable to the literature values owing to the high pore diameter. The average pore diameter is estimated to be 3.2 nm with the contribution of micropore volume being 50%. In comparison with the present process (i) the physical activation methods report very low yield (<15%), with high surface area (≈1000–1500 m^2/g) utilizing a high activation temperature (800–1000 °C), and activation time (1–2 h), (ii) the combination of physical and chemical activation method reports surface areas to range around 1500 m^2/g, with the activation temperatures and activation times much similar to the physical activation methods, with the yields being substantially higher than physical activation method in the range of 25–35%, (iii) the chemical activation methods report surface area less than 1250 m^2/g with the phosphoric acid activation method indicating a yield of 40% at an activation temperature of 500 °C, with an activation time of 2 h. The present process in comparison with the literature reported chemical activation methods, utilizes a self-generated atmosphere (no nitrogen purging), with significantly lower activation temperature and activation time. The textural characteristics of the activated carbon prepared in the present study, well compares with the surface area reported using chemical activation method, however with a substantially higher amounts of mesopores, with higher mean pore diameter. A significant rise of 40% increase in mesopore volume using self-generated atmosphere as compared to activation in an inert atmosphere has also been reported by Vernersson et al. [32]. The significant quantity of mesopores well suggests the activated carbon utility for the adsorption of bigger molecules that are suitable for liquid phase adsorption.

Fig. 3 shows the nitrogen adsorption capacity of activated carbon with respect to the nitrogen relative pressure (P/P_0). The sharp rise in the amount of nitrogen adsorbed at low relative pressures well indicates the amount of micropores available with the activated carbon. The pore volume continued to progressively increase with increase in the relative pressure with a shape rise at high relative pressure. The progressive rise in pore volume indicates the availability of mesopores and the process of multilayer filling of the

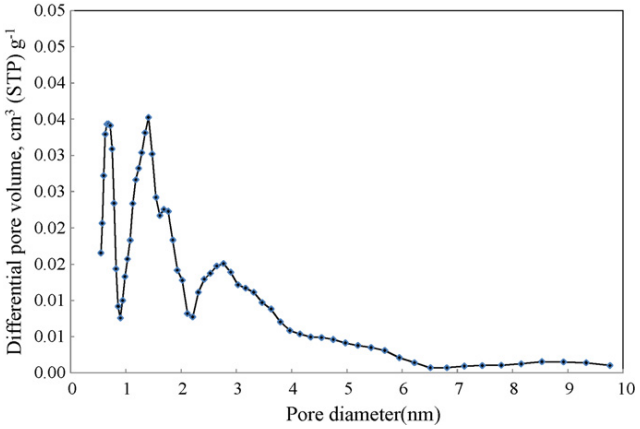

Fig. 4. Pore size distribution of the activated carbon prepared at an impregnation ratio of 3, activation temperature of 425 °C and activation time of 30 min.

pores. The isotherm exhibits a pattern of type II isotherm, under the IUPAC classification of isotherms, based on the progressive increase in the adsorption capacity beyond the relative pressure of 0.1. The sharp rise beyond a relative pressure of 0.9 and the formation of hysteresis loop, while desorbing, indicate a type IV isotherm. This type of isotherm is a general characteristic of porous carbons that have large sized pores. The pore size distribution shown in Fig. 4 substantiates the amount of pores in the mesoporous range, with the average pore diameter estimated to be 3.2 nm. The pore size distribution shows a twin peak in the micropore region, contributing nearly to the 50% of total pore volume.

4. Conclusion

With the objective to develop activated carbon with good textural characteristics at low activation temperature and activation time with significant yield a phosphoric based activation process is chosen with palm shell based precursors. The yield of activated carbon has not been found effected by the impregnation ratio at an activation temperature of 425 °C and 30 min of activation time. However the textural characteristic is found to improve with increase in the impregnation ratio up to 2.0, characterized by the iodine number of 1210 mg/g. The yield of activated carbon has been found to be around 50%, while the BET surface area of the activated corresponding to an iodine number of 1035 mg/g is estimated to be 1109 m^2/g, with a pore volume of 0.903 cm^3/g, and an average pore diameter of 3.2 nm. The adsorption isotherm of the activated carbon indicates multilayer filling, characteristic of activated carbon with significant mesopores.

References

[1] S.H. Moon, J.W. Shim, J. Colloid Interface Sci. 298 (2006) 523–528.
[2] E. Ayranci, O. Duman, J. Hazard. Mater. 136 (2006) 542–552.
[3] S.E. Iyuke, W.R.W. Daud, A.B. Mohamad, Chem. Eng. Sci. 55 (2000) 4745–4755.
[4] A.M. Ribeiro, J.M. Loureiro, Chem. Eng. Sci. 57 (2002) 1621–1626.
[5] A.M. Fuente, G. Pulgar, F. González, C. Pesquera, J. Appl. Catal. A: Gen. 208 (2001) 35–46.
[6] A. Yuan, Q. Zhang, J. Electrochem. Commun. 8 (2006) 1173–1178.
[7] H. Oda, Y. Nakagawa, Carbon 41 (2003) 1037–1047.
[8] S. Biloe, V. Goetz, A. Guillot, Carbon 40 (2002) 1295–1308.
[9] D. Lozano-Castello, M.A. Lillo-Rodenas, D. Cazorla-Amoros, A. Linares-Solano, Carbon 39 (2001) 741–749.
[10] D. Adinata, W.M.A.W. Daud, M.K. Aroua, Bioresour. Technol. 98 (2007) 145–149.
[11] J. Guo, W.S. Xu, Y.L. Chen, A.C. Lua, J. Colloid Interface Sci. 281 (2005) 285–290.
[12] Global Oils and Fats Business magazine, Regional Review, KDN No. PP 10311/10/2008 (007203), vol. 6, 2009.
[13] World Activated Carbon to 2012—Market Research, Market Share, Market Size, Sales, Demand Forecast, Market Leaders, Company Profiles, Industry Trends, The Freedonia Group Inc., 2008.
[14] M.A. Ahmad, W.M.A.W. Daud, M.K. Aroua, Colloids Surf. A: Physicochem. Eng. Aspects 312 (2008) 131–135.
[15] Z. Hu, M.P. Srinivasan, Micropor. Mesopor. Mater. 43 (2001) 267–275.
[16] J. Guo, A.C. Lua, Mater. Chem. Phys. 80 (2003) 114–119.
[17] P. Patnukao, P. Pavasant, Bioresour. Technol. 99 (2008) 8540–8543.
[18] B.S. Girgis, M.F. Ishak, Mater. Lett. 39 (1999) 107–114.
[19] C. Srinivasakannan, M.Z. Abu Bakar, Biomass Energy 27 (2004) 89–96.
[20] M.K.B. Gratuito, T. Panyathanmaporn, R.A. Chumnanklang, N. Sirinuntawittaya, A. Dutta, Bioresour. Technol. 99 (2008) 4887–4895.
[21] A. Mianowski, M. Owczarek, A. Marecka, Energy Sources A: Recovery Util. Environ. Effects 9 (2007) 839–850.
[22] B. Bestani, N. Benderdouche, B. Benstaali, M. Belhakem, A. Addou, Bioresour. Technol. 99 (2008) 8441–8444.
[23] L.H. Noszko, A. Bota, A. Simay, L.G. Nagy, Chem. Eng. 28 (1984) 293–297.
[24] S.J. Gregg, K.S.W. Sing, Adsorption, Surface Area and Porosity, second ed., Academic Press, London, 1982.
[25] M.M. Dubinin, Progress in Surface and Membrane, vol. 9, Academic Press, New York, 1975.
[26] C. Lastoskie, K.E. Gubbins, N. Quirke, Characterization of Porous Solids. Studies in Surface Science and Catalysis, vol. 87, Elsevier, New York, 1994.
[27] R. Arriagada, R. Garcia, M. Molina-Sabio, F. Rodriguez-Reinoso, Micropor. Mater. 8 (1997) 123–130.
[28] B.S. Girgis, S.S. Yunis, A.M. Soliman, Mater. Lett. 57 (2002) 164–172.
[29] M. Jagtoyen, F. Derbyshire, Carbon 36 (1998) 1085–1097.
[30] M.C. Baquero, L. Giraldo, J.C. Moreno, F. Suarez-Garcıa, A. Martınez-Alonso, J.M.D. Tascon, J. Anal. Appl. Pyrolysis 70 (2003) 779–784.
[31] Y. Munoz-Gonzalez, R. Arriagada-Acuna, G. Soto-Garrido, R. Garcıa-Lovera, J. Chem. Technol. Biotechnol. 84 (2009) 39–47.
[32] T. Vernersson, P.R. Bonelli, E.G. Carrella, A.L. Cukierman, Bioresour. Technol. 83 (2002) 95–104.
[33] M.Z. Hussein, R.S.H. Tarmizi, Z. Zainal, R. Ibrahim, M. Badri, Carbon 34 (1996) 1447–1454.
[34] J. Guo, A.C. Lua, Sep. Purif. Technol. 18 (2000) 47–55.
[35] Z. Hu, H. Guo, M.P. Srinivasan, Y. Ni, Sep. Purif. Technol. 31 (2003) 47–52.
[36] J. Guo, A.C. Lua, Sep. Purif. Technol. 30 (2003) 265–273.
[37] I.A.W. Tan, A.L. Ahmad, B.H. Hameed, Desalination 225 (2008) 13–28.
[38] J. Guo, A.C. Lua, Micropor. Mesopor. Mater. 32 (1999) 111–117.
[39] J. Guo, Y. Luo, A.C. Lua, R. Chi, Y. Chen, X. Bao, S. Xiang, Carbon 45 (2007) 330–336.
[40] J. Hayashi, T. Horikawa, I. Takeda, K. Muroyama, F.N. Ani, Carbon 40 (2002) 2381–2386.
[41] A.C. Lua, J. Guo, Carbon 38 (2000) 1089–1097.
[42] A.C. Lua, J. Guo, Langmuir 17 (2001) 7112–7117.
[43] J. Guo, A.C. Lua, Mater. Lett. 55 (2002) 334–339.
[44] J. Guo, A.C. Lua, J. Colloid Interface Sci. 251 (2002) 242–247.
[45] S. Sumathi, S. Bhatia, K.T. Lee, A.R. Mohamed, Bioresour. Technol. 100 (2009) 1614–1621.
[46] W.M.A.W. Daud, W.S.W. Ali, Bioresour. Technol. 93 (2004) 63–69.
[47] A.C. Lua, J. Guo, Colloids Surf. A: Physicochem. Eng. Aspects 179 (2001) 151–162.
[48] Q. Jia, A.C. Lua, Chem. Eng. J. 136 (2008) 227–235.
[49] Q. Jia, A.C. Lua, J. Anal. Appl. Pyrolysis 83 (2008) 175–179.
[50] W.M.A.W. Daud, W.S.W. Ali, M.Z. Sulaiman, Carbon 38 (2000) 1925–1932.
[51] M. Ahmad, W.M.A.W. Daud, M.K. Aroua, J. Porous Mater. 14 (2007) 393–399.
[52] J. Guo, A.C. Lua, J. Anal. Appl. Pyrolysis 46 (1998) 113–125.
[53] D. Adinata, W.M.A.W. Daud, M.K. Aroua, Fuel Process. Technol. 88 (2007) 599–605.
[54] J. Guo, A.C. Lua, Biomass Bioenergy 20 (2001) 223–233.
[55] J. Guo, A.C. Lua, J. Colloid Interface Sci. 254 (2002) 227–233.
[56] J. Guo, A.C. Lua, Chem. Eng. Res. Des. 81 (2003) 585–590.

Separation Science and Technology, 47: 886–895, 2012

ISSN: 0149-6395 print/1520-5754 online
DOI: 10.1080/01496395.2011.627078

Taylor & Francis
Taylor & Francis Group

Preparation of High Surface Area Mesoporous Activated Carbon: Kinetics and Equilibrium Isotherm

W. C. Lim,[1] C. Srinivasakannan,[2] and V. Doshi[1]
[1]*Chemical Engineering Department, Monash University, Sunway Campus, Bandar Sunway, Malaysia*
[2]*The Petroleum Institute, Abudhabi, UAE*

Activated carbon prepared from palm shell by phosphoric acid impregnation, at significantly favorable experimental conditions is characterized for the porous nature and adsorption of methylene blue dye molecules. The activation is carried out using a 2-stage activation process with the activation in a self-generated atmosphere. An activation temperature of 500°C, with an activation time of 75 minutes using a phosphoric acid impregnation ratio of 3 has yielded an activated carbon having unique characteristics. An activated carbon with a yield of 48%, total pore volume of 1.9 cm^3/g, surface area of 1956 m^2/g, an average pore diameter of 3.8 nm, with the ratio of the mesopore to the total surface area in excess of 75% has been prepared. The activated carbon exhibits a high methylene blue equilibrium adsorption capacity of 438 mg/g with the adsorption isotherm increasing with an increase in the adsorption temperature. Among the various adsorption isotherm models, the Langmuir model is able to explain the adsorption process well, evidenced by the proximity of the model with the experimental data. Among the different kinetic models tested with the experimental kinetic data, a pseudo-second-order model is found to fit the experimental data with close proximity.

Keywords activated carbon; adsorption kinetics; methylene blue; phosphoric acid; pore size distribution

INTRODUCTION

Activated carbons with highly developed surface area are widely used in a variety of industries for applications which include separation/purification of liquids and gases, removal of toxic substances, as catalysts and catalyst support (1–5). Liquid phase separations involving high molecular compounds typically involving biological material and dye compounds demand larger pores in accordance with their molecular diameter. It has been well established that the pore structure and pore size distribution are key factors that determine the adsorption capacity of activated carbon. The pore size should be sufficiently big enough to accommodate the molecule of specific interest with adequate binding force. High molecular weight compounds such as dyes and pigments demand a large pore size owing to their larger molecular diameter. Hence conventional activated carbons which are predominantly microporous have inferior adsorption capacity although they have a large surface area. The development of mesopores in activated carbon is crucial in decolorization (6). It is a common challenge to develop carbon materials with properties such as high surface area with specific pore size distribution from low cost precursors and at low temperature while ensuring a reasonably high yield (7). Further, a thorough literature scan revealed that the majority of the published literature only reports the pore structure and pore characteristics of the activated carbon, without the details on the yield of activated carbon.

Phosphoric acid (H_3PO_4), a strong dehydrating agent, has been reported for low activation temperature (below 600°C) on various biomass such as bamboo (7), *Eucalyptus camaldulensis Dehn* bark (8), cotton stalks (9), coconut shell (10), *Arundo donax* cane (11), and rubber wood (12). Marsh and Rodriguez-Reinoso (13) have reported that the amount of phosphorus introduced into the precursor is the main factor for porosity development and the degree of mesoporosity.

The objective of the present study is to produce activated carbon from palm shell using relatively low activation temperature and holding time under self-generated atmosphere and to characterize the product for yield, porous nature through surface area analysis, and Scanning Electron Microscope analysis. Further, the activated carbon is assessed for its appropriateness to adsorb methylene blue (MB), a basic industrial dye. The adsorption experiments, attempt to establish the adsorption isotherm and kinetics of adsorption, further to suitably modeling the adsorption isotherms and kinetics.

MATERIALS AND METHOD

Materials

Wet palm shells generated from the process line of palm oil mill, provided by Nam Bee Oil Palm Estate Sdn Bhd, have been utilized for experiments. The palm shells are water washed and dried at 105°C in a hot air oven until

Received 22 March 2011; accepted 22 September 2011.
Address correspondence to W. C. Lim, Chemical Engineering Department, Monash University, Jalan Lagoon Selatan, Bandar Sunway, Malaysia. E-mail: [redacted]

it is completely dry, which are then crushed, sieved to size 2.0 to 2.5 mm and stored in airtight containers for further experimentation. Analytical grade MB supplied by Sigma-Aldrich (M) Sdn Bhd, is used as adsorbate without further purification. The concentration of this dye is determined using a spectrophotometer (Hach, DR2800) at 665 nm wavelength.

Preparation of Palm Shell Activated Carbon (PSAC)

10 g of dried palm shell is impregnated with 46.15 mL of 65%(wt/wt) H_3PO_4 solution, so it has to have an impregnation ratio of 3:1(wt. H_3PO_4: wt. Palm shell). The H_3PO_4 soaked sample is left overnight and the excess water is evaporated in an oven at 100°C to ensure complete absorbance of the H_3PO_4 on to the palm shell powder. The acid soaked samples are semi-carbonized in a hot air oven (OSAW Industrial) at a preset furnace temperature of 170°C for 1 h. The semi-carbonized material is activated in a muffle furnace (Protherm Furnace, PLF120/5) at a desirable activation temperature of 500°C for a duration of 75 min under a self-generated atmosphere. The feasibility and benefits of using 2-stage chemical activation method in a self generated atmosphere are well documented in literature and are due to Srinivasakannan and Abu Bakar (12), Toles et al. (14), Garcia et al. (15), Ahmedna et al. (16), and Diao et al. (17). After activation, the samples are washed repetitively with distilled water to remove residual acid. The completeness of the washing process is confirmed with the conductivity of wash liquor less than 50 μS, using a conductivity meter. The product is finally air dried at 105°C, before being manually ground to a fine powder and sieved to a size below 120 μm, which are utilized for product characterization.

Carbon Textural Characterization

The pore structure of the PSAC is characterized by N_2 adsorption at −196°C with an accelerated surface area porosimetry system (Autosorb-1-C, Quantachrome) using the standard procedure (18). Texture surfaces of the PSAC samples are examined by scanning electron microscopy (SEM).

MB Adsorption Isotherms

The adsorption isotherm experiments are conducted with a fixed amount of 0.2 g of PSAC mixed with 100 mL MB solutions of various concentrations ranging from 600 to 1400 mg/L in the isothermal shaker bath for 24 hours at constant temperature of 30, 40, and 50°C without altering the pH of the MB solution. Preliminary experiments are carried out to ensure that the adsorption process reached equilibrium within 24 hours. The amount of MB adsorbed by the PSAC is estimated based on the difference in the concentration of the MB solution before and after completion of the experiment, with simple mass balance. The MB concentrations are measured using a spectrophotometer at 665 nm.

Effect of pH on MB Adsorption Isotherm

The effect of pH on MB adsorption is carried out with the initial pH range of 1-11. The initial pH of the solution is adjusted by using 0.1 N HCl or 0.1 N NaOH. Dose of 0.2 g PSAC is added to 100 mL of solution having 1400 mg/L of MB into 250-mL Erlenmeyer flasks. The flasks are then capped and constantly shaken in an isothermal shaker at 100 Hz and 30°C for 24 hours. The pH is measured by using a pH meter (Ecoscan, EUTECH Instruments). The MB concentration is estimated using a spectrophotometer.

MB Adsorption Kinetics

The adsorption kinetics experiments are conducted with a fixed PSAC dose of 0.2 g at constant temperature and pH (30°C and pH 7) with initial MB concentration of 600, 800, and 1200 mg/L. The change in concentration of the MB bath is monitored at intervals of time until no significant change in the concentration of the MB bath is observed. A significant variation in the concentration of the bath is observed until an adsorption time of only 120 min; however the experiments are continued for duration of 240 min.

RESULTS AND DISCUSSION

Characterization of PSAC

The textural characteristic of the PSAC prepared in the present study is listed in Table 1. As can be seen, a total pore volume of 1.9 cm^3/g is substantially higher than the pore volumes normally reported in literature. A compilation of the yields and porous nature of the activated carbon from palm shells has been due to Lim et al. (18), which clearly indicates the ranges of pore volumes using palm shells. The PSAC prepared in the present study is substantially mesoporous, with the mesopore volume being 85% of the

TABLE 1
Physical properties of activated carbon from palm shell by chemical activation with H_3PO_4

Sample	Values
Impregnation ratio, wt_{H3PO4}/wt_{PS}	3.0
Activation temperature, °C	500
Activation time, min	75
Yields, $\%wt_{PSAC}/wt_{PS}$	48.1
S_{BET}, m^2/g	1956
S_{me}, m^2/g	1501
S_{me}/S_{BET}, %	76.7
V_{total}, cm^3/g	1.90
V_{me}, cm^3/g	1.636
Average pore diameter, nm	3.88

total volume. Such an activated carbon with high amount of mesopores has not been reported in literature and it owes to the activation process followed in the present study. Although the pore volumes are high with a relative high contribution of mesopores, the total surface area corresponds only to $1956\,m^2/g$, due to the large average pore size of 3.8 nm. The unique nature of the porous carbon prepared in the present study, is expected to facilitate adsorption of a large quantum of high molecular weight compounds with ease, owing to the pore size and the surface area. Activation in a self-generated atmosphere is certainly simpler than conventional activation which involved thermal treatment of the impregnated precursor in inert conditions. Furthermore, a large amount of heat energy is discharged together with inert gas flow in the conventional method. As seen in the result, the presence of some air during activation in this experiment would not affect the process since the sample would constantly be blanketed by decomposition gases formed by the process. This is in agreement with works by Celis et al. (19) who observed activated carbon with high BET surface area ($2281\,m^2/g$) from *P. ruscifolia* wood activated using similar method.

In addition to the porous nature of the activated carbon, the yield of the activated carbon is a desirable parameter to assess effectiveness of the activation process, as it relates to process economics. The yield is defined as the ratio of, weight of activated carbon produced to the dry weight of precursor. An attempt to compile the range of yields using different activation processes has been due to Lim et al. (18). The yield of PSAC utilizing the present process is 48.1%, which is the highest of yield reported for palm shell based precursor. Guo and Lua (20) have reported a yield of 40%, while Hu et al. (21) have reported a yield of 37% with the activation using a combined physical-chemical activation using CO_2-$ZnCl_2$. However, both the above works reported a surface area less than $1200\,m^2/g$, substantially lower than the surface area and the pore volume generated in the present process.

During thermal decomposition of lignocellulosic precursors, the presence of H_3PO_4 in the interior of the precursor restricts the formation of tar as well as other liquids such as acetic acid and methanol by formation of cross-links, and inhibits the shrinkage of the precursor particle by occupying certain substantial volumes (22,23). The H_3PO_4 forms a layer of linkage such as phosphate and polyphosphate esters, which could protect the internal pore structure and thus prevent the adsorbent from excessive burn-off. As the pore evolution for the chemical process commences at much lower temperatures, a higher yield is expected than the thermal process where excessive burn-off is encountered at higher temperature.

Carbon Textural Characterization

Figure 1 shows the N_2 adsorption–desorption isotherms at $-196°C$ for PSAC produced. The significant rise in the adsorption capacity beyond $P/P_o > 0.1$ indicates the development of mesopores confirming the considerable amount of mesopores in the sample. The large hysteresis loop corresponds to the capillary condensation of N_2 molecules indicating the PSAC exhibited type IV isotherm. Such isotherms may exhibit hysteresis where the mechanism of filling by capillary condensation in mesopores, differs from that of mesopore emptying (13). The observed isotherm does not exhibit a plateau in the high relative pressure region, confirming their mesoporous nature.

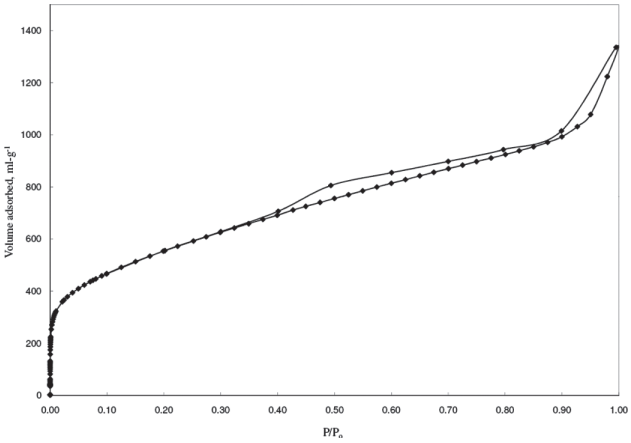

FIG. 1. Adsorption and desorption N_2 isotherms at $-196°C$ of PSAC prepared by H_3PO_4 impregnation.

The use of activated carbons for liquid or gas adsorption demands not only high surface areas but also appropriate pore sizes that are significantly higher than the size of the polluting molecules that can be retained by the carbon. An activated carbon that possesses a predominantly microporous structure would not adsorb large molecules such as MB, as the molecule would not be able to diffuse into the active adsorption sites (24). The pore size distribution along

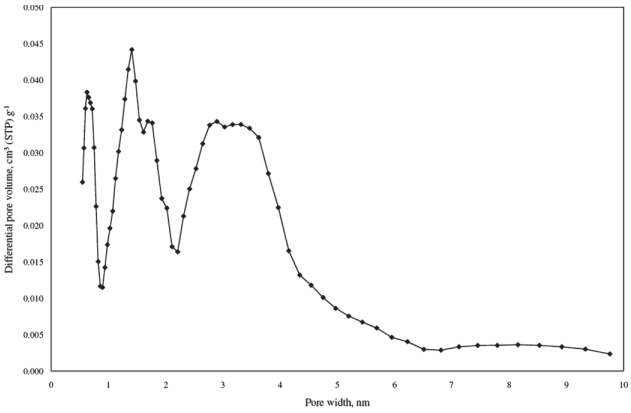

FIG. 2. Pore size distribution of PSAC prepared with H_3PO_4 at 3.0 impregnation ratio, 500°C and 75 min.

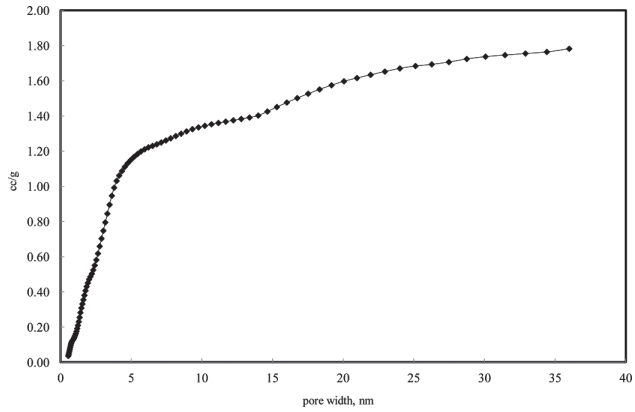

FIG. 3. DFT/Monte-Carlo cumulative pore volume plot.

with cumulative pore size distribution of the PSAC prepared in the present study is shown in Figs. 2 and 3, which shows three peaks with the first peak in the ultra-micropore range having pore size less than 1 nm, while the second peak within the range of 1 to 2 nm and the third one with a peak in the range of 2 to 4 nm. The presence of significant amounts of pores in the size range in excess of 2 nm is well evidenced from the figure, with the contribution of mesopores being 76.7% of the total surface area.

SEM analysis of PSAC samples are conducted to observe the pore structure of the activated carbon and are shown in Figs. 4a and b. As can be seen, the PSAC attests the presence of a substantial amount of pores created due to the activation of H_3PO_4. The carbon surface exhibits large amounts of clear porous structures, indicating H_3PO_4 is effective in creating well-developed pores and large surface area in PSAC. A relatively smooth external surface Fig. 4a is observed as compared to the "nodule-like" structures in the interior of the particles Fig. 4b.

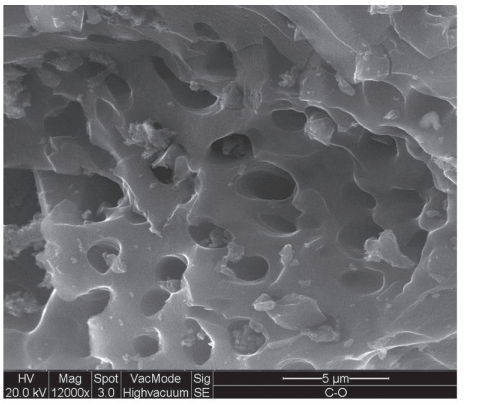

(a)

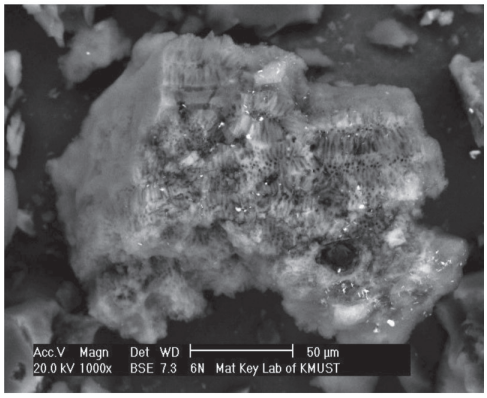

(b)

FIG. 4. SEM photograph of PSAC: (a) Particle outlook (X 12,000); (b) Internal porous (X 1000).

Adsorption Equilibrium

The influence of temperature on the MB adsorption rate and equilibrium on PSAC is investigated at three different temperatures of 30, 40, and 50°C at an initial MB concentration of 1200 mg/L. Figure 5 is a typical plot of the equilibrium adsorption of MB in the solid phase corresponding to the MB concentration in the liquid phase, showing the effect of temperature. A sharp rise in the equilibrium adsorption capacity at low concentration of MB in the liquid is observed, which reaches an asymptote at higher liquid phase MB concentration. Figure further evidence the increase in the equilibrium adsorption capacity of the PSAC with increase in temperature of the adsorption process.

An increase in the equilibrium adsorption capacity with increase in temperature indicates the adsorption process being endothermic. The increasing temperature aids increasing the number of MB molecules to acquire sufficient energy to penetrate the external boundary layer of PSAC particles to enable the interaction with active site at the surface. Hameed et al. (25) reported an increase in temperature may produce a swelling effect within the

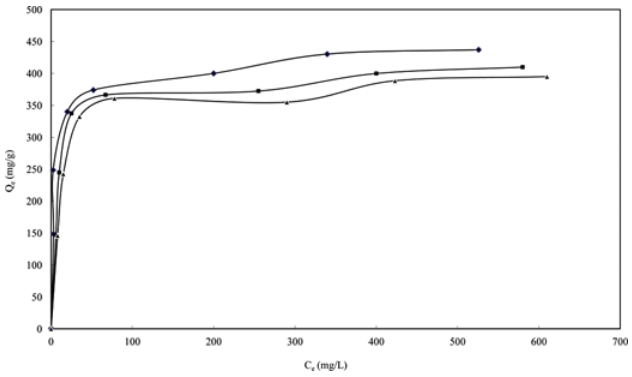

FIG. 5. The effect of temperature to the adsorption of MB onto PSAC (▲: 30°C; ■: 40°C; ◆: 50°C). (Color figure available online)

TABLE 2
Langmuir, Freundlich and Temkin isotherm constants for MB adsorption onto PSAC

Isotherm	Parameters
Langmuir	$Q_0 = 434.7$ mg/g
	b = 0.1729 L/mg
	$R^2 = 0.9998$
Freundlich	$K_F = 227$ (mg/g)(L/mg)$^{1/n}$
	$1/n = 0.1097$
	$R^2 = 0.9694$
Temkin	A = 336.97 L/g
	B = 36.859
	$R^2 = 0.9868$

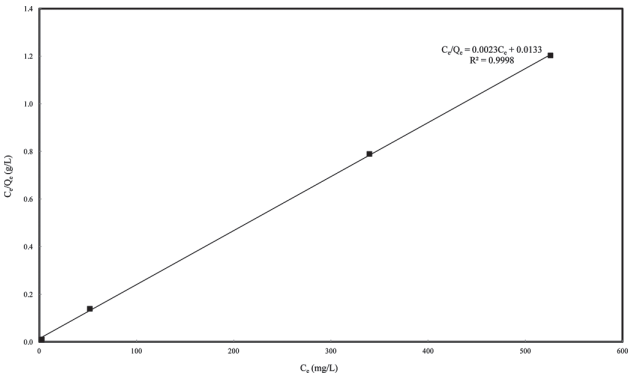

FIG. 6. Langmuir isotherm for the adsorption of MB onto PSAC.

internal structure of the adsorbent that enabling large dye to penetrate further. Meanwhile, Dogan et al. (26) suggested a possible mechanism of interaction is the reaction between the chromophere groups such as alcoholic, carboxylic, and phenolic of the adsorbent surface and the cationic group in the dye molecule; such a reaction could be favored at higher temperatures. It is also stated that increasing the temperature would result in increasing the diffusion rate of adsorbate molecules across the external film layer and into the internal pores of the adsorbent particle (27,28). An increase in temperature would also result in the shift of adsorption equilibrium due to Le- Chatelier Principle.

The quantity of dye that could be taken up by an adsorbent is a function of both the concentration of the dye and the temperature (29). The adsorption isotherms generated at different temperature for the PSAC are tested with popular adsorption isotherm models to identify the appropriate mechanism of adsorption. The experimental adsorption isotherms are fitted with the Langmuir, Freundlich and Temkin isotherm models to evaluate the model parameters by minimizing error between the experimental data and the model equation. The correlation coefficients, R^2, served as an indicator to check the appropriateness of the model. The evaluated model parameters are listed in Table 2.

Adsorption Isotherm

Langmuir Isotherm

The Langmuir equation, which is applicable to homogeneous sorption, can be described by the linearized form:

$$C_e/Q_e = 1/Q_0 b + C_e(1/Q_0)$$

The Langmuir constants Q_0 (mg/g) and b (L/mg) are determined from the slope and intercept of the plot of specific adsorption, C_e/Q_e against the equilibrium concentration, C_e as presented in Fig. 6. The close proximity of the experimental data with the model equation evidenced from the R^2 value (Table 2) of 0.999 demonstrates suitability of the Langmuir isotherm model.

Freundlich Isotherm

The logarithmic form of Freundlich isotherm is given by the following equation:

$$\log Q_e = \log K_F + (1/n) \log C_e$$

where K_F (mg/g)(L/mg)$^{1/n}$ and n are the Freundlich adsorption constant. $1/n$ is the heterogeneity factor that measure of the adsorption intensity as well as its favorability. The linearised Freundlich plot of logQ_e versus logC_e is shown in Fig. 7 along with Freundlich constants K_F and $1/n$. The R^2 value is shown in Table 2, and it corresponds to 0.9694, demonstrating the magnitude of variation between the experimental data and the model equation.

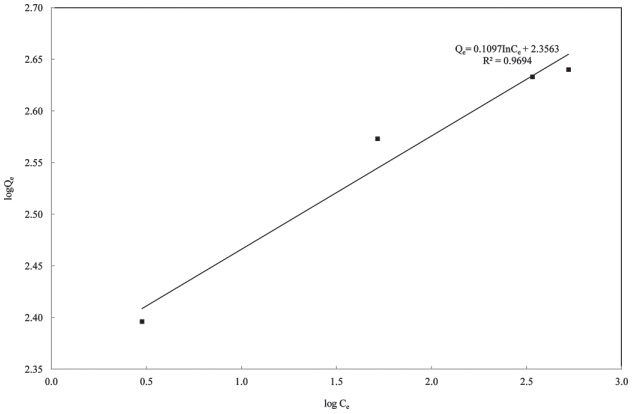

FIG. 7. Freundlich isotherm for the adsorption of MB onto PSAC.

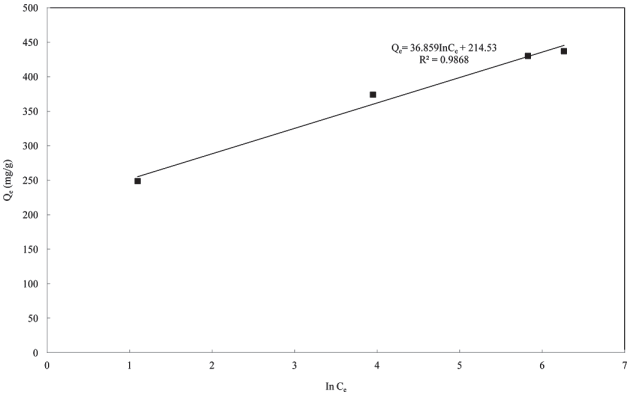

FIG. 8. Temkin isotherm for the adsorption of MB onto PSAC.

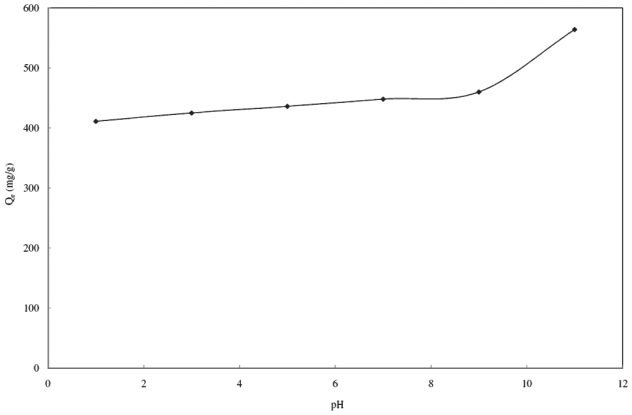

FIG. 9. pH effect on MB adsorption onto PSAC (MB concentration: 1400 mg/L; PSAC dose: 2 g/L).

Temkin Isotherm

Temkin isotherm considers the effects of indirect adsorbate/adsorbate interactions on adsorption isotherms (30). The linearized form of the Temkin isotherm is expressed as:

$$Q_e = (RT/b)\ln(A) + (RT/b)\ln C_e$$

where A (L/g) is the equilibrium binding constant corresponding to the maximum binding energy and B ($= RT/b$), is the Temkin constant, related to heat of sorption. R (8.314 J/mol K) is the universal gas constant, and T (K) is the absolute solution temperature. The plot of the above equation is shown in Fig. 8 along with the Temkin isotherm constants A and B. *The* R^2 value of the Temkin model is presented in Table 2 and it corresponds to 0.986.

From Table 2, the highest R^2 values correspond to Langmuir model with a R^2 value of 0.999, while the lowest value corresponds to Freundlich isotherm model with a R^2 value of 0.969. The perfect fit of the experimental data with the Langmuir isotherm model indicate the adsorption behavior to observe predominantly a monolayer adsorption, involving chemical and physical adsorption. This observation is in agreement with literature on MB adsorption onto activated carbon prepared from palm shell (31), palm fiber, coconut husk (32), jute fiber (33), and sunflower oil cake (34).

Effect of Solution pH on MB Uptake

The pH affects the surface charge of the adsorbents as well as the degree of ionization of different pollutants which may cause a shift in the equilibrium values of the adsorption process. As shown in Fig. 9, it is evident that pH does effect the MB adsorption onto PSAC significantly beyond a pH of 7, while its effect up to a pH of 7 is insignificant, although the figure shows a qualitative increase. Phosphoric or polyphosphoric acids react with the carbonaceous precursor to form phosphate or polyphosphate esters resulting in carbon adsorbents with strongly acidic surface groups (35). The acid surface of H_3PO_4 activated carbons is obviously due to phosphorus and oxygen-containing species such as phosphate or polyphosphate esters, along with carboxylic and phenolic groups.

At lower pH, the excess H^+ ions deter the electrostatic attractions between positively charged MB cations and positively charged acidic surface site, resulting in a net ionic repulsion effect. As the pH increases, the availability of OH^- ions increase the electrostatic attractions with the acidic surface sites of the PSAC. This transition enhances electrostatic interaction with MB cations and hence increase the dye uptake. This is in agreement with observation due to Senthilkumaar et al. (33), using carbon from H_3PO_4 activated jute fiber (*corchorus capsularis*),who have reported a significant increase in MB adsorption in the pH range from 7 to 10.

Tan et al. (36), using adsorbent from HCl-treated palm shell, reported a significant increase in MB adsorption from pH 7 onwards. While Karagoz et al. (34) found a significant increase in MB adsorption with pH only until pH 6 (after which MB adsorption became constant) for adsorbent from H_2SO_4 activated sunflower oil cake. A similar trend was reported by Hameed on untreated garlic peel. On the other hand, Lata et al. (37) reported an insignificant influence of pH, for carbon produced from H_3PO_4 activated biomass, (*Parthenium hysterophorus*) and Garg et al. (38) with untreated rosewood sawdust.

Adsorption Kinetics

Adsorption kinetics is known to vary with the concentration of the adsorbent, agitation rate, the adsorption temperature, the pH of the solution and size of the adsorbent. Figure 10 shows an increase in the rate of adsorption with increase in the initial concentration of MB from 600 to 1200 mg/L with the maximum adsorption corresponding to 306 to 421 mg/g. It is found that the removal of MB is

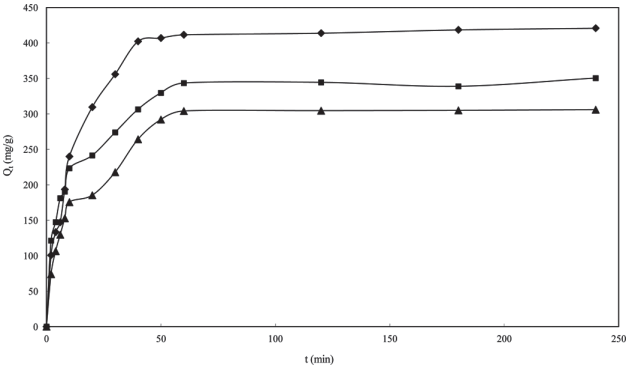

FIG. 10. The effect of initial dye concentration to the adsorption rate of MB onto PSAC (▲: 600 mg/L; ■: 800 mg/L; ◆ =: 1200 mg/L).

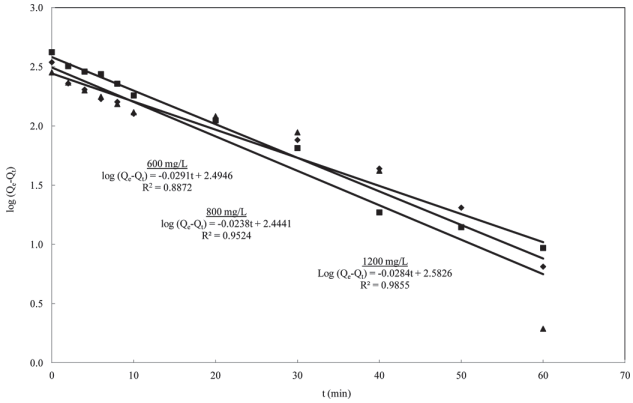

FIG. 11. Pseudo-first-order plots for different initial MB concentrations (A: 600 mg/L; ■: 800 mg/L; ◆: 1200 mg/L).

rapid during the initial period while the uptake slowdown with increase in time. The reduction in the rate of adsorption with no significant variation in the concentration of the solution indicates the existence of saturation adsorption condition, which could be achieved approximately around 70 min. No significant changes in the MB dye uptake are observed with further increase of contact time up to 24 hours. Similar observations have been reported in the literature for the removal of dyes such as MB (39), malachite green (40), and methyl violet (41). In batch adsorption systems, a monolayer of adsorbate is normally formed on the surface of the adsorbent, and the rate of removal of adsorbate species from aqueous solution is controlled primarily by the rate of transport of the adsorbate species from the exterior/outer sites to the interior site of the adsorbent particles (39,40). An increase in the initial MB concentration increases the mass transfer driving force to overcome all mass transfer resistances of molecules between the aqueous and solid phases (26).

The Pseudo-First-Order Kinetic Model

The pseudo-first-order kinetic Lagergren equation (42) is derived as:

$$\log(Q_e - Q_t) = \log Q_e - (k_1/2.303)t$$

where Q_e and Q_t are the amounts of MB adsorbed (mg/g) at equilibrium and at time t (min), respectively, and k_1 (min^{-1}) is the adsorption rate constant of pseudo-first-order adsorption. The validity of the model can be checked by linearised plot of log ($Q_e - Q_t$) versus t.

Figure 11 shows the linear plot of log ($Q_e - Q_t$) versus t, while Table 3 summarizes the model constants k_1 and Q_e along with R^2 values. The R^2 values which evidence the acceptability of the model in representing the experimental data is found to vary from 0.887 to 0.986 for MB concentration of 600–1200 mg/L.

The Second-Order Kinetic Model

The second-order kinetic model is conveniently expressed in the linearised form as:

$$t/Q_t = 1/k_2 Q_e^2 + t/Q_e$$

where Q_e and Q_t are the amounts of MB adsorbed (mg/g) at equilibrium and at time t (min), respectively, and k_2 is the rate constant (min^{-1}).

The linear plots of t/Q_t against t are shown in Fig. 12. It is found from Table 3, that there is a good agreement between the experimental and the calculated adsorption

TABLE 3
Non-linear kinetics parameters calculated for MB adsorption onto PSAC

	Pseudo-first-order				Pseudo-second-order			Intraparticle diffusion		
Initial MB concentration (mg/L)	$Q_{e,\,exp}$ (mg/g)	$Q_{e,\,cal}$ (mg/g)	k_1 (min^{-1})	R^2	$Q_{e,\,cal}$ (mg/g)	k_2 (x10^{-4}) (min^{-1})	R^2	K_p ($\text{mg}\cdot\text{g}^{-1}$ $\text{min}^{-1/2}$)	C	R^2
600	306	312	0.06702	0.8872	312.5	4.357	0.9974	34.408	42.386	0.9736
800	350	278	0.05481	0.9524	357.1	5.158	0.9987	33.713	91.046	0.9765
1200	421	382	0.06541	0.9855	434.8	3.527	0.9982	53.119	42.038	0.9561

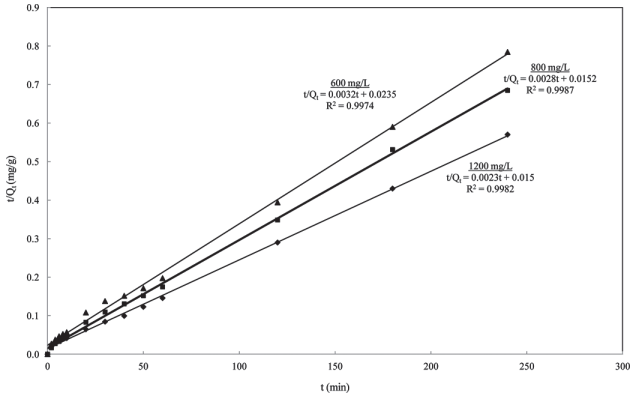

FIG. 12. Pseudo-second-order plots for different initial MB concentrations (A: 600 mg/L; ■: 800 mg/L; ◆: 1200 mg/L).

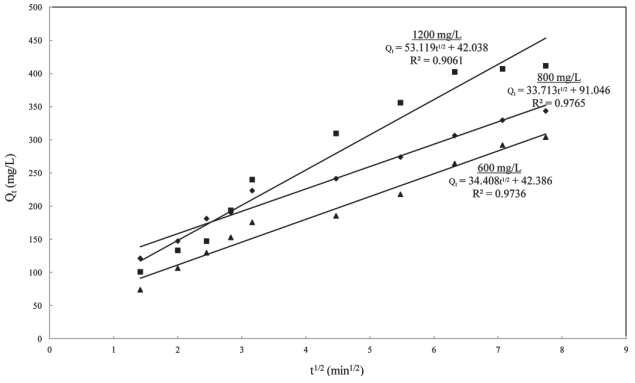

FIG. 13. Intraparticle diffusion plots for different initial MB concentrations (A: 600 mg/L; ■: 800 mg/L; ◆: 1200 mg/L).

$Q_{e,\mathrm{exp}}$ and $Q_{e,\mathrm{cal}}$. This is further supported by the correlation coefficient values for the second-order kinetic model which is almost equal to unity ($R^2 = 1$) for all MB concentrations, highlighting the suitability of pseudo-second-order kinetic model to describe the MB adsorption dynamics.

Intraparticle Diffusion Model

The intraparticle diffusion equation (43) can be described as:

$$Q_t = K_p t^{1/2} + C$$

Where C is the intercept and k_p is the intraparticle diffusion rate constant ($\mathrm{mg \cdot g^{-1}\,min^{-1/2}}$), which can be evaluated from the slope of linear plot of Q_t versus $t^{1/2}$. The linearized plot of the intraparticle model equation is shown in Fig. 13. The R^2 values for the Intraparticle diffusion is found to vary between 0.9061 to 0.9765 and is shown in Table 3.

For all MB concentration the R^2 values is more than 0.99 for pseudo-second-order kinetic model, which is higher than that of the pseudo-first-order kinetic model and intraparticle diffusion model. The high values of correlation coefficients show that the data conformed well to the pseudo-second-order rate kinetic model. This is in agreement with the literature reports on the adsorption of MB using activated carbons from various biomasses (32–34,42,44–46).

Comparison of MB Dye Adsorption with Carbon From Other Biomass

Table 4 shows the compilation of the various maximum MB adsorption capacities reported in literature for different biomass precursors. The maximum MB adsorption capacity of the activated carbon produced in the present study is well among the highest reported owing to the high pore volume

TABLE 4
Comparison of adsorption capacity between PSAC and other studied activated carbons for removal of MB from aqueous solutions

		Activation				Adsorption model	
Reference	Precursor	Reagent	Temp (°C)	Time (min)	Q_e (mg/g)	Isotherm	Kinetics
This work	Palm Shell	H_3PO_4	500	75	438	Langmuir	Pseudo-second-order
Hameed et al.	Bamboo	CO_2/KOH	850	120	454	Langmuir	Pseudo-second-order
Tan et al.	Coconut husk	CO_2/KOH	850	120	435	Langmuir	Pseudo-second-order
Altenor et al.	Vetiver roots	H_3PO_4	600	60	423	Redlich–Peterson	BWS equation
Hameed et al.	Oil palm fibre	CO_2/KOH	862	60	204	Langmuir	
Tan et al.	Palm shell	CO_2/KOH	850	120	244	Langmuir	Pseudo-second-order
Senthilkumaar et al.	Jut Fiber	H_3PO_4			226	Langmuir	Intraparticle diffusion
Demirbas et al.	Apricot stone	H_2SO_4	250	1440	221	Langmuir, Freundlich	Intraparticle diffusion

and the surface area with appropriate pore diameter. Among the different published literature only the report due to Hameed et al. (47), shows an MB adsorption capacity of 454.2 mg/g, for the bamboo precursor using combined physical-chemical activation. However, it should be noted that the bamboo-activated carbon were produced from a much more complex process i.e., carbonization at 700°C for 1 h under N_2 atmosphere followed by KOH (1:1 impregnation ratio) with activation temperature of 850°C for 2 h. Tan et al. (31) with the palm shell precursor using KOH activation have reported only 244 mg/g but at higher activation temperature of 850°C. In general the majority of the literature reports a lower MB adsorption capacity with the activation temperatures and time being significantly higher than that utilized in the present study. The higher adsorption capacity coupled with simplified experimental conditions of activation in a self-generated atmosphere, lower activation time and temperature, with significantly higher yield well augurs the present process commercially favorable, in comparison with the existing processes.

CONCLUSION

The following conclusions could be derived based on the present study pertaining to preparation of activated carbon from palm shells using H_3PO_4 impregnation,

1. A2-stage activation process with the activation temperature of 500°C, an activation time of 75 minutes, with a H_3PO_4 impregnation ratio of 3 results in an activated carbon with a yield of 48%, total pore volume of 1.9 cm^3/g, surface area of 1956 m^2/g, an average pore diameter of 3.8 nm, with the ratio of the mesopore to the total surface area in excess of 75%.
2. The above stated pore characteristics are highly favorable for adsorption of high molecular weight compounds. The activated carbon exhibits a high MB equilibrium adsorption capacity of 438 mg/g with the adsorption isotherm increasing with an increase in the adsorption temperature.
3. Among the various adsorption isotherm models, the Langmuir model is able to explain the adsorption process well, evidenced by the proximity of the model with the experimental data.
4. Among the different kinetic models tested with the experimental kinetic data, a pseudo-second-order model is found to fit the experimental data with close proximity.

REFERENCES

1. Moon, S.H.; Shim, J.W. (2006) A novel process for CO2/CH4 gas separation on activated carbon fibers-electric swing adsorption. *J. Colloid Interface Sci.*, 298: 523–528.
2. Ayranci, E.; Duman, O. (2006) Adsorption of aromatic organic acids onto high area activated carbon cloth in relation to wastewater purification. *J. Hazard. Mater.*, 136: 542–552.
3. Iyuke, S.E.; Daud, W.R.W.; Mohamad, A.B.; Kadhum, A.A.H.; Fisal, Z.; Shariff, A.M. (2000) Application of Sn-activated carbon in pressure swing adsorption for purification of H2. *Chem. Eng. Sci.*, 55: 4745–4755.
4. Ribeiro, A.M.; Loureiro, J.M. (2002) Simulation of toxic gases and vapours removal by activated carbon filters. *Chem. Eng. Sci.*, 57: 1621–1626.
5. Fuente, A.M.; Pulgar, G.; Gonzalez, F.; Pesquera, C.; Blanco, C. (2001) Activated carbon supported Pt catalysts: effect of support texture and metal precursor on activity of acetone hydrogenation. *Appl. Catal. A*, 208: 35–46.
6. Munoz-Gonzalez, Y.; Arriagada-Acuna, R.; Soto-Garrido, G.; Garcia-Lovera, R. (2009) Activated carbons from peach stones and pine sawdust by phosphoric acid activation used in clarification and decolorization processes. *J. Chem. Technol. Biotechnol.*, 84: 39–47.
7. Chan, L.S.; Cheung, W.H.; McKay, G. (2008) Adsorption of acid dyes by bamboo derived activated carbon. *Desalination*, 218: 304–312.
8. Patnukao, P.; Pavasant, P. (2008) Activated carbon from *Eucalyptus camaldulensis Dehn* bark using phosphoric acid activation. *Bioresour. Technol.*, 99: 8540–8543.
9. Girgis, B.S.; Ishak, M.F. (1999) Activated carbon from cotton stalks by impregnation with phosphoric acid. *Mater. Lett.*, 39: 107–114.
10. Gratuito, M.K.B.; Panyathanmaporn, T.; Chumnanklang, R.A.; Sirinuntawittaya, N.; Dutta, A. (2008) Production of activated carbon from coconut shell: Optimization using response surface methodology. *Bioresour. Technol.*, 99: 4887–4895.
11. Vernersson, T.; Bonelli, P.R.; Carrella, E.G.; Cukierman, A.L. (2002) *Arundo donax* cane as a precursor for activated carbon preparation by phosphoric acid activation. *Bioresour. Technol.*, 83: 95–104.
12. Srinivasakannan, C.; Abu Bakar, M.Z. (2004) Production of activated carbon from rubber wood sawdust. *Biomass Energy*, 27: 89–96.
13. Marsh, H.; Rodriguez-Reinoso, F. (2006) *Activated Carbon.* 1st Ed.; Elsevier Ltd.
14. Toles, C.A.; Marshall, W.E.; Johns, M.M. (1998) Phosphoric acid activation of nutshells from metal and organic remediation: Process optimization. *J. Chem. Technol. Biotechnol.*, 72: 255–263.
15. Garcia, F.S.; Alonso, A.M.; Tascon, J.M.D. (2002) Pyrolysis of apple pulp: Chemical activation with phosphoric acid. *J. Anal. Appl. Pyrolysis*, 63: 283–301.
16. Ahmedna, M.; Marshall, W.E.; Rao, R.M. (2000) Surface properties of granular activated carbons from agricultural by-products and their effects on raw sugar decolorization. *Bioresour. Technol.*, 71: 103–112.
17. Diao, Y.; Walawender, W.P.; Fan, L.T. (2002) Activated carbons prepared from phosphoric acid activation of grain sorghum. *Bioresour. Technol.*, 81: 45–52.
18. Lim, W.C.; Srinivasakannan, C.; Balasubramanian, N. (2010) Activation of palm shells by phosphoric acid impregnation for high yielding activated carbon. *J. Anal. Appl. Pyrolysis*, 88: 181–186.
19. Celis, J.D.; Amadeo, N.E.; Cukierman, A.L. (2009) *In situ* modification of activated carbons developed from a native invasive wood on removal of trace toxic metals from wastewater. *J. Hazard. Mater.*, 161: 217–223.
20. Guo, J.; Lua, A.C. (2003) Textural and chemical properties of adsorbent prepared from palm shell by phosphoric acid activation. *Mater. Chem. Phys.*, 80: 114–119.
21. Hu, Z.; Guo, H.; Srinivasan, M.P.; Ni, Y. (2003) A simple method for developing mesoporosity in activated carbon. *Sep. Purif. Technol.*, 31: 47–52.
22. Budinova, T.; Ekinci, E.; Yardim, F.; Grimm, A.; Bjornbom, E.; Minkova, V.; Goranova, M. (2006) Characterization and application of activated carbon produced by H_3PO_4 and water vapor activation. *Fuel Process. Technol.*, 87: 899–905.
23. Girgis, B.S.; Ishak, M.F. (1999) Activated carbon from cotton stalks by impregnation with phosphoric acid. *Mater. Lett.*, 39: 107–114.

24. Williams, P.T.; Reed, A.R. (2004) High grade activated carbon matting derived from the chemical activation and pyrolysis of natural fibre textile waste. *J. Anal. Appl. Pyrolysis.*, 71: 971–986.
25. Hameed, B.H.; Ahmad, A.A. (2009) Batch adsorption of methylene blue from aqueous solution by garlic peel, an agricultural waste biomass. *J. Hazard. Mater.*, 164: 870–875.
26. Dogan, M.; Abak, H.; Alkan, M. (2009) Adsorption of methylene blue onto hazelnut shell: Kinetics, mechanism and activation parameters. *J. Hazard. Mater.*, 164: 172–181.
27. Tan, I.A.W.; Ahmad, A.L.; Hameed, B.H. (2009) Adsorption isotherms, kinetics, thermodynamics and desorption studies of 2,4,6-trichlorophenol on oil palm empty fruit bunch-based activated carbon. *J. Hazard. Mater.*, 164: 473–482.
28. Karaca, S.; Gurses, A.; Acikyildiz, M.; Ejder (Korucu), M. (2008) Adsorption of cationic dye from aqueous solutions by activated carbon. *Microporous Mesoporous Mater.*, 115: 376–382.
29. Thinakaran, N.; Panneerselvam, P.; Baskaralingam, P.; Elango, D.; Sivanesan, S. (2008) Equilibrium and kinetic studies on the removal of Acid Red 114 from aqueous solutions using activated carbons prepared from seed shells. *J. Hazard. Mater.*, 158: 142–150.
30. Demiral, H.; Demiral, I.; Tumsek, F.; Karabacakoglu, B. (2008) Adsorption of chromium (VI) from aqueous solution by activated carbon derived from olive bagasse and applicability of different adsorption models. *Chem. Eng. J.*, 144: 188–196.
31. Tan, I.A.W.; Ahmad, A.L.; Hameed, B.H. (2008) Adsorption of basic dye using activated carbon prepared from oil palm shell: Batch and fixed bed studies. *Desalination*, 225: 13–28.
32. Tan, I.A.W.; Ahmad, A.L.; Hameed, B.H. (2008) Adsorption of basic dye on high-surface-area activated carbon prepared from coconut husk: Equilibrium, kinetic and thermodynamic studies. *J. Hazard. Mater.*, 154: 337–346.
33. Senthilkumaar, S.; Varadarajan, P.R.; Porkodi, K.; Subbhuraam, C.V. (2005) Adsorption of methylene blue onto jute fiber carbon: kinetics and equilibrium studies. *J. Colloid interface Sci.*, 284: 78–82.
34. Karagoz, S.; Tay, T.; Ucar, S.; Erdem, M. (2008) Activated carbons from waste biomass by sulfuric acid activation and their use on methylene blue adsorption. *Bioresour. Technol.*, 99: 6214–6222.
35. Puziy, A.M.; Poddubnaya, O.I.; Martinez-Alonso, A.; Suarez-Garcia, F.; Tascon, J.M.D. (2005) Surface chemistry of phosphorus-containing carbons of lignocellulosic origin. *Carbon*, 43: 2857–2868.
36. Tan, I.A.W.; Ahmad, A.L.; Hameed, B.H. (2008) Enhancement of basic dye adsorption uptake from aqueous solutions using chemically modified oil palm shell activated carbon. *Colloid Surf., A*, 318: 88–96.
37. Lata, H.; Garg, V.K.; Gupta, R.K. (2007) Removal of a basic dye from aqueous solution by adsorption using *Parthenium hysterophorus*: An agricultural waste. *Dyes Pigments*, 74: 653–658.
38. Garg, V.K.; Amita, M.; Kumar, R.; Gupta, R. (2004) Basic dye (methylene blue) removal from simulated wastewater by adsorption using Indian Rosewood sawdust: A timber industry waste. *Dyes Pigments*, 63: 243–250.
39. Kannan, N.; Sundaram, M.M. (2001) Kinetics and mechanism of removal of methylene blue by adsorption on various carbons- a comparative study. *Dyes Pigments*, 51: 25–40.
40. Malik, R.; Ramteke, D.S.; Wate, S.R. (2007) Adsorption of malachite green on groundnut shell waste based powdered activated carbon. *Waste Manage. (Oxford)*, 27: 1129–1138.
41. Ho, Y.S.; McKay, G. (1999) Pseudo-second order model for sorption processes. *Proc. Biochem.*, 34: 451–465.
42. Largegren, S. (1898) About the theory of so-called adsorption of soluble substances. *Kungliga Suensk Vetenskapsakademiens Handlingar*, 241: 1–39.
43. Weber, Jr., W.J.; Morris, J.C. (1963) Kinetics of adsorption on carbon from solution. *J. Sanit. Eng. Div. Am. Soc. Civil Eng.*, 89: 31–59.
44. Al-Ghouti, M.A.; Khraishehb, M.A.M.; Ahmad, M.N.M.; Allen, S. (2009) Adsorption behaviour of methylene blue onto Jordanian diatomite: A kinetic study. *J. Hazard. Mater.*, 165: 589–598.
45. Ho, Y.S.; McKay, G. (1998) Sorption of dye from aqueous solution by peat. *J. Chem. Eng.*, 70: 115–124.
46. Ho, Y.S.; McKay, G. (2000) The kinetics of sorption of divalent metal ions onto sphagnum moss peat. *Water Res.*, 34: 735–742.
47. Hameed, B.H.; Din, A.T.M.; Ahmad, A.L. (2007) Adsorption of methylene blue onto bamboo-based activated carbon: Kinetics and equilibrium studies. *J. Hazard. Mater.*, 141: 819–825.